PhD degree in Molecular Medicine, curriculum in Molecular Oncology,

European School of Molecular Medicine (SEMM),

University of Milan and University of Naples "Federico II"

Faculty of Medicine

Settore disciplinare: Bio/10

# Understanding the catalytic mechanisms of ubiquitin-E3 ligases

*Eleonora Valentini*

Fondazione IFOM, Milan

Matricola n. R09864

*Supervisor:* Dr. Simona Polo
Fondazione IFOM, Milan

Anno accademico 2014-2015

# TABLE OF CONTENTS

# LIST OF ABBREVIATIONS

**AMPK** AMP-activated protein kinase

**AMSH** Associated molecule with SH3 domain of STAM

**AREL1** Apoptosis-resistant E3 ubiquitin ligase

**AP-2** Adaptor protein-2

**APC/C** Anaphase-promoting complex/cyclosome

**Atg8** Autophagy 8

**Atg12** Autophagy 12

**ATP** Adenosine triphosphate

**CC** Coiled-coil domain

**DUB** Deubiquiting enzyme

**E1** Ubiquitin activating enzyme

**E2** Ubiquitin conjugating enzyme

**E3** Ubiquitin ligase

**E6-AP** E6 associated protein

**EGFR** Epidermal growth factor receptor

**ENaC** Epithelial sodium channel

**EPS15** Epidermal growth factor receptor protein substrate 15

**FGFR1** Fibroblast growth factor receptor 1

**GAP** Activating GTPase protein

**GEF** Guanine nucleotide exchange factor

**GST** Glutathione S-transferase

**HB** Helical bundle

**HOIP** HOIL-1 interacting protein

**HECT** Homologous to the E6-AP carboxyl terminus

**IB** Immunoblot

**IBR** In-between RING

**IP3** 1,4,5-trisphosphate

**ISG15** Interferon-stimulated gene 15

**ITC** Isothermal titration calorimetry

**JAMM** Jab1/Pab1/MPN domain containing protease

**$K_D$** Dissociation constant

**LUBAC** Linear ubiquitin chain assembly complex

**MIU** Motif interacting with ubiquitin

**MJD** Machado-Joseph domain containing protease

**MS** Mass spectrometry

**Nedd4** Neuronal precursor cell expressed developmentally downregulated gene 4

**Nedd8** Neuronal precursor cell-expressed developmentally downregulated

**NF-kB** Nuclear factor-kB

**OTU** Otubain domain ubiquitin binding proteins

**PHD** Plant homeodomain

**PINK1** PTEN-induced putative kinase protein-1

**PR** Proline rich

**Rabex-5** Rabaptin associated exchange factor for Rab5

**RAP80** Receptor associated protein 80

**RBR** RING-in between-RING

**RCC1** Regulator of chromosome condensation 1

**RING** Really interesting new gene

**RLD** RCC1-like domain

**SAXS** Small angle X-ray scattering

**SUMO** Small Ub-like modifier

**Ub** Ubiquitin

**UBA** Ubiquitin associated domain

**UBD** Ubiquitin binding domain

**Ubls** Ubiquitin-like proteins

**UBZ** Ubiquitin binding zinc

**UCH** Ubiquitin C-terminal hydrolases

**UFD** Ubiquitin fold domain

**UIM** Ubiquitin interacting motif

**USP** Ubiquitin specific protease

**WB** Western blot

**Y2H** Yeast two hybrid assay

**ZnF** Zinc finger

# FIGURES INDEX

# TABLES INDEX

# ABSTRACT

E3 ubiquitin ligases are key regulatory enzymes of the ubiquitination pathway as they are responsible for substrate specificity. This thesis aimed at deciphering the molecular mechanisms through which two different E3 ligases, Nedd4 and Rabex-5, exert their activity. Nedd4 is the prototype for HECT-E3 ligase while Rabex-5, containing an A20 zinc finger domain (ZnF_A20) instead of a canonical RING, could be defined as an atypical RING-E3 ligase.

In the case of Nedd4, we provided the first crystal structure of the catalytic intermediate of $HECT^{Nedd4}$~Ub in complex with Ub non-covalently bound to the UBD present in the N-lobe of $HECT^{Nedd4}$. Our structure represents the next step of the transfer of $Ub^D$ from the catalytic cysteine of E2 to the one of E3 in which the $Ub^D$ C-terminal tail is in an extended conformation primed for catalysis. Our data strongly supports the sequential addition model proposed for HECT proteins.

Within this study we also clarified some aspects of Rabex-5 as E3 ligase. By yeast-two-hybrid, GST-pull-down assays and ITC analysis, we identified specific E2 partners, Ube2D and Ube2E families, that bind Rabex-5 only when in their active Ub-loaded state. Performing *in vitro* auto-ubiquitination assay and disulfide stability assay we confirmed that ZnF_A20 is the minimal domain responsible for the catalytic activity. To obtain the structure of the Rabex-$5^{1-74}$:E2-Ub complex, we tested, unfortunately without success, crystallization trials and SAXS analysis with various samples.

We also analyzed Rabex-5 catalytic activity towards on H-Ras, which is the unique substrate of Rabex-5 so far identified, and we disproved that H-Ras is a Rabex-5 substrate. To identify candidate substrates we profiled 20.000 human proteins using a microarray-based ubiquitination screening. A list of 67 proteins represent the most statistically stringent and conservative estimate for Rabex-5 substrates that we are going to validate in

the nearest future, starting from the ones involved in the endocytic pathway.

# INTRODUCTION

## 1. Ubiquitin and Ubiquitin-like proteins

Cells use different kind of post-translational protein modifications to generate and transmit signals regulating cellular functions. Among the numerous post-translational modifications, a key role is played by the covalent attachment of one or more ubiquitin (Ub) molecules to epsilon-amino groups of protein lysines (Dye and Schulman, 2007).

Ub is a relatively small polypeptide of 76 amino acids, highly conserved in all eukaryotic cells (Pickart, 2001). This protein is extremely stable and adopts a compact β-grasp fold with the six residues at the C-terminal tail very flexible (Vijay-Kumar et al., 1987) (**Figure 1A**). It is an abundant protein present both in the cytoplasm and in the nucleus, in a free monomeric and target-conjugated form (Dantuma et al., 2006). In mammals, Ub is encoded by a multigene family; UBB and UBC encode Ub polyproteins with three and nine Ub coding units respectively, while UBA52 and UBA80 encode fusion between Ub and two ribosomal proteins (L40 and S27, respectively). The translation occurs from precursor proteins that are then processed into Ub monomers (Finley et al., 1989; Redman and Rechsteiner, 1989).

Ub is a family member of Ub-like modifiers (Ubls) together with Nedd8, SUMO and ISG15. The conjugation reaction to the specific substrate occurs through analogous but specific enzymes cascade determining the involvement in different cellular process (van der Veen and Ploegh, 2012). They are all very similar in structure with a common C-terminal glycine involved in the formation of the isopeptide bond with the substrate (**Figure 1B**). SUMO (small Ub-like modifier) is involved in nuclear transport and organization, transcription, chromatin remodeling, ribosome biogenesis and DNA repair (Gareau and Lima, 2010). Nedd8 (neuronal precursor cell-expressed developmentally downregulated) is a well-defined modifier of all members of Cullin family, able to activate

their ubiquitin ligase activity (Huang et al., 2009). Autophagy 12 (Atg12p) and autophagy 8 (Atg8p) are two Ubls involved in autophagy (Ohsumi and Mizushima, 2004). ISG15 (interferon-stimulated gene 15) is involved in the activation of antiviral immune response through IFN response (Zhao et al., 2005) and broadly targets newly synthesized proteins (Durfee et al., 2010).

Interestingly, recent data demonstrated that Ub could be itself modified by post-translational modification such as acetylation and phosphorylation, increasing the signaling repertoire of this multifunctional protein (Herhaus and Dikic, 2015). Among the various residues of Ub that can be phosphorylated, Ser65 residue has been extensively studied in the context of mitochondrial autophagy (mitophagy). This modification, not only changes the Ub surface properties adding a negative charge, but can also alter the activity of several E2 enzymes, E2/E3 complexes (Wauer et al., 2015) and impairs the activity for several deubiquitinating enzymes (Ordureau et al., 2015; Swaney et al., 2015). Alterations in PARKIN pathway are found in neurodegenerative disease such as in Parkinson. Recently it was demonstrated that PARKIN binding to the p-Ser65-Ub determines its conformational changes causing an increase of its E3 ligase activity (Kazlauskaite et al., 2015; Kumar et al., 2015; Ordureau et al., 2015).

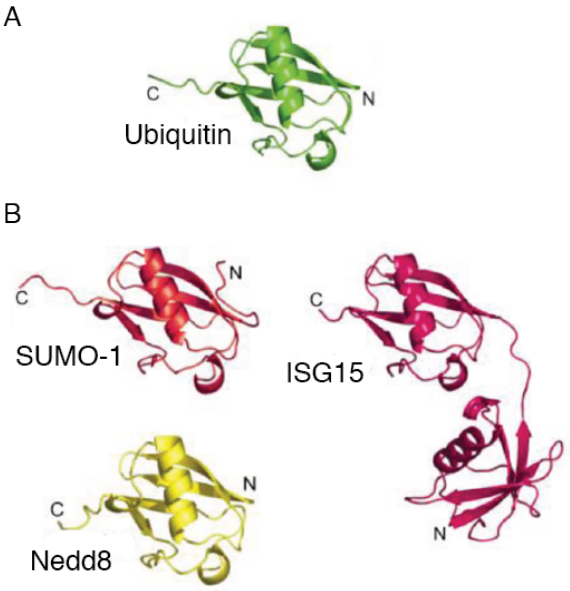


**Figure 1. Structures of ubiquitin-like modifiers (adapted from Dye BT, Annu Rev Biophys Biomol Struct. 2007).** (A) Ub posses a compact β-grasp structure with a flexible C-terminal tail. (B) Structures of some characterized Ubls. They adopt similar tridimensional conformation. SUMO and Nedd8 are composed by only one Ub-like unit respect ISG15 that is composed by two units.

### 1.1 Monoubiquitination and ubiquitin chains

Ub can be attached to the substrate as a single molecule (monoubiquitination or multi-monoubiquitination) or as a polymer composed by multiple Ub molecules called Ub chains (polyubiquitination).

Monoubiquitination usually determines a change in the interaction ability or in the localization of the target proteins (Hicke, 2001) and acts preferentially as a non-proteolytic signal to control gene expression, viral budding, DNA repair and endocytosis (Ramanathan and Ye, 2012).

Ub chains can be of different topology depending on how Ub molecules are connected. The linkage between Ubs can be through the N-terminus or through one of its seven lysines (Lys6, 11, 27, 29, 33, 48 e 63) (**Figure 2A**). These chains are considered homogenous if on each moiety the same residue is modified, or branched if different linkages are used (**Figure 2B**). Chains display distinct structural conformations depending on the linkage (Kulathu and Komander, 2012). The canonical Lys48-linked chains adopt compact conformation (Eddins et al., 2007), with those adjacent moieties interacting with each other. Other linkages, such as Lys6 and Lys11, cause Ub dimers to adopt a similar compact conformation (Matsumoto et al., 2010). In contrast, N-terminus and Lys63- chains display an open conformation, with no contact surfaces except for the linkage site (Datta et al., 2009; Komander et al., 2009b) (**Figure 3**). Recently, the crystal structure of the Lys33-linked diUb was solved showing that it adopts a symmetric compact conformation. In contrast, the Lys33-linked triUb in crystal structure shows an open extended conformation (Kristariyanto et al., 2015). Another group demonstrated that in solution the Lys33-linked and Lys29-linked diUb adopt an open conformation (Michel et al., 2015). Interestingly, also other Ub chains can adopt multiple conformations in solution (Varadan et al., 2002), highlighting the fact that the structural conformations are not a unique but rather a

preferred state of the chains that are indeed very flexible. The receptor proteins carrying the ubiquitin binding domains (UBDs, see below) exploited this flexibility.

From the functional point of view, two chains have been extensively studied: Lys48-linked polyubiquitin chains are involved in targeting proteins for degradation by 26S proteasome (Hershko and Ciechanover, 1998), and Lys63-linked polyubiquitin chains promote cell signaling, membrane protein trafficking or DNA damage response (Chen and Sun, 2009). Only recently a functional role also for other Ub chains linkages has been established. Lys11-linked Ub chains have recently been linked to the proteosomal degradation of cell-cycle proteins. The anaphase-promoting complex (APC/C), the E3 ligase critical for the mitotic degradation of cyclin B and securin, has been shown to act in concert with the E2 Ube2S generating Lys11-linked Ub chains on its substrates (Jin et al., 2008; Wickliffe et al., 2011). Linear-linked chains are involved in nuclear factor- $\kappa$ B (NF-$\kappa$ B) signalling and cell death and dysfunction in linear ubiquitination underlie chronic inflammation (Iwai et al., 2014). Lys33-Ub chains appear to have non-degradative functions working as negative regulator of T-cell antigen receptor (Huang et al., 2010) and of AMPK (AMP-activated protein kinase)-related protein kinase (Al-Hakim et al., 2008).

Finally, branched chain with mixed linkages can be formed *in vitro* (Ben-Saadon et al., 2006) and their role *in vivo* was established in recent work (Meyer and Rape, 2014). Rape and colleagues identified substrates that are specifically modified by branched ubiquitin chains and showed that these conjugates provide an improved signal for proteasomal degradation (Meyer and Rape, 2014).

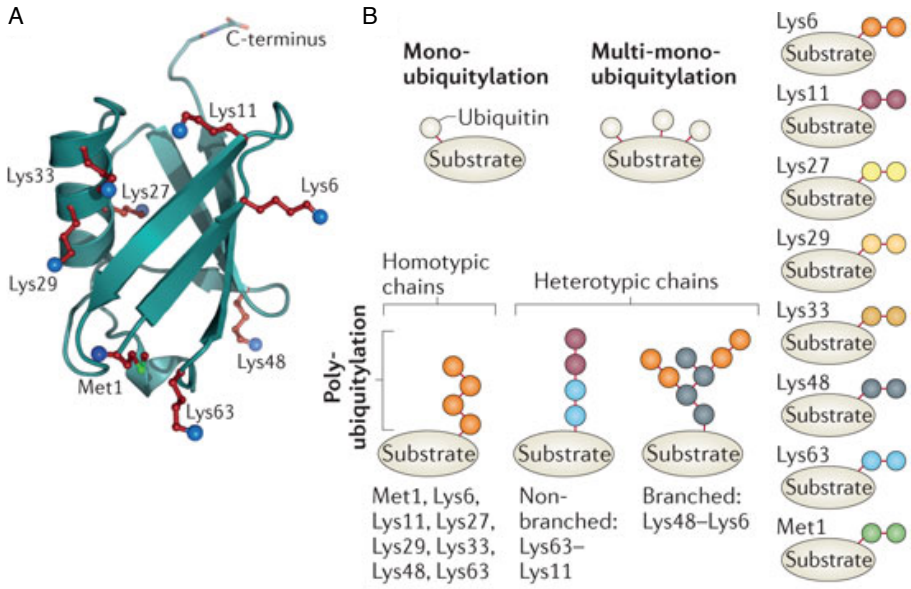


**Figure 2. Ub chains** (adapted from Kulathu, Nat. Rev. Mol. Cell Biol., 2012). (A) The Ubiquitin molecule. The N-terminus and all the lysine residues involved in chains formation are highlighted. (B) Schematic representation of all different types of substrate ubiquitination such as mono, multi-monoubiquitination and homogeneous or mixed in the case of Ub chains.

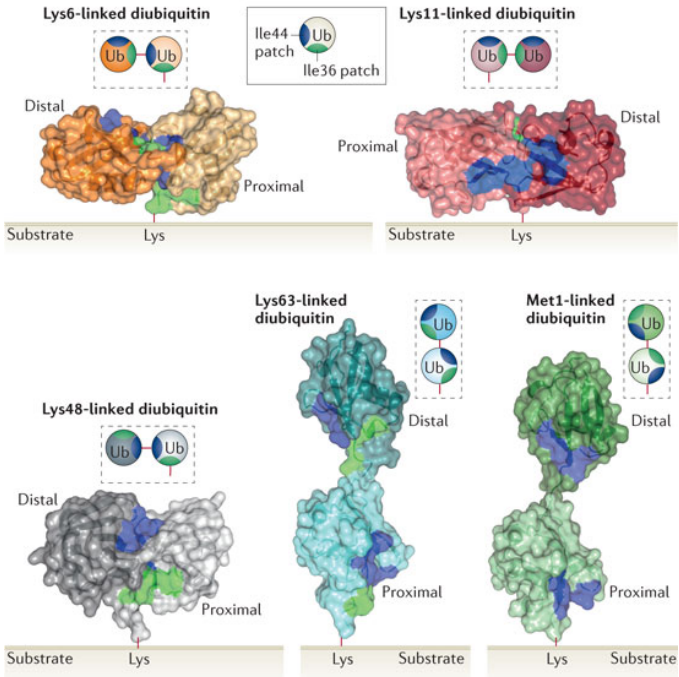


**Figure 3. Structures of some Ub chains with different linkages** (adapted from Kulathu, Nat. Rev. Mol. Cell Biol., 2012). Depending on the type of linkages, every Ub chains adopt different tridimensional structures that determine different functions. Ub chains with K48-, K6- and K11-linkage display a compact conformation instead of K63- and N-terminus adopt an open conformation. The hydrophobic patch centered on Ile44 is represented in blue and the interaction patch centered on Ile36 is represented in green.

### 1.2 Ubiquitin binding domain (UBD)

As stated before, each chain may assume distinct structure and function in the cell and this selective function is mediated by Ub receptors, proteins that contain Ub binding domains (UBDs) (Husnjak and Dikic, 2012).

UBDs are small domains (20-150 aa) able to bind non-covalently Ub (Hicke et al., 2005). A large amount of proteins (around 150 by a rough estimation) possess UBDs through which they can interact with ubiquitinated substrates. The abundance and localization of ubiquitin receptors is crucial for the generation of an ubiquitin network where the ability of ubiquitin to act as an interaction module works as a signalling cascade.

The binding affinity of single UBD is very low, with a dissociation constant ($K_D$) around 10-500 μM (Dikic et al., 2009); this is advantageous for the cell because it creates a dynamic network allowing rapid assembly and disassembly of the complexes.

The most common surface of interaction between UBDs and Ub involves the solvent-exposed hydrophobic patch of Ub, which includes Leu8, Ile44 and Val70. However, other UBDs interact with different residues of Ub, determining a large amount of structural folds and unique binding modes (Dikic et al., 2009). Few examples are: the ZnF_A20 of Rabex-5 binds Ub to a polar surface centered on Asp58 (Penengo et al., 2006), the ZnF UBP of DUB isopeptidase T interacts with the C-terminal Gly of Ub (Reyes-Turcu et al., 2006), the UEV (Ubc E2 variant) domain contacts a hydrophilic site centered on Gln62 of Ub (Sundquist et al., 2004). In addition, single UBDs can have multiple ubiquitin binding surfaces. For example DUIM, which possess one α-helix UIM domain, is able to interact simultaneously with two Ub molecules using opposite surface on the same α-helix (Hirano et al., 2006).

Binding to UBDs can modify Ub chains topology generating a range of inter-moiety arrangements as demonstrated for Ub chains Lys48-linked, Lys63-linked and N-terminus-linked (Dikic et al., 2009). For example, Lys63-linked diUb is usually present in

open conformation with the linker region that connects the two Ub moieties very flexible. However, it assumes an extended conformation when in complex with the UBD of the endosome-associated Ub isopeptidase AMSH (associated molecule with the SH3 domain of STAM) to facilitate the cleavage of the isopeptide bond (Sato et al., 2008). By contrast, Lys63-linked diUb can assume a more compact conformation when it interacts with specific antibodies able to recognize it (Newton et al., 2008).

The number of identified UBDs are constantly growing and now includes at least twenty domains: UBA, UIM, MIU, DUIM, CUE, GAT, NZF, ZnF_A20, UBP, UBZ, Ubc, UEV, UBM, GLUE, Jab1/MPN, VHS, PRU, SH3, UBAN and PFU (**Table 1**).

| UBD abbreviations | Structure | Ubiquitin surface | Type of ubiquitin binding | Proteins with specific UBDs |
|---|---|---|---|---|
| UBA | Three-helix bundle | Ile44 | mUb<br>polyUb ( > K48)<br>UBL | PLIC1/2, HHR23A/B, Ddi1, p62/SQSTM1, NBR1, Cbl-b, USP5, UBC1, HERC2 |
| CUE | Three-helix bundle | Ile44 | mUb | Cue2 (monomeric), Vps9 (dimeric) |
| UIM | Single α-helix, often present in tandem | Ile44 | mUb<br>pUb (K48, K63)<br>UBL | S5a, Vps27, USP28, ataxin-3, EPS15, STAM, RAP80 |
| MIU/IUIM | Single α-helix[b] | Ile44 | mUb | Rabex-5 |
| DUIM | Single α-helix, binds two ubiquitin molecules[c] | Ile44 | mUb | Hrs |
| VHS | Superhelix of eight α-helices | Ile44 | mUb | STAM, Hrs |
| GAT | Three-helix bundle | Ile44 | mUb | GGA3, TOM1 |
| NZF | Zinc finger, four β-strands | Ile44 | mUb<br>pUb (K63) [d] | Npl4, VPS36, TAB2, TAB3, HOIP, HOIL-1L |
| ZnF A20 | Zinc finger | Asp58[e] | mUb (Rabex-5)<br>Lys63 (A20) | A20, Rabex-5 |
| ZnF UBP | Zinc finger, a globular fold with a deep cleft and pocket to accommodate ubiquitin's tail | Leu8, Ile36, tail | pUb (unanchored) | USP5, HDAC6, BRAP2 |
| UBZ | Zinc finger, ββα -fold | Ile44 | mUb<br>pUb | Polymerase η , polymeraseκ, FAN1, NDP52, TAX1BP1, WRNIP1 |
| UBC | β-sheet | Ile44 | mUb | UbcH5C |
| UEV | αβ -sequence, lacks E2 catalytic Cys | Ile44 | mUb | VPS23, TSG101 |
| UBM | Helix turn helix, helices separated by an invariant Leu-Pro motif | Leu8 | mUb | Polymerase ι , polymerase Rev1 |
| GLUE | Split-pleckstrin homology domain | Ile44 | mUb | EAP45 |
| PRU | Pleckstrin homology domain, three loops bind ubiquitin | Ile44 | mUb (Ile44)<br>pUb (K48 linker)<br>UBL | Rpn13 |
| Jab1/MPN | Inactive variant of Jab1/MPN domain lacking key residues in the motif | Ile44 | mUb | Prp8p |
| PFU | Four β-strands and two αhelices | Ile44 | mUb<br>pUb | Doa1, PLAA |
| SH3, variant | β-barrel fold, hydrophobic groove binds ubiquitin | Ile44 | mUb | Sla1, CIN85, amphiphysin |
| UBAN | Parallel coiled-coil dimer | Ile44<br>Phe4<br>linker | Met1-diUb | NEMO, optineurin, ABIN1-3 |
| WD40 repeat β-propeller | Top surface of WD40 repeaβ-propeller | Ile44 | mUb | Doa1/UFD3 |

**Table 1: Summary of ubiquitin binding domains and their main characteristics** (adapted from Husnjak and Dikic, Annu. Rev. Biochem. 2012).

Most UBDs bind the hydrophobic patch of Ub through an α-helical-based structure. Some UBDs such as ubiquitin-interacting motif (UIM), inverted UIM (MIU), double-sided ubiquitin-interacting motif (DUIM) are composed by a single α-helix, others such as ubiquitin-associated domain (UBA) and CUE domain bind Ub through two discontinuous α-helices(Hurley et al., 2006)(**Figure 4A**).

The second largest family of UBDs is represented by ZnFs and this family is composed by NZF domain, A20_ZnF domain, ZnF UBP and UBZ domains. They use a single zinc-binding site that coordinates a zinc atom (**Figure 4B**).

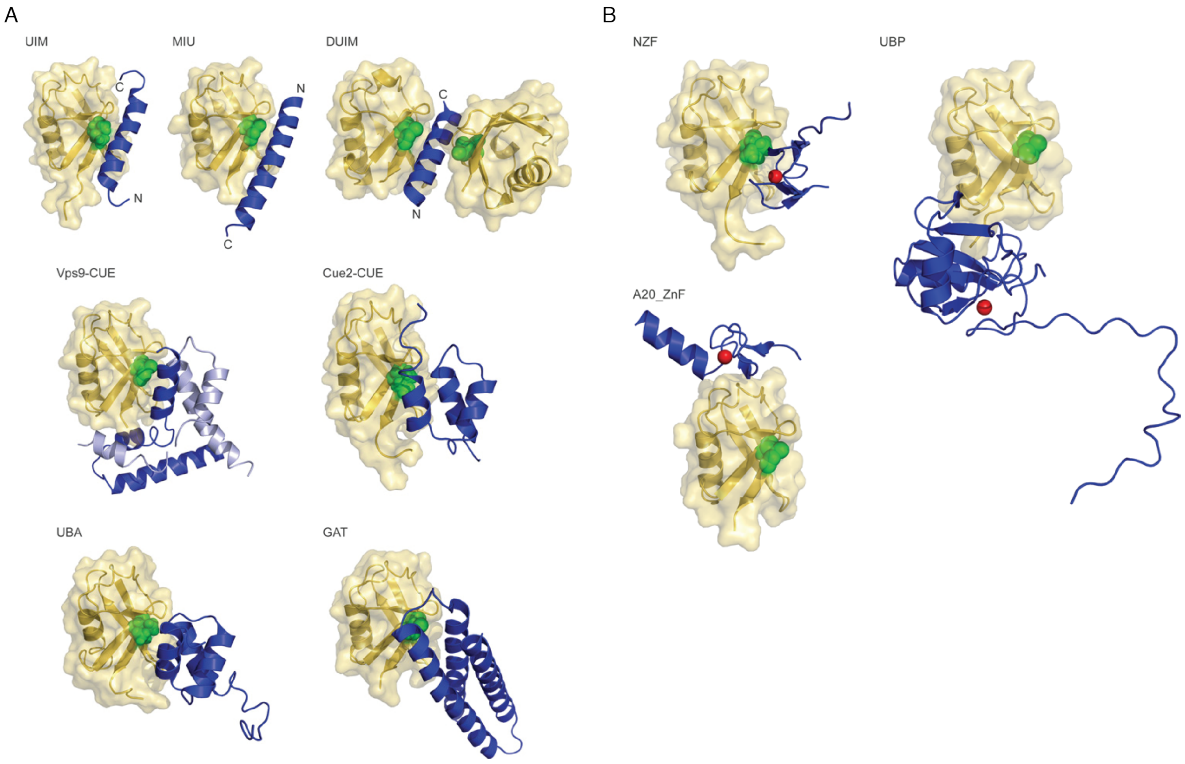


**Figure 4. Structures of different ubiquitin binding domains** (adapted from Hurley, Biochem J. 2006). (A) Representation of some UBDs characterized by the α-helix. Ub molecule is represented in yellow and the helical domain in blue. The canonical hydrophobic patch involved in the binding is depicted as green spheres. (B) Representation of three UBDs, shown in blue, those possess the ZnF domain where the zinc ions are highlighted as red sphere. Ub is depicted in yellow and the canonical hydrophobic patch in green spheres to show that they recognize different surface on Ub.

These zinc-finger-based structures possess more diversity in recognition and affinity than the α-helix domains because they recognize different surfaces on the Ub. An example is

represented by the ZnF4 domain which is able to bind three separate Ub molecules using unique interaction interface (Bosanac et al., 2010).

Many proteins carry more than one UBD (tandem UBDs), either of the same or of different structure, causing specific network (Husnjak and Dikic, 2012) (**Figure 5**). An example of tandem UBDs is Rabex-5 that is composed by the N-terminal ZnF_A20 domain fused to the MIU domain, a zinc finger and α-helix domains respectively (Lee et al., 2006a; Penengo et al., 2006).

Proteins containing tandem UBDs can interact each other through their UBDs forming multi-protein complexes. This process can also determine an increase in the Ub binding affinity due to the avidity effect, promoting the Ub:UBD interaction. Many endocytic proteins possess multiple UIMs such as epidermal growth factor receptor protein substrate 15 (Eps15) and Eps15R that have double-sided UIMs. UIMs bind to mono-Ub with low affinity however multiple UIMs cooperate to increase the affinity and could bind multiple monoubiquitinated proteins (Hofmann and Falquet, 2001).

Tandem UBDs can also define the interaction with Ub chains of specific linkage, such as RAP80 (receptor associated protein 80) that specifically binds Lys63-linked but not Lys48-linked Ub chains through its two UIMs (Sims and Cohen, 2009).

In the case of the transcriptional activator Met4, the two tandem UBDs, UIM and UIM-like domains (Tyrrell et al., 2010) exert a different function regulating the enzyme activity. Preventing its proteasomal degradation, these two UBDs interact with the Lys48-linked Ub chains blocking the interaction of Met4 with the promoter (Kaiser et al., 2000).

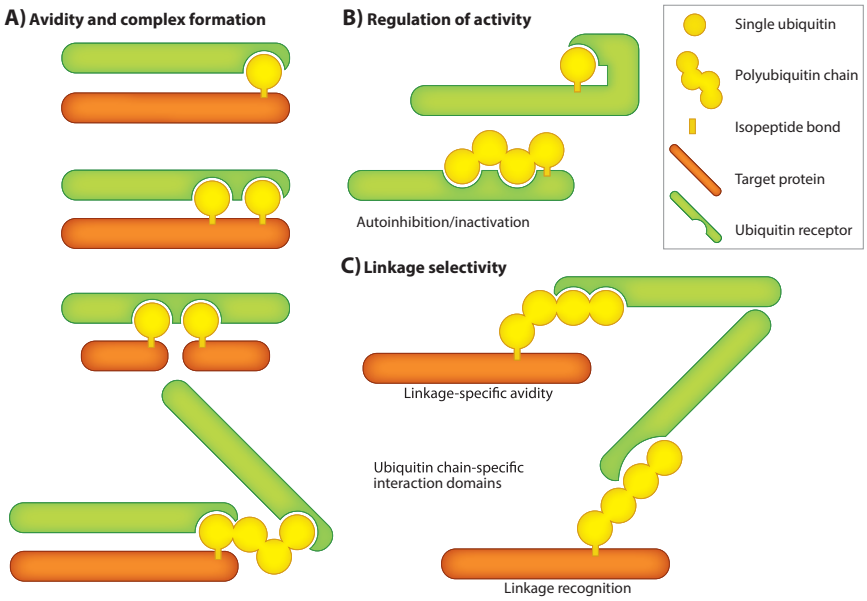


**Figure 5. Models of possible role of tandem UBDs** (adapted from Husnjak and Dikic, Ann. Rev. Biochem. 2012). (A) Tandem UBDs can help the formation of multi-protein complex causing an increase in the binding affinity to an avidity effect. (B) Binding with specific Ub chains or mono-Ub can positively or negatively regulate the protein activity. (C) Tandem UBDs can discriminate between different Ub chains conferring linkage specificity of the protein.

## 2. The Ubiquitin Machinery

The ubiquitin pathway is comprised of many enzymes and regulators that process, activate, attach and detach ubiquitin to substrates. In the ubiquitination cascade three different enzymes are involved: Ub-activating enzymes (E1s), Ub-conjugating enzymes (E2s) and Ub-ligases (E3s). The cascade mechanism allows the prompt modification of a large number of diverse substrates, in many distinct ways (Scheffner et al., 1995). For covalent conjugation to occur, the ubiquitin C-terminus has to be activated. This happens through the action of an activating enzyme (E1), that forms a thioester with the carboxyl group of the C-terminal Ub residue, Gly76. Subsequently, this transient thioester is transferred to the cysteine of a conjugating enzyme (E2). This second enzyme carries the activated Ub to

a third enzyme, the ubiquitin ligase (E3), which catalyzes the transfer of Ub to the lysine residue of the substrate, generating a stable isopeptide bond (**Figure 6**).

In the ubiquitin pathway two E1 enzymes are involved in the activation and transfer of Ub to a limited number of E2s, which interact with several E3s determining an increase in specificity along the cascade. Indeed each E3 recognizes and ubiquitinates a panel of substrates with high specificity (Hershko and Ciechanover, 1998).

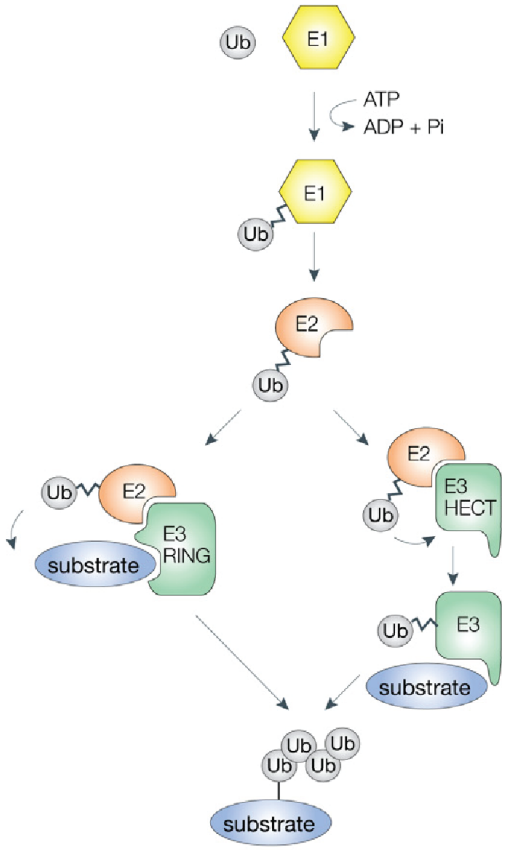


**Figure 6. Schematic representation of the ubiquitin pathway** (adapted from Woelk, Cell Div. 2007). Substrate ubiquitination occurs via the stepwise transfer of Ub moieties from Ub-activating enzyme (E1), to an Ub-conjugating enzyme (E2) and finally to the protein substrate in a ligation reaction catalyzed by the E3 ligase. The two major classes of E3 ligases are depicted.

### 2.1 Ub-activating enzyme (E1)

In mammals there are two E1 (UBA1 and UBA6) involved in the ubiquitin activation (Pelzer et al., 2007). Structural studies have shown that E1s contain at least three distinct regions involved in the biochemical activities of the enzyme: two pseudosymmetric adenylation domains that are involved in ATP-$Mg^{2+}$ and Ub binding, a catalytic cysteine

domain (Cys domain) that is involved in the E1~Ub thioester bond formation and a Ub fold domain (UFD) important for the E2 interaction (Lee and Schindelin, 2008).

The enzyme undergoes remarkable conformational changes during the process of activation. The first step of the reaction is guided by the binding of ATP- $Mg^{2+}$ and Ub in the adenylation domain that adenylates the C-terminal glycine of Ub. Once the Ub is adenylated the E1 releases the pyrophosphate, generating an 130° rotation of the Cys domain. Cys domain rotation facilitates the nucleophilic attack and the transfer of Ub from the adenylation site to the catalytic site with the formation of a thioester bond. Once the thioester bond is formed, the AMP is released and another conformational change occurs. This favours a second cycle of adenylation starting from the binding of ATP- $Mg^{2+}$-Ub (Olsen and Lima, 2013) (**Figure 7**). A fully loaded E1 carries two Ub molecules, one as thioester and the second as adenylate. The thiol-linked Ub is then transferred from the E1 to the second enzyme of the ubiquitination cascade, the E2.

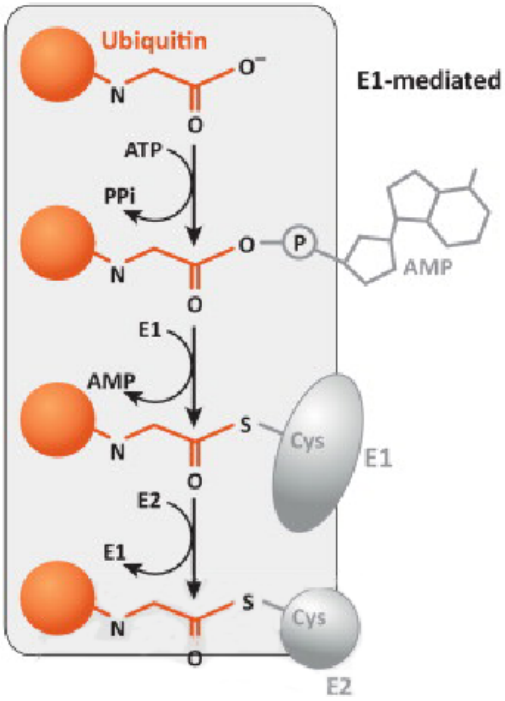


**Figure 7. Schematic representation of the first step of ubiquitination** (adapted from Kleiger, Trends Cell Biol. 2014). First step of the process is the activation of Ub through its adenylation mediated by the E1 using a molecule of ATP. Second step is the formation of the thiolester bond between Ub and the catalytic cysteine of the E1. Next, Ub is transferred from the E1 to the E2.

### 2.2 Ub-conjugating enzyme (E2)

E2s are functionally defined for their capability to accept the Ub thioester from the E1 ternary complex and to transfer ubiquitin to either an E3 or a substrate (**Figure 8**). There are 11 E2s in *Saccharomyces cerevisiae* and more than 40 in higher organisms (Metzger et al., 2012). This class of enzymes carries out distinct biological functions and their specificity of function is mainly related to their interactions with distinct E3s (Pickart, 2001).

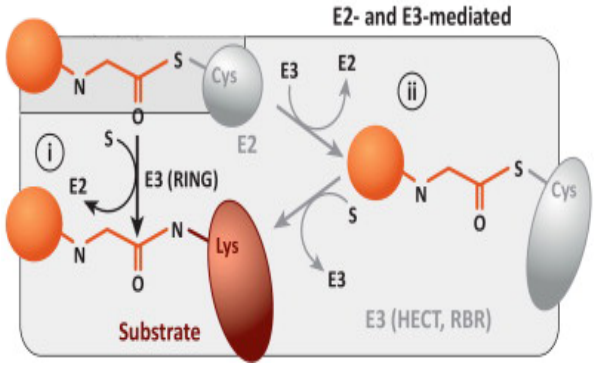


**Figure 8. Functions of E2** (adapted from Kleiger, Trends Cell Biol. 2014). E2 enzymes interacting with RING/RING-like E3s can directly transfer the Ub to the substrate as in (i). E2s that interact with E3s containing the HECT or RBR domain, as in (ii), require an additional *trans*-thioesterification step.

All E2s have a common conserved UBC core domain of ~150 residues important for the E1 recognition, for the binding and transfer of the activated Ub (Pickart, 2001). Depending on the domains that they possess, E2s can be divided in four major classes: Class I (e.g.Ube2D, UbcH7, Ubc13) possess only the UBC core domain, Class II (e.g. Ube2k) and Class III (e.g. UbcH6 and Ube2e2) possess a C-terminal and N-terminal extension from the UBC core domain respectively, Class IV possess both extensions. These amino acidic sequences contribute for the substrate specificity, as they can modulate both E3 interactions and cellular localization (Christensen et al., 2007).

It is known that the E2 binding to E1 and to E3 is mutually exclusive, as their binding sites on the E2 are partially overlapping. Thus, the E2-E3 interaction happens only when the E2 is disengaged from the E1. In addition, E1 preferentially associates with free E2s while E3 preferentially associates with Ub-thioester E2s, thus ensuring sequentiality in the cascade (Eletr et al., 2005). A recent analysis based on structural and computational

approach revealed that on the interaction surface there are structurally conserved residues among E2 proteins which appear to be essential for all E2−E3 interactions despite E3 characteristics (RING or HECT type E3s), while a particular loop in the structure likely plays important roles in E3 selectivity (Kar et al., 2012).

A specific HPN motif surrounding the active site of the E2 has a crucial role in isopeptide bond formation, positioning the incoming lysine and generating an environment that lowers the pKa of the lysine to promote the nucleophilic attack (Bernier-Villamor et al., 2002). In different E2s (e.g. Ube2D2) the conserved asparagine of the HPN motif can form an oxyanion intermediate interacting with the last glycine at the C terminus of Ub (Wu et al., 2003). During the nucleophilic attack of the thioester bond, the oxyanion intermediate facilitates the Ub transfer (Sakata et al., 2010) (**Figure 9**). In addition, the asparagine side chain has a structural role and it is required to maintain the correct tridimensional rearrangement of the active site loop (Berndsen et al., 2013).

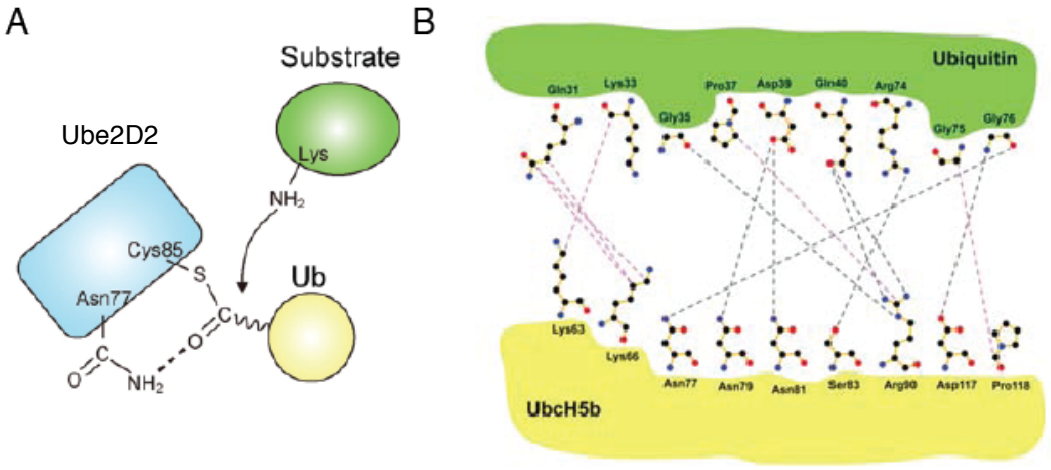


**Figure 9. Role of the Asparagine in HPN motif** (adapted from Sakata, Structure. 2010). (A) Model of oxyanion intermediate for nucleophilic attack on E2~Ub. (B) Schematic representation of the binding interface between Ub and E2 (e.g. Ube2D3) around the catalytic site. Black dashed lines represent hydrogen bonds and pink dashed lines are hydrophobic interactions.

Some members of E2 families, i.e. Ube2D3, have a non-covalent Ub-binding domain on the "back side" of the E2, centered on Ser22. Through this surface they interact

with Ub via the canonical hydrophobic patch of Ub composed by L8, I44 and V70 (**Figure 10A**). The Ub conjugated to the active site of the E2 cannot bind the backside UBD present in the same E2 molecule. Thus, each E2 can bind two different Ub molecules simultaneously: one non-covalently to the UBD and the other covalently linked to the catalytic cysteine (**Figure 10B**). It was initially proposed that this UBD is important for the processivity in Ub chain formation, as it creates E2~Ub self-associated oligomers that increase the local concentration of E2~Ub around the E3 (Brzovic et al., 2006). Indeed, the S22R mutation, which disrupts the interaction on the "back side", impaired the ability of E2s to form poly-Ub chains but not to monoubiquitinate (Brzovic et al., 2006; Buetow et al., 2015). More recently, it was proposed that the Ub, bound to the "back side" might have a positive allosteric activity on the E3-mediated Ub transfer. Indeed, it appears to stabilize the E3-E2~Ub complex in a catalytically favorable conformation (Buetow et al., 2015).

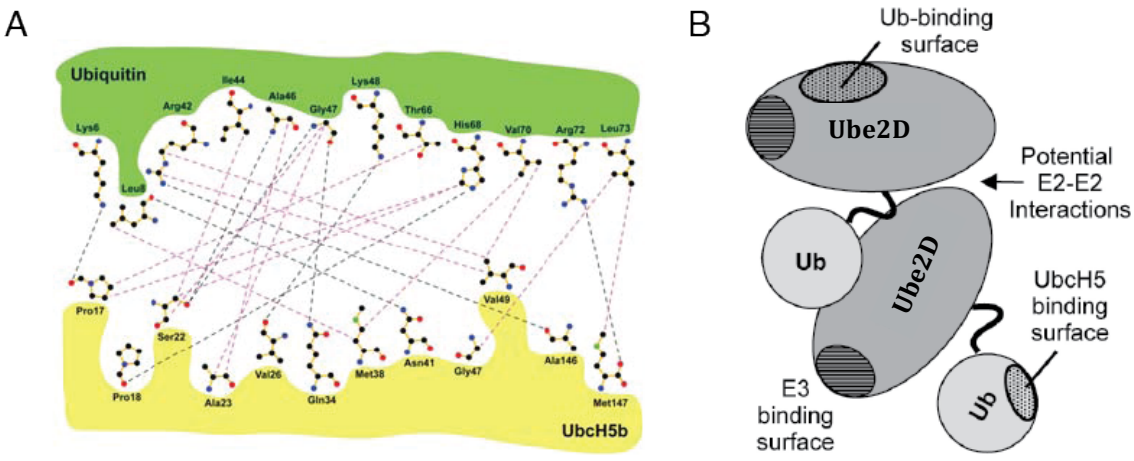


**Figure 10. UBD in the E2.** (A) (adapted from Sakata, Structure. 2010) Schematic representation of the non-covalent interaction between UBD of the E2 (e.g. Ube2D2) and Ub where residue S22 of E2 has a critical role. Black dashed lines represent hydrogen bonds and pink dashed lines are hydrophobic interactions. (B) (adapted from Brzovic, Mol Cell. 2006) Cartoon depicting the self-assembly of activated E2~Ub through the non-covalent interaction UBD:Ub that is important for the processivity. Each E2 interacts with two different Ub molecules.

### 2.3 Ub-ligase enzyme (E3)

The last enzymes of the ubiquitination machinery are the Ub-ligase E3s that in humans are estimated to be more than 600.

According to their properties, E3 ligases could be divided in three major classes: HECT, RING and RING-in-between-RING (RBR) domain-containing E3s. E3 ligases containing the HECT (homologous to the E6AP carboxyl terminus) domain (Rotin and Kumar, 2009) form an obligate thioester intermediate via a catalytic cysteine and subsequently transfer the Ub to the lysine of the substrate (**Figure 11A**). The vast majority of E3 ligases belong to the group of Really Interesting New Gene (RING) and RING-related E3s – such as plant homeodomain (PHD) and members of the U-box family (Deshaies and Joazeiro, 2009).

These enzymes do not contain catalytic cysteines but simultaneously bind the E2~Ub and the substrate to allosterically activate the donor Ub carried by the E2 enzyme (Dou et al., 2012; Plechanovova et al., 2012) and subsequently transfer it to the substrates (Deshaies and Joazeiro, 2009)(**Figure 11B**). The last class of E3 ligases is represented by the RBR, defined as RING-HECT hybrid, because it possesses both a RING-type domain and an atypical RING domain (RING2) containing a catalytic cysteine (Metzger et al., 2012; Wenzel and Klevit, 2012) (**Figure 11C**).

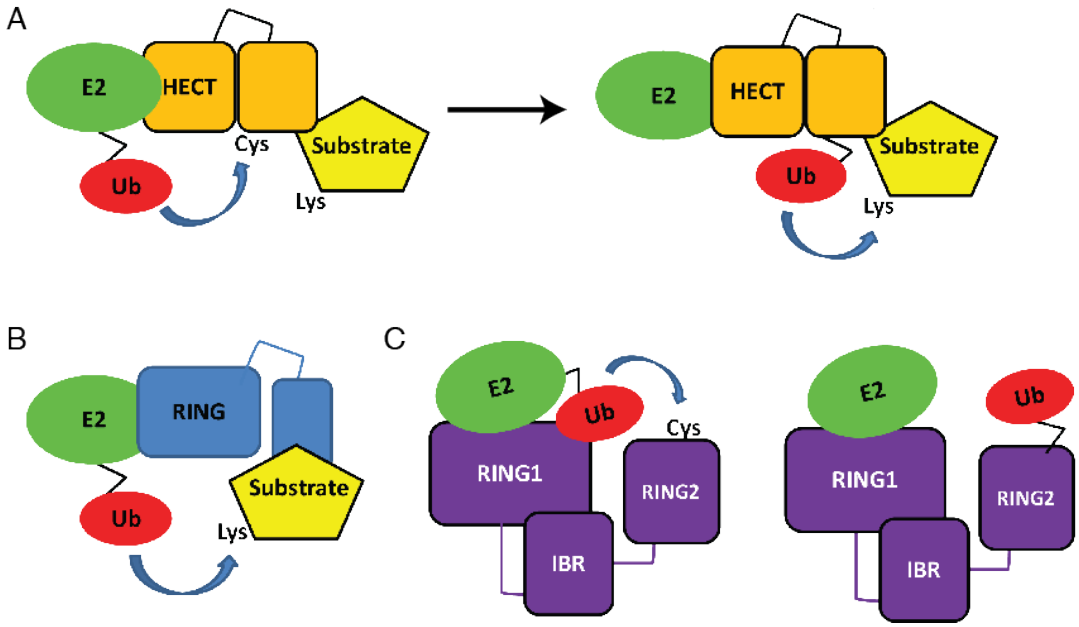


**Figure 11. Mechanisms of Ub transfer for different E3s** (adapted from Wenzel, BMC Biol. 2012). (A) E3 ligases containing the HECT domain bind the E2~Ub and the Ub is transferred to the catalytic cysteine forming a thioester intermediate. Next the E3s transfer Ub to the lysine of the substrate. (B) RING-E3 ligases act as scaffold facilitating the transfer of Ub from the E2~Ub to the lysine. (C) RBR domains act as RING-HECT hybrids. The E2~Ub binds the RING1 domain and Ub is transferred to the catalytic cysteine of the RING2 domain. Next Ub is transferred to the lysine of the substrate.

E3 ligases confer specificity in the ubiquitination reaction since they recognize specific target substrates and determine - alone or in combination with their cognate E2 - whether the substrate will be mono- or polyubiquitinated and the type of linkages that are formed (Christensen et al., 2007).

Little is known about how these enzymes can determine the linkage specificity during Ub-chains elongation. With few remarkable exceptions (Jin et al., 2008; Petroski and Deshaies, 2005; Wickliffe et al.) even if various models have been proposed (Hochstrasser, 2006) the mechanisms of Ub-chain assembly have not been clarified yet (**Figure 12**).

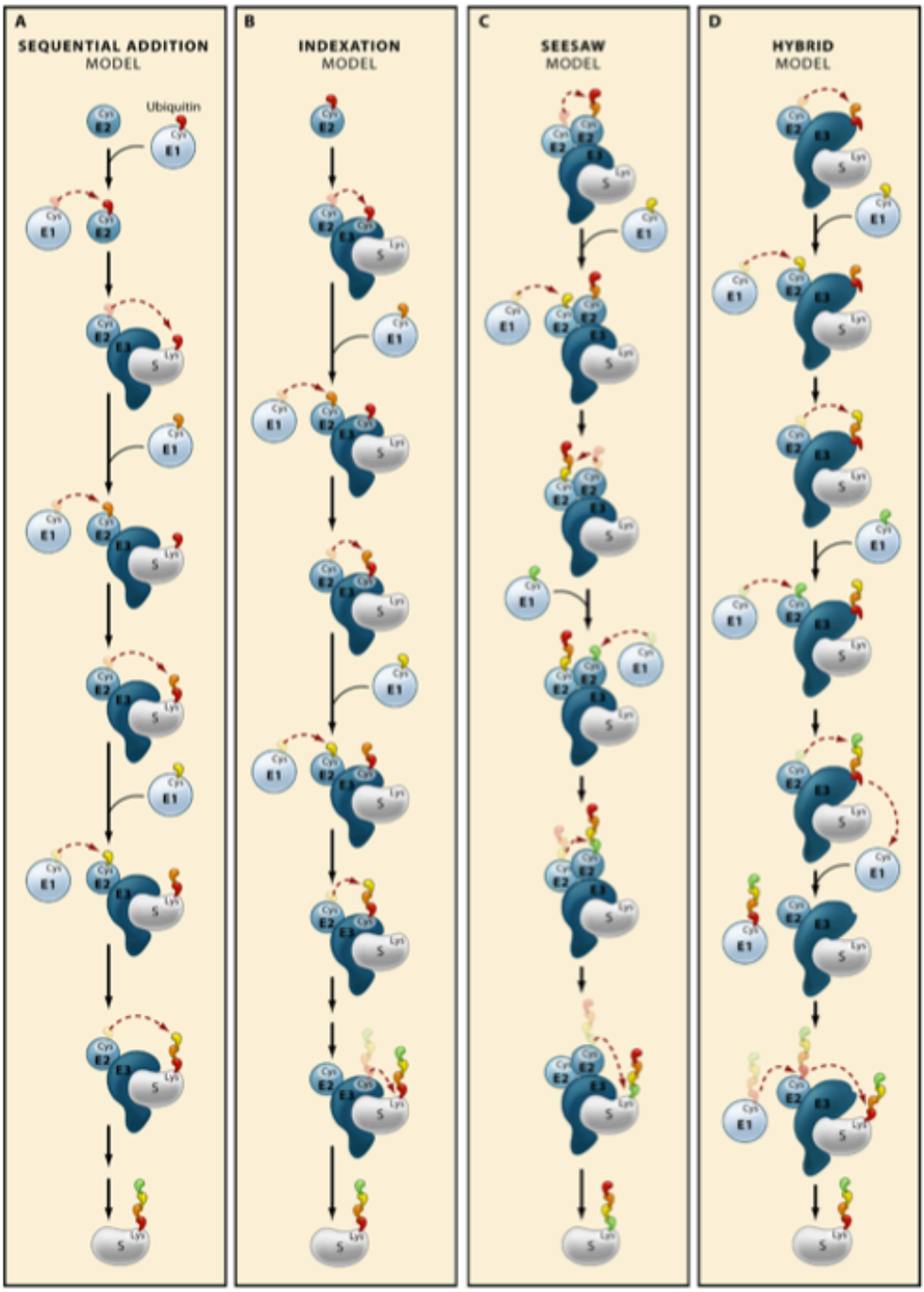


**Figure 12. Models for synthesis of polyubiquitin chain** (adapted from Hochstrasser, Cell 2005). (A) Sequential addition model in which a RING E3 (here depicted) attaches one Ub at a time, starting from the lysine of the substrate and then to the specific lysine on the distal Ub of the growing chain. (B) Indexation model in which the entire Ub chain is first built on the catalytic activity of the HECT E3 and then transferred to the lysine of the substrate. (C) Seesaw model shows a possible mechanism in which a pair of E2s (homo- or heterodimer) can built Ub chain prior the transfer to the substrate. The growing Ub chain passes back and forth between the two E2s. (D) In the hybrid model Ub chain is formed on the catalytic cysteine of the E3 but an additional step is necessary. The free end of the Ub chain has to be activated by the E1 then transferred to the cysteine of the E2 before the final transfer to the substrate.

### 2.3.1. HECT

The HECT E3s are enzymes characterized by the presence of a well-conserved catalytic domain, the HECT domain, a 350 residues module first characterized in the human ubiquitin protein ligase E6-associated protein E6AP (Huibregtse et al., 1995).

In mammals there are ~30 HECT domain E3s and they are divided in subfamilies, depicted in **Figure 13**, according to their protein-protein interaction domain architecture: the HERCs contain RCC1 (regulator of chromosome condensation 1)-like domains (RLDs); the Nedd4 family ligases contain a C2 and several WW domains, and HECT E3s that neither contain C2, RLDs nor WW domains (Rotin and Kumar, 2009; Scheffner and Kumar, 2014). They have different roles and functions in protein trafficking, immune response and different signaling pathways. Their deregulation is associated with several human diseases, including cancer (Rotin and Kumar, 2009; Scheffner and Kumar, 2014).

HECT-domain E3 ligases catalyze two distinct reactions: a transthiolation reaction, in which ubiquitin is transferred from the E2 to an active site cysteine in the HECT domain, and a subsequent attack on the HECT~Ub thioester by a substrate lysine (Huibregtse et al., 1995) (**Figure 11A**). For both reactions, the HECT domain is necessary and sufficient.

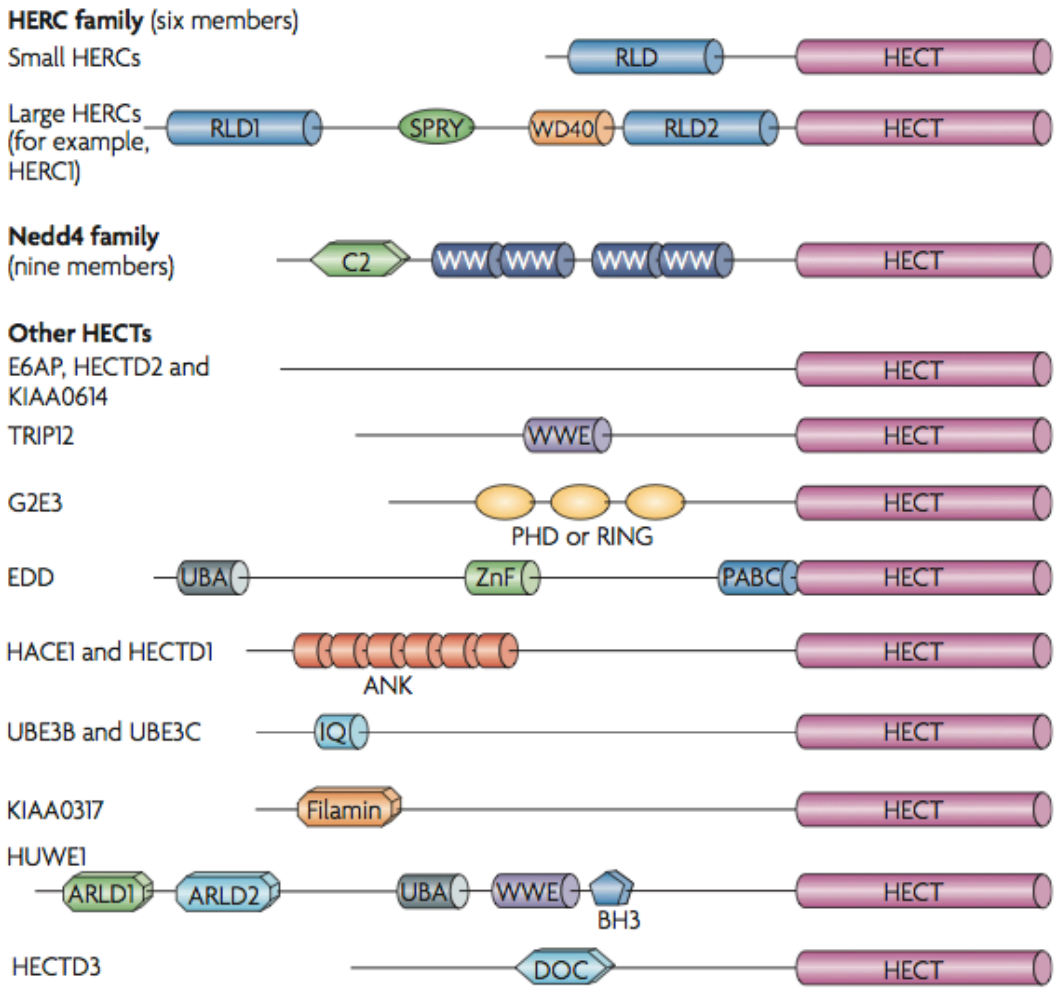


**Figure 13: Domain architecture of mammalian HECT E3s** (adapted from Rotin and Kumar, Nat. Rev. Mol. Cell Biol. 2009). In all cases the HECT domain is present at the C-terminus. The HERC family members can be divided in two group: the small HERCs contain only one regulator of chromosome condensation 1 (RCC1)-like domains (RLDs), the large HERCs contain more than one RLD and additional domains. Nedd4 family members shared common domain architecture, composed by an amino-terminal C2 domain and two to four WW domains. The other HECT family contains proteins composed by various domains (as shown). PABC, PABP (Poly (A)-binding protein) C terminus; ANK, ankyrin; UBA, ubiquitin-associated; ZnF, zinc finger. Not all these proteins have an E3 ligase activity, even if they possess the HECT domain, as it was proposed for G2E3 (Brooks et al., 2008).

From the structural point of view, the HECT domain is a bilobal structure composed by an N-terminal region (N-lobe) important for the E2 binding and a C-terminal region (C-lobe) that contains the conserved catalytic cysteine involved in thioester formation (Scheffner et al., 1995). The C- and N- lobes are connected by a hinge loop whose flexibility determines

the various conformations observed in the different solved structures (Huang et al., 1999) (**Figure 14**).

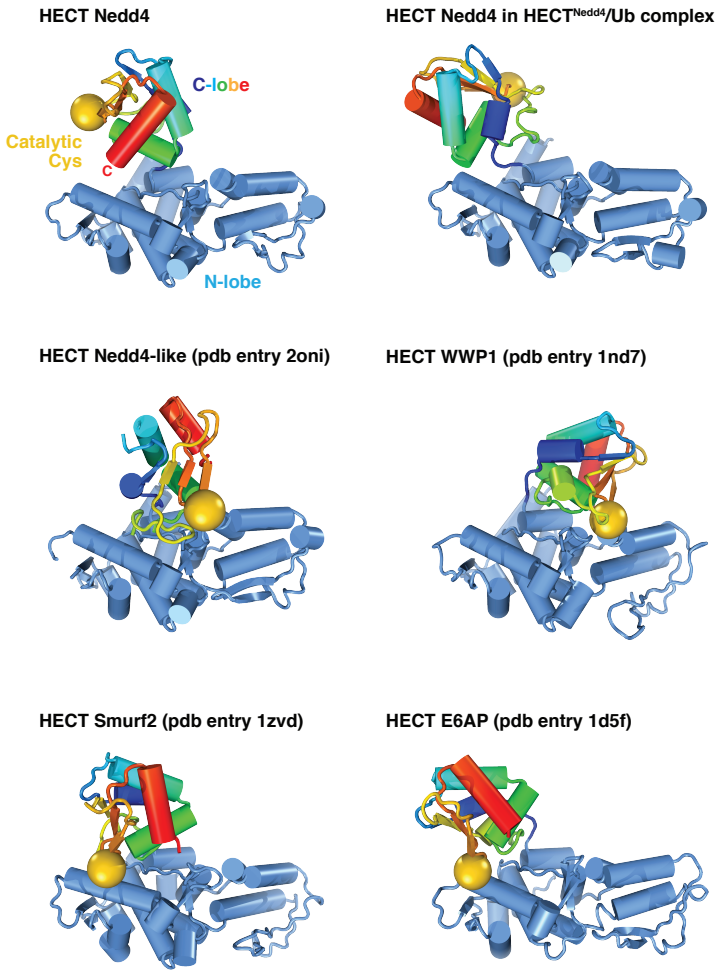


**Figure 14. Different orientation of the C-lobe in the structures of HECT domains** (adapted from Maspero E., EMBO Rep., 2011). Structures of the different HECT domains show that the C-lobe may assume different orientation respect the N-lobe. N-lobes are in light blue, while C-lobes are in a colour gradient, ranging from blue (residue linked to the N-lobe) to red (C-terminus of the HECT domains). The position of the catalytic cysteine is highlighted as yellow ball, representing the sulphur atom.

The flexibility of the hinge loop has a critical role in the ligase activity. It is required to bring in close proximity the cysteine residues of the E2 and the E3 during Ub transfer and for the nucleophilic attack of the target lysine to the HECT~Ub (Kamadurai et al., 2013; Kamadurai et al., 2009; Verdecia et al., 2003) (**Figure 15**).

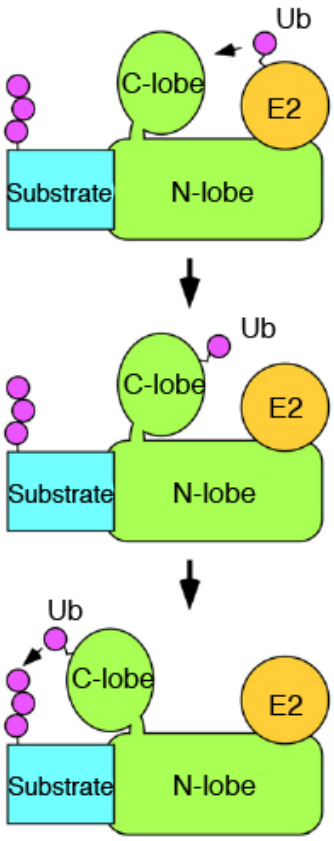


**Figure 15. Model of the catalytic activity of the HECT domain** (adapted from Kipreos E., WormBook 2005). The mechanism of the Ub-conjugation to the substrate by the HECT domain is shown. The E2~Ub binds the N-lobe of the HECT domain and transferred Ub to the catalytic cysteine of the C-lobe. The C-lobe rotates on the flexible hinge loop and catalyzes the transfer of Ub to the lysine of the substrate.

E3 ligases containing the HECT domain possess a wide range of linkage specificity: yeast Rsp5 and human Nedd4 synthesize Lys63-chains (Kim and Huibregtse, 2009; Maspero et al., 2011), E6AP assembles Lys48 and KIAA10/UBE3C promotes chains formation with Lys29 and Lys48 linkages (Wang and Pickart, 2005). The apoptosis-resistant E3 ubiquitin ligase (AREL1) is instead able to synthesize predominantly atypical Lys33-linked chains with a little percentage of Lys11-chains (Michel et al., 2015). For HECT-E3 ligases the linkage specificity is an inherent property of the HECT domain itself and does not depend on the interacting E2. It was demonstrated that the last C-terminal 60 amino acids of the C-lobe contain the critical determinant for the linkage specificity (Kim and Huibregtse, 2009). Our lab has recently demonstrated that the partial substitution of the last four residues of the HECT domain of Nedd4-1 with residues of E6AP produced a partial changing in linkage specificity from Lys63 to Lys48-linked Ub chains (Maspero et al., 2013). The last three or four residues present in the C-terminal part of the HECT domain

are important for the chain specificity, however other determinants present in the C-lobe might participate.

### 2.3.2. RING

The mammalian genome encodes for more than 600 potential RING finger E3s (Deshaies and Joazeiro, 2009). They regulate crucial cellular functions such as cell cycle, DNA repair, cell signaling and responses to hypoxia (Deshaies and Joazeiro, 2009).

In these enzymes, the catalytically critical domain is the RING. Thanks to the coordination of two structural $Zn^{2+}$ ions through eight Cys and His residues, the RING domain assumes a globular conformation similar to a cross brace structure (Petroski and Deshaies, 2005). The RING E3 has a dual role in substrate ubiquitination. First, it acts as a scaffold between the E2~Ub and the substrate and brings them together in close proximity (**Figure 11B**). Second, it induces conformational changes in the complex that allosterically activates the E2~Ub and correctly orients the thioester bond. Structural studies in which E2~Ub loaded form is captured in complex with RING domain E3, RNF4 (Plechanovova et al., 2012) or BIRC7 (Dou et al., 2012) show that the RING domain contacts an hydrophobic patch on the loaded ubiquitin. This contact immobilizes the C-terminus of the ubiquitin moiety in a structurally conserved groove in the E2, favoring a conformation that facilitates the lysine attack of the substrate lysine to the thioester bond (Dou et al., 2012; Plechanovova et al., 2012). Members of RING ligases can work as monomers, dimers or multi-subunit complexes (**Figure 16**).

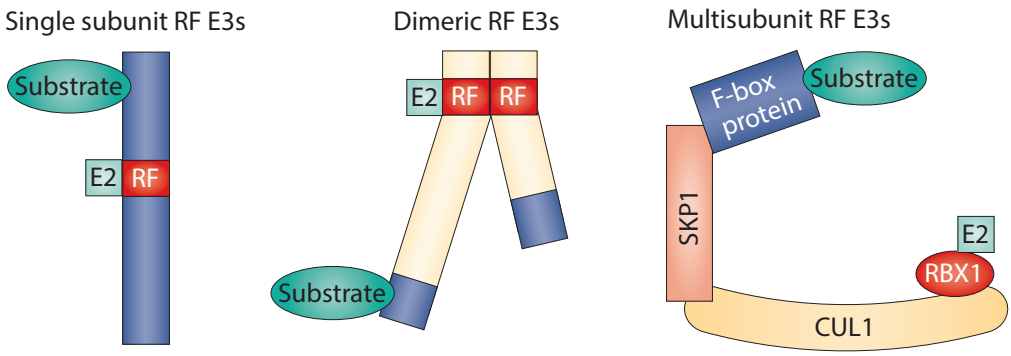


**Figure 16: RING E3s arrangement** (adapted from Lipkowitz, 2011). RING finger E3s can be single subunit in which the RING finger (RF) is surrounded by protein interacting motifs (shown in dark blue) or homodimers/heterodimers where the RING finger and/or surrounding regions serve as the site of dimerization. Finally they can exist as multisubunits E3s, which include a scaffold to assemble multiple proteins (as the Cullin protein) such as adaptor proteins and substrate targeting proteins.

Dimerization of RINGs often occurs through surrounding regions of the RING domain itself, forming homodimers or heterodimers (Lipkowitz and Weissman, 2011). One example of homodimers is represented by the Rnf8 E3 ubiquitin-protein ligase complex that plays a key role in DNA damage signaling (Nakada et al., 2012; Peuscher and Jacobs, 2011). In the case of heterodimers, generally one RING is not active and is involved in the stabilization of the active E2 binding RING domain. A well-studied example is given by E3 ligase Mdm2 that can function as homodimer or heterodimer with MDMX in regulating the tumor suppressor p53 (Linke et al., 2008). Another example is Brca1-Bard1, a RING finger complex where the two proteins are associated through the N-terminal regions. In this complex, only Brca1 has a role in E2 binding and E3 activity, instead Bard1 has only a structural role as it does not even contact the E2 (Brzovic et al., 2003).

Examples for multi-subunit RING ligases are the APC/C (anaphase-promoting complex/cyclosomes) and the Cullin family ligases (Culling-RING ligases, CRLs) (Hua and Vierstra, 2011). The APC/C has a critical role in the correct progression of the cell cycle. It is composed of several subunits including co-activators that confer substrate specificity and associate with the APC/C at specific stages of the cell cycle (Buschhorn

and Peters, 2006). Cell cycle regulation depends also on the action of another family of multi-subunit E3s, the SCF (Skp1-Cul1-F-box) (Lydeard et al., 2013). The SCF is a modular class of E3 ubiquitin ligases that use an interchangeable set of substrate adaptors termed F box proteins (Bai et al., 1996). The SCF complex is the prototypic Cullin E3 where a Cullin protein serves as a scaffold to assemble multiple proteins, including a small RING finger protein (RBX1), adaptor proteins (such as SKP1) (Feldman et al., 1997) and substrate targeting proteins (such as F-box) (Deshaies, 1999).

In addition to the classical RING domain other similar domains were demonstrated to have similar E3 properties. U-box proteins are an evolutionary variant of the RING domain, with similar folding and function but with a hydrophobic core in place of structural metal ions (Ohi et al., 2003).

The PHD domain represents another variant of the RING finger that includes a cysteine rather than a histidine in the fourth coordinating position and an invariant tryptophan before the seventh zinc-binding residue (Aravind and Koonin, 2000; Capili et al., 2001). Another variation of the theme is represented by proteins that contain a zinc finger (ZnF) domain. Among them, the ZnF_4 of the A20 protein (Bosanac et al., 2010) and the ZnF_A20 of Rabex-5, have been shown to possess catalytic activity (Lee et al., 2006a; Xu et al., 2010).

### 2.3.3. RING in between RING (RBR)

The RING-between-RING E3s family has only recently burst upon the scene as a mechanistically distinct class of E3s that shares features of both RING and HECT E3s, yet catalyze ubiquitination and auto-regulate their activity in a distinct manner. These E3 ligases contain RING and RING-like domains separated by a conserved sequence called in-between-RING (IBR) (Aguilera et al., 2000). The first RING domain is important to recruit the E2 and the second RING possesses the catalytic cysteine to form a thioester

intermediate in a HECT-like mechanism (Wenzel et al., 2011) (**Figure 11C**). The presence of the second RING, which acts as an HECT domain, determines the linkage specificity.

Members of this E3 family mediate diverse processes as regulation of post-translation modifications and protein stability, cellular and stress signaling, cell-cycle control, transcription, RNA metabolism and translation (Eisenhaber et al., 2007).

The most studied RBR enzymes are Parkin, whose mutations in the RBR domain are associated with Parkinson's disease (Shimura et al., 2012), and HOIP (HOIL-1 interacting protein) that is a component of the complex LUBAC (linear ubiquitin chain assembly complex). The LUBAC complex regulates the translation and activates the NF-kB signaling (Wenzel and Klevit, 2012). These proteins are regulated in different ways like intramolecular auto-inhibition or they are potential targets of protein kinase (Spratt et al., 2014). As example, phosphorylation of residue Ser65 on Parkin Ub-like (Ubl) domain, mediated by PINK1 (PTEN-induced putative kinase protein 1) (Kazlauskaite et al., 2014), has a critical role in Parkin activation (Kumar et al., 2015). This modification increases the affinity for p-Ser65-Ub by 20-fold determining an increase in Parkin activation (Kondapalli et al., 2012; Ordureau et al., 2015).

### 2.4. De-ubiquitinating enzymes (DUBs)

Ubiquitination is a reversible and dynamic process thanks to the action of deubiquitinating enzymes (DUBs). These enzymes specifically cleave the isopeptide bond between the ε-amino group of lysine side chains of target proteins and the C-terminal group of ubiquitin or disassemble Ub-chains. Human genome encodes for about 100 DUBs and more than 60% of these DUBs are not well characterized.

The critical role of DUBs is to maintain the pool of free-Ub by processing linear fusion products (UBC and UBB), ubiquitin precursors (Clague et al., 2012), Ub chains preformed or Lys48-Ub chains to rescue the Ub from proteasomal degradation (Hanpude

et al., 2015)(**Figure 17a, e, b**). They have an additional role in non-proteasomal degradation pathway by removing Ub signal and by editing the Ub chains and generating alternative Ub signaling (Chen and Sun, 2009)(**Figure 17c, f**). These proteins are composed of multi-domains as the catalytic DUB domain and the UBDs involved in the binding of ubiquitinated-substrate and/or subcellular localization domains (Hanpude et al., 2015).

DUBs can be classified into 5 distinct families: ubiquitin C-terminal hydrolases (UCH), the ubiquitin specific proteases (USP/UBPs), Otubain domain ubiquitin binding proteins (OTU), Machado-Joseph domain-containing (MJD) proteases, Jab1/Pab1/MPN domain-containing (JAMM) protease (Nijman et al., 2005). All DUBs families are cysteine proteases, except for protease containing the JAMM domain that are the only DUBs classified as Zn metalloproteases because required a $Zn^{2+}$ ion for their function (Nijman et al., 2005).

A large group of DUBs, i.e. most of USP family members, disassemble Ub chains independently of the linkage (Komander et al., 2009a). Other DUBs display specificity toward one or few linkages. Examples include Cezanne that specifically cleaves Lys11-linked Ub chains (Bremm et al., 2010) and OTUB1 that is specific for Lys48-linkages (Mevissen et al., 2013). A20 acts as DUB removing Lys63-linkage Ub chains from the substrate thanks to the N-terminal ovarian tumor (OTU) domain (Bosanac et al., 2010; Wertz et al., 2004).

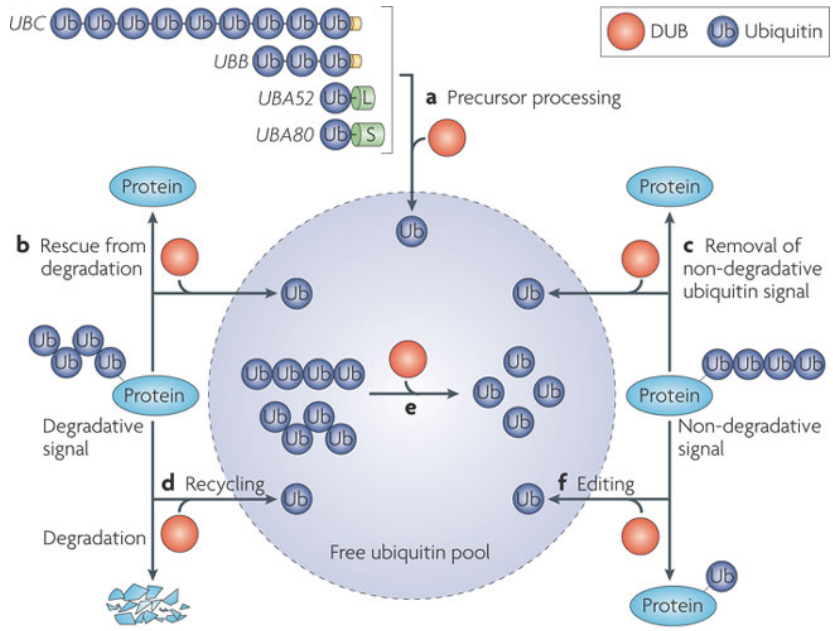


**Figure 17. General cellular role of DUBs** (adapted from Komander, Nat Rev Mol Cell Biol. 2009). (a) Ub is formed as a fused precursor protein consisting in multiple copies of Ub and DUBs which help in the formation of monomeric Ub. (b) Elimination of degradation signals from proteins by cleaving Ub chains. (c) DUBs can remove non-degradative Ub signal. (d) DUBs prevent Ub proteasome degradation with conjugated proteins. (e) Disassembling Ub chains to form monomeric Ub and increase the free Ub pool. (f) By editing Ub chains DUBs can generate other Ub signaling.

# 3. NEDD4

## 3.1 Domain description

The Nedd4 (neuronal precursor cell-expressed developmentally downregulated gene 4) family of HECT domain E3 ligases is a well-characterized class of enzymes and conserved from yeast to mammals. In humans there are 9 members (Nedd4-1, Nedd4-2, ITCH, Smurf1, Smurf2, WWP1, WWP2, NEDL1 and NEDL2) of this family and all of these proteins share common domains (Ingham et al., 2004; Rotin and Kumar, 2009) (**Figure 18A**).

They present a conserved modular organization with an N-terminal C2 domain critical for membrane localization, between two and four WW domains that recognize substrates and adaptor proteins that contain PY motif or phosphoserine/threonine residues and a C-terminal HECT catalytic domain always positioned at the C-terminus of the protein (**Figure 18B**).

The C2 domain, folded in an eight-stranded β-sandwich structure, is a calcium-binding domain. Upon $Ca^{2+}$ binding the C2 domain interacts with phospholipids and mediates intracellular targeting to the plasma membrane, endosomes and multivescicular bodies (Dunn et al., 2004). In addition, the C2 domain has a critical role; it exerts the auto-inhibitory function through the binding to the HECT domain (Mari et al., 2014; Wiesner et al., 2007).

The name of WW domain derives from the presence of two highly conserved tryptophan residues and a conserved proline residue in a sequence of ~35 amino acids (Harvey et al., 1999). This domain is composed by a hydrophobic core surrounded by three stranded antiparallel β-sheets and binds proteins that contain small proline-rich sequences, called PY motif (Huang et al., 2000; Sudol, 1996).

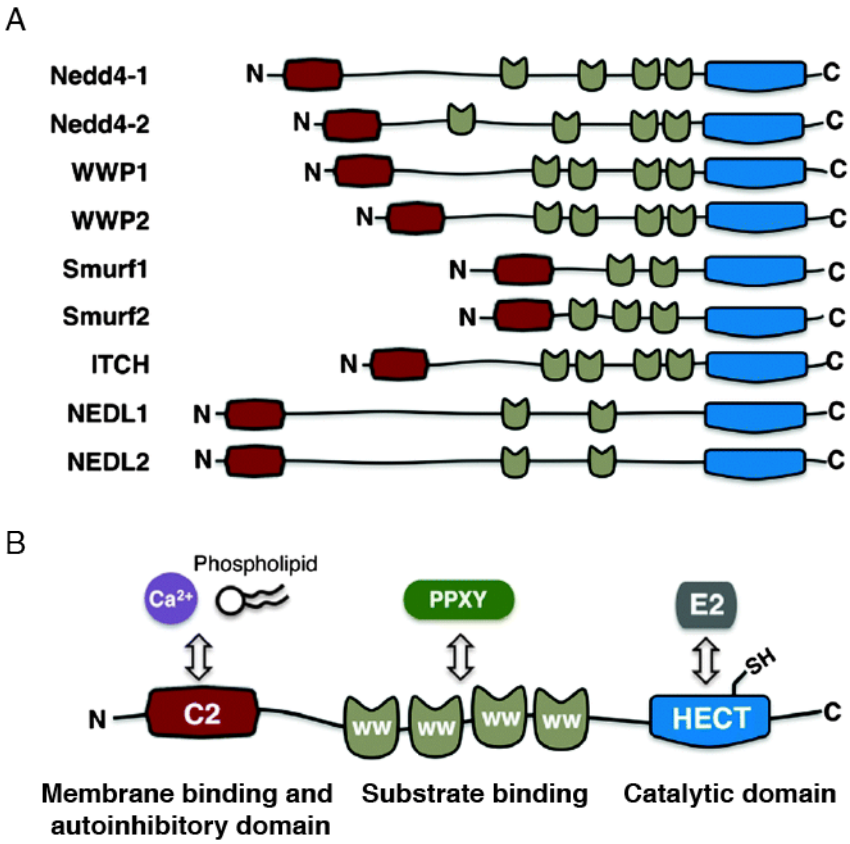


**Figure 18. Schematic representation of the structure of Nedd4 family** (adapted from An H, Mol Biosyst. 2014). (A) All 9 members of Nedd4 family shared common domains. (B) Nedd4 family members have N-terminal C2 domain involved in membrane binding and auto-inhibitory function, from 2 to 4 WW domains involved in substrate binding and the catalytic HECT domain at the C-terminal.

### 3.2 Functional role of Nedd4

Each members of Nedd4 family are diversely implicated in a wide range of biological processes such as endocytosis, protein trafficking, viral budding, signaling, cellular growth and proliferation (Rotin and Kumar, 2009; Yang and Kumar, 2010). They modulate important cellular functions and their alterations play a critical role in cancer (Scheffner and Kumar, 2014).

Nedd4-1 is widely expressed in mammalian tissues and has a conserved function in endocytosis and sorting of numerous proteins through mono- (Polo et al., 2002; Woelk et al., 2006) and Lys63-linked polyubiquitination (Rotin and Kumar, 2009).

The first Nedd4's polyubiquitinated substrate identified was the epithelial $Na^+$ channel (Katz et al., 2002) that is involved in the maintenance of salt ($Na^+$) and fluid balance in cells (Harvey et al., 2001; Kamynina et al., 2001). Nedd4 (and even better Nedd4-2) through their WW domains, directly bind the PY motif present at the C-terminal tail of ENaC. Subsequently, ENaC ubiquitination caused by these ligases promotes its endocytosis and degradation (Rotin et al., 2001; Staub et al., 1996). Mutations or deletions of PPxY motif determined the disruption of the interaction between Nedd4 and ENaC causing the Liddle's syndrome, a severe disorder that consists of sodium retention and hypertension (Lifton et al., 2001).

A possible oncogenic role of Nedd4 was ascribed to its effect on the tumor suppressor proteins PTEN. It was published that Nedd4 mediates the polyubiquitination of PTEN in the cytosol determining its proteasomal degradation (Wang et al., 2007). However, the role of Nedd4 on PTEN fate was not validated in Nedd4 knockout studies (Fouladkou et al., 2008), leaving a controversy in the field.

Nedd4 has been implicated in the down-regulation of different receptors like epidermal growth factor receptor (EGFR) (Katz et al., 2002). EGFR trafficking is modulated by a variety of endocytic adaptors (i.e. eps15, eps15R and epsins) that interact through their UIM with the ubiquitinated receptor and through other domains with different components of the endocytic machinery, like clathrin and adaptor protein-2 (AP-2) (Acconcia et al., 2009). In particular, Eps15 contains two copies of UIM. Upon EGF stimulation, the second UIM is involved in the recruitment of Nedd4, which then leads to Eps15 monoubiquitination via a process called coupled monoubiquitination (Polo et al., 2002; Woelk et al., 2006). Using Eps15 as a model system our lab clarified the molecular mechanism of coupled monoubiquitination. This involves the interaction between a "competent" UIM in the Ub receptor and a HECT-type E3 ligase (Nedd4, in the case of eps15), which has itself been covalently modified by ubiquitination. This modified E3

enzyme is then able to transfer another thiolester-conjugated Ub from the catalytic Cys residue to the Lys acceptor site in the substrate (Woelk et al., 2006).

### 3.3 Characteristics of the HECT domain of Nedd4

The HECT domain is the minimal region of the HECT-E3 enzymes that is necessary and sufficient to promote ubiquitination. As described in paragraph 2.3.1, the HECT domain is divided in two structural lobes tethered by a flexible linker. In the N-terminal N-lobe resides the E2 binding domain that is critical for the interaction with active E2~Ub, while the C-terminal C-lobe contains the catalytic cysteine critical for the enzymatic activity.

Several studies have demonstrated that members of the Nedd4 family possess two Ub-interaction surfaces within the HECT domain. A study published by Schulman and co-workers provided the crystal structure of Ube2D2~Ub in complex with the HECT domain of Nedd4-2 giving insights into how Ub, covalently bound to the E2, is correctly positioned to be transferred to the catalytic cysteine of the HECT domain (Kamadurai et al., 2009). This study discovered the first non-covalent ubiquitin-binding surface in the C-lobe. This surface is essential for the Ub transfer from the E2 to the E3 (Kamadurai et al., 2009). Several hydrophobic contacts involve an Ub surface centered on Ile36, Leu71 and Leu73.

Other studies identified a different ubiquitin-binding surface present in the N-lobe of the HECT domain. This was first identified in Rsp5 (French et al., 2009), the yeast homologue of Nedd4, and subsequent in Smurf2 (Ogunjimi et al., 2010), another member of Nedd4 family. However, these two studies reached different conclusions on about the role of this Ub-binding surface. In the case of Rsp5, it was proposed that the UBD acted to restrict polyubiquitination (French et al., 2009), while for Smurf2 the UBD was shown to facilitate the substrate polyubiquitination (Ogunjimi et al., 2010).

Our lab characterized the UBD in the N-lobe of Nedd4 through the crystal structure of HECT$^{Nedd4}$:Ub complex (Maspero et al., 2011). We demonstrated that only a subset of Nedd4 family members binds Ub, namely Nedd4, Nedd4-2 and Smurf2 (Maspero et al., 2011).

Our results confirmed the essential role of the non-covalent binding surface in the N-lobe for enzyme processivity. Indeed a point mutation in the UBD, capable of abrogating the Ub interaction, impaired the polyubiquitination of known Nedd4 substrates but not their monoubiquitination. Kim et al. reached similar conclusions solving the structure of Rsp5 in complex with Ub (Kim et al., 2011).

Based on these results we proposed a model in which once the first Ub moiety is attached to the substrate, the Ub occupies the UBD present in the N-lobe and this interaction is essential for the retention of the ubiquitinated substrate to the E3, keeping the correct conformation of the N-lobe that favors enzyme processivity (Maspero et al., 2011) (**Figure 19**).

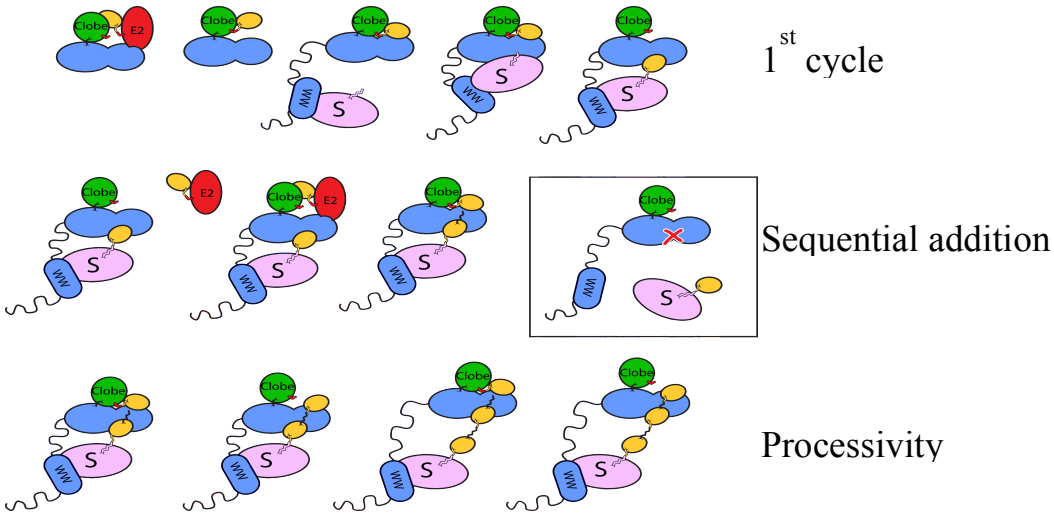


**Figure 19. Model of the role of UBD of the HECT domain in enzyme processivity.** Model for substrate polyubiquitination, in pink is depicted the substrate, in yellow ubiquitin, the WW and N-lobe of the HECT domain in blue while in green the C-lobe. We demonstrated that the UBD present in the N-lobe of the HECT domain is not essential for the first cycle of substrate ubiquitination while it has a critical role for the enzyme processivity. Our model proposed that the UBD kept in close proximity the lysine of Ub to the catalytic cysteine. Mutation of the UBD impaired substrate polyubiquitination but not the monoubiquitination.

### 3.4 Regulation of Nedd4 ligase activity

The ligase activity of Nedd4 family proteins is finely regulated at several levels that span from intra-molecular interactions to adaptor protein interactions and post-translational modifications (Rotin and Kumar, 2009; Shearwin-Whyatt et al., 2006).

As stated before, in resting conditions the C2 domain forms an intra-molecular interaction with the HECT domain (**Figure 20**). The C2:HECT interaction inhibits the E3 ligase activity to possibly protect both the enzyme and the substrates from premature ubiquitination (Wiesner et al., 2007). Recent efforts from our and Wiesner lab resulted in the structural characterization of the Nedd4 and Smurf auto-inhibited conformation (Mari et al., 2014). NMR data and biochemical analyses on Smurf2 and Nedd4 showed that the C2 domain has the capacity to regulate E3 activity by maintaining the HECT domain in a low-activity state where its ability for transthiolation and noncovalent Ub binding are impaired (Mari et al., 2014) This *in cis* autoinhibition can be relieved by binding of the adaptor protein SMAD7 to the Smurf2 HECT domain (Ogunjimi et al., 2005), by an increase of $Ca^{2+}$ intracellular content (Wang et al., 2010) or by post-translational modifications caused by upstream signaling in the case of Nedd4 (Persaud et al., 2014) (**Figure 20**). It has been proposed that the C2 domain interacts with $Ca^{2+}$ and inositol 1,4,5-trisphosphate ($IP_3$) using the same surface involved in the HECT interaction (Escobedo et al., 2014). Our lab in collaboration with Rotin lab, has recently demonstrated the specific role of post-translational modifications for the dissociation of the auto-inhibitor C2:HECT interaction in Nedd4 (Persaud et al., 2014).

Upon EGF stimulation, EGFR is activated by dimerization and auto-trans-phosphorylation of tyrosine residues in the kinase domain (Schlessinger, 2002). The phosphorylated form of EGFR recruits phospho-binding proteins as c-Src, promoting its activation and signaling transduction (Osherov and Levitzki, 1994). Our lab found that, once activated by the EGFR, c-Src phosphorylates Nedd4 in 5 different sites ($Tyr^{43}$, $Tyr^{111}$,

Tyr [332], Tyr[585] and Tyr[647]). Two tyrosines, Tyr[43] in the C2 domain and Tyr[585] in the HECT domain, were particularly relevant as they are located near the regions involved in the C2-HECT interaction. Phosphorylation of these Tyr induces the dissociation of the auto-inhibition C2:HECT interaction, increasing the catalytic activity of Nedd4 (Persaud et al., 2014) (**Figure 20**). Same sites and mechanism are in place in the case of the fibroblast growth factor receptor 1 (FGFR1) that is a substrate of Nedd4 (Persaud et al., 2009).

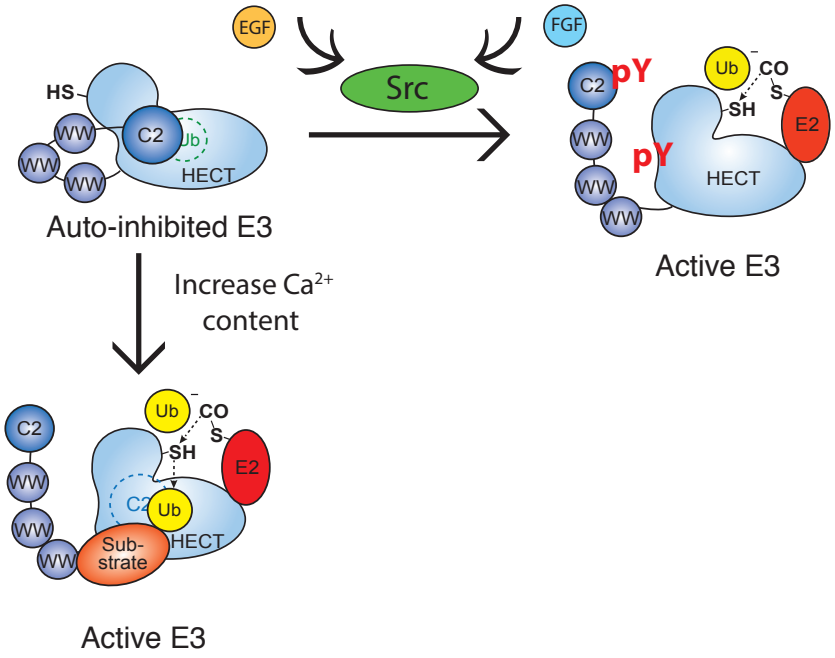


**Figure 20. Schematic representation of the regulation of intra-molecular inhibition C2:HECT domains** (adapted from Mari, Structure, 2014). Here it is represented Nedd4-1. On the left, the C2 domain binds and inhibits the catalytic activity of the HECT domain through the interaction with the UBD present in the HECT domain. Specific signals (i.e. increase of $Ca^{2+}$ content-bottom panel) or post-translational modifications (i.e. specific phosphorylation on Tyr[43] and Tyr[585]-right panel) could disrupt the C2:HECT interaction generating a fully activated Nedd4.

## 4. RABEX-5

Rabex-5 (RABapitin associated EXchange factor for rab5) is a guanine nucleotide exchange factor (GEF) for Rab-5 that is an important regulator of endosomal trafficking (**Figure 21A**). The small GTPase Rab-5 regulates the transport of clathrin coated vesicles from the plasma membrane to the early endosomes (Mattera et al., 2006) and cycles between an active (GTP bound) state and inactive (GDP bound) state. Rab-5 activity is crucially regulated by enzymes as exchange factors (GEFs) and activating GTPase proteins (GAPs).

Rabex-5 working as a GEF activates Rab-5 by stimulating GDP release and facilitating the GTP binding. Rabex-5 is present in the cytosol in complex with its activator Rabaptin-5 and subsequently is recruited to the plasma membrane of the endosome to exert its GEF activity (Haas et al., 2005). The Vps9-homology domain and the adjacent N-terminal helical bundle (HB) composed the GEF catalytic core that is responsible for the GEF activity (Delprato et al., 2004). To increase this activity, accelerating the Rab-5 activation (Lippe et al., 2001), Rabex-5 binds Rabaptin-5 through the coiled-coil (CC) domain and together they form a large multiprotein complex (Horiuchi et al., 1997) (**Figure 21B**).

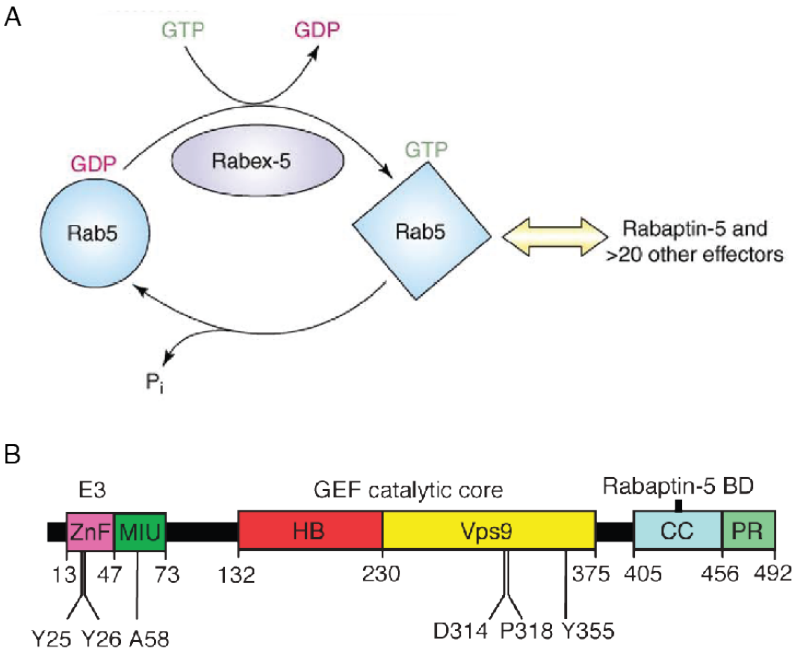


**Figure 21. Function and domain organization of Rabex-5.** (A) (adapted from Raiborg, Trends Biochem Sci. 2006) Rabex-5 is a GEF of Rab-5 through the exchange of GDP with GTP. (B) (adapted from Mattera, EMBO J. 2008) Schematic representation of Rabex-5 domains. The helical bundle (HB) and the Vps9 domains are the GEF catalytic core, respectively in red and yellow. In light blue the coiled-coil (CC) domain involved in the binding of Rabaptin-5. In green the C-terminal prolin rich domain (PR). Zinc finger and MIU domain are two UBDs, respectively depicted in pink and green.

Rabex-5 plays an oncogene role in the formation and development of different malignant tumors; its up-regulation promotes tumor growth, migration and invasion of cancer cells. Recent studies demonstrated that Rabex-5 is overexpressed in several cancers like colorectal cancer (Nimmrich et al., 2000), breast cancer (Zhang et al., 2013), prostate cancer (Zhang et al., 2014) and gastric cancer (Wang et al., 2014).

### 4.1 UBDs of Rabex-5

Our lab demonstrated that Rabex-5 binds Ub through two independent UBDs: 1) the MIU domain that recognizes the canonical hydrophobic surface of Ub centered on Ile44, Leu8, Val70 through Ile51, Leu57 and Ala58 on Rabex-5; 2) the A20 zinc finger (ZnF_A20) domain that interacts through Tyr25 and Tyr26 with Asp58 of Ub (Lee et al., 2006a; Mattera et al., 2006; Penengo et al., 2006). This second non-canonical interaction surface involves polar residues such as Arg54, Thr55, Ser57, Asp58, Tyr59 and Asn60 (**Figure 22**).

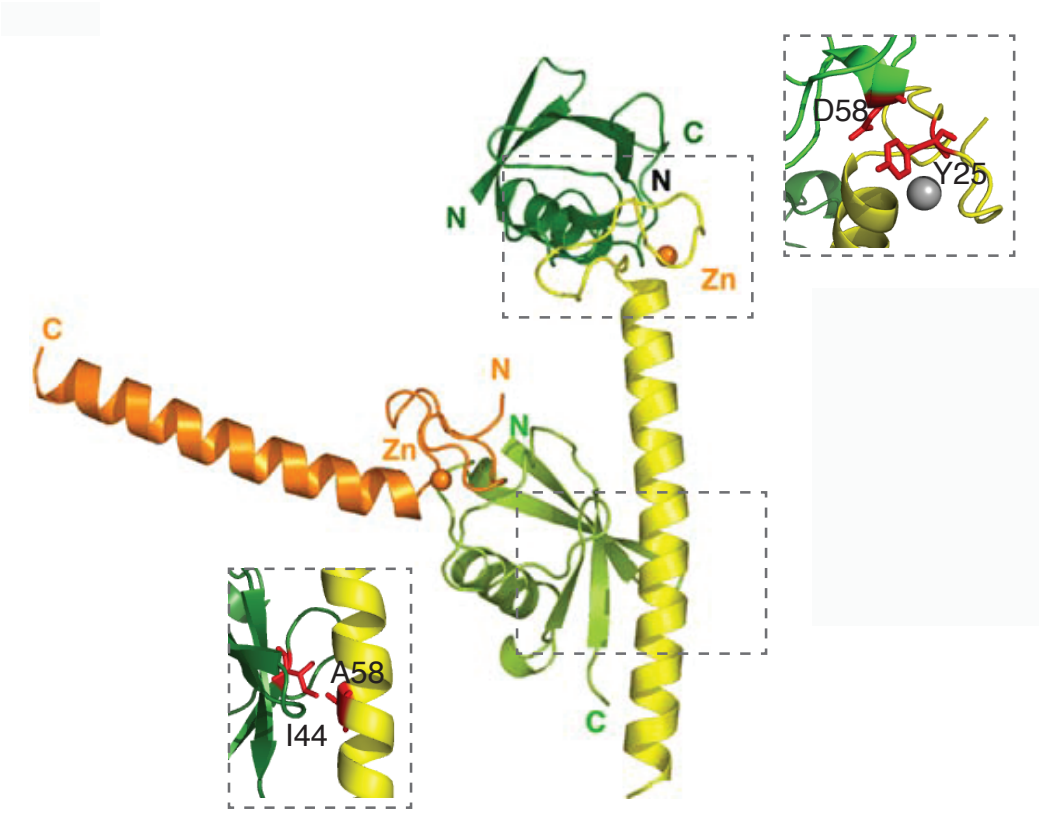


**Figure 22. Crystal structure of Rabex-5 in complex with Ub** (adapted from Penengo, Cell, 2006). Representation of the human Rabex-5 fragment (from 1 to 74 a.a.) in complex with Ub molecules. Rabex-$5^{1-74}$ is depicted in yellow and the two Ub molecules are in light and dark green. ZnF_A20 coordinates the $Zn^{2+}$ ion represented as a sphere. Magnification of each interaction of Ub with Rabex-5 is shown in dashed box indicating different residues (depicted in red) are used. Ub interacts with the MIU domain through the Ile44 and with the ZnF_A20 using a non canonical Asp58 surface.

The MIU domain (48-74a.a.) is an amphipathic α-helix and possesses the same sequence as the well-described ubiquitin-interacting motif (UIM) found in many proteins but with the opposite orientation (Hicke et al., 2005). The interaction between the MIU domain and Ub has the dissociation constant ($K_D$) of 28 μM (Penengo et al., 2006) that is lower respect the UIMs versus Ub ($K_D$ ~ 100-500 μM) (Hicke et al., 2005).

The presence of four cysteines (Cys19, Cys23, Cys35 e Cys38) at the N-terminus (2-49a.a.) that interact with $Zn^{2+}$ ion identifies in Rabex-5 a zinc finger module belonging to the ZnF_A20 family. This domain interacts with Ub on a different surface centered on Asp58 and the $K_D$ measured is around 12 μM (Lee et al., 2006b; Penengo et al., 2006).

Each domain can interact with Ub independently and a single Ub molecule can interact with two Rabex-5 moieties (Penengo et al., 2006). Rabex-5 binds to the activated form of EGFR, which is known to be ubiquitinated, and ZnF_A20 or MIU domain mediates this binding (Penengo et al., 2006). It has been suggested that Rabex-5 UBDs are important for Rabex-5 localization at the plasma membrane and for their co-trafficking with Ub-cargoes (Penengo et al., 2006). Indeed, mutations on the UBDs that impaired the Ub binding strongly reduce Rabex-5 endosomal localization (Mattera and Bonifacino, 2008). In addition, Rabex-5 undergoes coupled monoubiquitination driven by the MIU domain (Penengo et al., 2006).

### 4.2 Rabex-5 as E3 ligase

The GEF activity of Rabex-5 was extensively studied while little is known on the role of Rabex-5 as E3 ligase and the molecular mechanism that it used to perform substrate ubiquitination is still unclear. Rabex-5 has been proposed as E3 ligase based on its ability to self-ubiquitinate (Lee et al., 2006a). Having an A20 zinc finger domain (ZnF_A20) instead of a canonical RING, Rabex-5 can be considered as an atypical RING-E3.

Ras proteins were identified as possible substrates of the E3 ligase activity of Rabex-5. Ras proteins are small guanine nucleotide binding proteins involved in signal transduction regulating cellular growth, proliferation (Malumbres and Pellicer, 1998), survival (Cox and Der, 2003), differentiation and cell mobility. Being central hubs in these intracellular pathways they are the most common oncogenes in human cancer (Bos, 1989). These proteins can switch between active GTP-bound states and, upon GTP hydrolysis, in inactive GDP-bound states (Cox and Der, 2003). In the GTP-active state H-Ras can interact and activate a wide range of downstream effectors like ERK, PI3K and Raf (Malumbres and Pellicer, 1998). Studies performed by Dafna Bar-Sagi and co-workers have demonstrated that Rabex-5 is able to mono- and di-ubiquitinate both H-Ras and N-Ras and that these modifications can promote their endosomal association leading to an attenuation of Ras-ERK signaling (Jura and Bar-Sagi, 2006; Xu et al., 2010).

# MATERIALS AND METHODS

## 1. Solutions

1.1 TRIS-HCl (1 M)

The solution was prepared by using TRIS base, dissolving 121.1g in 800 ml distilled H2O. The pH was adjusted to 7.4, 7.6 or 8.0 with HCl and ddH20 was added to bring volume to 1 litre.

1.2 10x TRIS EDTA (pH 7.4-8.0)

100 mM Tris HCl (pH 7.4-8.0)

10 mM EDTA (pH 8.0)

1.3 50x TAE (Tris-Acetate-EDTA)

242 g/L Tris base

57.1 ml/L Acetic acid 0.5 M

20 ml/L EDTA pH 8

The pH was adjusted to 8.5 with HCl.

1.4 TRIS-Buffered saline (TBS)

137 mM NaCl

2.7 mM KCl

25 mM TRIS pH 7.4

The pH was adjusted to 7.4 with HCl.

1.5 1X SDS-PAGE Sample Buffer (Laemmli)

2% SDS

50 mM TRIS pH 6.8

10 % glycerol

0.1 % saturated Bromophenol blue

SDS-PAGE Sample Buffer was prepared as a 5X stock solution. 5 % (v/v) β-Mercaptoethanol (14M) or 100 mM DTT was added to the stock solution before use. The solution was stored at -20°C and protected from light.

1.6 10X SDS-PAGE Running Buffer

192 mM Glycine

250 mM TRIS, pH 8.3

1% SDS

1.7 Buffer for preparation of Tris-Tricine gels (TRIS-Cl/ SDS)

3 M TRIS-HCl

0.3% SDS

The pH was adjusted to 8.45 with HCl. The buffer was stored at 4°C.

1.8 Running Buffers for Tris-Tricine gels

1X Cathode buffer:

0.1 M TRIS base

0.1 M Tricine

0.1% SDS

5X Anode buffer:

0.2 M TRIS-HCl, pH 8.9

The pH was adjusted to 8.9 with HCl. The Cathode buffer was added in the upper chamber (-) of the gel apparatus and the Anode buffer in the lower chamber (+).

1.9 10X Western Transfer Buffer

250 mM TRIS, pH 8.3

192 mM Glycine

20% v/v methanol or ethanol

1.10 1x RIPA buffer

50 mM Tris Hcl pH 7.6

150 mM NaCl

1% NP-40

0.1% SDS

0.5% Deoxycholic acid

Phosphatases and protease inhibitors were added freshly to lysis and wash buffers:

20 mM Na pyrophosphate pH 7.5

50 mM NaF

2 mM PMSF in ethanol

10 mM Na vanadate in HEPES pH 7.5

Protease Inhibitor Cocktail 1:500 (Calbiochem)

1.11 1x YY buffer

50 mM Na-HEPES pH 7.5

150 mM NaCl

1mM EDTA

1mM EGTA

10% glycerol

1% triton-100

1.12 1x ubiquitination buffer

25 mM Tris–HCl pH 7.6

5 mM $MgCl_2$

100 mM NaCl

0.2 mM dithiothreitol

2 mM ATP

1.13 1x isopeptide buffer

50 mM Tris–HCl pH 10.0

5 mM $MgCl_2$

150 mM NaCl

1.14 1x ITC buffer

20mM Tris-HCl pH 8.0

200 mM NaCl

5% glycerol

1mM DTT (freshly added)

## 2. Reagents

Polyubiquitin Lys63-linked chains were purchased from Enzo Life Sciences. Biotinylated Ub was purchased from BostonBiochem. Ub (from bovine red blood cells), ATP, TCEP and DTT were purchased from Sigma. Imperial Protein Stain and Instant blue were purchased from Thermo Scientific and Expedeon respectively.

2.1 Antibodies

The following antibodies were used: mouse monoclonal anti-MIU and CUE domain respectively at N- and C-terminal part of Rabex-5 (generated in-house); mouse monoclonal anti-Ub ZTA10 (generated in-house); polyclonal anti-GST (generated in-house); streptavidin-HRP (Pierce); polyclonal anti-Ube2D (Santa Cruz).

## 3. Cloning techniques

3.1 Agarose gel electrophoresis

DNA samples were loaded on 0.8%-2% agarose gels along with DNA markers. Gels were made in TAE buffer containing Gel Red (Biotium), according to the manufacturer's instructions, and run at 90 V until desired separation was achieved. DNA bands were visualized under a UV lamp.

3.2 Minipreps

Clones picked from individual colonies were used to inoculate 2 ml LB (containing the appropriate antibiotic) and grown overnight at 37°C. Bacteria were pelleted for 5 minutes at 16,000 *g*. Minipreps were performed with the Wizard Plus SV Minipreps Kit (Promega) following the manufacturer's instructions. The plasmids were eluted in 50 µl nuclease free $H_2O$.

3.3 Diagnostic DNA restriction

0.5-2 µg DNA were digested for 2 hours at 37°C with 10-20 units of restriction enzyme (New England Biolabs). For digestion, the volume was brought to 20-50 µl with the appropriate buffer and distilled $H_2O$.

3.4 Large Scale Plasmid Preparation

Plasmid DNA was isolated from 200 ml of bacterial culture using the Qiagen Maxi-prep kit according to the manufacturer's instructions.

3.5 Transformation of competent cells

50 µl of competent cells Top10 (Promega) (both for cloning and DNA preparation) or BL21-CodonPlus (Promega) (for GST or His-tagged proteins production), were thawed on ice prior to the addition of plasmid DNA. Cells were incubated with DNA on ice for 30 minutes and then subjected to a heat shock for 45 seconds at 42°C. Cells were replaced on ice for 5 additional minutes. Then, 500 µl of SOC was added and the cells were left at 37°C for another 60 minutes before plating them onto plates with the appropriate antibiotic. Plates were incubated overnight at 37°C.

3.6 PCR (Polymerase Chain Reaction)

Sense and an antisense oligo of 20-30 nucleotides each were generated, one annealing in 5' (forward) and the other in 3' (reverse) to the target sequence. The primers were designed of similar length and annealing temperature (calculated by running the primers on simulated PCR reactions, using the Ape programme). Primers were used in a PCR reaction together with the DNA template and the high fidelity Phusion DNA polymerase (BioLabs).

Reaction mixture

10 µl reaction buffer 5x

50 ng DNA template

0.5 µM primer forward

0.5 µM primer reverse

0.2 mM dNTPs mix

0.01 U of Phusion enzyme

distilled $H_2O$

The PCR reaction (denaturation, annealing and extension) was repeated for various number of cycles (see table below). This was done on an automated cycler (GeneAmp PCR system 9700, Applied Biosystems.

Cycling parameters:

| **Step** | **Temperature** | **Time** | **Cycles** |
|---|---|---|---|
| 1 | 98°C | 30 seconds | 1 |
| 2 | 98°C<br>40-44°C (calculated for each primer pair)<br>72°C | 30 seconds<br>30 seconds<br>60 seconds | 5 |
| 3 | 98°C<br>50-55°C (calculated for each primer pair)<br>72°C | 30 seconds<br>30 seconds<br>60 seconds | 25 |
| 4 | 72°C | 7 minutes | 1 |
| 5 | 4°C | ∞ | 1 |

| **Construct** | **Oligonucleotides** |
|---|---|
| Rabex-5 1-74 | For:ATCGGATCCACCATGAGCCTTAAGTCTGAACGCCGA<br>Rev: CTTTGCCAGTCAGAGCTAACAAGGGCCCAATCCCT |
| Rabex-5 1-49 | For: ATCGGATCCACCATGAGCCTTAAGTCTGAACGCCGA<br>Rev: CAAAGCCAGGCAGAAGTAGATTCAGGAGGACTG |
| Rabex-5 48-74 | For: ATCGGATCCACCATGAGCCTTAAGTCTGAACGCCGA<br>Rev:CTTGCCAGTCAGAGCTAACAAGGGCCCAATCCCT |

3.7 Site directed mutagenesis

Site directed mutagenesis was performed using the Quick Change Mutagenesis Kit (StrataGene), following the manufacturer's instructions. Briefly, a sense and an antisense oligo, carrying the desired mutation in the middle of the sequence, were generated and used in a PCR reaction using the wild type construct (50 ng). The PCR was performed using the Pfu TURBO polymerase for 12-18 cycles. After amplification, 1 μl of DpnI restriction enzyme, which selectively cuts methylated DNA at the GATC sequence, was added to digest the wild-type parental DNA. After 1 hour of incubation at 37℃, the PCR product was used to transform competent *Escherichia coli* cells. Single colonies were picked, plasmid DNA extracted (Miniprep) and sequenced for the presence of the desired mutation and the absence of other, unwanted, base changes.

For the amplification step, 12-18 PCR cycles were performed with a denaturation step of 30 seconds at 95°C followed by an annealing step of 1 minute at 55°C and an extension step at 68°C of 2 minutes/ kb of plasmid length. All the constructs were cloned in pGEX6P2 or pet14b vectors.

In the table are shown the oligonucleotides used for the generation of each construct.

| **Construct** | **Oligonucleotides** |
|---|---|
| HECT C778S | For: CTAGAGCTTCTTATGTCTGGACTGGGAGATGTTG<br>Rev: CAACATCTCCCAGTCCAGACATAAGAAGCTCTAG |
| HECT IDCNP | For: AATCCAAACTCTGGAATCAACCCAGATCACCTCTC<br>Rev: GAGAGGTGATCTGGGTTGATTCCAGAGTTTGGATT |
| HECT C627A | For: CCAAACTCTGGATTGGCTAACGAAGATCACCTC<br>Rev: GAGGTGATCTTCGTTAGCCAATCCAGAGTTTGG |
| HECT C627S | For: CCAAACTCTGGATTGTCTAACGAAGATCACCTC<br>Rev: GAGGTGATCTTCGTTAGACAATCCAGAGTTTGG |

| | |
|---|---|
| HECT DC627 | For: CCAAACTCTGGATTGAACGAAGATCACCTC<br>Rev: GAGGTGATCTTCGTTCAATCCAGAGTTTGG |
| HECT DC627NP | For: AATCCAAACTCTGGATTGAACCCAGATCACCTCTC<br>Rev: GAGAGGTGATCTGGGTTCAATCCAGAGTTTGGATT |
| HECT F707A | For: CATAGATGAAGAACTTGCTGGACAGACACATC<br>Rev: GATGTGTCTGTCCAGCAAGTTCTTCATCTATG |
| Ub G76C | For: CTCCGTCTCAGAGGTTGCTAGGGATCCGGCTGC<br>Rev: GCAGCCGGATCCCTAGCAACCTCTGAGACGGAG |
| Ube2D3 C21S | For: GACCCTCCAGCACAATCTTCTGCAGGTCCAGTTG<br>Rev: CAACTGGACCTGCAGAAGATTGTGCTGGAGGGTC |
| Ube2D3<br>C107S/C111S | For: GTTCTTTTATCCATTTCTTCACTGCTATCTGATCCAAACCCAG<br>Rev:CTGGGTTTGGATCAGATAGCAGTGAAGAAATGGATAAAAGAAC |
| Ube2D3 S22R | For: GACCCTCCAGCACAATGTCGTGCAGGTCCAGTTGGG<br>Rev: CCCAACTGGACCTGCACGACATTGTGCTGGAGGGTC |
| Ube2D3 C85K | For: CAGTAATGGCAGCATTAAGCTCGATATTCTAAGATCAC<br>Rev: GTGATCTTAGAATATCGAGCTTAATGCTGCCATTACTG |
| Ube2D3 C21S/S22R | For: GACCCTCCAGCCACAATCTCGTGCAGGTCCAGTTGGG<br>Rev: CCCAACTGGACCTGCACGAGATTGTGCTGGAGGGTC |
| Ube2D3 C85S | For: CAGTAATGGCAGCATTTCTCTCGATATTCTAAGATCAC<br>Rev: GTGATCTTAGAATATCGAGAGAAATGCTGCCATTACTG |

| | |
|---|---|
| Rabex-5 A58G | For: AGGACTGGGAGCTGGAGAGAGCGACTCCAGCG<br>Rev: CGTGGAGTCGCTCCCAAGCTCCCAGTCCT |
| Rabex-5<br>Y25F | For: AGAAAGGATGTGGTTTCTACG<br>Rev: GCAGGGTTGCCGTAGAAACCACATCCTTTCT |
| Rabex-5 Y/A | For: TGCAAGAAAGGATGTGGTGCCGCCGGCAAACCCTGCCTGGCAG<br>Rev: CTGCCAGGCAGGGTTGCCGGCGGCACCACATCCTTTCTTGCA |

## 4. Protein procedures

### 4.1 SDS-PolyAcrylamide Gel Electrophoresis (SDS-PAGE)

Gels for resolution of proteins were made from a 30%, 37,5:1 mix of acrylamide: bisacrylamide (Sigma). As polymerisation catalysts, 10% Ammonium PerSulphate (APS) and TEMED were used.

Separating gel mix

| **Gel %** | **6** | **8** | **10** | **15** |
|---|---|---|---|---|
| Acrylamide mix (ml) | 2 | 2.7 | 3.3 | 5 |
| 1.5M Tris HCl pH 8.8 (ml) | 2.5 | 2.5 | 2.5 | 2.5 |
| Distilled $H_2O$ (ml) | 5.3 | 4.6 | 4 | 2.3 |
| 10% SDS (ml) | 0.1 | 0.1 | 0.1 | 0.1 |
| 10% APS (ml) | 0.1 | 0.1 | 0.1 | 0.1 |
| TEMED (ml) | 0.01 | 0.01 | 0.01 | 0.01 |
| TOTAL (ml) | 10 | 10 | 10 | 10 |

Stacking gel mix

| | |
|---|---|
| Acrylamide mix (ml) | 1.68 |
| 1M Tris HCl pH 6.8 (ml) | 1.36 |
| Distilled $H_2O$ (ml) | 6.8 |
| 10% SDS (ml) | 0.1 |
| 10% APS (ml) | 0.1 |
| TEMED (ml) | 0.01 |
| TOTAL (ml) | 10 |

To obtain a good resolution of small proteins like Ub, proteins were run on Tris-Tricine protein gels. For these gels a 30%, 29:1 mix of acrylamide: bisacrylamide (Sigma) was used.

Separating gel mix (11%)

| | |
|---|---|
| Acrylamide mix (ml) | 21.72 |
| Tris HCl/ SDS (ml) | 20 |
| Distilled $H_2O$ (ml) | 11.94 |
| Glycerol (ml) | 6.34 |
| 10% APS (ml) | 0.1 |
| TEMED (ml) | 0.03 |
| TOTAL (ml) | 60 |

Stacking gel mix (4%)

| | |
|---|---|
| Acrylamide mix (ml) | 6.66 |
| Tris HCl/ SDS (ml) | 12.4 |
| Distilled $H_2O$ (ml) | 30.94 |
| 10% APS (ml) | 0.2 |

| | |
|---|---|
| TEMED (ml) | 0.12 |
| TOTAL (ml) | 50 |

**4.2 Western Blot**

Desired amounts of proteins were loaded onto 1-1.5 mm SDS-PAGE gels for electrophoresis (Biorad). Proteins were transferred in western transfer tanks (Biorad) to nitrocellulose membranes (Schleicher and Schnell) in 1x Western Transfer buffer (supplemented with 20% methanol) at 30V overnight or 100V for 1 hour. Ponceau staining was used to roughly reveal the amount of protein transferred to the membranes. Membranes were blocked 1 hour (or overnight) in 5% milk in TBS supplemented with 0.1% Tween (TBS-T).

After blocking, membranes were incubated with the primary antibody, diluted in TBS-T 5% milk for 1 hour at room temperature, followed by three washes of 5 minutes each in TBS-T and then incubated with the appropriate horseradish peroxidase-conjugated secondary antibody diluted in TBS-T for 30 minutes. After the incubation with the secondary antibody, the membranes were washed three times in TBS-T and the bound secondary antibody was revealed using the Enhanced ChemiLuminescence (ECL) method (Amersham). The images were acquired by using Chemidoc instrument and ImageLab software (Biorad).

**4.3 Anti-Ubiquitin WB**

After SDS-PAGE or tris–tricine gel, proteins were transferred on a PVDF (polyvinylidene fluoride) membrane (Immobilion P, Millipore), previously activated by incubation in 100% MetOH for 1 minute at room temperature. Ponceau staining was avoided since it might interfere with antibody recognition. After transfer, membranes were subjected to a denaturing treatment in a dedicated solution (see Denaturing solution) for 30 minutes at

4°C. This treatment denatures Ub and facilitates the recognition of latent Ub epitopes by anti-Ub antibody resulting in intensification of the anti-Ub signal. After extensive washing in TBS-T buffer, filters were blocked overnight at 4°C in 5% BSA (dissolved in TBS-T). After blocking, membranes were incubated with antibodies against Ub, diluted in TBS-T 5% BSA, for 1 hour at room temperature, followed by three washes of 10 minutes each in TBS-T and then incubated with the horseradish peroxidase-conjugated secondary antibody diluted in TBS-T 3% BSA for 30 minutes at room temperature. After incubation with the secondary antibody, the membranes were washed three times in TBS-T (5 minutes each) and the bound secondary antibody was revealed using the ECL method (Amersham). The images were acquired by using Chemidoc instrument and ImageLab software (Biorad).

Denaturing solution

6 M Guanidium Chloride

20 mM TRIS, pH 7.4

1 mM PMSF (freshly added)

5 mM b-mercaptoethanol (freshly added)

## 5. Protein production and purification

### 5.1 GST-fusion proteins production

BL21 cells were picked from individual colonies and transformed with the indicated GST-fusion constructs, and used to inoculate 50 ml LB (containing 25 μg/ml ampicillin) and grown overnight at 37°C. The 50 ml overnight culture was diluted in 1 litre of LB and grown at 37°C until it reached approximately OD=0.6. Then, 0.5-1mM IPTG was added and the culture was grown at 18°C overnight. The cells were then pelleted at 4000 rpm for 10 minutes at 4°C and pellets were resuspended in GST-lysis solution (20 ml/L of bacteria). Samples were sonicated 5 times for 20 seconds/each on ice and were pelleted at

14000 rpm for 30 minutes at 4°C. 1 ml of glutathione-sepharose beads (Amersham) (1:1 slurry), previously washed 3 times with GST-lysis buffer, were added to the supernatants and samples were incubated 3-4 hours at 4°C on a rocking wheel. The beads were then washed 3 times in PBS containing 1% triton, and additional 2 times in PBS alone. The beads were finally resuspended in 1:1 volume of GST-maintenance solution and stored at –80°C.

GST-lysis solution

50 mM Hepes pH 7.5

200 mM NaCl

1 mM EDTA

0.1% NP40

5% glycerol

Protease Inhibitors (Calbiochem)

GST-maintenance solution

50 mM Tris pH 7.4

100 mM NaCl

1 mM EDTA

10% glycerol

1 mM DTT

Protease Inhibitors (Calbiochem)

**5.2 Cleavage of GST-fusion proteins**

GST-fusion proteins were cleaved with PreScission Protease (GE). 1 unit of enzyme for 100 μg of fusion protein was added to the beads in the presence of GST-maintenance

solution and either incubated over night at 4°C. After cleavage the supernatant containing the cleaved protein was collected and the beads were washed twice to allow the complete recovery of the cleaved protein.

### 5.3 His-fusion proteins production

BL21 cells picked from individual colonies and transformed with the His-constructs were used to inoculate 50 ml LB and grown overnight at 37°C. The 50 ml overnight culture was diluted in 1 litre of LB and was grown at 37°C until it reached approximately OD=0.6. Then, 1 mM IPTG was added and the culture was grown at 18°C overnight. Cells were then pelleted at 4000 rpm for 10 minutes at 4°C and pellets were resuspended in Buffer A. Samples were sonicated 5 times for 20 seconds/each on ice and were pelleted down at 14000 rpm for 30 minutes at 4°C. 1 ml of Ni-NTA beads (QIAGEN), previously washed 3 times with buffer A, was added to the supernatants and samples were incubated for 2 hours at 4°C, on a rocking wheel. The beads were then washed once with buffer A, once in the same solution plus 1 M NaCl, and once in the same solution plus 20 mM imidazole. His-fusion proteins were eluted in two steps, first with buffer A plus 200 mM imidazole and second with buffer A plus 500 mM imidazole. Dialysis was then performed in GST-maintenance buffer overnight, using Tris pH 6.8.

Buffer A

50 mM $NaH_2PO_4$ pH 7.8

300mM NaCl

10 % glycerol

10 mM imidazole

Protease inhibitors (Calbiochem)

### 5.4 Production of untagged Ub

Ub G76C and Ub WT are expressed in BL21 (Amp). BL21 cells picked from individual colonies and transformed with the constructs were used to inoculate 50 ml LB and grown overnight at 37°C. The 50 ml overnight culture was diluted in 1 litre of LB and was grown at 37°C until it reached approximately OD=0.6. Then, 1 mM IPTG was added and the culture was grown at 18°C overnight. Cells were then pelleted at 4000 rpm for 10 minutes at 4°C and pellets were resuspended in a specific buffer:

25mM ammonium acetate pH 7.0

10% glycerol

10mM β-mercaptoethanol

protease inhibitors

Samples were sonicated 5 times for 20 seconds/each on ice and were pelleted down at 14000 rpm for 30 minutes at 4°C. The supernatant adjusted to pH 4.5-5.0 with concentrated acetic acid because acid-precipitable proteins were removed by centrifugation (15000 rpm for 30 min) and the supernatant containing the ubiquitin monomers was passed through a 0.45 mm PES filter.

To change the buffer, dialysis (o.n. in tubes with 3.5 Kd MWCO) was performed against:

20 mM Tris HCl pH 8

200 mM NaCl

5% glycerol

1mM EDTA

1mM DTT

Eventually Ub can be concentrated after dialysis using concentrator (centricon of 3.0 kDa of cut-off) and purified by a Superdex 75 column.

### 5.5 Protein purification

After cleavage from the GST tag (for GST-fusion proteins) or elution from Ni-NTA beads (for His-fusion proteins) proteins were purified using either size exclusion chromatography or ion exchange chromatography. Prior to run on a Superdex 200 or 75 size exclusion column, the samples were concentrated using Vivaspin (of different dimension and different molecular weight cut off according to the protein of interest) and centrifuged at 4000 rpm at 4°C. The concentrated sample was run onto a Superdex size exclusion column of different sizes according to the total amount of protein using a specific gel filtration buffer.

Gel filtration buffer

20 mM Tris pH 8.0

200 mM NaCl

1 mM EDTA

1 mM DTT

5% glycerol

The desired protein was eluted in a clear, well isolated peak according to its size and shape. Purity of the peak was assayed by SDS-PAGE gel and Coomassie staining. The desired fractions were collected, pooled and concentrated using Vivaspin tubes.

Other proteins were purified using ion exchange chromatography (Resource S or Q) depending on its isoelectric point. Samples were diluted with the purification buffer without NaCl to reduce the concentration to 30 mM of NaCl in order to allow the binding of the proteins to the ion exchange column. The samples were applied on the column pre-equilibrated with the buffer without salt and eluted using a gradient (20 column volume) from 30 mM to 500 mM NaCl in the same buffer. Fractions were analysed by SDS-PAGE

or Tris-tricine gel and the desired fractions were pooled and concentrated using Vivaspin tubes. The final concentration of the samples was obtained as the ratio between the measured absorbance at 280 nm and the theoretical molar extinction coefficient at 280 nm, according to Lambert–Beer's law.

## 6. Pull-down experiments

For pull-down experiments, 2μM of GST proteins were incubated with 250 ng of K63 chains or 2 mM of mix composed by 1/3 Ub-loaded E2 and 2/3 E2 for 2 hours at 4°C in YY buffer. After four washes of the GST proteins with YY buffer, specifically bound proteins were resolved on tris-tricine gel and detection was obtained by immunoblotting using specific antibodies.

## 7. Pull-down Experiments with *In vitro* translated E2s

*In vitro* translated E2 was obtained by adding 1 μg of circular plasmid DNA, containing a T7 promoter, coding for E2 protein to an aliquot of the $T_NT$ Quick master mix (Promega) and 20μCi of [$^{35}$S]-methionine. 50 μl reaction was then incubated for 90 minutes at 30°C and the radioactive protein was analysed by SDS-PAGE.

For pull down experiments, 4 μM GST-Rabex-5 WT or mutants immobilized onto GSH beads were incubated with 8 μl of *in vitro* translated E2 for 2 h at 4°C in a buffer containing 50 mM Hepes pH 7.5, 150 mM NaCl, 10% glycerol and 1% Triton X-100. Three washes with YY buffer were made. Specifically bound proteins were resolved on Tris-Tricine-PAGE and transferred on nitrocellulose membrane. Ponceau staining of the

membrane was performed to show the loading of GST-fusion protein. Films were exposed and developed after 24h of incubation.

## 8. *In vitro* Ubiquitination assay

Ubiquitination assays were performed at 37°C using purified enzymes. In particular, auto-ubiquitination reactions contained 20 nM E1, 500 nM $His_6$-tagged Ube2D3, 500 nM GST-Rabex-5 WT or mutants, 2.5 μM of ubiquitin in ubiquitination buffer (25 mM Tris–HCl, pH 7.6, 5 mM $MgCl_2$, 100 mM NaCl, 0.2 μM dithiothreitol, 2 mM ATP). GST-tagged Rabex-5 was used immobilized on glutathione beads. For substrate ubiquitination assay 20 nM E1, 500 nM Ube2D3, 500 nM Rabex-5 produced as GST fusion protein, cleaved with PreScission protease and purified, 5μM of Ub-biotinylated and 500 nM of substrate (GST-$Ras^{1-166}$ or GST-H-Ras) were added to the reaction mixture. At the indicated time points samples were centrifuged to separate the beads ("pellet"), containing the ubiquitinated E3s or the ubiquitinated substrate, from the supernatant, containing unbound enzymes. The pellet was washed four times in RIPA buffer (50 mM Tris HCl pH 7.6, 150 mM NaCl, 1% NP-40, 0.1% SDS, 0.5% Deoxycholic acid) before loading on SDS–PAGE. Detection was performed by immunoblotting, using specific antibody. For Ub-biotinylated the detection was performed using HRP-streptavidin. A coomassie-stained membrane was used to show the loading of GST-fusion protein after immunoblotting

## 9. *In vitro* Transthiolation assay

Different new E1 concentrations were simultaneously tested comparing with 100ng of E1 in used. The reaction was performed with 100ng of E1 in presence of 1mg of Ub-

biotenylated and 2 mM ATP in *in vitro* Ub-buffer (25 mM Tris–HCl, pH 7.6, 5 mM $MgCl_2$, 100 mM NaCl, 0.2 μM dithiothreitol) at 37°C for 30 minutes. The reaction was stopped by addition of laemmli without DTT in order to detect the amount of E1~Ub. Samples were loaded on a SDS-PAGE gel and detection was made using HRP-streptavidin.

## 10. Directed yeast two-hybrid screen

10.1) Yeast growth conditions and strain

Yeast cells were grown in rich medium (YPD; 1% yeast extract, 2% peptone, 2% glucose) or synthetic minimal medium (0,67% yeast nitrogen base without amino acids) with glucose 2% (SD), galactose 2% (SGal) or raffinose 2% (SRaf) as carbon source and amino acids as required. Yeast strain used for the screen is AH109 (Clontech).

| **Yeast strain** | **Reporter gene** | **Transformation markers** |
|---|---|---|
| AH109 | HIS3, ADE2, lacZ, MEL1 | Trp1, Leu2 |

10.2) Constructs and plasmids for yeast two hybrid screening

DNA encoding for Rabex-5 (1-74) domain was obtained by PCR amplification and subcloned into pGBKT7- bait vector (Clontech) and the construct was sequence verified. The E2s DNA cloned into pACT2-prey vector (Clontech) were kindly provided by Rachel Klevit(Christensen et al., 2007).

pGBKT7 contains TRP1 nutritional gene, whereas pACT2 contains LEU2 nutritional gene to allow yeast growth on limiting synthetic media.

10.3) High-efficiency LiAc transformation

AH109 cells were inoculated in an appropriate volume of YPD complete medium to obtain $5x10^6$ cells/ml culture. After o.n. growth at 28-30°C cells were centrifuged at 4000 rpm for 3 minutes at room temperature and pellets were resuspended in 2 ml of LiAc/TE solution (LiAc 0,1 M/TE 1x) and incubated for 40 minutes-1h at 28-30°C. Competent cells were then centrifuge at 4000 rpm for 3 minutes at room temperature and pellets were resuspended in 400µl of LiAc/TE solution, and incubated (100µl of cells per transformation) for 40 minutes at room temperature with plasmid DNA to be transformed (100 ng), along with excess carrier DNA (100µg). 1 ml solution of 40% Polyethylene glycol (PEG) 6000 in LiAc/TE is then added and the mixture of DNA and yeast cells and incubated for additional 40minutes-1hour. After the incubations, the cells were heat shocked for 30 minutes at 42°C, to allowed the DNA to enter the cells. The cells are then plated on the appropriate medium to select for transformants containing the introduced plasmid(s).

10.4) TCA yeast protein extraction

Yeast protein extraction was performed with Tricloroacetic acid (TCA). This method is very efficient to avoid proteolytic phenomena when cells are broken.

Cells from an exponentially growing colture were collected and centrifuged for 5 minutes at 4000 rpm. Then cells were washed with 1ml of TCA 20%, vortexed, transferred to 2 ml microfuge tubes and centrifuged for 2 minutes at 14000 rpm. The pellet was resuspended in 100 µl of TCA 20% and an equal volume of acid-washed glass beads (Sigma) was added, leaving a layer of supernatant over the beads. The samples were then vortexed continuously for 4 minutes in order to break the cells. Lysed cells were transferred to a fresh tube, and the beads were washed twice with 100 µl of TCA 5%. In this way, each

tube contains 300 µl of liquid with 10% TCA final concentration. Samples were centrifuged at 4000 rpm for 10 minutes. The pellet was resuspended in 50 µl Laemmli buffer 1x (mix colour should be yellow). To neutralize the acid pH 25 µl of Tris Base 1M were added to each sample (mix colour should turn blue). Then the protein extract was boiled at 95°C for 3 minutes and centrifuged again at maximum speed. Finally, the supernatant, containing the final protein extract, was collected in a new tube and extracts were stored at -20°C.

## 11. Disulfide bond reaction

The formation of the disulfide bond was conducted as described in reference (Serniwka and Shaw, 2009) with a dialysis treatment in disulfide-bond buffer (100 mM $Na_2HPO_4^-$ $NaH_2PO_4$, pH 7.5, 200 mM NaCl, 5% glycerol and 25 µM $CuCl_2$) at room temperature. Disulfide bond formation was monitored by nonreducing SDS-PAGE until Ub G76C monomer depletion. HECT~Ub complex was obtained by mixing together 100µM of HECT C778S/IΔC$^{627}$NP with 100µM of UbG76C and subsequently the complex was purified through anionic exchange column (Resource Q) in the following buffer: 20mM Tris-HCl pH 8.0, 5% glycerol, 10mM of $CuCl_2$ using a NaCl gradient from 2 mM to 500 mM. The Ube2D3~Ub complex was obtained mixing together 100µM of E2 (C21S/C107S/C111S) mutant with 500µM of UbG76C in a molar ratio of 1:5. Purification step performed on an anionic exchange column (HiTrap S) using a NaCl gradient form 30mM to 500mM and fraction's composition was analyzed by loading on a non-reducing SDS-PAGE gel. With this column we were able to purify the E2 species from $Ub_2$ and Ub alone due to the difference of the isoelectric points. Fractions were collected and concentrated with centricon of 3kDa of cut-off.

## 12. Isopeptide bond reaction

The enzymatic reaction was performed by incubating 200μM of Ube2D3 S22R/C85K with 200μM of $His_6$-tagged ubiquitin and 1μM of E1 at 37°C for 26h in a buffer containing 3mM ATP, 5mM $MgCl_2$, 50mM Tris-HCl pH 10.0, 150mM NaCl. The E2-Ub conjugate was purified by $Ni^{2+}$-affinity chromatography and the E2-Ub was eluted from beads using 200mM imidazole. The last purification step was done by size exclusion chromatography, using a Superdex 75. Fraction's composition was analyzed by loading on a reducing SDS-PAGE gel and the most pure fractions were collected and concentrated with concentricon of 3kDa of cut-off.

## 13. Disulfide bond stability assay

The kinetic experiments were performed by incubating 60μM of purified E2~Ub (see Material and Methods paragraph 11) in the presence of 5μM of Rabex-$5^{1-74}$ WT or mutants in ubiquitination buffer (25mM Tris-HCl pH 7.6, 5 mM $MgCl_2$, 100 mM NaCl) at 37°C. E2~Ub disulfide disruption was monitored by quenching the reaction at different time points with Laemmli buffer without reducing agent (i.e. DTT) and analyzing the presence of free-Ub by immunoblot with anti-Ub (ZTA10, generated in house, dilution 1:5).

## 14. Isothermal Titration Calorimetry

ITC measurements were performed on a MicroCal VP-ITC (MicroCal, Inc.) instrument at 24°C. All proteins were extensively dialyzed against ITC buffer (20mM tris HCl pH 8.0, 200mM NaCl, 5% glycerol and 1mM DTT). Rabex-$5^{1-74}$ WT at a concentration of 0.74-0.91mM was injected into 2ml of solution containing 35μM of Ube2D3-Ub or Ub alone in

injection of 4µl. Experimental heats were corrected by subtracting the blank measurements and analyzed using the Origin software package. Binding constants and other thermodynamic parameters were calculated by fitting the integrated titration data assuming a single binding site.

## 15. Crystallization trays

The crystallization screening experiments were performed with a Honeybee Cartesian nano-dispenser robot by sitting-drop vapor diffusion method at 20°C and 4°C, allowing us to screen at the same time 96 different conditions using commercially available kits (Hampton, Qiagen). To screen for initial crystallization conditions, 100nl of protein solution, at specific concentration, was mixed with 100nl reservoir solution and equilibrated against 150ml of reservoir solution. Different commercial crystallization screens were tested such as the Morpheus, Midas, JCSG+, PACT, Pro-complex, Index.

## 16. Small Angle X-ray Scattering (SAXS)

SAXS data were collected at the BM29 beamline of the European Synchrotron Radiation Facility (Grenoble). Data were collected for HisUb-loaded UbcH5c S22R/C85K through the isopeptide bond, Rabex-$5^{1-74}$ A58G and the complex formed in a ratio 1:1 at 250mM in a final volume of 90ml. Rabex-$5^{1-74}$ A58G and the complex were run on a size exclusion chromatography (Superdex 75) using a SAXS compatible buffer (20mM Tris-HCl pH 8.0, 200mM NaCl, 5% glycerol and adding fresh TCEP). Next, they are analyzed by X-Ray scattering. On the contrary the E2-Ub was directly analyzed by SAXS due to it is homogeneous.

## 17. *In vitro* ubiquitination assay using protein microarray (Life Sensor)

### 17.1 Array Hybridization

Protein microrrays were removed from -80°C storage and placed at room temperature (RT) for 15 minutes in a sealed, dessicated container before opening, to avoid formation of condensate. The arrays were rehydrated in a solution of 1M urea, 0.5M ethanolamine, pH 7.5, 25% glycerol, 20mM glutathione, and 1mM DTT for 30 min at RT. The arrays were washed twice in PBST (PBS containing 0.1% Tween-20) and then blocked for 1 hour at RT in PBST containing 20mM reduced glutathione, 1mM DTT, 5% BSA, and 25% glycerol. Each array was ubiquitylated with TAMRA-labeled ubiquitin (Ub-TMR), ubiquitin activating enzyme (UBE1), 100nM UBE2D3, and His-MBP-Rabex-5 full length for 120 minutes RT. The ubiquitylation buffer also contained 20mM Hepes, pH 7.4, 150mM NaCl, 0.5mM DTT, 1mM ATP, 2mM $MgCl_2$, and an ATP regeneration system consisting of creatine phosphate, creatine phosphokinase, and inorganic pyrophosphatase. A control array was treated with the same reaction mixture minus the E3. Arrays were washed with three changes PBST, four changes 0.2 micron-filtered water, and then centrifugally dried (1000 RPM for 5 minutes at RT). The arrays were scanned using a GenePix 4100A Microarray Scanner (Molecular Devices, Inc.) using the 532nm channel.

### 17.2 Data Analysis

Microarray images were gridded and quantitated using GenePix Pro (v7) software. Median intensities (features and local backgrounds) were utilized and median feature intensities minus background were calculated (F-B). Negative F-B values were assigned a value of one relative fluorescence unit for further calculations. F-B values for all both arrays, control (null), Rabex5-treated, were log(base 2) transformed and subjected to Quantile Normalization (Bolstad, Irizarry et al. 2003; Reimers 2010) to normalize intensity ($I_N$)

between arrays and remove technical sources of error (print-tip and location). Control $I_N$ values were subtracted from experimental $I_N$ values to yield the final estimate of magnitude change ($M_N$). Duplicate features (representing identical proteins) were used to calculate the average (avg $M_N$) and standard deviation. *Note that although calculation of standard deviation technically requires three data points, Excel will report a value from two, useful for estimating reproducibility.* T-test (paired, 2 tailed) was used to assess the probability that the experimental $I_N$ value was different from the control $I_N$ value. A threshold of 95% confidence ($p < 0.05$) was employed to filter data.

# RESULTS

## Characterization of E3 ligase activity of HECT$^{Nedd4}$

Nedd4 is a well-characterized E3 ligase able to catalyze the formation of Lys63-linked chains through a sequential addition mechanism. By solving the structure of the HECT domain in complex with free Ub we have structurally characterized the UBD, present in the N-lobe, which interacts with Ub in a non-covalently manner (Maspero et al., 2011). We have shown that this surface plays a critical role in the enzyme processivity to promote substrate polyubiquitination (Maspero et al., 2011) (**Figure 19**). Yet, the mechanism used by Nedd4 to achieve linkage specificity remains poorly understood.

We aimed at to understanding the detailed molecular mechanism of how HECT$^{Nedd4}$ domain transfers the donor Ub (Ub$^{D}$) from the catalytic cysteine to the growing chain on the substrate. Our goal was to solve the structure of a catalytic intermediate formed by the Ub$^{D}$-charged HECT$^{Nedd4}$ domain and the acceptor Ub molecule non-covalently bound to the UBD.

### 1. Catalytic intermediate of the HECT$^{Nedd4}$ domain

To crystallize the catalytic intermediate (HECT~Ub$^{D}$:Ub) we needed an HECT~Ub complex stable in crystallization conditions and easy to produce in a large amount. In the case of naturally occurring thioester bond, we envisioned two major caveats: i) the low yield of the enzymatic production of the HECT~Ub intermediate, ii) the short life of the thioester HECT~Ub bond that is prone to rapid transfer Ub$^{D}$ from the catalytic cysteine to any acceptor lysine (even of the enzyme itself).

To overcome these problems we replaced the thioester bond with a stable disulfide bond that we chemically generated between the catalytic cysteine (C867) of the HECT domain and a modified form of the Ub$^{D}$ (**Figure 23A**). NMR studies have shown that the

disulfide bond nicely mimics the native thioester bond, most likely thanks to the flexibility of Gly76 in the thioester, able to compensate for the extra bond length distance present in the S-S bridge (Serniwka and Shaw, 2009). The Ub protein does not possess any Cys. Thus, to mimic the thioester bond we replaced the last Gly (G76) of the Ub moiety with a Cys residue generating the UbG76C mutant.

The chemical reaction needed to generate the disulfide bond is, in principle, not able to distinguish between the catalytic cysteine and the other cysteines present in the HECT domain. Thus, we mutagenized the two additional non-catalytic Cys of the HECT domain, C627 and C778, which are positioned in the UBD of the N-lobe and in close proximity to the flexible linker, respectively.

Once mutated to Ser we verified whether the Ub binding ability of the generated mutants was altered. A pull-down assay was performed incubating 2μM of GST-HECT mutants with 250ng of K63-linked Ub chains for 2h (**Figure 23B**). We used GST-HECT wild type as positive control for the binding while as negative control either GST alone or the GST-HECT F707A mutant, previously demonstrated to be impaired in the Ub binding (Maspero et al., 2011). Results showed that single point mutation of C778 residue did not affect Ub binding ability (**Figure 23B**) whereas the mutation of C627 residue caused a severe impairment in Ub binding. This is possibly due to its position in the middle of the UBD.

We thus decided to replace C627 and its surrounding residues with the amino acids sequence of Nedd4 yeast counterpart, Rsp5, which naturally does not possess Cys residue in this region (**Figure 23C**) but has the same structural folding of the $HECT^{Nedd4}$ (**Figure 23D**). Therefore we mutagenized the HECT C778S in the context of a few amino acids substitution ($I\Delta C^{627}NP$, details in the materials and methods) generating the double mutant HECT $I\Delta C^{627}NP$/C778S that was subsequently tested in pull-down assay with K63-linked

Ub-chains. Results demonstrated that the IΔC$^{627}$NP mutation was able to restore the Ub binding ability of the HECT domain lacking the two non-catalytic cysteines (**Figure 23E**).

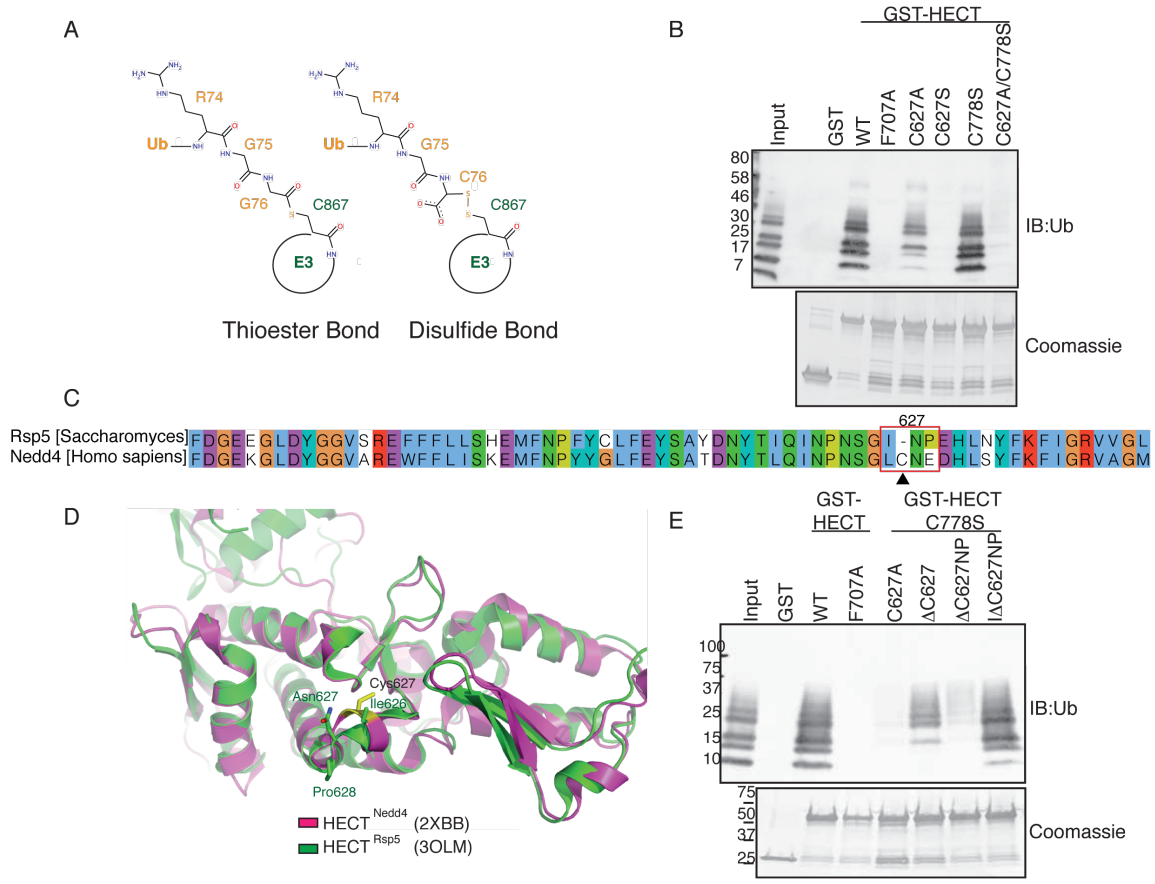


**Figure 23. Generation of the HECT mutant for the disulfide bond.** (A) Schematic drawing of the naturally occurring thioester bond between the catalytic cysteine (Cys867) of the HECT$^{Nedd4}$ domain and the C-terminal of Ub. To mimic the short-lived thioester bond we replaced it with a stable disulfide bond chemically produced between the Cys867 of the HECT domain and the cysteine of Ub (G76C) mutant. (B) Different HECT mutants were tested for their ability to bind Ub by GST pull-down assay. The indicated GST-fusion proteins were incubated for 2h at 4°C in YY buffer with synthetic K63-polyUb chains and analyzed by immunoblotting (IB) anti-Ub as indicated. Coomassie staining shows comparable loading of GST proteins. (C) Sequence alignment, color-coded according to ClustalX, of the region surrounding the Cys627 of the HECT domains of human Nedd4 and yeast Rsp5, performed with Muscle program. Region mutated in the HECT$^{Nedd4}$ to produce the stable disulfide bridge with Ub is indicated with a red box and the Cys627 is highlighted by a black triangle. (D) Cartoon representation of the region surrounding the Cys627 of the HECT$^{Nedd4}$ WT (in purple, PDB:2XBB) superposed to HECT$^{Rsp5}$ (in green, PDB:3OLM) showing the difference in the secondary structure of the region of interest. (E) As in (B), different HECT mutants were tested for their ability to bind Ub using synthetic K63-polyUb chains by GST pull-down assay. GST and GST-HECT F707A were negative control, GST-HECT WT was a positive control.

Next, the HECT C778S/IΔC$^{627}$NP mutant was produced in bacteria as GST-tagged protein. We removed the GST tag by Prescission protease cleavage (**Figure 24A**) and purified the HECT by size exclusion chromatography (Superdex 200 column) (**Figure 24B**). The untagged ubiquitin G76C mutant was produced and purified through an acid precipitation (**Figure 24C**) (for details see Materials and Methods). Then it was purified by a size exclusion chromatography (Superdex 75 column) in which the UbG76C was eluted from 70 to 90ml of elution volume (**Figure 24D**). Proteins and nucleic acids composed other peaks as contaminants.

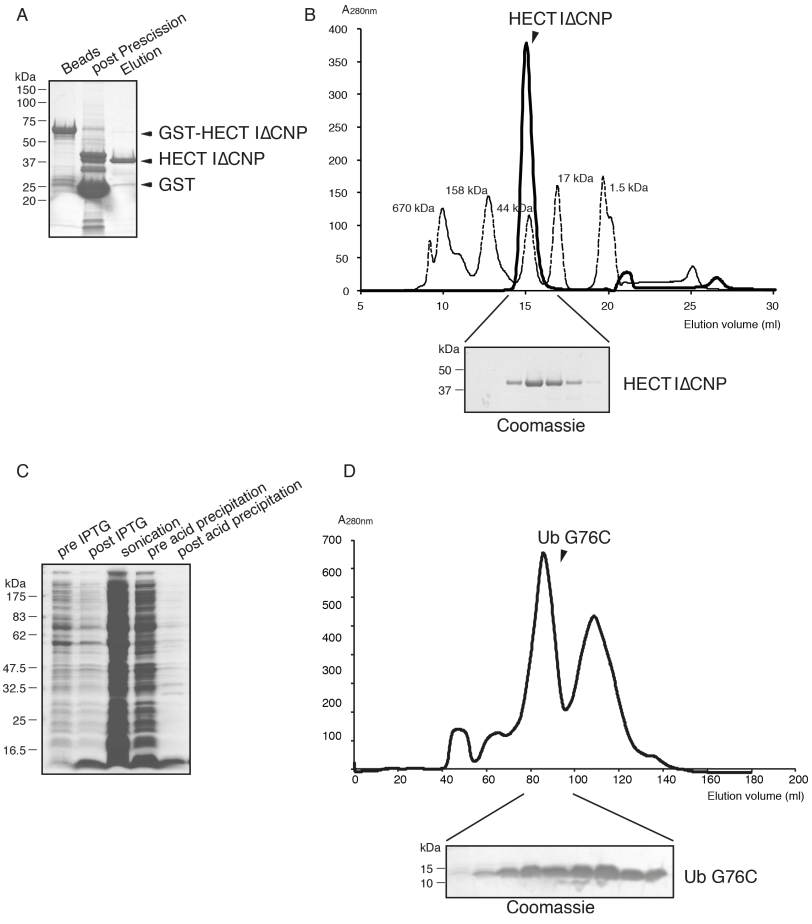


**Figure 24. HECT C778S/IΔC$^{627}$NP and UbG76C production and purification**. (A) Example of HECT C778S/IΔC$^{627}$NP cleavage from glutathione beads incubating with Prescission protease. First and second lanes were beads before and after cleavage, respectively. In the third line there was the HECT sample needed to be purified. (B) Elution profile of cleaved HECT C778S/IΔC$^{627}$NP on a size exclusion column (Superdex 200). Fractions depicted were loaded on a reducing SDS-PAGE gel and Coomassie staining was performed. (C) Example of UbG76C production. Lane 1 and 2 were bacteria lysates pre and post-induction with IPTG. Lane 3 was

bacteria lysate post-sonication. Lane 4 and 5 were respectively pre and post-acid precipitation. (D) Chromatogram from size exclusion chromatography (Superdex 75 column). Lower panel's fractions from the peak loaded on a reducing SDS-PAGE gel.

Once we obtained the purified proteins, we set up the disulfide bond reaction with a dialysis treatment in disulfide bond buffer supplemented with 25μM of $CuCl_2$ (Merkley et al., 2005). The reaction was performed mixing together the two proteins at 1:1 molar ratio with a final concentration of 100μM/each. The disulfide bond formation was stopped by adding laemmli without DTT and was monitored by non-reducing SDS-PAGE. After 48h the free UbG76C was exhausted and large amount of HECT~Ub was obtained (**Figure 25A**).

For successful crystallization trials, homogeneous, highly pure and concentrated sample is required. Since it is a chemical reaction, we obtained not only the heterodimer HECT~Ub but also HECT~HECT and Ub~Ub homodimers as well as single, not-modified proteins. To purify the HECT~Ub from the mixture, we performed an anionic exchange column (Resource Q), taking advantage of a sizeable difference in isoelectric points of the different species. Fractions were monitored by a non-reducing SDS-PAGE followed by a Coomassie staining. In these conditions we were able to separate the HECT~Ub from other proteins, and in particular from the HECT domain alone. Pure fractions comprised between 140-160 ml of elution volume were collected (**Figure 25B**).

To obtain the complex for crystallization, we mixed together the purified HECT~Ub with free Ub wild type in a 1:2 molar ratio in order to saturate the UBD in the N-lobe. The complex was subsequently concentrated until 37 mg/ml using Centricon column (Millipore) with a cut-off of 3kDa.

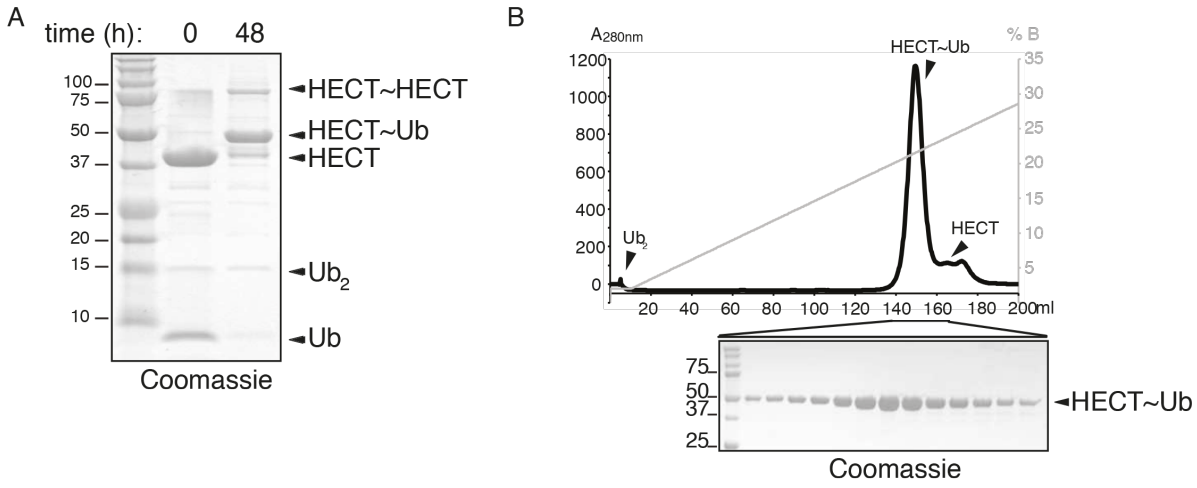


**Figure 25. Preparation of HECT$^{Nedd4}$~Ub$^{D}$ complex.** (A) Disulfide bond reaction between HECT C778S/IΔCNP and Ub G76C, in specific dialysis buffer supplemented with $CuCl_2$, monitored by non-reducing SDS-PAGE and Coomassie staining. At 48h the reaction was stopped due to Ub monomer depletion. (B) Elution profile of anionic exchange column, based on a NaCl gradient, showing the separation of HECT C778S/IΔCNP~Ub from HECT C778S/IΔCNP dimer, monomer and Ub dimer. Lower panel, Coomassie staining shows fractions composition from the peak containing HECT C778S/IΔCNP~Ub, loaded on non-reducing SDS-PAGE.

## 2. Crystal structure of the catalytic intermediate (HECT$^{Nedd4}$~Ub$^{D}$:Ub)

We tested several crystallization conditions with a number of commercially available nanovolume crystallization screening trays, performed at the High Throughput Crystallization Laboratory (HTX Lab) of the EMBL Grenoble outstation. Crystals were then reproduced in house, in collaboration with the Crystallization Unit at the IFOM-IEO campus, using a Honeybee liquid Cartesian robot by sitting drops vapor diffusion method, allowing us to monitor with an automated imaging system (CF400, Bruker) the 96-well plates.

Diffracting crystals were obtained at 4 °C in 2.4–2.6 M sodium malonate, pH 5.7–6.2 (**Figure 26A**). Crystals were harvested from the 96-well plate and directly vitrified in liquid nitrogen and data were collected at the European Synchrotron Radiation Facility (Grenoble). Data collection, data processing, model building and refinement was carried

out by the head of the crystallization facility, Sebastiano Pasqualato, who previously solved the HECT:Ub structure (Maspero et al., 2011). The crystal structure of the complex ($HECT^{Nedd4}$~$Ub^{D}$:Ub) was determined at 2.51Å resolution (**Table 2**).

**Table 2: Data collection and refinement statistics**

| | $HECT^{Nedd4}$~$Ub^{D}$–Ub |
|---|---|
| Data collection | |
| Space group | R 32:h |
| Cell dimensions | |
| a, b, c (Å) | 196.54, 196.54, 98.77 |
| α, β, γ (°) | 90, 90, 120 |
| Resolution (Å) | 56.74–2.51 (2.57–2.51) |
| $R_{merge}$ | 8.8 (88.5) |
| $I / \sigma I$ | 16.6 (2.9) |
| Completeness (%) | 100.0 (100.0) |
| Redundancy | 7.4 (7.5) |
| Refinement | |
| Resolution (Å) | 56.74–2.51 |
| No. reflections | 22,567 |
| $R_{work}$ / $R_{free}$ | 18.4 / 22.9 |
| No. atoms | |
| Protein | 4,381 |
| Water | 112 |
| B factors | |
| Nedd4 HECT domain | 52.8 |
| $Ub^{D}$ | 50.4 |
| Ub | 82.3 |
| Water | 46.1 |
| r.m.s. deviations | |
| Bond lengths (Å) | 0.008 |
| Bond angles (°) | 1.12 |

[a]Values in parentheses are for highest-resolution shell.

As expected, loading of the $Ub^{D}$ onto $HECT^{Nedd4}$ catalytic cysteine is compatible with non-covalently Ub binding. The N-lobe adopts the same conformation in the presence

or absence of $Ub^D$ (root-mean-square deviation -rmsd- of 0.8 Å over 258 Cα) with free Ub kept in the binding site crafted by the N-lobe subdomains (Maspero et al., 2011).

Previous structures of various HECT domains have already shown the extreme flexibility between the N- and C-lobes (**Figure 14**). This was the first structure of an Ub-loaded HECT E3 ligase primed for catalysis and showed an "inverted T" shape conformation with the C-lobe sited at the middle of the N-lobe.

The overall HECT domain structure remarkably resembles that of Nedd4-like HECT domain ($HECT^{Nedd4L}$) crystallized in complex with Ube2D2~Ub (Kamadurai et al., 2009), (**Figure 26B**, superposition with a rmsd of 1.1 Å over 369 Cα). This is the first time that two C-lobes from different HECTs show the same orientation. Strikingly, the $Ub^D$ in the $HECT^{Nedd4}$~$Ub^D$:Ub structure sits in the same position as the Ub loaded on the E2 in $HECT^{Nedd4L}$: Ube2D2~Ub structure (Kamadurai et al., 2009).

As the interaction pattern between the C-lobe and $Ub^D$ is unaltered with respect to what described by Schulman and coworkers we conclude that we have trapped the following step in the E3-mediated ubiquitination reaction, in which $Ub^D$ has been handed over to the C-lobe, and is ready to be transferred to the substrate.

Differently from the bulk of conserved contacts between $Ub^D$ and the C-lobe (**Figure 26B**), the last three residues of $Ub^D$ display a dramatic re-arrangement with respect to the $HECT^{Nedd4\text{-}Like}$:Ube2D2~Ub structure (**Figure 26C**). The $Ub^D$ tail zips onto β-strand β9, upstream of the catalytic Cys867, and organizes a hydrogen bond pattern that results in β-sheet augmentation, a common motif in protein-protein interactions. These residues are thus locked in an extended conformation that causes the "stretch" of the Ub tail.

This re-arrangement of the $Ub^D$ tail orients the thioester bond, held on the HECT domain, resulting in an optimal conformation for nucleophilic attack by the incoming lysine residue of the substrate (Dou et al., 2012; Plechanovova et al., 2012).

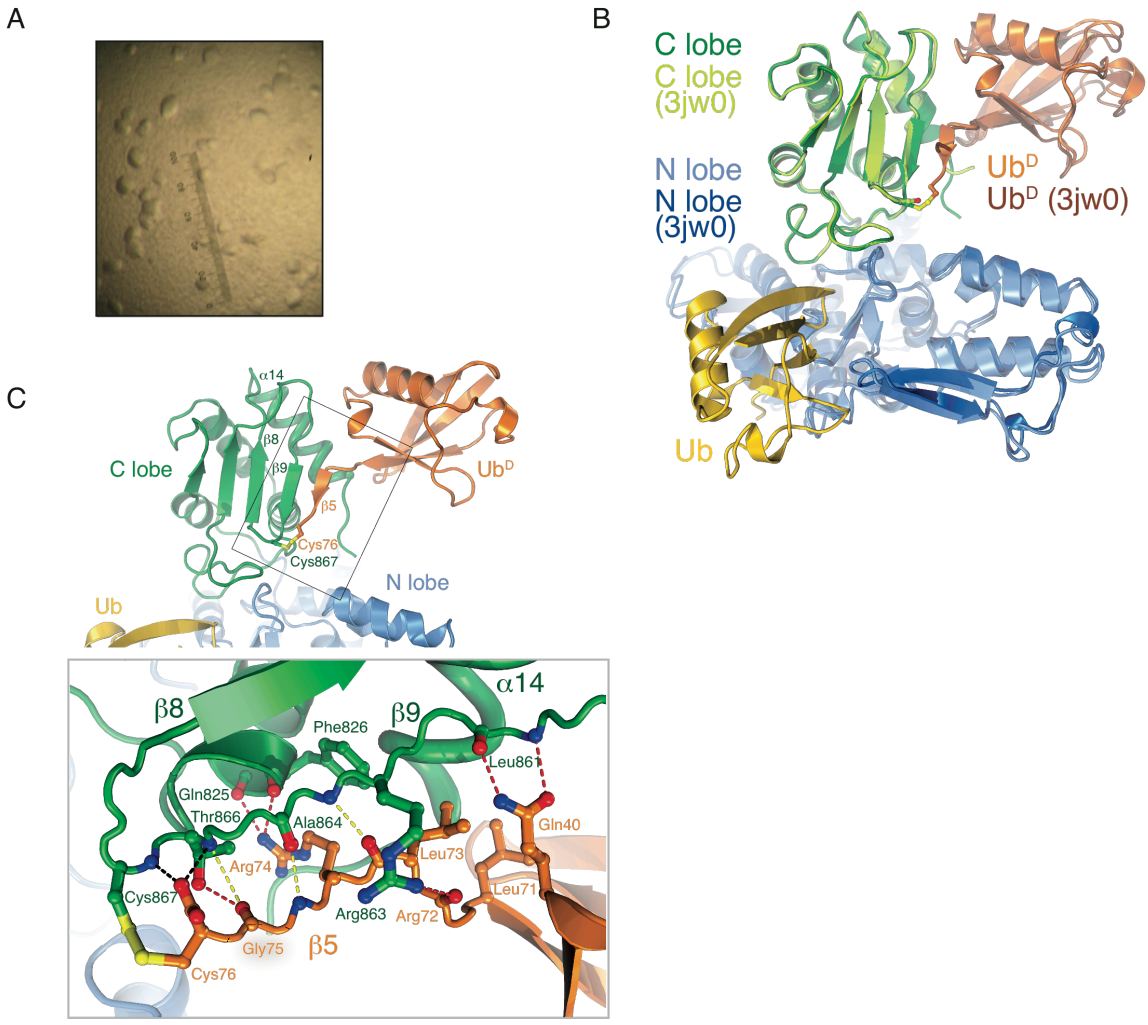


**Figure 26. Structure of the Ub-loaded HECT in complex with Ub.** (A) Image of diffracting crystals composed by HECT$^{Nedd4}$~Ub$^{D}$:Ub obtained at 4 °C in 2.4–2.6 M sodium malonate, pH 5.7–6.2. (B) Cartoon representation of the superposition of HECT$^{Nedd4}$~Ub$^{D}$:Ub with HECT$^{Nedd4L}$:Ube2D2~Ub (PDB:3jw0). Ube2D2 is not shown to allow a better view of the HECT and Ub superposition. N- and C-lobe of HECT$^{Nedd4}$ are in light blue and in dark green respectively; Ub$^{D}$ is in orange, non-covalently-bound Ub is in yellow. In the case of HECT$^{Nedd4L}$ N-, C-lobe and loaded Ub are in dark blue, light green and in brown, respectively. (C) Close-up of the Ub tail in the crystal structure of HECT$^{Nedd4}$~Ub$^{D}$:Ub. When bound to the catalytic cysteine of HECT$^{Nedd4}$, the ubiquitin tail zips onto β-strand β9, upstream the catalytic Cys867, and organizes a hydrogen bond pattern that results in a β-sheet augmentation.

## Characterization of Rabex-5 as E3 ligase

Rabex-5 is able to bind Ub through two independent UBDs, MIU domain and ZnF_A20 domain (**Figure 22**) (Lee et al., 2006b; Penengo et al., 2006). In addition, it has been demonstrated that Rabex-5 may exert an E3 ligase activity through its ZnF_A20 domain (Lee et al., 2006b). Due to the presence of A20 zinc finger domain (ZnF_A20) instead of a canonical RING domain, Rabex-5 can be defined as an atypical RING-E3 ligase. How Rabex-5 acts as E3 ligase is poorly understood and biochemical and structural information are lacking. Our aim was to validate the E3 ligase activity of Rabex-5 and to eventually characterize the molecular mechanism adopted by Rabex-5 to perform this activity.

### 3. Rabex-5$^{1-74}$ has an E2 binding domain

It is becoming clear that, at least for RING-type E3 enzymes, different combinations of E2/E3 enzymes catalyze the formation of different types of ubiquitin chains associated with distinct biological functions (Wickliffe et al., 2011; Williamson et al., 2009).

To determine which E2s can interact with Rabex-5, we carried out in the lab a yeast-two-hybrid screen (Y2H) using a library of E2s (Christensen et al., 2007) with Rabex-5$^{1-74}$ (containing both the ZnF_A20 and the MIU domains) as a bait (**Figure 27A**). This fragment has been previously shown to be sufficient for auto-ubiquitination (Lee et al., 2006b). Two families of E2s, Ube2D and Ube2E, were found to be positive for Rabex-5$^{1-74}$ interaction (**Figure 27A-B**). We therefore selected them for further validation.

First, we validated the Y2H by a pull-down assay, using *in vitro* translated Ube2D3 and Ube2L3 as negative control. Pull-down experiment was performed incubating 4μM of GST- Rabex-5$^{1-74}$ with 8μl of *in vitro* translated ([$^{35}$S]-methionine) E2s for 2h at 4°C. After washes with YY buffer, samples were loaded either on a reducing (100 mM DTT) SDS-PAGE gel (**Figure 27C**-left panel) or on a non-reducing SDS-PAGE gel (**Figure 27C**-

right panel) and detection of the binding was done by autoradiography.

As shown in **Figure 27C,** in both conditions the positive hit Ube2D3 showed a clear binding to GST-Rabex-5$^{1-74}$ while Ube2L3 was negative. This assay confirmed the Y2H result, demonstrating a specific recognition of the E2 moiety by Rabex-5$^{1-74}$. Based on these results, we used and referred to Ube2D3 as the specific E2 of Rabex-5. Caveat of this experiment is that the loading with Ub of the E2s, detected in the input in absence of DTT (**Figure 27C**-right panel), is less efficient in the case of Ube2L3 respect Ube2D3.

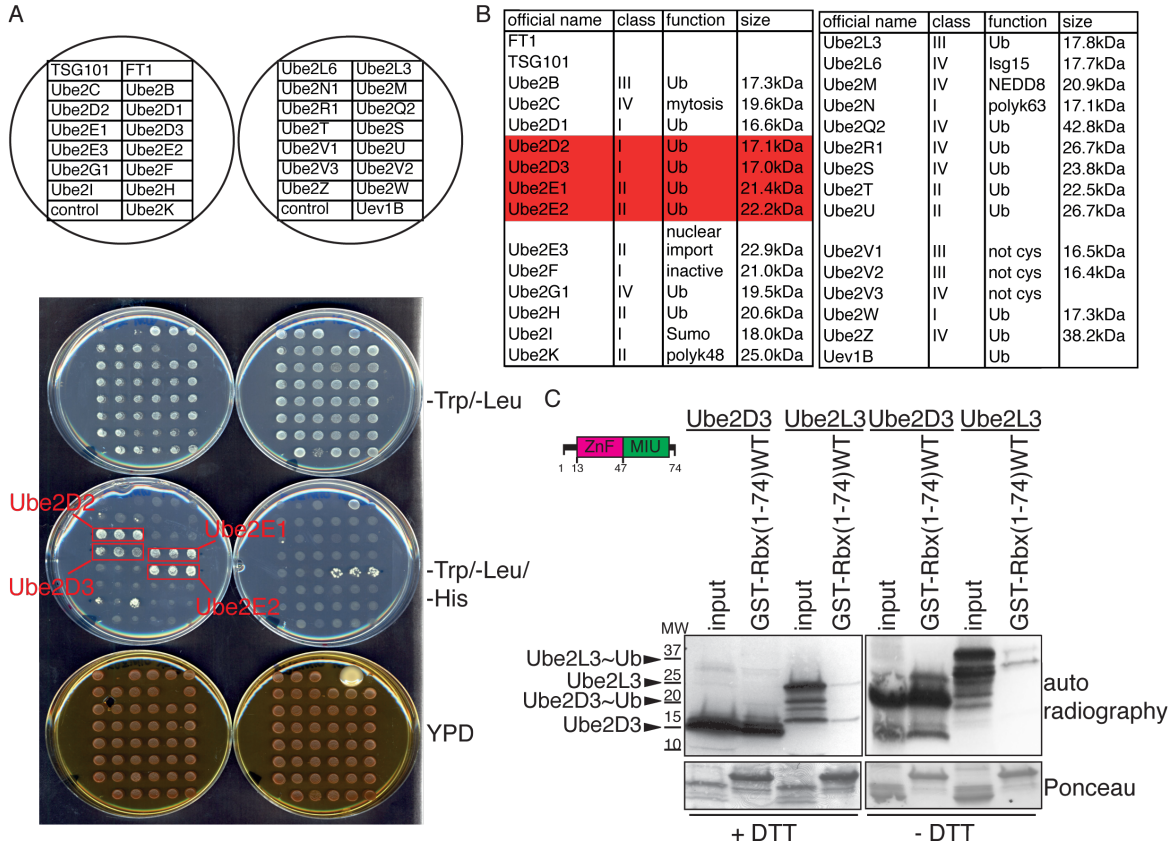


**Figure 27. Interaction between Rabex-5 and specific E2s.** (A) Schematic representation of the plated transformants. Rabex-5$^{1-74}$ was expressed in fusion with GAL4 DNA binding (Kim et al., 2007) protein and its interaction with different E2 proteins fused with GAL4 activation domain (AD) was tested by yeast two-hybrid assay. Triplicate of yeast transformants were grown on SD medium lacking indicated amino acids. Protein interaction was assessed from growth on SD -Trp -Leu -His medium (middle panel). The presence of both the fusion proteins was assessed from growth on SD -Trp -Leu (top panel) and yeast strain viability was assessed from growth of complete medium (bottom panel). (B) Panel of the different E2 screened showing their main features. Four E2s are highlighted in red as positive interactors of Rabex-5$^{1-74}$. (C) Pull-down assay performed with GST-Rabex-5$^{1-74}$ and *in vitro* translated E2s ($^{35}$S-methionine), Ube2D3 and

Ube2L3, respectively a positive and negative hit in Y2H. On the left washes of pull-down experiments were made in buffer containing 100mM DTT and on the right all the experiment is performed in absence of reducing agent to score the loaded statues of the E2s. Detection was made by autoradiography.

**4. The interaction between Rabex-5 and Ube2D3 is mediated by ubiquitin**

To better characterize whether the E2:Rabex-5 interaction is Ub-dependent or independent, we performed the same pull-down experiment with *in vitro* translated Ube2D3(C85S) mutant. We mutagenized the catalytic cysteine (C85) of Ube2D3 to a less-reactive serine to obtain a stable *in vitro* translated Ub-loaded-E2 through oxyester bond (Plechanovova et al., 2011). Using this mutant we can visualize and distinguish in the input not only the E2 alone but also the Ub-loaded-E2 (**Figure 28A**-first line). We then performed a pull-down assay using 4μM of GST-Rabex-$5^{1-74}$ wild type with 8μl of *in vitro* translated Ube2D3 C85S for 2h at 4°C. As shown in **Figure 28A**, Rabex-5 clearly demonstrated a preference for the Ub-loaded Ube2D3 even if the stoichiometry of the E2 species in the input was unbalanced towards the E2 alone. With this assay we proved that Ub plays a critical role in the binding to activated E2.

Next, we intend to determine which UBD of Rabex-5 is involved in the binding. To this end, we tested GST-Rabex-$5^{1-74}$ constructs with specific mutations that abrogate the binding with ubiquitin: Y25F for the ZnF_A20 domain and A58G for the MIU domain (Penengo et al., 2006). Our analysis suggested that both UBDs participate to the binding to Ub-loaded E2 as only the double mutant showed a clear impairment (**Figure 28A**).

The same experiment was repeated with GST-Rabex-5 full-length protein and also in this case we found a preferential binding for the Ub loaded form of the E2 (**Figure 28B**). As shown in **Figure 28B** Rabex-5 full-length and Rabex-$5^{1-74}$ bind Ub loaded E2 in comparable manner, suggesting that no additional domains are required.

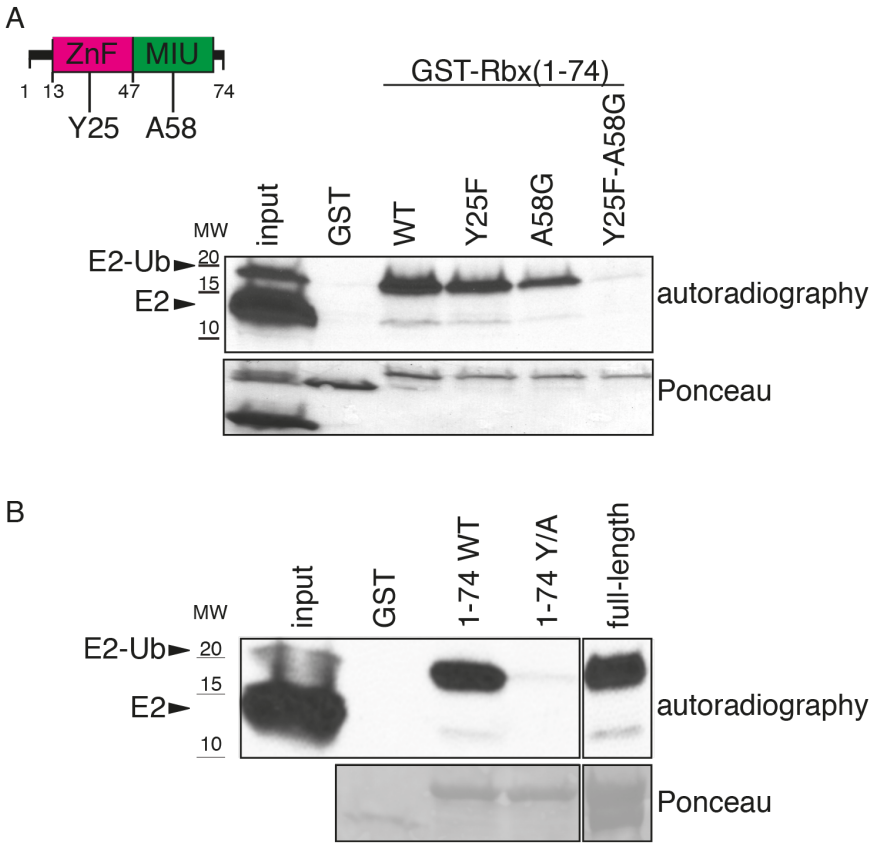


**Figure 28. Interaction between Rabex-5 and Ube2D3 is mediated by Ub.** (A) Pull-down assay performed with GST as negative control, GST-Rabex-$5^{1-74}$ WT and UBDs mutants (Y25F for the ZnF_A20 domain and A58G for the MIU domain) with *in vitro* translated Ube2D3 C85S. Ube2D3 C85S formed a non-reducible oxyester bond with Ub (input line). Washes were made with buffer containing 100mM DTT and detection was made by autoradiography. (B) Same as in (A), using GST-Rabex-$5^{1-74}$, GST-Rabex-5 full-length and GST-Rabex-$5^{1-74}$ Y/A (double mutants in Y25F and A58G)

We also performed a pull-down experiment with the isolated UBDs. To skip ([$^{35}$S]-methionine labeling of the E2, we used a Ube2D3 modified with an isopeptide bond between the E2 and Ub. This strategy has been recently proved to be successful to mimic the thioester bond E2-Ub in the crystallization of the E2-Ub:RNF4 complex (Plechanovova et al., 2012). This product was obtained as described later (paragraph 5.2). The isolated UBDs of Rabex-5, Rabex-$5^{1-49}$ (ZnF_A20 domain) and Rabex-$5^{48-74}$ (MIU domain), either wild type or harboring single point mutation were produced as GST proteins. To mimic competition, as for the previous experiments, we mixed the E2-Ub and E2 alone in a 1:3

molar ratio. Pull-down assay was performed incubating 2μM of GST-proteins with 2μM of the E2 mix for 2h at 4°C. After washes with YY buffer, samples were loaded on a reducing SDS-PAGE gel. Detection was performed using anti-Ube2D antibody.

Also in this case, results were not conclusive regarding the relative importance of the two UBDs. We confirmed selective binding to the E2-Ub also for GST-Rabex-$5^{1-49}$ and GST-Rabex-$5^{48-74}$ and, we found that single point mutants on the UBD were able to impair E2-Ub binding **(Figure 29)**.

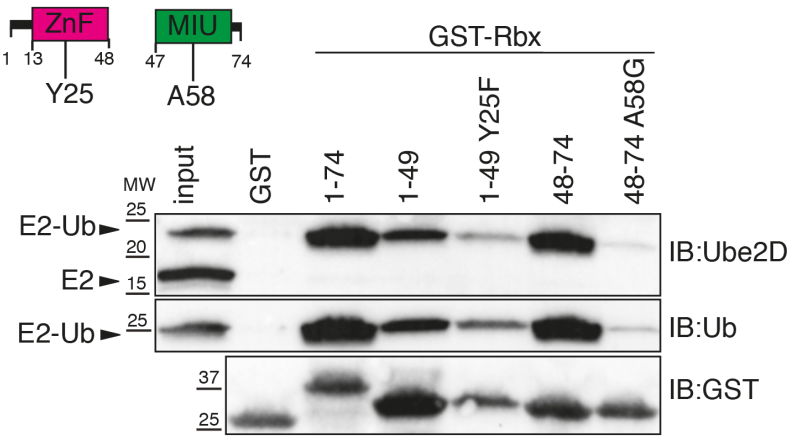


**Figure 29. Interaction between Rabex-5 fragments and Ube2D3.** Pull-down assay performed with GST, GST-Rabex-5 UBDs fragments and mutants (Y25F for the ZnF_A20 domain and A58G for the MIU domain) with a mix composed by a 3:1 molar ratio of Ube2D3 C85K and the Ub modified E2 (E2-Ub). Washes were made with buffer containing 100mM DTT and analyzed by IB as indicated.

Finally, we measured the binding affinity between Rabex-$5^{1-74}$ wild type and Ub-loaded Ube2D3 performing the isothermal titration calorimetry (ITC). This technique allows the measurement of the affinity constant (the reciprocal of the dissociation constant $K_D$) between two proteins in solution. For the ITC experiment, Rabex-$5^{1-74}$ was produced as GST protein, cleaved from GST tag by Prescission protease treatment and purified by size exclusion chromatography (Superdex 75 column) using an ITC compatible buffer (20mM Tris-HCl pH 8.0, 200mM NaCl, 5% glycerol and 1mM DTT). The ITC measurements were performed titrating 740μM of Rabex-$5^{1-74}$ into 2ml of solution

containing 35μM of the Ube2D3-Ub (isopeptide bond) protein. Experimental heats were corrected by subtracting the blank measurements and analyzed using the Origin software package. Binding constants and other thermodynamic parameters were calculated by fitting the integrated titration data assuming a single binding site. The measured $K_D$ is 2.67 ± 0.06 μM (**Figure 30**, left panel).

Not surprisingly, direct binding with the E2 alone was impossible to measure. To evaluate the contribution of the E2 binding, we repeated the ITC measurement between Rabex-$5^{1-74}$ and Ub. Untagged Ub was produced by acid precipitation method and purified by size exclusion chromatography (Superdex 75 column) using the ITC buffer. 35μM Ub was titrated with 912μM Rabex-$5^{1-74}$. In this case we determined a $K_D$ of 5.9 ± 0.2 μM (**Figure 30**, right panel). Comparing the two $K_D$, we can assume that Rabex-$5^{1-74}$ has an E2 binding domain, which minimally contributes to the binding affinity. Thus, the initial interaction seems to be mediated by binding to Ub. The minimal E2 binding may facilitate the correct positioning of the E2 on Rabex-5. We are currently investigating which is the binding affinity for each GST-Rabex-5 fragments.

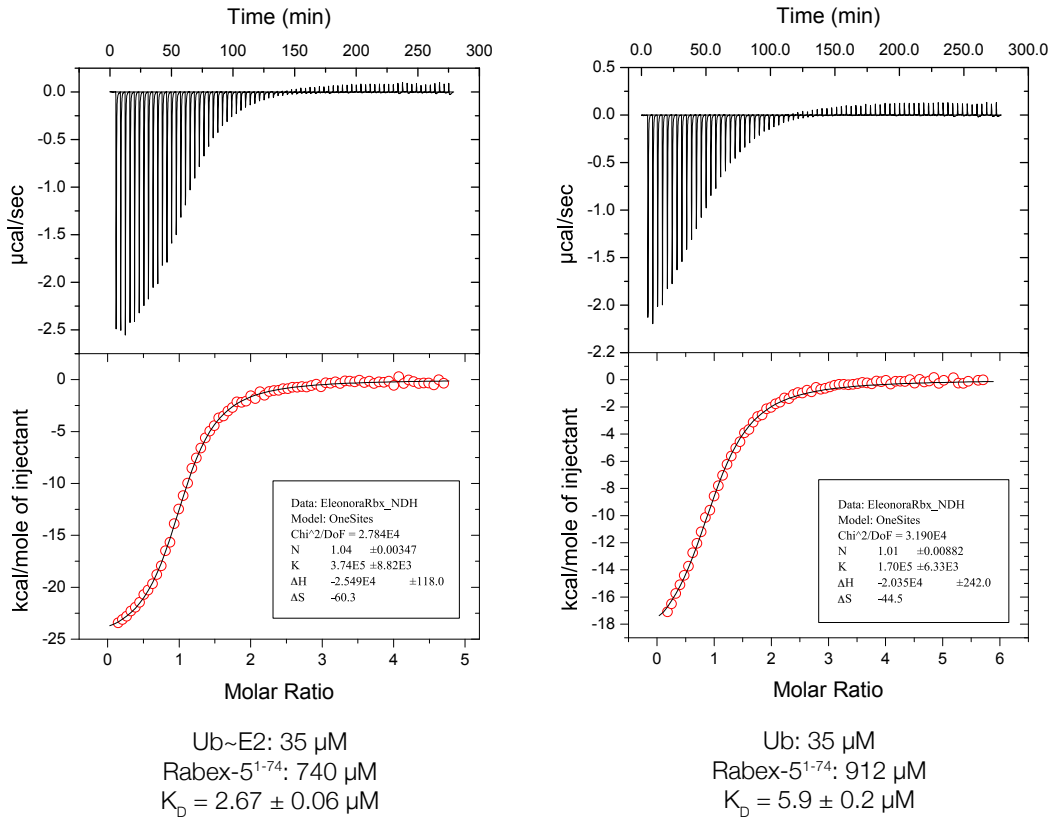


Ub~E2: 35 µM
Rabex-5$^{1-74}$: 740 µM
$K_D$ = 2.67 ± 0.06 µM

Ub: 35 µM
Rabex-5$^{1-74}$: 912 µM
$K_D$ = 5.9 ± 0.2 µM

**Figure 30. Isothermal Titration Calorimetry Assays.** Representative ITC curves are shown and the average $K_D$ with standard deviation for each data set is reported under each panel. Data were acquired and analyzed using the Origin software package. For each titration, the heat released upon E2-Ub:Rabex-5$^{1-74}$ WT or Ub:Rabex-5$^{1-74}$ WT association in the course of the ITC experiment, y axis, is displayed as a function of time, x axis (top quadrant). The integrated heats for each injection are plotted against the E2-Ub:Rabex-5$^{1-74}$ WT or Ub:Rabex-5$^{1-74}$ WT molar ratio together with the fitted curve (bottom quadrant).

## 5. Structure of the complex Rabex-5$^{1-74}$:Ube2D3~Ub

To understand the molecular mechanism exerted by Rabex-5 in the ubiquitination process, we set to crystallize a complex composed of our positive hit Ube2D3 loaded with Ub and Rabex-5$^{1-74}$. The latter product is soluble, easy to produce and purify (Penengo et al., 2006). The thioester-linked E2~Ub is a short-lived bond and highly unstable in crystallization conditions. To overcome this problem we tried different strategies.

### 5.1. Disulfide bond

As first strategy, we used the same approach that we successfully undertook to produce a stable Ub-loaded HECT (**Figure 23**). We replaced the thioester bond with a stable disulfide bond chemically produced between the catalytic Cys85 of the Ube2D3 and the one we introduced in Ub (G76C) (**Figure 31A**). To favor the catalytic Cys85 of Ube2D3 during the disulfide bond formation, we mutagenized all surface exposed Cys present in the E2 to Ser. We generated the E2 mutant containing the following mutations C21S/C107S/C111S by site directed mutagenesis. To verify whether this mutant maintains the tridimensional structure we carried out a pull-down assay using 4μM of GST-Rabex-$5^{1-74}$ and *in vitro* translated Ube2D3 C21S/C107S/C111S (C/S) mutant in absence of reducing agent (DTT). As positive control of the reaction we used the previously described Ube2D3 C85S. As shown in **Figure 31B** the Ube2D3 C/S mutant formed a thioester adduct very efficiently. In addition, similar to the E2 C85S~Ub, the Ube2D3 C/S~Ub was able to specifically interact with GST-Rabex-$5^{1-74}$ wild type. Thus, we confirmed that the triple mutations do not alter the structural conformation and function of the E2.

We then proceeded with the generation of a large scale Ube2D3 C/S~Ub. Ube2D3 C21S/C107S/C111S was produced and purified using a size exclusion column (Superdex 75). The reaction was performed mixing together 100μM of E2 (C21S/C107S/C111S) mutant and 500μM of UbG76C against a disulfide bond buffer supplemented with 25μM $CuCl_2$ at room temperature. The disulfide bond formation was stopped by adding laemmli without DTT and was monitored by non-reducing SDS-PAGE. After 72h the free UbG76C was exhausted (**Figure 31C**).

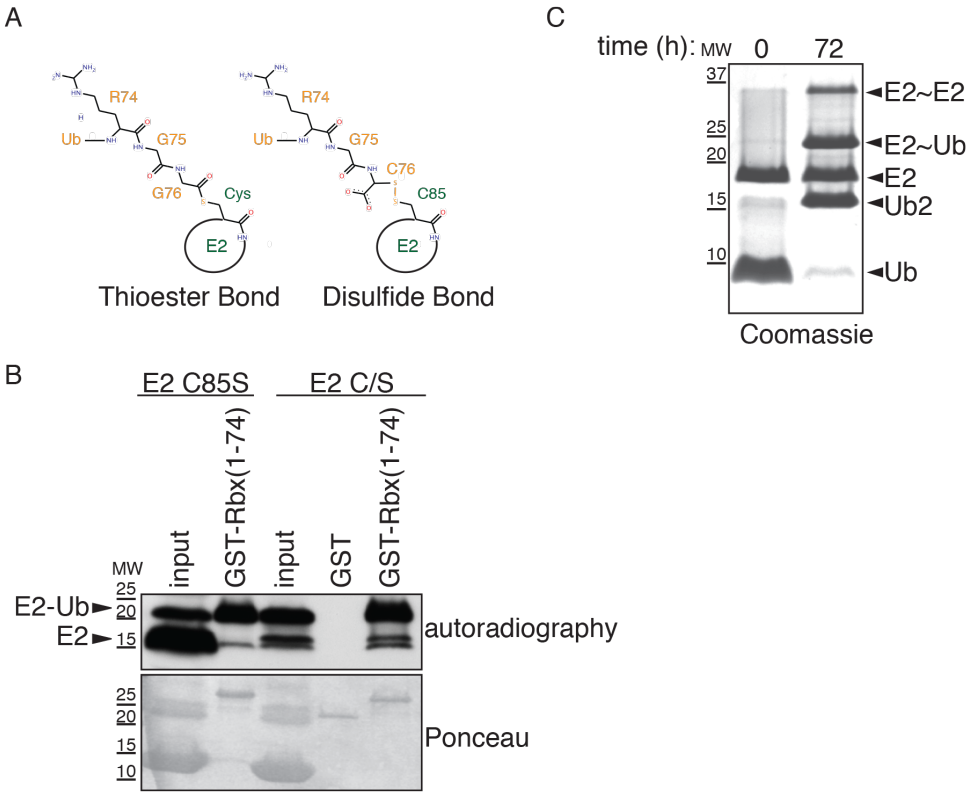


**Figure 31. Disulfide bond formation between E2 and Ub.** (A) Schematic drawing of the naturally occurring thioester bond between the catalytic cysteine (C85) of the E2 enzyme and the C-terminal of Ub. To mimic the short-lived thioester bond, we replaced it with a stable disulfide bond, chemically produced between the Cys85 of E2 and the cysteine of Ub (G76C) mutant. (B) Pull-down assay performed with GST-Rabex-$5^{1-74}$ WT and *in vitro* translated Ube2D3 C85S (positive control) and Ube2D3 C21S/C107S/C111S mutant (indicated as E2 C/S). Washes were made in non-reducing condition and detection was made by autoradiography. (C) Disulfide bond reaction between E2 (C21S/C107S/C111S) mutant and UbG76C, in specific dialysis buffer supplemented of $CuCl_2$, monitored by non-reducing SDS-PAGE and Coomassie staining. After 72h the reaction was stopped because the monomeric Ub was exhausted.

We then purified the E2~Ub from the other side products of the reaction, by a two steps purification protocol. The first anionic exchange column (HiTrap S) allowed us to separate E2 species from $Ub_2$ and Ub alone due to the difference of the isoelectric points (**Figure 32A**). Fractions from F6 to H1 (**Figure 32A**) were collected, concentrated and loaded on a size exclusion column (Superdex 75) to purify the E2~Ub from the other E2 species. We analyzed the composition of single fractions of the peak by a non-reducing SDS-PAGE gel (**Figure 32B**). Unfortunately, separation was suboptimal as the molecular

weights of the various species were too similar.

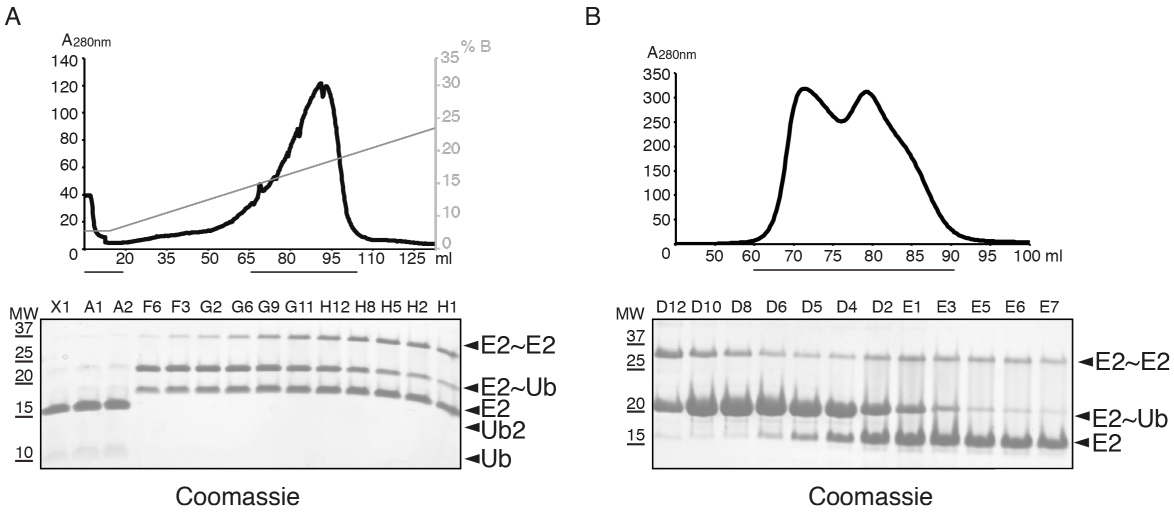


**Figure 32. Purification of the disulfide E2~Ub complex.** (A) Elution profile of the disulfide bond E2~Ub complex on an anionic exchange column (HiTrapS) using a NaCl gradient. Fractions depicted with a black line were loaded on a non-reducing SDS-PAGE and Coomassie staining was performed. (B) Chromatogram of the E2~Ub sample purified on a size exclusion column (Superdex 75). Lower panel shows fractions from the peak loaded on a non-reducing SDS-PAGE.

As alternative strategy, we decided to take advantage of the ability of Rabex-$5^{1-74}$ to bind selectively the E2~Ub. First, we ran an analytical size exclusion chromatography. A Superdex 75 column was loaded with the two separated proteins, Rabex-$5^{1-74}$ or E2~Ub mixture at 100μM concentration (**Figure 33).**

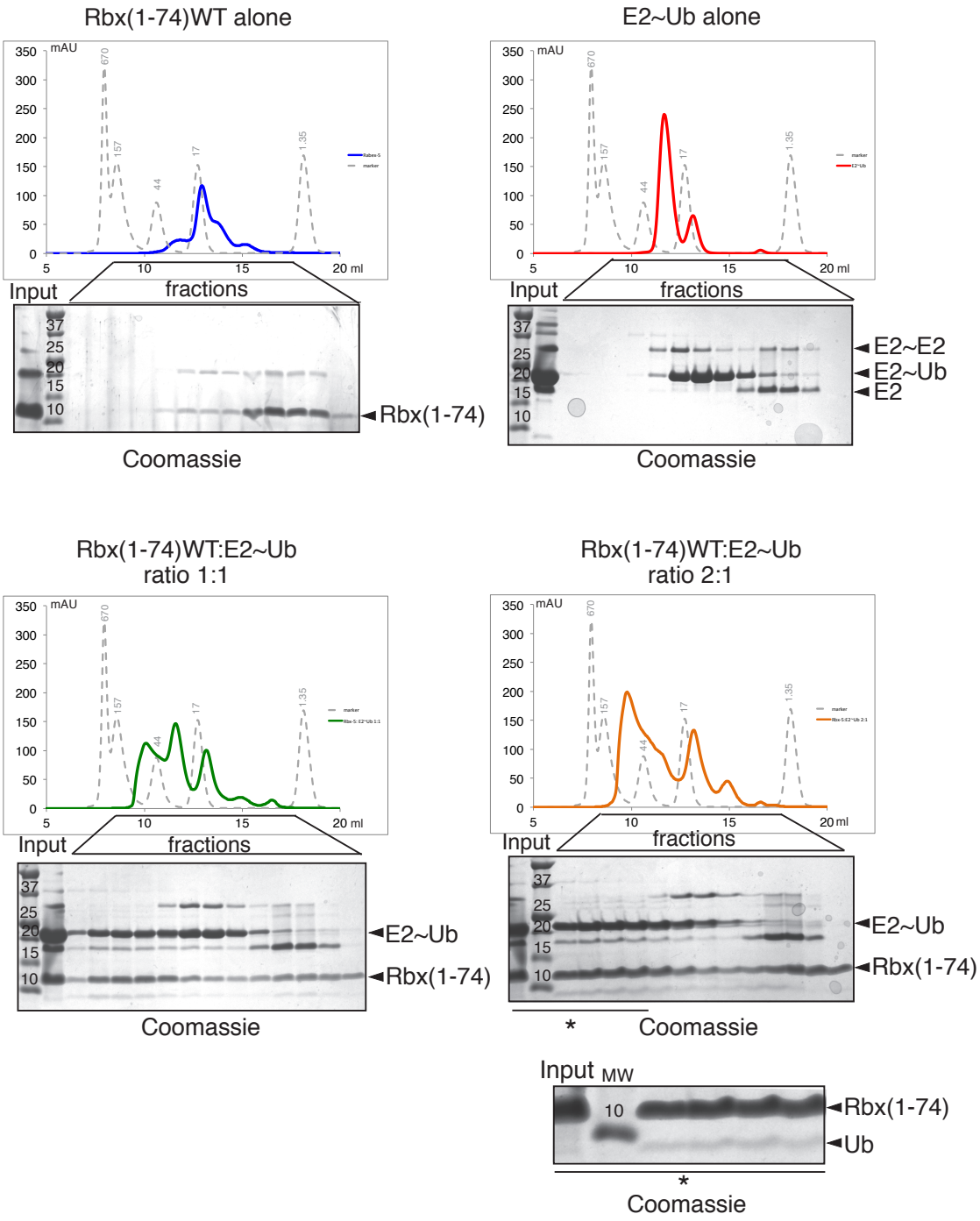


**Figure 33. E2~Ub purification strategy.** Analytical size exclusion analysis of the E2~Ub mixture, obtained from previous purifications, and Rabex-5$^{1-74}$ WT. Elution profile of the E2~Ub mixture is represented as a red line, Rabex-5$^{1-74}$ WT alone as a blue line, the two complexes obtained mixing together the E2~Ub mixture:Rabex-5$^{1-74}$ WT in a ratio 1:1 and 1:2 are respectively green and orange. The E2~Ub curve showed a peak shift upon addition of different concentration of Rabex-5. Fractions from 9 to 15 ml (indicated with a black line in the graph) of each run were analyzed by Tris-tricine PAGE and Coomassie staining. Lower panel represented a magnification of the upper panel (depicted by the black line and asterisk) to show the presence of an additional band, not present in the input and corresponding to free Ub, upon Rabex-5 incubation with E2~Ub sample.

In blue is represented the elution profile of Rabex-$5^{1-74}$ alone, while the red line represented the one of the E2~Ub mixture. Fractions of the two runs were loaded on a non-reducing SDS-PAGE gel. Rabex-$5^{1-74}$ alone is eluted at the expected molecular weight and the species of the E2~Ub were co-eluted as in **Figure 32B**.

Then, 100μM of the E2~Ub mixture was incubated with Rabex-$5^{1-74}$ in a 1:1 molar ratio and subsequently ran on the size exclusion column. The elution profile (**Figure 33**, green line) showed the appearance of an additional peak at higher molecular weight corresponding to the formation of Rabex-$5^{1-74}$:E2~Ub complex. Analysis of the fractions confirmed the appearance of the complex (third panel, **Figure 33**). Importantly, both the E2 homodimer and the E2 alone did not change their elution profile in presence of Rabex-5 confirming that Rabex-$5^{1-74}$ binds specifically the Ub-loaded form of the E2. Increasing the concentration of Rabex-$5^{1-74}$ to a 2:1 molar ratio (**Figure 33**, orange line) caused a further increase in the intensity of the complex formation.

Close inspection of the gel, revealed the appearance of a faint band at the same molecular weight of free Ub (magnification-bottom panel **Figure 33**). Since no free Ub was present in the input, we hypothesized that Rabex-$5^{1-74}$ was able to disrupt the disulfide bond on the E2.

While this can be seen as a possible proof of its E3 ligase activity, it prevents further use of the complex for crystallization purpose as the complex is not stable in presence of Rabex-$5^{1-74}$.

### 5.2. Isopeptide bond

To generate a stable complex for crystallization trials, we therefore decided to generate a more stable isopeptide bond between Ube2D3 and Ub, according to a recently published protocol (Plechanovova et al., 2012) (**Figure 34A**). To this purpose, we created a mutant

Ube2D3 in which we mutagenized the catalytic Cys85 into a Lys as well as Ser22 into Arg. The newly generated Lys85 in the E2 (C85K) is in an optimal position to perform the nucleophylic attack on the catalytic Cys of the Ub-loaded E1 (**Figure 34B**). Mutation S22R destroys a non-covalent interaction with Ub, present in the backside of the E2 and previously shown to be necessary for the enzyme's processivity (Brzovic et al., 2006). This mutation increases the yield of E2-Ub product in the enzymatic reaction (Plechanovova et al., 2012).

We set up an enzymatic reaction with E1, the E2 S22R/C85K mutant and free N-terminal His-tagged-Ub. To obtain a reasonable amount of E2-Ub, we produced the single components in large amount and we purified them through chromatographic passages: an anionic exchange (HiTrap S column) and a size exclusion (Superdex 200 column) for the E1 enzyme and a single size exclusion (Superdex 75 column) for His-Ub and Ube2D3 S22R/C85K. The isopeptide bond formation was generated mixing together 200μM Ube2D3 S22R/C85K, 200μM His-tagged Ub and 1μM E1 at 37°C in a buffer containing 3mM ATP, 5mM $MgCl_2$, 50mM Tris-HCl pH 10.0 and 150mM NaCl. After 26h the reaction was stopped because the His-Ub was almost exhausted (**Figure 34C**).

To purify the E2-HisUb from the enzymatic mixture we performed a first purification step using nickel beads, which bind both E2-HisUb and His-Ub (Fraction 7 and 8 **Figure 34D**). Those two proteins were subsequently purified through a size exclusion column (Superdex 75), taking advantage of their molecular weight difference (**Figure 34E**).

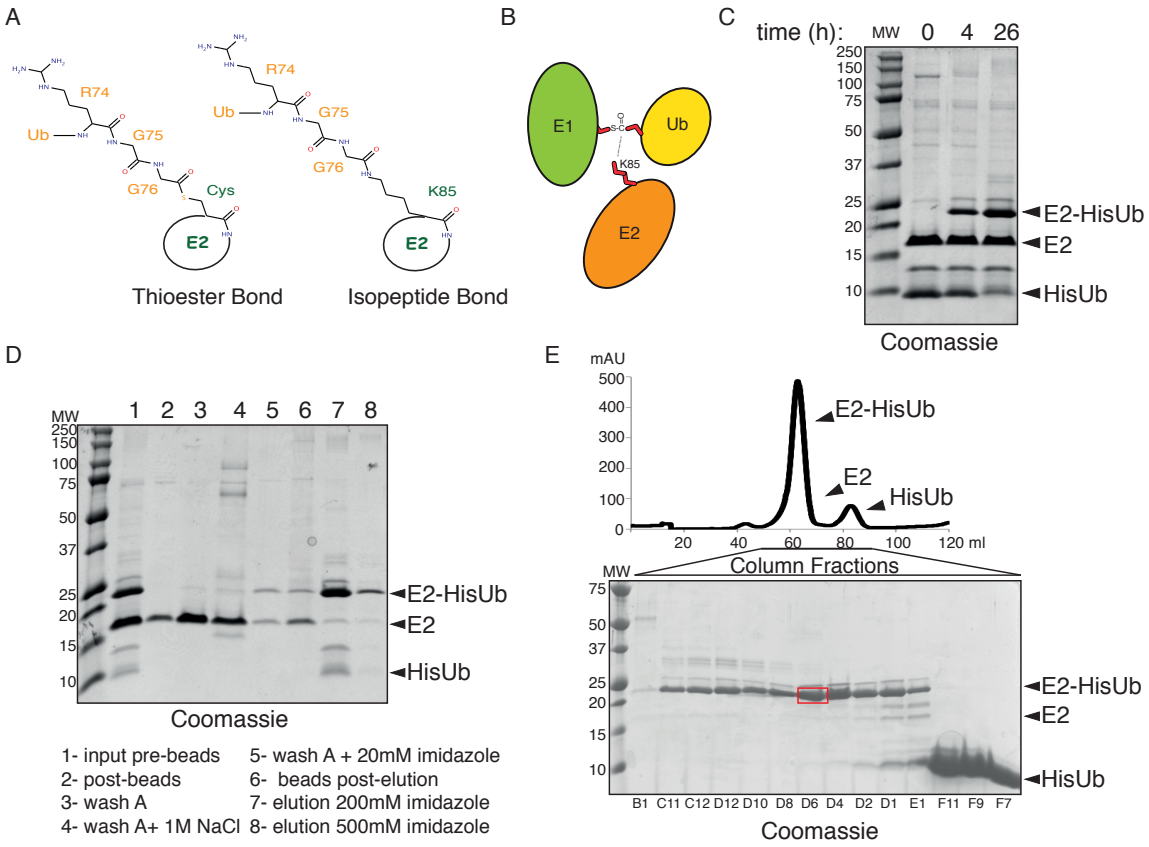


**Figure 34. Isopeptide bond formation between E2 and Ub.** (A) Schematic drawing of the naturally occurring thioester bond between the catalytic cysteine (Cys85) of the E2 and Ub. To mimic the short-lived thioester bond with a more stable bond we enzymatically produced an isopeptide bond between the lysine of E2 mutant (C85K) and Ub. (B) Cartoon representation of a nucleophilic attack of K85 of E2 towards an Ub~loaded E1, allowing the formation of E2-Ub. (C) Isopeptide bond reaction was monitored by a reducing SDS-PAGE and Coomassie staining. After 26h the reaction was almost completed due to formation of the largest amount of our target E2-Ub. (D) Purification of E2-HisUb by incubation with nickel beads for 2h at 4°C. Beads were washed with 1M NaCl (Fraction 4) and 20mM imidazole (Fraction 5) before elution with 200mM (Fractions 7) and 500mM (Fraction 8). Fractions were loaded on a reducing SDS-PAGE and Coomassie staining was performed. (E) Elution profile of purified E2-HisUb (Fraction 7 of D) on a size exclusion column (Superdex 75). Indicated fractions were analyzed by reducing SDS-PAGE and Coomassie staining. Fraction depicted with a red box was analyzed by Mass-Spectrometry.

Before proceeding with the following steps, we analyzed by mass spectrometry (MS) the major band of the E2-HisUb purified peak (depicted with a red box in **Figure 34E**).

MS data confirmed that the band is exclusively made of E2-Ub with Ub attached on residue Lys 85 (**Figure 35**).

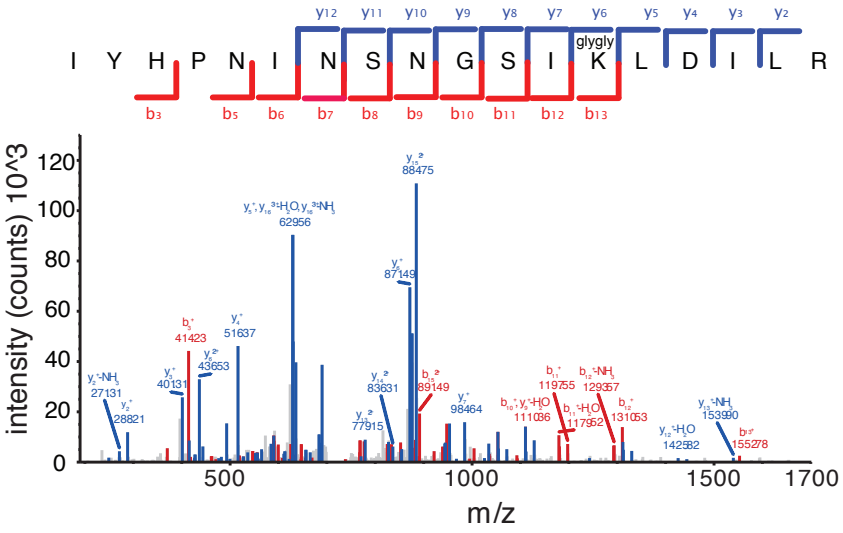


**Figure 35. Mass-spectrometry of isopeptide E2-Ub.** MS/MS spectrum of the Ube2D3 C85K peptide with the diglycine-modified lysine residue. Peptide sequence was shown with the annotation of the identified matched *b* ions in red and the *y* ions in blue.

We also noticed other bands appearing above the one of interest that were further analyzed by MS (**Figure 34**). Results demonstrated that additional natural lysines were modified by the Gly-Gly peptide, sign of ubiquitination: Lys8, Lys133 and Lys144. Thus, even if at low stoichiometry, additional lysines may be directly modified by the E1. To reduce this side effect of the reaction, we generated a triple K8R/K133R/K144R mutant by site directed mutagenesis. Unfortunately, this E2 variant was not soluble and impossible to purify (data not shown). This behavior prevented further experiments with this mutant.

Since the multi-Ub E2-HisUb represented a minimal percentage of the total E2-HisUb obtained, we decided to proceed with the Ube2D3 S22R/C85K-Ub being selective with the fractions collection upon purification. As shown in **Figure 34E,** we collected fractions from D10 to D2, and we concentrated our sample to 6mg/ml. This sample was used for pull-down experiments and ITC analysis shown before (**Figure 29-30**) and for crystallization purpose as described below.

### 5.3. Rabex-$5^{1-74}$:Ube2D3-Ub complex and crystallization trays

Purified Ube2D3 S22R/C85K-Ub, was mixed with Rabex-$5^{1-74}$ wild type in a 1:2 molar ratio and the mix was concentrated until a final concentration of 60μM.

We evaluated the complex by size exclusion column (Superdex 75) and aliquots of fractions were run in a reducing SDS-PAGE (**Figure 36**). As shown in the chromatogram of **Figure 36** (red line), the complex Rabex-$5^{1-74}$ wild type:Ube2D3-Ub was eluted at higher molecular weight than the nominal one. This was possibly due to the fact that the two UBDs of Rabex-$5^{1-74}$ may engage multiple interactions with modified E2-Ub generating a not homogeneous complex. Being the two surface of interaction different, Ub could act as a bridge between two molecules of Rabex-$5^{1-74}$ wild type, and these molecules could in turn bind other Ubs, thus creating long 'chains' of not necessarily identical Rabex-5:E2-Ub units. To overcome this problem we decided to include in the crystallization screening, Rabex-$5^{1-74}$ A58G mutant (MIU-impaired mutant) that apparently shows a wild type catalytic activity. Our previous data (shown in paragraph 6) seems in fact to confirm that the ZnF_A20 domain is the domain responsible for the E3 ligase activity of Rabex-5 (Lee et al., 2006b; Xu et al., 2010).

Rabex-$5^{1-74}$ A58G was produced as GST tagged protein, cleaved from the GST tag with Prescission protease, and purified using a size exclusion column (Superdex 75). We analyzed its behavior alone (**Figure 36**-blu line) or in complex with E2-Ub in a ratio 1:2 at final concentration of 60μM (**Figure 36**-green line). Compare to the complex made with Rabex-$5^{1-74}$ wild type, the complex of Rabex-$5^{1-74}$ A58G:Ube2D3-Ub eluted at the expected molecular weight, indication of a more homogenous and monodisperse sample.

Unfortunately, in both cases, we scored several peaks, including the one of Ube2D3-Ub that ran immediately after the peak of the complex. To have a more homogeneous sample we were quite stringent in choosing the fractions. For E2-Ub:Rabex-$5^{1-74}$ wild type

complex we collected fractions from E4 to E7 while for E2-Ub:Rabex-$5^{1-74}$ A58G complex we collected fractions from E7 to E9 (**Figure 36**). Then, complexes were concentrated and tested in several crystallizations trays. For E2-Ub:Rabex-$5^{1-74}$ wild type complex we tested two different concentrations, 13mg/ml and 30mg/ml, while E2-Ub:Rabex-$5^{1-74}$ A58G complex was tested at 20mg/ml. Trays were set-up at two different temperatures (20°C and 4°C), using commercial screens: PACT, JCSG+ and Procomplex from Qiagen, Stura/Macrosol, Morpheus and Structure screen 1⁄2 from Molecular Dimension, Crystal screen 1⁄2 and Index from Hampton. Unfortunately, no reproducible crystals were obtained.

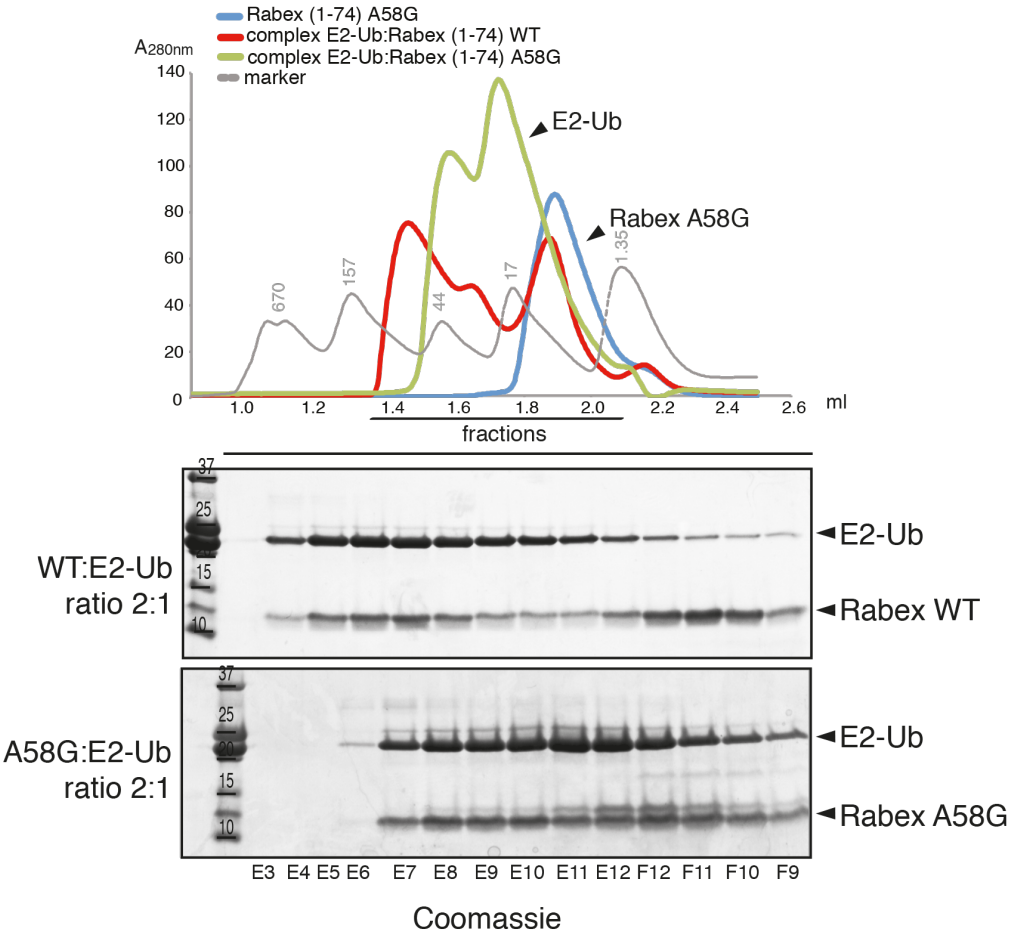


**Figure 36. Rabex-5$^{1-74}$:Ube2D3-Ub complex.** Size exclusion column of the E2-Ub:Rabex-5$^{1-74}$ complex. Elution profile of E2-Ub:Rabex-5$^{1-74}$ WT complex is depicted in red, E2-Ub:Rabex-5$^{1-74}$A58G complex is depicted in green and Rabex-5$^{1-74}$A58G alone in blue. The curves of the complexes showed peak shifts respect to Rabex-5$^{1-74}$ alone. Fractions from 1.4 to 2.1 ml were monitored in the lower panels by reducing SDS-PAGE and Coomassie staining.

## 5.4. SAXS

Since all our structural efforts failed, we decided to use Small Angle X-ray Scattering (SAXS) to get an idea of the tridimensional arrangement of the Rabex-5$^{1-74}$:Ube2D3-Ub complex. In collaboration with Sebastiano Pasqualato at IEO (Milan), Adam Round and Martha Brennich of the BM29 beamline at the European Synchrotron Radiation Facility (Grenoble), we performed SAXS analysis obtaining technically good spectra.

We described results obtained with Rabex-5$^{1-74}$A58G and not with Rabex-5$^{1-74}$ wild

type, even if we tested both, due to the unsuccessful results obtained with the wild type protein. Even if we previously ran Rabex-$5^{1-74}$ wild type:Ube2D3-Ub complex on a size exclusion chromatography (Superdex 75 column) the complex formed aggregates at high molecular weight, as shown in **Figure 36**, with a low intensity of scattering. Therefore, elaboration of data from the spectrum was not possible.

First, we subjected to X-Ray scattering the two single proteins, Rabex-$5^{1-74}$A58G and the isopeptide Ube2D3 S22R/C85K-Ub sample. We decided to test Rabex-$5^{1-74}$A58G mutant as it maintained the catalytic domain intact (see below, chapter 6.2) and behaved as homogeneous sample.

We ran Rabex-$5^{1-74}$A58G sample on a size exclusion chromatography (Superdex 75) to isolate the scattering of the monodisperse sample from that of aggregated or oligomerized one. The isopeptide Ube2D3 S22R/C85K-Ub sample was directly tested by X-Ray scattering without size exclusion chromatography, because the sample was sufficiently homogeneous and monodisperse (data not shown). The obtained spectra were analyzed using as model the crystal structures of Rabex-$5^{1-74}$ (PDB:2C7N) (Penengo et al., 2006) and of various E2~Ub. Indeed, the E2~Ub can assume various conformations (Pruneda et al., 2011) therefore we chose crystal structure of E2-Ub alone (PDB:3UGB (Page et al., 2012), PDB:3A33 (Sakata et al., 2010), PDB:1FXT (Hamilton et al., 2001)) or in complex with RING-E3 ligase (PDB:4AP4) (Plechanovova et al., 2012) or HECT-E3 ligase (PDB:3JW0) (Kamadurai et al., 2009).

As shown in **Figure 37A**, theoretical scattering (the curve depicted in orange) calculated from the crystal structure of Rabex-$5^{1-74}$ A58G perfectly fits the experimental data. This data confirmed the correct tridimensional arrangement of our sample. In the case of E2~Ub, each theoretical scattering was generated from the structures indicated in **Figure 37B.** Our experimental scattering fits well with curves generated from PBD 3UGB and 3JW0 that are obtained from crystal structure of E2-Ub alone or in complex with the

HECT domain of Nedd4-2. On the contrary, theoretical curves obtained using 4AP4 (E2-Ub in complex with the RING protein-RNF4), does not fit well, suggesting that in solution our E2-Ub sample adopts a conformation different from the active 'folded back' conformation assumed in the complex with RNF4 (Plechanovova et al., 2012).

Next, we analyzed the complex E2-Ub:Rabex-$5^{1-74}$ A58G obtained mixing together the two proteins to have a final concentration of 250μM. We performed the size exclusion chromatography (Superdex 75) and then we analyzed by SAXS the eluted sample. X-ray scattering did not allow the unambiguous *ab-initio* positioning of the E2 molecule, due to the very low scattering provided by the small E2. We thus decided to analyze the complex based on models that we generated from crystal structures, to see if one of their theoretical curves might fit the experimental data. We based our models on all the E2-Ub tested before, positioning the Ub in the ZnF_A20 domain as in the previous crystallized complex Rabex-$5^{1-74}$:Ub (Penengo et al., 2006). As shown in **Figure 37C** the experimental data did not fit with any theoretical models, suggesting that the complex can assume a different conformation respect from what we proposed. Unfortunately, we cannot resolve the tridimensional arrangement of our complex Rabex-$5^{1-74}$ A58G:E2-Ub from the experimental data due to the low intensity of scattering and high degree of flexibility of the complex.

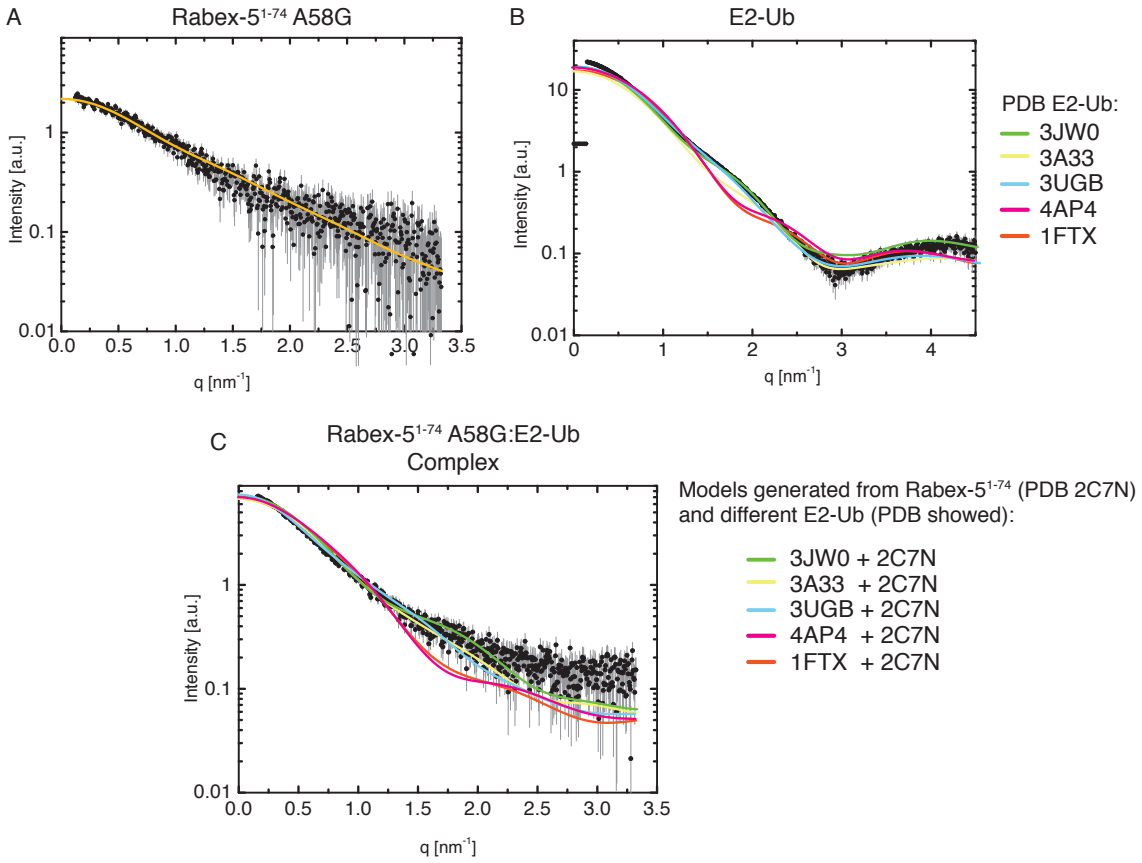


**Figure 37. SAXS analysis.** A) Dots representing the SAXS profile of Rabex-5$^{1-74}$ A58G that we fitted with the curve calculated with the crystal structure of Rabex-5$^{1-74}$ in complex with Ub(Penengo et al., 2006) (PDB:2C7N). B) Dots represented the SAXS profile of Ub-loaded Ube2D3 S22R/C85K through the isopeptide bond. All curves are obtained from different E2 loaded with Ub crystallized alone or in complex with an E3. C) Dots are the analysis of the complex Rabex-5$^{1-74}$ A58G:E2-Ub by SAXS. In this case curves are obtained by modeling the different E2-Ub structures on Rabex-5$^{1-74}$ (PDB:2C7N) considering the mutation A58G.

## 6. Characterization of E3 ligase activity of Rabex-5

### 6.1 Rabex-5 can alter the stability of E2~Ub disulfide bond

During the preparation of Rabex-5$^{1-74}$:Ube2D3~Ub complex for crystallography we realized that the disulfide bond of E2~Ub was not stable in the presence of Rabex-5$^{1-74}$. We hypothesized that this was due to the E3 ligase activity of Rabex-5.

To prove our hypothesis further, we performed a disulfide bond stability assay in which 60 μM of the E2~Ub mixture was incubated with 5μM of Rabex-$5^{1-74}$ wild type in a time course reaction at 37°C. As a source of E2~Ub we used an E2~Ub mixture, containing both E2~E2 dimer as well as E2~Ub, previously obtained from in the anionic exchange column (**Figure 32A**). Reaction was stopped by addition of laemmli buffer without DTT and loaded on a non-reducing SDS-PAGE. The detection was performed by immunoblot anti-Ub (**Figure 38A**). To control the stability of the E2~Ub alone in the reaction conditions, the E2~Ub was incubated for 2h at 37°C in the same buffer without DTT, alone or in the presence of 5μM of GST. No free Ub was detected, demonstrating that the E2~Ub is stable in these conditions. Incubation of E2~Ub with 5μM Rabex-$5^{1-74}$ wild type induced disruption of disulfide bond detected by increased amount of free Ub. The same effect is visible upon addiction of 1μM of $HECT^{Nedd4}$, a well-characterized E3 ligase. We thus, consider this phenotype as a validation of E3 ligase activity of Rabex-5 (**Figure 38A**).

To understand which domain is responsible for the Ub detachment, we performed the same assay, adding to the E2~Ub either 5μM of Rabex-$5^{1-74}$ wild type or single mutants in one of the two UBDs of Rabex-5 (Rabex-$5^{1-74}$Y25F and Rabex-$5^{1-74}$A58G). As negative control, we used GST alone while, as positive control, the GST-$HECT^{Nedd4}$ domain. E2~Ub was also incubated with DTT to break entirely the disulfide bond (**Figure 38B**). Through the detection of free Ub, we confirmed that the incubation of Rabex-$5^{1-74}$ wild type with E2~Ub induced disruption of disulfide bond. A detectable amount of free Ub was observed also when the E2~Ub is incubated with Rabex-$5^{1-74}$ A58G. However no free Ub was scored in the case of Rabex-$5^{1-74}$ Y25F (**Figure 38B**).

Thus, also with this assay, we can ascribe to the ZnF_A20 domain the ligase activity of Rabex-5, as previously suggested by other groups (Lee et al., 2006a; Xu et al., 2010).

The disulfide bond disruption could be an unspecific effect of the presence of the

thiol (-SH) group of Cys residue in the proteins. However we scored a different behavior between Rabex-$5^{1-74}$ A58G and Rabex-$5^{1-74}$ Y25F to disrupt the disulfide bond. We proposed this effect as prove of the E3 ligase activity of Rabex-5.

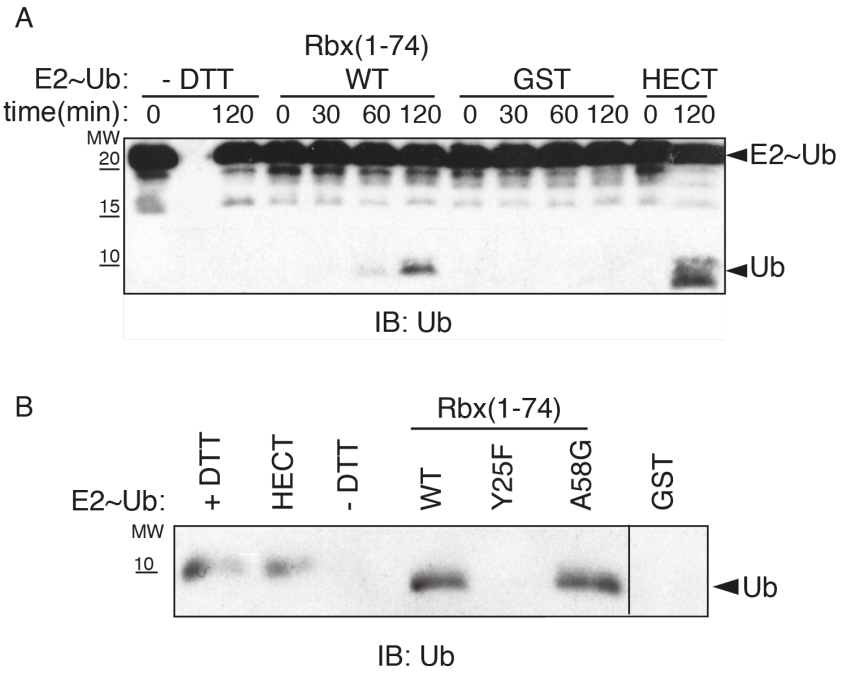


**Figure 38. E2~Ub disulfide bond stability in the presence of Rabex-5.** (A) Incubation of purified E2~Ub in presence of Rabex-$5^{1-74}$ WT, at 37°C for the indicated time. As control E2~Ub alone was incubated in a buffer without DTT or together with GST or GST-HECT. At different time point, reaction was blocked by addition of laemmli buffer without DTT. Detection of free Ub was performed with IB anti-Ub. (B) E2~Ub was incubated in the presence of Rabex-$5^{1-74}$ either WT or mutants in the ZnF_A20 domain (Y25F) and the MIU domain (A58G) at 37°C for 2h. GST alone, $HECT^{Nedd4}$ and E2~Ub in presence or absence of DTT in the buffer were added as control reaction. Free Ub was detected by IB anti-Ub.

### 6.2. Self-ubiquitination of Rabex-5

We then performed a classical *in vitro* auto-ubiquitination assay. We tested either GST-Rabex-$5^{1-74}$ wild type or full-length protein in order to verify if the N-terminal fragment is sufficient to drive catalysis. The assay was performed using 500 nM GST-proteins in presence of 20 nM E1, 500 nM Ube2D3 and 2.5 µM Ub in ubiquitination buffer. At the indicated time points the reaction was stopped by addition of laemmli with DTT and the

detection was performed by anti-Ub.

As shown in **Figure 39A,** GST-Rabex-$5^{1-74}$ and GST-Rabex-5 full-length were both able to sustain self-ubiquitination but apparently with different kinetics; full length Rabex-5 seems to be faster than Rabex-$5^{1-74}$ (**Figure 39A**). In both cases, only few Ub molecules (possibly one in case of Rabex-$5^{1-74}$) were attached to the E3s. We also performed *in vitro* auto-ubiquitination assay in the previous conditions, using GST-Rabex-$5^{1-74}$ wild type and single mutants in the two UBDs (Rabex-$5^{1-74}$Y25F and Rabex-$5^{1-74}$A58G). The reaction was stopped at the indicated time points adding laemmli with DTT. The Ub modification was detected by anti-Ub (**Figure 39B**).

We confirmed that GST-Rabex-$5^{1-74}$ wild type is able to ubiquitinate itself and we showed that this activity is reduced when the ZnF_A20 domain is mutated at residue Y25. Instead, the A58G mutation on the MIU domain of GST-Rabex-$5^{1-74}$ did not affect its activity. Only when both UBDs are mutagenized the enzyme was completely dead (**Figure 39B**). We also performed the *in vitro* auto-ubiquitination reaction using single UBDs, GST-Rabex-$5^{1-49}$ and GST-Rabex-$5^{48-74}$. In this case again, only constructs containing an intact ZnF_A20 domain were able to sustain ubiquitination reaction as well as the GST-Rabex-$5^{1-74}$ (**Figure 39C**).

From the sum of these assays we can confirm literature's data concluding that the ZnF_A20 is the main responsible for the ligase activity shown by Rabex-5.

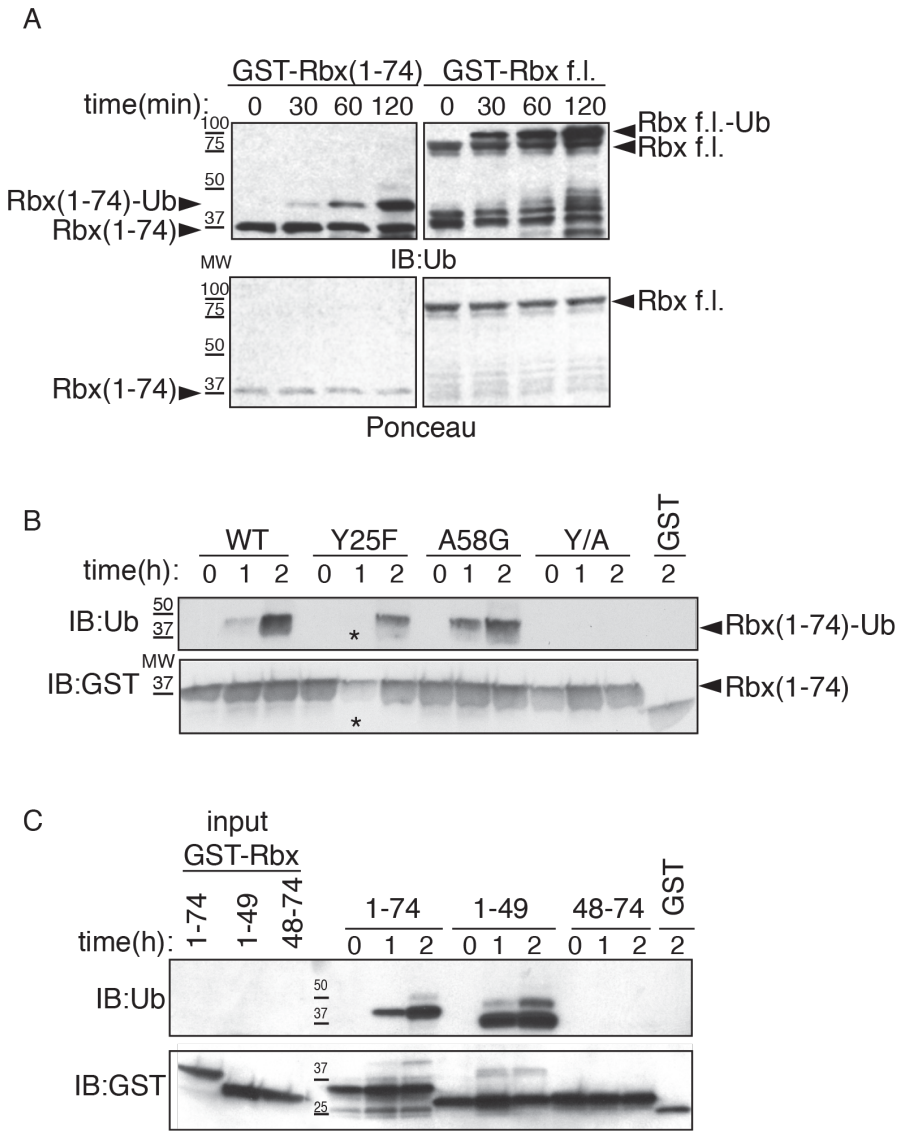


**Figure 39. E3 ligase activity of Rabex-5.** (A) *In vitro* auto-ubiquitination assay carried out with GST-Rabex-$5^{1-74}$ (MW 34kDa) and GST-Rabex-5 full length (MW 84kDa) in presence of E1 and the specific E2 (Ube2D3). Reactions were performed at 37°C and at different time points beads were collected and washed with RIPA buffer three times. Ubiquitinated form of Rabex-5 was detected with IB anti-Ub and sample loading by direct ponceau staining of the membrane. (B) *In vitro* auto-ubiquitination assay performed with GST-Rabex-$5^{1-74}$ WT and mutants. Reactions were performed at 37°C and at different time points beads were collected and washed with RIPA buffer three times. Modified and unmodified form of Rabex-5 were detected by IB anti-Ub and anti-GST, respectively. (C) *In vitro* auto-ubiquitination assay carried out with GST-Rabex-5 fragments of single UBDs (1-49 contains the ZnF_A20 domain and 48-74 contains the MIU domain). GST-Rabex-$5^{1-74}$ and GST alone were included as control in the reaction. Reactions were performed at 37°C and at different time points beads were collected and washed with RIPA buffer three times. Ubiquitination was detected by IB anti-Ub.

## 7. Substrates Identification

Once we demonstrated that Rabex-5 has the ability to self-ubiquitinate, we analyzed its catalytic activity towards possible substrate candidates.

### 7.1. H-Ras is not a real Rabex-5 substrate

We focused our attention on H-Ras, which is the unique substrate of Rabex-5 so far identified. Xu and colleagues demonstrated that H-Ras become mono- and di-ubiquitinated by Rabex-$5^{1-76}$ and that mutation in ZnF_A20 impaired the catalytic activity of the enzyme (Xu et al., 2010).

Initial experiments were made using $Ras^{1-166}$ fragment, which lacks the hypervariable C-terminal part that confers biochemical diversity between the three isoforms of Ras (H-Ras, K-Ras and N-Ras). The construct was kindly provided by Dr. Campbell (Baker et al., 2013). We produced and purified GST-$Ras^{1-166}$.

We performed an *in vitro* substrate ubiquitination assay using 500 nM GST-$Ras^{1-166}$ as substrate and 500 nM Rabex-$5^{1-74}$ as E3 ligase at 37°C for the indicated time points (**Figure 40A**). As negative control of the reaction we performed the same reaction without the E2 or without the E3. During the time course we scored an increase in GST-$Ras^{1-166}$ monoubiquitination but at the same level as in the absence of Rabex-$5^{1-74}$ (**Figure 40A**).

We hypothesized that the C-terminal part of Ras could have a critical role in Rabex-5 recognition and consequently may determine a different mode of substrate ubiquitination. We tested several conditions both *in vivo* and *in vitro*, using H-Ras full-length and both Rabex-$5^{1-74}$ or full-length, always with negative results (data not shown). We thus decided to use the same settings of the published protocol (Xu et al., 2010) performing the reaction with 20 nM E1, 500 nM Ube2D3, 3 μM Rabex-$5^{1-74}$ cleaved and purified, 2,5 μM GST-H-Ras and 5μM Ub-biotinylated. The reaction was stopped adding laemmli with DTT at the

indicated time points (**Figure 40B**). A parallel sample was performed in the absence of Rabex-$5^{1-74}$. Negative control was the same reaction using GST alone as substrate. Using biotinylated-Ub, the detection was performed using HRP-streptavidin. As shown in **Figure 40B** we scored increasing level of monoubiquitination of GST-H-Ras during the time course. Unfortunately, once again we detected Ras monoubiquitination also in the absence of Rabex-5 as E3 ligase. We concluded that Ube2D3 is sufficient to trigger the Ub modification of Ras. This is not surprising as when particularly high concentration of enzymes is used, the E2 alone is able to ubiquitinate a substrate (Hoeller et al., 2007).

Unfortunately, we never scored an effect of Rabex-5 on Ras, not even an anticipated kinetics, thus we concluded that H-Ras is not a Rabex-5 target protein.

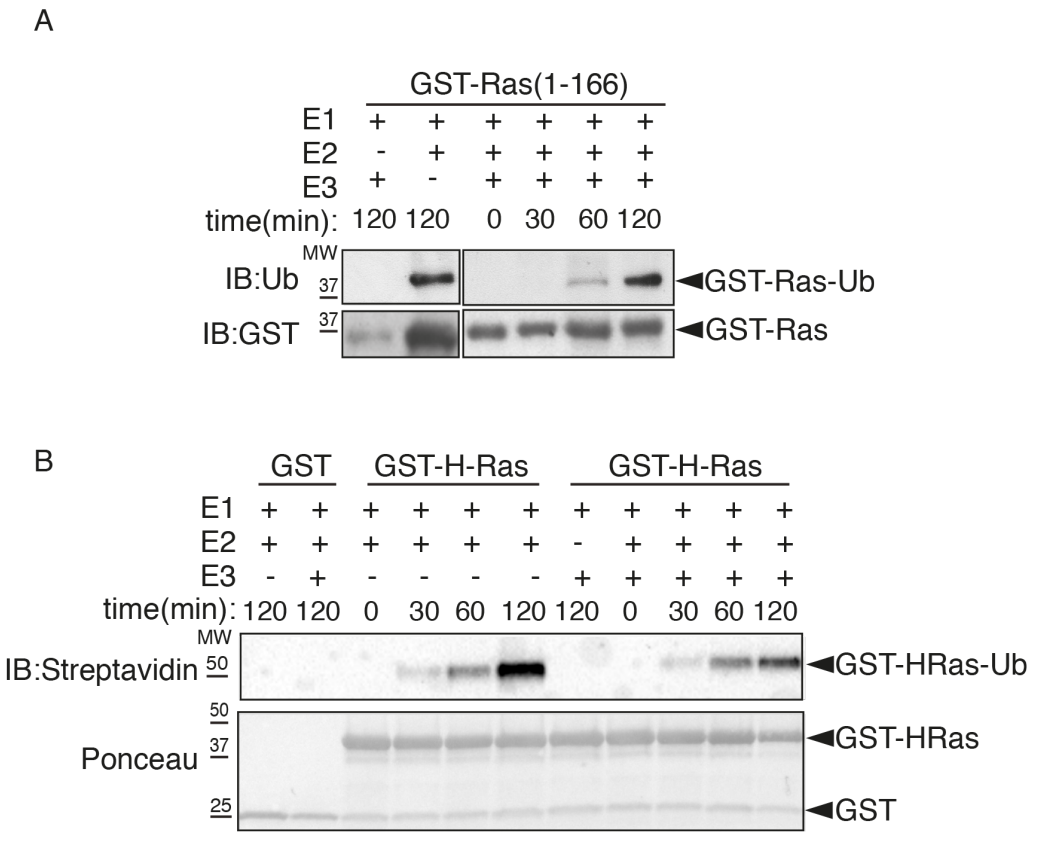


**Figure 40. *In vitro* Ras ubiquitination.** (A) *In vitro* substrate ubiquitination assay carried out using E1, Ube2D3 as E2, Rabex-$5^{1-74}$ as E3 ligase, GST-Ras (1-166, lacking the hypervariable region) as substrate. Reactions were performed at 37°C and different time points were collected. Beads were then washed with RIPA buffer three times. Ubiquitination was detected by IB anti-Ub and sample loading by IB anti-GST. (B) *In vitro* substrate ubiquitination assay carried out using

E1, Ube2D3, Rabex-$5^{1-74}$, GST-H-Ras as substrate and biotinylated-Ub. Reactions were performed at 37°C and different time points were collected. Beads were then washed with RIPA buffer three times. GST alone was used as negative control. Ubiquitination was detected with HRP-conjugated streptavidin and sample loading by ponceau.

### 7.2. Substrate identification using protein microarray

To characterize possible substrates of Rabex-5 E3 ligase with an unbiased approach, we performed an *in vitro* ubiquitination assay using protein microarray as candidate substrates (Persaud et al., 2009). Life Sensors performed for us the *in vitro* ubiquitination assay on microarray as well as the substrate profiling. For this assay we decided to use the CDI microarray in which there were spotted 20.000 human proteins produced in yeast. The reaction was performed on the array using a mixture composed by the E1, the E2 candidate (Ube2D3), the E3 candidate and fluorescent-Ub. Ubiquitinated substrates were identified by the detection of fluorescent-Ub that remains covalently attached to the proteins after washing. The control array was treated with the same ubiquitylation machinery without the E3.

#### 7.2.1 Production and purification of His-MBP-Rabex-5 full-length

We decided to use Rabex-5 full-length protein instead of the minimal region Rabex-$5^{1-74}$ in order to allow a correct recognition of the substrates by the E3 ligase. Ideally for the screening we should avoid GST-tagged protein, thus we subcloned Rabex-5 in pET43a vector that carries two different tags at the N-terminus: His and MBP. His-MBP Rabex-5 was purified from bacterial lysate using nickel beads and subsequently eluted from the beads using 200mM of imidazole. Each fraction of the washes and elutions were loaded on a reducing SDS-PAGE gel (**Figure 41A**). Fraction 7 was collected and extensively dialyzed to eliminate imidazole, then loaded on a cationic exchange column (HiTrap Q)

(**Figure 41B**). We analyzed the composition of the single fractions on a gel. We also performed an immunodetection with an anti-CUE antibody that specifically recognize the C-terminus of Rabex-5 full length (**Figure 41B**-lower panel). Fractions from 18 to 21 ml were collected and further purified on a size exclusion column (Superdex 200) to separate Rabex-5 full length from the degradation products. We collected fractions from 11,5 ml to 13,5 ml (**Figure 41C**). The sample was loaded on a SDS-PAGE gel and the band at 100kDa was analyzed by mass spectrometry (data not shown). The MS data confirmed that the band is made exclusively by His-MBP-Rabex-5.

Prior to send the target protein to the Life Sensor Company, we analyzed its activity by *in vitro* self-ubiquitination assay. The reaction was performed with 20 nM E1, 500 nM His-Ube2D3, 500 nM His-MBP-Rabex-5 full length and 2.5 μM of Ub-biotinylated in ubiquitination buffer for 2h at 37°C (**Figure 41D**). As positive control, we used GST-Rabex-5 full length. Detection of ubiquitination was done by HRP-streptavidin while detection of the level of Rabex-5 was performed with an anti-MIU antibody. His-MBP-Rabex-5 full length was active and able to perform self-monoubiquitination in the same way as the GST-Rabex-5 full length (**Figure 41D**).

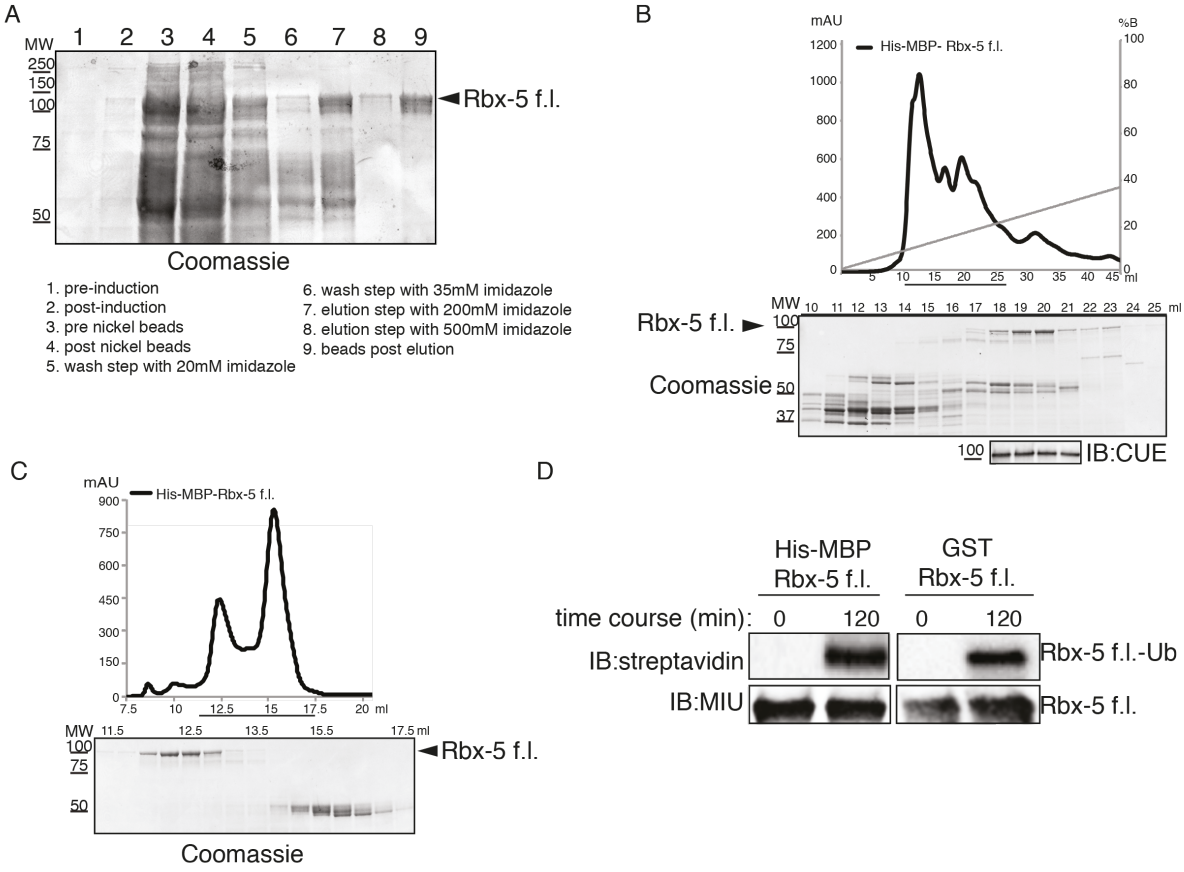


**Figure 41. His-MBP-Rabex-5 f.l. production and purification.** (A) Example of His-MBP-Rabex-5 f.l. production. Fraction 1 and 2 were bacteria lysates pre and post-induction with IPTG. His-MBP-Rabex-5 was purified from bacterial lysate (fraction 3) by incubation with nickel beads (fraction 4-supernatant post-beads) for 2h at 4°C. Specifically bound proteins were washed with 20mM imidazole (fraction 5) and 35mM imidazole (fraction 6) before elution with 200mM (fractions 7) and 500mM (Fraction 8). Fractions were loaded on a reducing SDS-PAGE and Coomassie staining was performed. (B) Elution profile of purified His-MBP-Rabex-5 f.l. (Fraction 7 of A) on a cationic exchange column (HiTrapQ) using a NaCl gradient. Fractions depicted with a black line were loaded on a reducing SDS-PAGE gel and Coomassie staining was performed. Fractions containing bands corresponding to the molecular weight of the target protein were analyzed by IB anti-CUE, a specific antibody against the CUE domain present at C- terminus of Rabex-5 f.l. (C) Chromatogram from size exclusion chromatography (Superdex 200 column). Lower panel showed fractions from the two peaks loaded on a reducing SDS-PAGE gel. (D) *In vitro* auto-ubiquitination assay performed with His-MBP-Rabex-5 f.l. using E1, Ube2D3 and biotinylated-Ub. GST-Rabex-5 f.l. was used as positive control. Reactions were performed at 37°C for 2h and beads were then washed with RIPA buffer three times. Modified Rabex-5 was detected with HRP-conjugated streptavidin and sample loading was assessed by IB anti-MIU.

### 7.2.2 Identification of possible substrates

Of roughly 20,000 human proteins on the microarray, 1007 features showed a significant difference ($p<0.05$) in ubiquitination between the Rabex-5-treated and the control arrays. Of these, 629 showed increased ubiquitination. In **Table 3** we reported the top 67 "hits", which were filtered first by $M_N$ value, which is the magnitude change estimated from the normalized intensity of experimental values subtracting the control value, and then by F-B value, calculated by median feature intensities minus background, using an arbitrary cut-off of F-B ≥50RFU. These were also the features that showed the highest fluorescent intensities on the experimental arrays (by visual inspection). This list represents the most statistically stringent and conservative estimate for Rabex-5 substrates. Interestingly, the large number of positive hits on the Rabex-5 treated arrays showed low signal intensities that we interpreted as most likely indicating mono- or di-ubiquitination events. This well fits with our previous results. This effect is also visible in **Figure 42**, which shows block 15 from both the control (A) and Rabex-5 treated arrays (B).

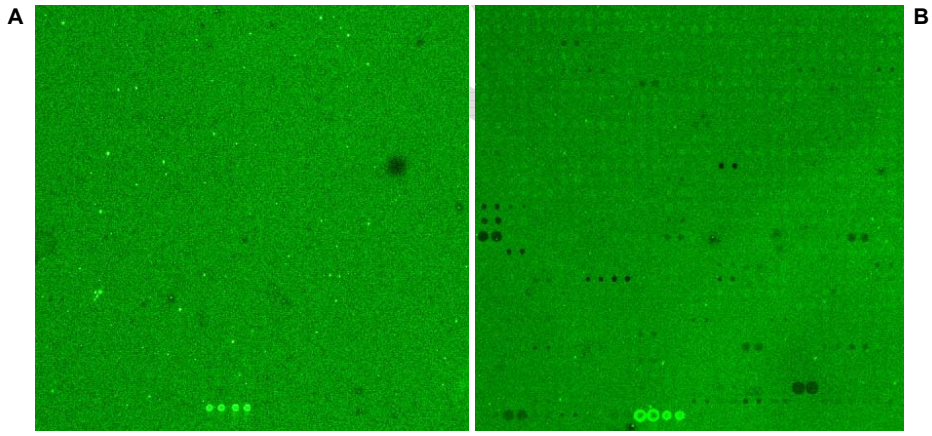


**Figure 42. Representative sub-arrays from control and Rabex-5-treated arrays.** The four bright features at the bottom of each sub-array were controls labeled with a fluorescent dye.

Based on the knowledge that Rabex-5 is involved in the regulation of Rab-5 GTPases and aspects of the endocytic pathway, on the list of the top 67 hits (**Table 3**), we

have highlighted six hits that appear to function in Rho GTPase pathways (light red) and five that may be involved in secretion/endocytic pathways (light green). These proteins will be the first to validate in the nearest future.

Table 3. Potential Rabex-5 substrates

| Index | Block | Column | Row | Name | ID | AvgMN | Stdev | pval | | Notes |
|---|---|---|---|---|---|---|---|---|---|---|
| 42447 | 43 | 15 | 25 | TGFB3 | NM_003239.2 | 6.33 | 0.289 | 0.021 | | transforming growth factor beta-3 |
| 17049 | 18 | 25 | 6 | TRMT61A | NM_152307.2 | 5.92 | 0.138 | 0.011 | | Catalytic subunit of tRNA (adenine-N(1)-)-methyltransferase |
| 9141 | 10 | 21 | 7 | CDIPT | NM_006319.2 | 5.67 | 0.310 | 0.025 | | biosynthesis of phosphotidylinositol |
| 10961 | 12 | 17 | 2 | HYLS1 | BC015047.1 | 5.65 | 0.270 | 0.022 | | unknown function |
| 26007 | 27 | 23 | 7 | CDC26 | NM_139286.3 | 5.62 | 0.006 | 0.000 | | component of APC/C |
| 36735 | 38 | 31 | 1 | TMEM27 | NM_020665.2 | 5.53 | 0.121 | 0.010 | | regulates SNARE complex function |
| 34915 | 36 | 3 | 7 | MGC9913 | BC008651.1 | 5.51 | 0.007 | 0.001 | | unknown function |
| 20927 | 22 | 31 | 3 | POP4 | NM_006627.1 | 5.46 | 0.595 | 0.049 | | May function as a negative regulator of NF-kappa-B |
| 13161 | 14 | 9 | 9 | OR5H14 | NM_001005514.1 | 5.38 | 0.568 | 0.047 | | olfactory GPCR |
| 17995 | 19 | 11 | 5 | LSM7 | NM_016199.1 | 5.36 | 0.450 | 0.038 | | Binds specifically to the 3'-terminal U-tract of U6 snRNA |
| 42675 | 44 | 19 | 1 | ALG8 | BC001133.2 | 5.33 | 0.140 | 0.012 | | dolichol glycosyltransferase |
| 25081 | 26 | 25 | 9 | OR2K2 | NM_205859.1 | 5.28 | 0.038 | 0.003 | | olfactory GPCR |
| 25979 | 27 | 27 | 6 | TRIM41 | BC009762.2 | 5.28 | 0.408 | 0.035 | | E3 ligase that catalyzes degradation of protein kinase C |
| 24957 | 26 | 29 | 5 | LAMA4 | BC004241.1 | 5.27 | 0.401 | 0.034 | | unknown function |
| 25913 | 27 | 25 | 4 | CCKBR | NM_176875.2 | 5.20 | 0.048 | 0.004 | | gastrin/cholecystokinin GPRC |
| 18277 | 19 | 5 | 14 | CHST3 | NM_004273.2 | 5.18 | 0.009 | 0.001 | | catalyze the transfer of sulfate to N-acetylgalactosamine (GalNAc) |
| 27299 | 28 | 3 | 17 | MYBBP1A | BC050546.1 | 5.17 | 0.098 | 0.009 | | May activate or repress transcription |
| 13073 | 14 | 17 | 6 | KCNK17 | BC025726.1 | 5.15 | 0.223 | 0.020 | | Outward rectifying potassium channel |
| 34923 | 36 | 11 | 7 | ARL17A | BC000924.3 | 5.11 | 0.169 | 0.015 | | GTP-binding protein that functions as an allosteric activator. Involved in protein trafficking |
| 18039 | 19 | 23 | 6 | HDGFRP3 | NM_016073.2 | 5.09 | 0.189 | 0.017 | | hepatoma-derived growth factor 3 |
| 30787 | 32 | 3 | 2 | SCAMP1 | NM_004866.4 | 5.08 | 0.043 | 0.004 | | Functions in post-Golgi recycling pathway |
| 25113 | 26 | 25 | 10 | AKT1S1 | BC016043.1 | 5.07 | 0.043 | 0.004 | | Subunit of mTORC1. Inhibits RHEB-GTP-dependent mTORC1 activation |
| 27267 | 28 | 3 | 16 | GCSAM | NM_001008756.1 | 5.07 | 0.130 | 0.012 | | positive regulator of the RhoA signaling pathway |
| 34203 | 35 | 27 | 15 | ATOH1 | NM_005172.1 | 5.06 | 0.264 | 0.023 | | unknown function |
| 33915 | 35 | 27 | 6 | RPL14 | BC009294.2 | 5.05 | 0.195 | 0.017 | | ribosome constituent |
| 21849 | 23 | 25 | 1 | C9 | NM_001737.2 | 5.03 | 0.178 | 0.016 | | complement C9 |
| 25041 | 26 | 17 | 8 | TMEM135 | NM_022918.2 | 5.03 | 0.197 | 0.018 | | unknown function |
| 20857 | 22 | 25 | 1 | WSB1 | NM_015626.8 | 5.03 | 0.216 | 0.019 | | Probable substrate-recognition component of a SCF-like ECS E3 ubiquitin ligase |
| 25863 | 27 | 7 | 3 | ZC3H14 | NM_207662.2 | 5.03 | 0.402 | 0.036 | | binds polyA RNA |
| 37767 | 39 | 7 | 3 | IMAGE:4072062 | BC022851.1 | 5.03 | 0.099 | 0.009 | | |
| 23081 | 24 | 9 | 9 | OR2T8 | NM_001005522.1 | 5.03 | 0.315 | 0.028 | | olfactory GPCR |
| 13593 | 14 | 25 | 22 | C19orf66 | BC026180.1 | 5.01 | 0.055 | 0.005 | | unknown function |
| 34913 | 36 | 1 | 7 | C3AR1 | NM_004054.2 | 4.99 | 0.239 | 0.022 | | C3a anaphylatoxin chemotactic GPCR |

| | | | | | | | | | | |
|---|---|---|---|---|---|---|---|---|---|---|
| 18057 | 19 | 9 | 7 | DPH3 | NM_206831.1 | 4.98 | 0.010 | 0.001 | | Essential for the first step in the synthesis of diphthamide; possible role in the secretion process |
| 30639 | 31 | 15 | 28 | UGT2A1 | NM_006798 | 4.94 | 0.068 | 0.006 | | UDP-glucuronosyltransferase; seems to be involved in olfaction |
| 29807 | 31 | 15 | 2 | MAL2 | NM_052886.2 | 4.93 | 0.515 | 0.047 | | involved in polarized transport of endosomes |
| 12983 | 14 | 23 | 3 | RPP30 | NM_006413.2 | 4.93 | 0.048 | 0.004 | | Component of ribonuclease P |
| 12905 | 14 | 9 | 1 | TSSK6 | NM_032037.2 | 4.90 | 0.129 | 0.012 | | Testis-specific kinase 6 |
| 3187 | 4 | 19 | 7 | NAT14 | NM_020378.2 | 4.86 | 0.183 | 0.017 | | Probable acetyltransferase |
| 24849 | 26 | 17 | 2 | GFAP | NM_002055.2 | 4.85 | 0.284 | 0.026 | | a cell-specific marker |
| 18319 | 19 | 15 | 15 | LDLRAD4 | NM_181481.2 | 4.84 | 0.297 | 0.028 | | negative regulator of TGF-beta signaling |
| 22923 | 24 | 11 | 4 | GTF2F1 | BC000120.1 | 4.84 | 0.387 | 0.036 | | general transcription initiation factor |
| 23077 | 24 | 5 | 9 | OR11L1 | NM_001001959.1 | 4.83 | 0.114 | 0.011 | | olfactory GPCR |
| 17747 | 18 | 19 | 28 | MGAT5 | NM_002410 | 4.81 | 0.344 | 0.032 | | alpha-1,6-mannosylglycoprotein 6-beta-N-acetylglucosaminyltransferase activity |
| 31165 | 32 | 29 | 13 | KLK13 | NM_015596.1 | 4.80 | 0.335 | 0.031 | | Kallikrein 13 |
| 13007 | 14 | 15 | 4 | NOP56 | BC004937.1 | 4.80 | 0.232 | 0.022 | | Involved in 60S ribosomal subunit biogenesis |
| 42661 | 44 | 5 | 1 | IKBKB | BC006231.2 | 4.78 | 0.465 | 0.044 | | I-kappa-B-kinase beta |
| 21495 | 22 | 23 | 21 | P2RY4 | BC096068.1 | 4.78 | 0.456 | 0.043 | | purinergic nucleotide GPCR |
| 21055 | 22 | 31 | 7 | TFAP2A | NM_001032280.2 | 4.77 | 0.290 | 0.027 | | Sequence-specific DNA-binding protein to regulate transcription of selected genes |
| 26627 | 27 | 3 | 27 | C6 | BC035723 | 4.77 | 0.290 | 0.027 | | Complement C6 |
| 26213 | 27 | 5 | 14 | EYA2 | NM_172113.1 | 4.76 | 0.408 | 0.039 | | Functions both as protein phosphatase and as transcriptional coactivator for SIX1 |
| 33307 | 34 | 27 | 18 | FICD | NM_007076.2 | 4.74 | 0.242 | 0.023 | | Adenylyltransferase able to inactivate Rho GTPases in vitro by adding AMP to RhoA, Rac and Cdc42 |
| 34055 | 35 | 7 | 11 | PNLIPRP1 | BC025784.2 | 4.71 | 0.357 | 0.034 | | Inactive pancreatic lipase-related protein 1 |
| 26893 | 28 | 13 | 4 | NUCB1 | NM_006184.3 | 4.67 | 0.436 | 0.042 | | Major calcium-binding protein of the Golgi |
| 38239 | 39 | 31 | 17 | NBPF1 | BC034418.1 | 4.56 | 0.495 | 0.049 | | unknown function |
| 32095 | 33 | 31 | 11 | PLXNA2 | BC032125.2 | 2.44 | 0.050 | 0.009 | | Coreceptor for SEMA3A and SEMA6A |
| 9921 | 11 | 1 | 1 | ARF6 | NM_001663.2 | 2.26 | 0.044 | 0.009 | | GTP-binding protein involved in protein trafficking that regulates endocytic recycling |
| 46023 | 47 | 7 | 13 | CLMN | BC068482.1 | 2.00 | 0.093 | 0.021 | | unknown function |
| 18067 | 19 | 19 | 7 | PSMA1 | NM_002786.2 | 1.99 | 0.209 | 0.047 | | proteasome component |
| 39225 | 40 | 25 | 17 | AAAS | NM_015665.3 | 1.64 | 0.083 | 0.023 | | Plays a role in the normal development of the peripheral and central nervous system |
| 31999 | 33 | 31 | 8 | GABRA4 | NM_000809.2 | 1.61 | 0.011 | 0.003 | | GABA receptor subunit |
| 22025 | 23 | 9 | 7 | MLST8 | NM_022372.3 | 1.42 | 0.029 | 0.009 | | component of mTORs, mTORC2 fxns upstream of Rho GTPases |
| 4271 | 5 | 15 | 10 | RNF115 | NM_014455.1 | 1.30 | 0.139 | 0.048 | | endosomal trafficing of receptors |
| 33149 | 34 | 29 | 13 | UXS1 | NM_025076.3 | 1.19 | 0.102 | 0.039 | | Catalyzes the NAD-dependent decarboxylation of UDP-glucuronic |
| 13595 | 14 | 27 | 22 | CLSTN2 | BC103506.1 | 1.18 | 0.028 | 0.011 | | May modulate calcium-mediated postsynaptic signals |
| 8963 | 10 | 3 | 2 | BBS10 | BC026355.1 | 1.05 | 0.055 | 0.023 | | Probable molecular chaperone |
| 20945 | 22 | 17 | 4 | ZNF346 | NM_012279.2 | 1.02 | 0.061 | 0.027 | | dsRNA binding protein |
| | | | | | | | | | | |

**ID** = GenBank accession number; $\mathbf{M_N}$ = duplicate-summarized, normalized, $\log_2$ transformed fluorescence intensity from the protein, values obtained from the experimental array minus those obtained from the negative control array; **SD** = standard deviation of the difference above (standard deviation of two numbers subtracted was the square root of the sum of squares of the standard deviations associated with each of the two numbers); **pVal** = p value from 2-tailed, paired T-test for significance of change.

# DISCUSSION

E3 ubiquitin ligases are key regulatory enzymes of the ubiquitination pathway as they are responsible for substrate specificity. This thesis aimed at deciphering the molecular mechanisms through which two different E3 ligases, Nedd4 and Rabex-5, exert their activity.

Nedd4 is the prototype for HECT-E3 ligase while Rabex-5, containing an A20 zinc finger domain (ZnF_A20) instead of a canonical RING, could be defined as an atypical RING-E3 ligase.

## 1. Dissecting the mechanism of catalysis of Nedd4

Nedd4 belongs to the family of E3 enzymes known as HECT. Homologous to E6-AP C terminus (HECT) E3 ligases recognize and directly catalyze ligation of Ub to their substrates. The HECT domain is the catalytic portion of these E3 enzymes and is necessary and sufficient to promote ubiquitination. This region is composed of two lobes, the N-lobe and the C-lobe, that are connected by a flexible linker. Intriguingly, previous structural studies suggested that these lobes might adopt a variety of positions with respect to each other (**Figure 14**). This flexibility is absolutely required for catalysis (Kamadurai et al., 2013; Verdecia et al., 2003).

Nedd4 and other HECT E3s function through a two-step mechanism. First, ubiquitin is transferred from the catalytic cysteine of an E2 enzyme to that on the E3 HECT domain. This produces a transient HECT~ubiquitin intermediate that is linked by a thioester bond. Next, ubiquitin is transferred from the HECT E3 cysteine to either a substrate protein, or to a specific lysine on the surface of ubiquitin to generate a chain. This process is often compared to a relay, where ubiquitin is the baton transferred between athletes (e.g. E2, E3,

substrate, and eventually ubiquitin linked to substrate). Chains are thought to be generated by a sequential addition mechanism (Kim and Huibregtse, 2009) (**Figure 19**). Molecular details of this process remain unknown.

In particular, no one has ever been able to "see" the transient intermediate with ubiquitin linked at a HECT E3 catalytic cysteine, because such complexes are extremely unstable. We overcame this challenge by using an alternative, more stable bond to link the active site of the Nedd4 HECT and ubiquitin. The crystal structure of the complex ($HECT^{Nedd4}$~$Ub^{D}$:$Ub^{A}$) was determined at 2.51Å resolution (**Table 2 and Figure 26**). Our structure was the first capturing the elusive HECT~ubiquitin intermediate, after transfer of ubiquitin from E2 (Maspero et al., 2013).

### 1.1 Molecular validation of the sequential addition model

The $HECT^{Nedd4}$~Ub transitory intermediate provides a structural basis for the proposed sequential addition mechanism. The Ub of the $HECT^{Nedd4}$~Ub interacts with the C-lobe of the HECT in the same position as in the crystal structure of Nedd4-like HECT domain in complex with Ub-loaded Ube2D2 (Kamadurai et al., 2009). The relative orientation between the N- and C-lobe and between the C-lobe and $Ub^{D}$ is also maintained (**Figure 26B**). To our knowledge this is the first time that two C-lobes from different HECT structures show the same orientation. Based on that, we can conclude that our structure represents the step that immediately follows the transfer of the thioester bond from the E2 to the E3, in which $Ub^{D}$ has been handed over to the C-lobe, and is ready to be transferred to the substrate.

One of the key features that we found is that, after the transfer of $Ub^{D}$ from the E2 to the E3, the non-covalent interaction between the C-lobe and the $Ub^{D}$ is conserved (Kamadurai et al., 2009). Thus, due to steric hindrance, a second Ub-loaded E2 enzyme is unable to access the C-lobe Ub binding site until the E3 transfers its transiently bound Ub

to the substrate or to the growing Ub chain. Only after this has occurred, another cycle of transthiolation reaction between the E2~Ub and the E3 can take place. This discovery strongly supports the sequential addition model proposed for some HECT ligases in which single Ub moiety are added at one time (Kim and Huibregtse, 2009; Maspero et al., 2011).

### 1.2 Implications for the $Ub^D$ C-terminal tail-locking

Differently from most of the conserved contacts between $Ub^D$ and the C-lobe, the last three residues of $Ub^D$ display a dramatic rearrangement with respect to the $HECT^{Nedd4L}$:Ube2D2~Ub structure. The $Ub^D$, transferred from the E2, acquired an extra surface of interaction with the C-lobe. Clearly visible in our structure, the Ub C-terminal tail, generally flexible, is locked in an extended conformation due to the hydrogen bond pattern that generates a β-sheet augmentation, common motif in protein-protein interaction (**Figure 26C and Figure 37A**).

This stretched conformation shows the catalytic bond suitably positioned for attack by the substrate protein's lysine. A similar $Ub^D$ tail stretch conformation was recently observed in other E3s structures such as the one of RNF4:Ube2D1~Ub (Plechanovova et al., 2012) and of BIRC7:Ube2D2~Ub complex (Dou et al., 2012) (**Figure 43B-C**). The authors demonstrated that the Ub tail held on the E2, is in an optimal conformation for nucleophilic attack by the incoming lysine residue of the substrate. In addition, the same tail stretch was displayed by SUMO~RanGAP1-Ubc9-Nup358 complex even if the SUMO modifier is just transferred to the substrate (Reverter and Lima, 2005) (**Figure 43D**). Therefore, we propose that docking the flexible C-terminal tail of Ub in an extended conformation might be a common, evolutionary-conserved, mechanism adopted by both E2s and E3s to prime the $Ub^D$ for catalytic transfer to the substrate.

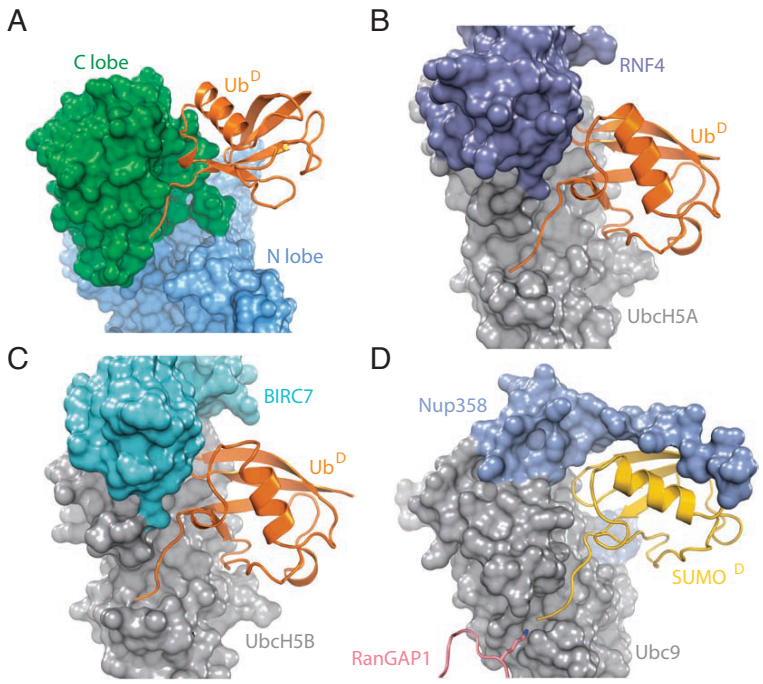


**Figure 43. The tail stretch of Ub$^{D}$ primed for catalysis** (adapted from Maspero E., Nat. Struct. Mol. Biol. 2013). Extended conformation of the Ub$^{D}$ tail (orange) or SUMO C-terminal tail (yellow) when formed the complex HECT$^{Nedd4}$~Ub(Maspero et al., 2013) (A), or in the complex RNF4-Ube2D1~Ub(Plechanovova et al., 2012) (B), BIRC7-Ube2D2-Ub(Dou et al., 2012) (C) and SUMO~RanGAP1-Ubc9-Nup358 complex(Reverter and Lima, 2005) (D).

### 1.3 Role of the UBD in the N-lobe

Our data elucidated some aspects of the molecular mechanism by which the HECT domain of the E3 ligase Nedd4 exerts its catalytic activity. However, several important questions remained. As predicted (Maspero et al., 2011), loading of the Ub$^{D}$ onto HECT$^{Nedd4}$ catalytic cysteine is compatible with free Ub bound to the Ub binding region embedded in the N-lobe of the HECT. Previously, we have characterized this UBD present in Nedd4, by solving the structure of the HECT domain in complex with free Ub (Maspero et al., 2011). We have postulated that this site is important to keep the acceptor Ub from the growing chain in close proximity to the catalytic cysteine favoring enzyme processivity. In a

parallel study, Huibregtse and colleagues reached the same conclusion about the role of the UBD in Rsp5 (Kim et al., 2011).

Once we solved the structure of the Ub-loaded E3 in complex with Ub, the position of the non-covalently bound Ub molecule in the crystal structure did not provide any clue on how ubiquitination should work, as Lys63 of the "acceptor" Ub ($Ub^A$) is far away from the HECT catalytic cysteine. Thus, we concluded that the free Ub bound to the UBD is not the $Ub^A$. One possibility is that the Ub bound to UBD is instead the last before the $Ub^A$ of the chain. To solve this issue we intend to determine the crystal structure of the Ub-loaded E3 in complex with Ub Lys63 dimer or trimer.

Another intriguing possibility is that the non-covalently bound Ub may work as an allosteric activator of the HECT, as it was recently found for the Ub bound to the "back side" of the E2 enzyme (Buetow et al., 2015). Using RNF38 as model system, Huang and colleagues found that the free Ub bound the UBD in the back side of the E2 has a primary role to stabilize a catalytic favorable conformation of the RING E3:Ube2D2-Ub interaction. This catalytic favorable conformation facilitates the Ub transfer including initial Ub transfer to a substrate lysine (Buetow et al., 2015). It could be possible that the binding of Ub in the UBD of the HECT domain may induces a similar allosteric activation, promoting enzyme processivity, even if our initial observation using KO ubiquitin (data not shown) seems to disprove this idea.

### 1.4 Nedd4 polyubiquitination: chain elongation is different from the first Ub addition?

After our study, Schulman and co-workers have captured the moment in which Rsp5, the HECT enzyme essential in yeast, transfers ubiquitin to a lysine residue within a target protein called Sna3 (Kamadurai et al., 2013). The authors took a chemical approach to substitute the substrate lysine acceptor with a bifurcated crosslinker conjugated to a

modified Ub Cys75 and the HECT catalytic Cys. The structure suggests that both specific orientation between the N- and the C-lobes of the HECT domain and unique active site conformation are required for the selection of the target Lys and ligation. Importantly, Kamadurai et al. revealed that a dramatic re-arrangement of the C-lobe of the HECT domain is required to transfer the Ub to the lysine of the substrate. They described a C-lobe swiveling of ~130° to place the thioester in proximity to a substrate lysine (**Figure 44**)(Kamadurai et al., 2013).

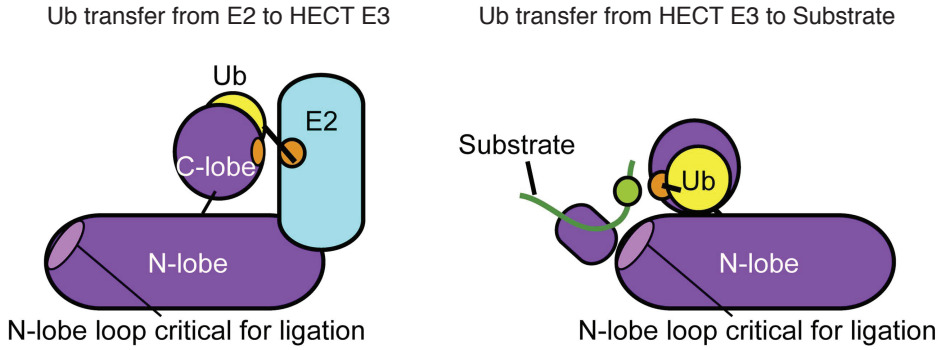


**Figure 44. Substrate ubiquitination performed by HECT$^{Rsp5}$ domain** (adapted from Kamadurai, eLIFE, 2013). Schematic view of the E2-to-E3 transfer of Ub (on the left) and the next step of the transfer of Ub from the catalytic cysteine of the HECT$^{Rsp5}$ domain to the lysine of the substrate (on the right). These steps required a dramatic re-arrangement of the C-lobe.

This re-arrangement fits well with the previous studies showing the importance of the flexible linker between the N- and the C-lobe (Kamadurai et al., 2013; Kamadurai et al., 2009; Verdecia et al., 2003), and with the various crystal structures that show variability in the reciprocal orientation of the two subdomains (**Figure 14**). This structure, though, does not help in rationalizing the role of the UBD.

The sum of our and Schulman's lab data led us to propose an intriguing model. First Nedd4 faces E2 to receive ubiquitin. After ubiquitin transfer to the Nedd4 HECT domain, a new beta sheet stabilizes the intermediate. Then, the Nedd4 HECT E3 turns around to face the substrate and deliver the ubiquitin to the first lysine. After the first

ubiquitin has been attached, the HECT might continue to receive Ub from the E2 and to polymerize ubiquitin chains, without the C-lobe rotation and stabilizing the interaction with the growing chain thanks to the UBD. This hypothesis is based on the observation that a point mutation in the UBD of the HECT domain, which abrogates the Ub interaction, impairs the polyubiquitination of the substrate without altering the addition of the first Ub moiety (Maspero et al., 2011). It is also supported by computational docking data we are generating in collaboration with Anna Tramontano in Rome. In essence, we propose that monoubiquitination and polyubiquitination mediated by Nedd4 occurs via two distinct mechanisms that have different requirements. For monoubiquitination we need the swinging of the C-lobe but not the UBD while for chain elongation the UBD is required while the C-lobe rotation is not.

To provide a clear picture about the role of the UBD, other structural studies with Nedd4 in complex with ubiquitinated substrate or Ub chains are required. To trap the catalytic step we will use the same approach as in HECT~$Ub^D$:Ub complex in which the HECT domain is loaded with $Ub^D$ (active state) through a non reducible covalent bond. It will be interesting to see if HECT E3s can also be 'caught in the act' of assembling a chain, as this could reveal how multiple interactions contributed by several domains of the enzyme establish catalytic efficiency and specificity.

## 2. Characterization of Rabex-5 as E3 ligase

Our lab demonstrated that Rabex-5 binds Ub through its two UBDs, MIU domain and the ZnF_A20 domain, determining its coupled monoubiquitination and allowing interaction *in vivo* with the ubiquitinated form of EGFR (Penengo et al., 2006). Rabex-5 was also proposed to be an E3 ligase thanks to its ability to ubiquitinate itself via the ZnF_A20 domain (Lee et al., 2006a) and its substrate H-Ras (Xu et al., 2010). Still unclear is how

Rabex-5 exerts its E3 ligase activity. This thesis intended to clarify some aspects of the E3 ligase activity of Rabex-5.

### 2.1 Efforts to solve the structure of Rabex-5 with its specific E2

In most of the studied cases the E2-E3 interaction is selective. Few E2s are expected to function with a given E3 and each E2-E3 pairs may be selective for putative substrates and for their type of Ub modification (Christensen et al., 2007). So the first step in the Rabex-5 characterization as E3 ligase was the identification of possible E2 partners.

In order to define the E2s, we set up a yeast-two-hybrid screening between Rabex-$5^{1-74}$ and a complete library of human E2s and we demonstrated that Rabex-$5^{1-74}$ interacts specifically only with a subset of them (**Figure 27**). These E2s are members of the Ube2D and Ube2E families.

The E2-E3 interaction is usually transient and of modest affinity, and indeed we found that the binding between Rabex-$5^{1-74}$ and the specific E2 was significant only when the E2 is in its active state, loaded with Ub (**Figure 28A**). Using either single point mutants in the UBDs on Rabex-$5^{1-74}$ as well as isolated UBDs (ZnF_A20 and MIU domains) we are unable to define which was the UBD required for the interaction as both seem to be necessary (**Figure 28A-29**). In addition, Rabex-5 full length binds the E2-Ub in a comparable manner respect to the Rabex-$5^{1-74}$ fragment suggesting that no additional domains are required (**Figure 28B**).

ITC analysis confirmed our biochemical data, proving that the contribution of the E2 in binding Rabex-$5^{1-74}$ is very limited and that the interaction between the two proteins is mainly mediated by the Ub carried by the E2 and the UBDs of Rabex-5 (**Figure 30**). Thus, we propose that the initial binding occurs through this interaction that drives the correct positioning of the E2, possibly allowing activation of the E2. As the two UBDs of Rabex-5 are able to interact with Ub using different surface (Penengo et al., 2006) we hypothesize a

possible different role of the two in substrate ubiquitination.

To characterize Rabex-5 as E3 ligase it is crucial to obtain the structure of the Rabex-$5^{1-74}$:E2-Ub complex. We tried different strategies to obtain a stable Rabex-$5^{1-74}$:Ube2D3-Ub complex, enough pure and homogeneous for crystallization purpose and for SAXS analysis.

Our first attempt was the generation of a disulfide bond between the catalytic cysteine of the E2 and Ub (G76C) mutant. This approach was unsuccessful due to the instability of the disulfide E2~Ub in presence of Rabex-$5^{1-74}$. Indeed, we considered the ability of Rabex-5 to break down the disulfide bond, releasing free Ub a clear sign of its E3 activity (**Figure 33**, further discussed below). To mimic an E2 loaded with Ub, we decided to create an isopeptide bond between the C-terminal of Ub and the artificially created Lys of the E2 C85K mutant. Mixing together the isopeptide E2-Ub with Rabex-$5^{1-74}$ and purified the complex on a size exclusion chromatography (Superdex 75 column), we obtained a suitable sample that we used both in crystallization trays and in SAXS analysis. In this context, we generated complexes using either Rabex-$5^{1-74}$ wild type or Rabex-$5^{1-74}$ A58G. This MIU mutant generates a more homogenous sample, maintaining the catalytic activity of the ZnF_A20 domain (**Figure 36**).

Unfortunately, in none of the conditions tested we obtained reproducible crystals. One possible reason for this failure is that the samples were not enough pure or homogeneous. Indeed, the isopeptide bond is formed via an *in vitro* reaction and analyzing our samples we found that the ubiquitination occurs at our target Lys 85 (**Figure 35**) but also at the natural Lys (K8, K133 and K144) present in the E2 determining the presence of these different species impossible to eliminate with purification procedures (**Figure 34**). A second possible explanation could arise from the constructs we used. To improve the rate of isopeptide reaction we used an E2 mutated in the backside (S22R, (Plechanovova et al., 2012)) while to avoid aggregation we used a MIU mutant (A58G, (Penengo et al., 2006)).

As previously discussed, a recent paper underlined the importance of the interaction between the backside E2 and the allosteric activator free Ub (Buetow et al., 2015). A future effort will be to repeat the crystallization trays with E2-Ub:Rabex-$5^{1-74}$ wild type complex in presence of free Ub.

SAXS analysis was also disappointing and we did not obtain any information about the tridimensional arrangement of the complex. We initially tested Rabex-$5^{1-74}$ wild type (data not shown) but the presence of high aggregation in size exclusion chromatography and low scattering intensity precluded data elaboration. With the Rabex-$5^{1-74}$ A58G:E2-Ub complex we obtained technically good spectra but we failed to obtain an unambiguous *ab-initio* positioning of the E2 molecule due to its small size and consequent low scattering intensity.

To overcome this problem we generated models of Rabex-$5^{1-74}$:E2-Ub interaction based on the crystal structure of Rabex-$5^{1-74}$ wild type (Penengo et al., 2006) and different crystal structures of E2-Ub alone (Hamilton et al., 2001; Page et al., 2012; Sakata et al., 2010) and in complex with a RING-E3 ligase (Plechanovova et al., 2012) or with an HECT-E3 ligase (Kamadurai et al., 2009). Unfortunately, all models generated did not fit with the experimental data suggesting that the complex assume a different conformation that we are unable to determine in these conditions (**Figure 37**).

### 2.2 Ligase activity of Rabex-5

It has been reported that Rabex-5 possessess an E3 ligase activity thanks to its ability to ubiquitinate itself (Lee et al., 2006a) and its substrate H-Ras (Xu et al., 2010). Using *in vitro* ubiquitination assay, Lee et al. demonstrated that Rabex-5 undergoes polyubiquitination that is impaired once the ZnF_A20 domain is mutated in specific tyrosine residues (Y25 and Y26) critical for Ub binding (Lee et al., 2006b; Penengo et al.,

2006). Two parallel studies proved, by *in vivo* experiments, that Rabex-5 undergoes to monoubiquitination and for this process the MIU domain is required (Mattera et al., 2006; Penengo et al., 2006). Later, H-Ras was found as a possible substrate of the E3 ligase activity of Rabex-5 by *in vivo* and *in vitro* assays. H-Ras becomes mono- and di-ubiquitinated in presence of Rabex-5 wild type while the ubiquitination is impaired when the ZnF_A20 domain mutant (Y25/Y26A) is used (Xu et al., 2010). This modification can promote endosomal association leading to attenuation of Ras-ERK signaling (Jura and Bar-Sagi, 2006; Xu et al., 2010).

### 2.2.1 Ability to perform self-ubiquitination

To clarify whether Rabex-5 as E3 ligase is able to perform self-ubiquitination by adding one or multiple Ub moieties, we set up an *in vitro* self-ubiquitination assays in which we scored monoubiquitination of Rabex-$5^{1-74}$ and of the full-length protein. Interestingly, full-length kinetics seems to be faster than the Rabex-$5^{1-74}$ kinetics, a difference that we intend to investigate further (**Figure 39A**).

Taking advantage of point mutants on Rabex-$5^{1-74}$ as well as of the isolated UBD domains, we confirmed the important role of the ZnF_A20 domain in self-ubiquitination (**Figure 39B-C**). We also proved the E3 ligase activity of Rabex-5 using a second assay that measure the disruption of the disulfide bond of the E2~Ub in the presence of Rabex-5 fragments. Incubation of the E2~Ub with Rabex-$5^{1-74}$ wild type increases free Ub over the time while we did not score the same effect when we used the Rabex-$5^{1-74}$ mutated in the ZnF_A20 (**Figure 38**). The disulfide bond disruption could be ascribed as an unspecific effect due to the presence of a Cys residue in the protein. However mutation on the putative ZnF_A20 domain responsible for the E3 ligase activity is impaired in the disulfide bond disruption. Based on this result we proposed that the scored effect is a specific

behavior of Rabex-5 related to the E3 ligase activity.

We speculate that Rabex-5 may act as an E3 ligase via the evolutionary conserved mechanism we discussed for Nedd4 (**Figure 43**) that primes the $Ub^D$ linked to the active site for catalysis. Unfortunately, in the absence of the Rabex-5:E2-Ub structure we did not have the possibility to prove/disprove our hypothesis so far.

### 2.2.2 Substrate ubiquitination

An important validation for the putative role of Rabex-5 as E3 ligase is the identification of substrates proteins. Except for H-Ras (Xu et al., 2010), no other substrates of Rabex-5 are identified to date. As a first approach, we tested H-Ras protein using different *in vivo* and *in vitro* conditions and evaluating both Rabex-5 full length and Rabex-$5^{1-74}$. We were able to score H-Ras monoubiquitination only in an *in vitro* assay but this was evident also in the absence of Rabex-5 (**Figure 40**). As not even a difference in reaction kinetics was visible between the two conditions, we concluded that Rabex-5 is not an E3 for H-Ras. Positive results are possibly due to the high concentration of E2 used that can force the reaction to proceed in the absence of an E3 (Hoeller et al., 2007).

We then decided to search for new Rabex-5 substrates with an unbiased approach using a protein microarray and a fluorescence-Ub-based assay provided by LifeSensor. To be sure about the specificity of the Rabex-5 ligase activity we ran the assay also in the absence of the Rabex-5 but in the presence of the E2.

From all 20,000 human proteins tested, 1007 hits showed a significant difference in fluorescence respect to the negative control. Interestingly, all positive hits showed low fluorescence intensity suggesting that they could be only mono or di-ubiquitinated. This result fits well with our *in vitro* data. At first glance, 629 out of 1007 were considered positive hits as they showed an increase of intensity in ubiquitination, but most of them are

borderlines. Starting from these 629 possible substrates we selected the top 67 hits based on their highest fluorescent intensities (**Table 3**). We are going to validate these possible substrates starting from proteins that are involved in the endocytic pathway.

In conclusion, we have elucidated some aspects of how Rabex-5 may act as E3 ligase but much more needs to be done. At this point we can only speculate about how Rabex-5 exerts its activity and about the role of self-ubiquitination. An important question that remains to be answered is the role of the two different UBDs in Rabex-5. While the ZnF_A20 domain is apparently required, similar to the RING, to promote catalysis, we still do not have clues on the function of the MIU.

It could be possible that the MIU in Rabex-5 works in a way similar to the UBD present in the N-lobe of Nedd4, maintaining the binding of ubiquitinated substrates and promoting their polyubiquitination by the ZnF_A20 domain. Alternatively, the binding of the MIU with free Ub may allosteric activate Rabex-5 (Buetow et al., 2015). We tend to exclude that the MIU may bind the Ub bound to the backside of the E2 as both domains requires the same hydrophobic patch centered on Ile44. It worth mentioning that the MIU domain may also trigger coupled monoubiquitination (Penengo et al., 2006), similar to what occurs in several UIM-containing endocytic proteins (Woelk et al., 2006).

From the functional point of view, the MIU together with the ZnF_A20 domain are critical for the interaction with the ubiquitinated form of EGFR (Penengo et al., 2006) and are required for Rabex-5 recruitment to the endosomes (Mattera and Bonifacino, 2008). Once Rabex-5 is associated with the endosome it exerts its GEF activity to Rab-5 promoting homo- and heterotypic endosomes fusion (Mattera and Bonifacino, 2008). Bonifacino‘s lab also provided evidence that MIU-dependent coupled monoubiquitination may lead to Rabex-5 dissociation from the endosome. The authors proposed a model

whereby the UBDs interact with the Ub moiety covalently attached to Rabex-5 (Mattera and Bonifacino, 2008)(**Figure 45**). Also this hypothesis remains to be tested.

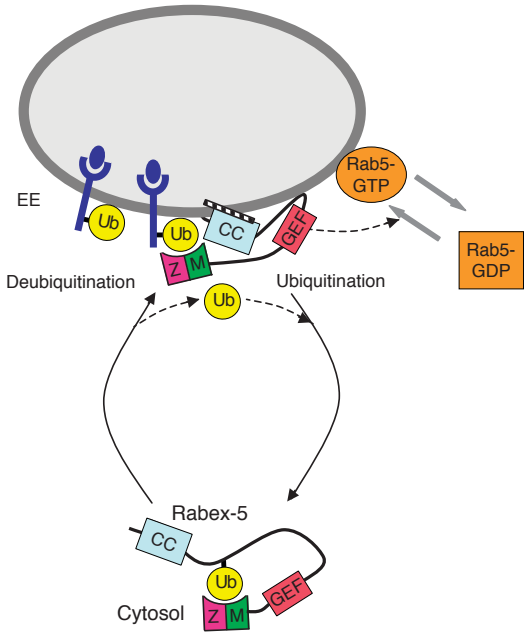


**Figure 45. Proposed model of the role of UBDs or Rabex-5 and its monoubiquitination** (adapted from Mattera and Bonifacino, Embo J, 2008). Rabex-5 is recruited to the endosome by the interaction between the two UBDs, ZnF_A20 (Z) and MIU (M) domains, and the ubiquitinated cargoes. At the endosome Rabex-5 activates Rab-5 via its GEF activity, determining endosome fusion. Dissociation from endosome with consequent Rabex-5 release in the cytosol occurs thanks to its monoubiquitination that causes an intra molecular interaction.

# REFERENCES


Acconcia, F., Sigismund, S., and Polo, S. (2009). Ubiquitin in trafficking: the network at work. Experimental cell research *315*, 1610-1618.

Aguilera, M., Oliveros, M., Martinez-Padron, M., Barbas, J.A., and Ferrus, A. (2000). Ariadne-1: a vital Drosophila gene is required in development and defines a new conserved family of ring-finger proteins. Genetics *155*, 1231-1244.

Al-Hakim, A.K., Zagorska, A., Chapman, L., Deak, M., Peggie, M., and Alessi, D.R. (2008). Control of AMPK-related kinases by USP9X and atypical Lys(29)/Lys(33)-linked polyubiquitin chains. The Biochemical journal *411*, 249-260.

Aravind, L., and Koonin, E.V. (2000). The U box is a modified RING finger - a common domain in ubiquitination. Curr Biol *10*, R132-134.

Bai, C., Sen, P., Hofmann, K., Ma, L., Goebl, M., Harper, J.W., and Elledge, S.J. (1996). SKP1 connects cell cycle regulators to the ubiquitin proteolysis machinery through a novel motif, the F-box. Cell *86*, 263-274.

Baker, R., Lewis, S.M., Sasaki, A.T., Wilkerson, E.M., Locasale, J.W., Cantley, L.C., Kuhlman, B., Dohlman, H.G., and Campbell, S.L. (2013). Site-specific monoubiquitination activates Ras by impeding GTPase-activating protein function. Nature structural & molecular biology *20*, 46-52.

Ben-Saadon, R., Zaaroor, D., Ziv, T., and Ciechanover, A. (2006). The polycomb protein Ring1B generates self atypical mixed ubiquitin chains required for its in vitro histone H2A ligase activity. Molecular cell *24*, 701-711.

Berndsen, C.E., Wiener, R., Yu, I.W., Ringel, A.E., and Wolberger, C. (2013). A conserved asparagine has a structural role in ubiquitin-conjugating enzymes. Nat Chem Biol *9*, 154-156.

Bernier-Villamor, V., Sampson, D.A., Matunis, M.J., and Lima, C.D. (2002). Structural basis for E2-mediated SUMO conjugation revealed by a complex between ubiquitin-conjugating enzyme Ubc9 and RanGAP1. Cell *108*, 345-356.

Bos, J.L. (1989). ras oncogenes in human cancer: a review. Cancer Res *49*, 4682-4689.

Bosanac, I., Wertz, I.E., Pan, B., Yu, C., Kusam, S., Lam, C., Phu, L., Phung, Q., Maurer, B., Arnott, D*., et al.* (2010). Ubiquitin binding to A20 ZnF4 is required for modulation of NF-kappaB signaling. Molecular cell *40*, 548-557.

Bremm, A., Freund, S.M., and Komander, D. (2010). Lys11-linked ubiquitin chains adopt compact conformations and are preferentially hydrolyzed by the deubiquitinase Cezanne. Nature structural & molecular biology *17*, 939-947.

Brooks, W.S., Helton, E.S., Banerjee, S., Venable, M., Johnson, L., Schoeb, T.R., Kesterson, R.A., and Crawford, D.F. (2008). G2E3 is a dual function ubiquitin ligase required for early embryonic development. The Journal of biological chemistry *283*, 22304-22315.

Brzovic, P.S., Keeffe, J.R., Nishikawa, H., Miyamoto, K., Fox, D., 3rd, Fukuda, M., Ohta, T., and Klevit, R. (2003). Binding and recognition in the assembly of an active BRCA1/BARD1 ubiquitin-ligase complex. Proceedings of the National Academy of Sciences of the United States of America *100*, 5646-5651.

Brzovic, P.S., Lissounov, A., Christensen, D.E., Hoyt, D.W., and Klevit, R.E. (2006). A UbcH5/ubiquitin noncovalent complex is required for processive BRCA1-directed ubiquitination. Molecular cell *21*, 873-880.

Buetow, L., Gabrielsen, M., Anthony, N.G., Dou, H., Patel, A., Aitkenhead, H., Sibbet, G.J., Smith, B.O., and Huang, D.T. (2015). Activation of a primed RING E3-E2-ubiquitin complex by non-covalent ubiquitin. Molecular cell *58*, 297-310.

Buschhorn, B.A., and Peters, J.M. (2006). How APC/C orders destruction. Nat Cell Biol *8*, 209-211.
Capili, A.D., Schultz, D.C., Rauscher, I.F., and Borden, K.L. (2001). Solution structure of the PHD domain from the KAP-1 corepressor: structural determinants for PHD, RING and LIM zinc-binding domains. The EMBO journal *20*, 165-177.
Chen, Z.J., and Sun, L.J. (2009). Nonproteolytic functions of ubiquitin in cell signaling. Molecular cell *33*, 275-286.
Christensen, D.E., Brzovic, P.S., and Klevit, R.E. (2007). E2-BRCA1 RING interactions dictate synthesis of mono- or specific polyubiquitin chain linkages. Nature structural & molecular biology *14*, 941-948.
Clague, M.J., Coulson, J.M., and Urbe, S. (2012). Cellular functions of the DUBs. Journal of cell science *125*, 277-286.
Cox, A.D., and Der, C.J. (2003). The dark side of Ras: regulation of apoptosis. Oncogene *22*, 8999-9006.
Dantuma, N.P., Groothuis, T.A., Salomons, F.A., and Neefjes, J. (2006). A dynamic ubiquitin equilibrium couples proteasomal activity to chromatin remodeling. The Journal of cell biology *173*, 19-26.
Datta, A.B., Hura, G.L., and Wolberger, C. (2009). The structure and conformation of Lys63-linked tetraubiquitin. Journal of molecular biology *392*, 1117-1124.
Delprato, A., Merithew, E., and Lambright, D.G. (2004). Structure, exchange determinants, and family-wide rab specificity of the tandem helical bundle and Vps9 domains of Rabex-5. Cell *118*, 607-617.
Deshaies, R.J. (1999). SCF and Cullin/Ring H2-based ubiquitin ligases. Annu Rev Cell Dev Biol *15*, 435-467.
Deshaies, R.J., and Joazeiro, C.A. (2009). RING domain E3 ubiquitin ligases. Annual review of biochemistry *78*, 399-434.
Dikic, I., Wakatsuki, S., and Walters, K.J. (2009). Ubiquitin-binding domains - from structures to functions. Nature reviews Molecular cell biology *10*, 659-671.
Dou, H., Buetow, L., Sibbet, G.J., Cameron, K., and Huang, D.T. (2012). BIRC7-E2 ubiquitin conjugate structure reveals the mechanism of ubiquitin transfer by a RING dimer. Nature structural & molecular biology *19*, 876-883.
Dunn, R., Klos, D.A., Adler, A.S., and Hicke, L. (2004). The C2 domain of the Rsp5 ubiquitin ligase binds membrane phosphoinositides and directs ubiquitination of endosomal cargo. The Journal of cell biology *165*, 135-144.
Durfee, L.A., Lyon, N., Seo, K., and Huibregtse, J.M. (2010). The ISG15 conjugation system broadly targets newly synthesized proteins: implications for the antiviral function of ISG15. Molecular cell *38*, 722-732.
Dye, B.T., and Schulman, B.A. (2007). Structural mechanisms underlying posttranslational modification by ubiquitin-like proteins. Annu Rev Biophys Biomol Struct *36*, 131-150.
Eddins, M.J., Varadan, R., Fushman, D., Pickart, C.M., and Wolberger, C. (2007). Crystal structure and solution NMR studies of Lys48-linked tetraubiquitin at neutral pH. Journal of molecular biology *367*, 204-211.
Eisenhaber, B., Chumak, N., Eisenhaber, F., and Hauser, M.T. (2007). The ring between ring fingers (RBR) protein family. Genome biology *8*, 209.
Eletr, Z.M., Huang, D.T., Duda, D.M., Schulman, B.A., and Kuhlman, B. (2005). E2 conjugating enzymes must disengage from their E1 enzymes before E3-dependent ubiquitin and ubiquitin-like transfer. Nature structural & molecular biology *12*, 933-934.

Escobedo, A., Gomes, T., Aragon, E., Martin-Malpartida, P., Ruiz, L., and Macias, M.J. (2014). Structural basis of the activation and degradation mechanisms of the E3 ubiquitin ligase Nedd4L. Structure *22*, 1446-1457.
Feldman, R.M., Correll, C.C., Kaplan, K.B., and Deshaies, R.J. (1997). A complex of Cdc4p, Skp1p, and Cdc53p/cullin catalyzes ubiquitination of the phosphorylated CDK inhibitor Sic1p. Cell *91*, 221-230.
Finley, D., Bartel, B., and Varshavsky, A. (1989). The tails of ubiquitin precursors are ribosomal proteins whose fusion to ubiquitin facilitates ribosome biogenesis. Nature *338*, 394-401.
Fouladkou, F., Landry, T., Kawabe, H., Neeb, A., Lu, C., Brose, N., Stambolic, V., and Rotin, D. (2008). The ubiquitin ligase Nedd4-1 is dispensable for the regulation of PTEN stability and localization. Proceedings of the National Academy of Sciences of the United States of America *105*, 8585-8590.
French, M.E., Kretzmann, B.R., and Hicke, L. (2009). Regulation of the RSP5 ubiquitin ligase by an intrinsic ubiquitin-binding site. The Journal of biological chemistry *284*, 12071-12079.
Gareau, J.R., and Lima, C.D. (2010). The SUMO pathway: emerging mechanisms that shape specificity, conjugation and recognition. Nature reviews Molecular cell biology *11*, 861-871.
Haas, A.K., Fuchs, E., Kopajtich, R., and Barr, F.A. (2005). A GTPase-activating protein controls Rab5 function in endocytic trafficking. Nat Cell Biol *7*, 887-893.
Hamilton, K.S., Ellison, M.J., Barber, K.R., Williams, R.S., Huzil, J.T., McKenna, S., Ptak, C., Glover, M., and Shaw, G.S. (2001). Structure of a conjugating enzyme-ubiquitin thiolester intermediate reveals a novel role for the ubiquitin tail. Structure *9*, 897-904.
Hanpude, P., Bhattacharya, S., Dey, A.K., and Maiti, T.K. (2015). Deubiquitinating enzymes in cellular signaling and disease regulation. IUBMB life.
Harvey, K.F., Dinudom, A., Cook, D.I., and Kumar, S. (2001). The Nedd4-like protein KIAA0439 is a potential regulator of the epithelial sodium channel. The Journal of biological chemistry *276*, 8597-8601.
Harvey, K.F., Dinudom, A., Komwatana, P., Jolliffe, C.N., Day, M.L., Parasivam, G., Cook, D.I., and Kumar, S. (1999). All three WW domains of murine Nedd4 are involved in the regulation of epithelial sodium channels by intracellular Na+. The Journal of biological chemistry *274*, 12525-12530.
Herhaus, L., and Dikic, I. (2015). Expanding the ubiquitin code through post-translational modification. EMBO reports *16*, 1071-1083.
Hershko, A., and Ciechanover, A. (1998). The ubiquitin system. Annual review of biochemistry *67*, 425-479.
Hicke, L. (2001). Protein regulation by monoubiquitin. Nature reviews Molecular cell biology *2*, 195-201.
Hicke, L., Schubert, H.L., and Hill, C.P. (2005). Ubiquitin-binding domains. Nature reviews Molecular cell biology *6*, 610-621.
Hirano, S., Kawasaki, M., Ura, H., Kato, R., Raiborg, C., Stenmark, H., and Wakatsuki, S. (2006). Double-sided ubiquitin binding of Hrs-UIM in endosomal protein sorting. Nature structural & molecular biology *13*, 272-277.
Hochstrasser, M. (2006). Lingering mysteries of ubiquitin-chain assembly. Cell *124*, 27-34.
Hoeller, D., Hecker, C.M., Wagner, S., Rogov, V., Dotsch, V., and Dikic, I. (2007). E3-independent monoubiquitination of ubiquitin-binding proteins. Molecular cell *26*, 891-898.

Hofmann, K., and Falquet, L. (2001). A ubiquitin-interacting motif conserved in components of the proteasomal and lysosomal protein degradation systems. Trends in biochemical sciences *26*, 347-350.
Horiuchi, H., Lippe, R., McBride, H.M., Rubino, M., Woodman, P., Stenmark, H., Rybin, V., Wilm, M., Ashman, K., Mann, M.*, et al.* (1997). A novel Rab5 GDP/GTP exchange factor complexed to Rabaptin-5 links nucleotide exchange to effector recruitment and function. Cell *90*, 1149-1159.
Hua, Z., and Vierstra, R.D. (2011). The cullin-RING ubiquitin-protein ligases. Annu Rev Plant Biol *62*, 299-334.
Huang, D.T., Ayrault, O., Hunt, H.W., Taherbhoy, A.M., Duda, D.M., Scott, D.C., Borg, L.A., Neale, G., Murray, P.J., Roussel, M.F.*, et al.* (2009). E2-RING expansion of the NEDD8 cascade confers specificity to cullin modification. Molecular cell *33*, 483-495.
Huang, H., Jeon, M.S., Liao, L., Yang, C., Elly, C., Yates, J.R., 3rd, and Liu, Y.C. (2010). K33-linked polyubiquitination of T cell receptor-zeta regulates proteolysis-independent T cell signaling. Immunity *33*, 60-70.
Huang, L., Kinnucan, E., Wang, G., Beaudenon, S., Howley, P.M., Huibregtse, J.M., and Pavletich, N.P. (1999). Structure of an E6AP-UbcH7 complex: insights into ubiquitination by the E2-E3 enzyme cascade. Science *286*, 1321-1326.
Huang, X., Poy, F., Zhang, R., Joachimiak, A., Sudol, M., and Eck, M.J. (2000). Structure of a WW domain containing fragment of dystrophin in complex with beta-dystroglycan. Nature structural biology *7*, 634-638.
Huibregtse, J.M., Scheffner, M., Beaudenon, S., and Howley, P.M. (1995). A family of proteins structurally and functionally related to the E6-AP ubiquitin-protein ligase. Proceedings of the National Academy of Sciences of the United States of America *92*, 5249.
Hurley, J.H., Lee, S., and Prag, G. (2006). Ubiquitin-binding domains. The Biochemical journal *399*, 361-372.
Husnjak, K., and Dikic, I. (2012). Ubiquitin-binding proteins: decoders of ubiquitin-mediated cellular functions. Annual review of biochemistry *81*, 291-322.
Ingham, R.J., Gish, G., and Pawson, T. (2004). The Nedd4 family of E3 ubiquitin ligases: functional diversity within a common modular architecture. Oncogene *23*, 1972-1984.
Iwai, K., Fujita, H., and Sasaki, Y. (2014). Linear ubiquitin chains: NF-kappaB signalling, cell death and beyond. Nature reviews Molecular cell biology *15*, 503-508.
Jin, L., Williamson, A., Banerjee, S., Philipp, I., and Rape, M. (2008). Mechanism of ubiquitin-chain formation by the human anaphase-promoting complex. Cell *133*, 653-665.
Jura, N., and Bar-Sagi, D. (2006). Mapping cellular routes of Ras: a ubiquitin trail. Cell Cycle *5*, 2744-2747.
Kaiser, P., Flick, K., Wittenberg, C., and Reed, S.I. (2000). Regulation of transcription by ubiquitination without proteolysis: Cdc34/SCF(Met30)-mediated inactivation of the transcription factor Met4. Cell *102*, 303-314.
Kamadurai, H.B., Qiu, Y., Deng, A., Harrison, J.S., Macdonald, C., Actis, M., Rodrigues, P., Miller, D.J., Souphron, J., Lewis, S.M.*, et al.* (2013). Mechanism of ubiquitin ligation and lysine prioritization by a HECT E3. eLife *2*, e00828.
Kamadurai, H.B., Souphron, J., Scott, D.C., Duda, D.M., Miller, D.J., Stringer, D., Piper, R.C., and Schulman, B.A. (2009). Insights into ubiquitin transfer cascades from a structure of a UbcH5B approximately ubiquitin-HECT(NEDD4L) complex. Molecular cell *36*, 1095-1102.
Kamynina, E., Debonneville, C., Bens, M., Vandewalle, A., and Staub, O. (2001). A novel mouse Nedd4 protein suppresses the activity of the epithelial Na+ channel. FASEB

journal : official publication of the Federation of American Societies for Experimental Biology *15*, 204-214.
Kar, G., Keskin, O., Nussinov, R., and Gursoy, A. (2012). Human proteome-scale structural modeling of E2-E3 interactions exploiting interface motifs. J Proteome Res *11*, 1196-1207.
Katz, M., 1, , K.S., 1, , Tal-Or, P., 1, , L.Y., 1, , Y.M*., et al.* (2002). Ligand-Independent Degradation of Epidermal
Growth Factor Receptor Involves Receptor
Ubiquitylation and Hgs, an Adaptor Whose Ubiquitin-
Interacting Motif Targets Ubiquitylation by Nedd4. Traffic.
Kazlauskaite, A., Kondapalli, C., Gourlay, R., Campbell, D.G., Ritorto, M.S., Hofmann, K., Alessi, D.R., Knebel, A., Trost, M., and Muqit, M.M. (2014). Parkin is activated by PINK1-dependent phosphorylation of ubiquitin at Ser65. The Biochemical journal *460*, 127-139.
Kazlauskaite, A., Martinez-Torres, R.J., Wilkie, S., Kumar, A., Peltier, J., Gonzalez, A., Johnson, C., Zhang, J., Hope, A.G., Peggie, M*., et al.* (2015). Binding to serine 65-phosphorylated ubiquitin primes Parkin for optimal PINK1-dependent phosphorylation and activation. EMBO reports *16*, 939-954.
Kim, H.C., and Huibregtse, J.M. (2009). Polyubiquitination by HECT E3s and the determinants of chain type specificity. Mol Cell Biol *29*, 3307-3318.
Kim, H.C., Steffen, A.M., Oldham, M.L., Chen, J., and Huibregtse, J.M. (2011). Structure and function of a HECT domain ubiquitin-binding site. EMBO reports *12*, 334-341.
Kim, H.T., Kim, K.P., Lledias, F., Kisselev, A.F., Scaglione, K.M., Skowyra, D., Gygi, S.P., and Goldberg, A.L. (2007). Certain pairs of ubiquitin-conjugating enzymes (E2s) and ubiquitin-protein ligases (E3s) synthesize nondegradable forked ubiquitin chains containing all possible isopeptide linkages. The Journal of biological chemistry *282*, 17375-17386.
Komander, D., Clague, M.J., and Urbe, S. (2009a). Breaking the chains: structure and function of the deubiquitinases. Nature reviews Molecular cell biology *10*, 550-563.
Komander, D., Reyes-Turcu, F., Licchesi, J.D., Odenwaelder, P., Wilkinson, K.D., and Barford, D. (2009b). Molecular discrimination of structurally equivalent Lys 63-linked and linear polyubiquitin chains. EMBO reports *10*, 466-473.
Kondapalli, C., Kazlauskaite, A., Zhang, N., Woodroof, H.I., Campbell, D.G., Gourlay, R., Burchell, L., Walden, H., Macartney, T.J., Deak, M*., et al.* (2012). PINK1 is activated by mitochondrial membrane potential depolarization and stimulates Parkin E3 ligase activity by phosphorylating Serine 65. Open biology *2*, 120080.
Kristariyanto, Y.A., Choi, S.Y., Rehman, S.A., Ritorto, M.S., Campbell, D.G., Morrice, N.A., Toth, R., and Kulathu, Y. (2015). Assembly and structure of Lys33-linked polyubiquitin reveals distinct conformations. The Biochemical journal *467*, 345-352.
Kulathu, Y., and Komander, D. (2012). Atypical ubiquitylation - the unexplored world of polyubiquitin beyond Lys48 and Lys63 linkages. Nature reviews Molecular cell biology *13*, 508-523.
Kumar, A., Aguirre, J.D., Condos, T.E., Martinez-Torres, R.J., Chaugule, V.K., Toth, R., Sundaramoorthy, R., Mercier, P., Knebel, A., Spratt, D.E*., et al.* (2015). Disruption of the autoinhibited state primes the E3 ligase parkin for activation and catalysis. The EMBO journal *34*, 2506-2521.
Lee, I., and Schindelin, H. (2008). Structural insights into E1-catalyzed ubiquitin activation and transfer to conjugating enzymes. Cell *134*, 268-278.
Lee, S., Tsai, Y.C., Mattera, R., Smith, W.J., Kostelansky, M.S., Weissman, A.M., Bonifacino, J.S., and Hurley, J.H. (2006a). Structural basis for ubiquitin recognition and autoubiquitination by Rabex-5. Nature structural & molecular biology *13*, 264-271.

Lee, S., Tsai, Y.C., Mattera, R., Smith, W.J., Kostelansky, M.S., Weissman, A.M., Bonifacino, J.S., and Hurley, J.H. (2006b). Structural basis for ubiquitin recognition and autoubiquitination by Rabex-5. Nature structural & molecular biology *13*, 264-271.
Lifton, R.P., Gharavi, A.G., and Geller, D.S. (2001). Molecular mechanisms of human hypertension. Cell *104*, 545-556.
Linke, K., Mace, P.D., Smith, C.A., Vaux, D.L., Silke, J., and Day, C.L. (2008). Structure of the MDM2/MDMX RING domain heterodimer reveals dimerization is required for their ubiquitylation in trans. Cell death and differentiation *15*, 841-848.
Lipkowitz, S., and Weissman, A.M. (2011). RINGs of good and evil: RING finger ubiquitin ligases at the crossroads of tumour suppression and oncogenesis. Nat Rev Cancer *11*, 629-643.
Lippe, R., Miaczynska, M., Rybin, V., Runge, A., and Zerial, M. (2001). Functional synergy between Rab5 effector Rabaptin-5 and exchange factor Rabex-5 when physically associated in a complex. Mol Biol Cell *12*, 2219-2228.
Lydeard, J.R., Schulman, B.A., and Harper, J.W. (2013). Building and remodelling Cullin-RING E3 ubiquitin ligases. EMBO reports *14*, 1050-1061.
Malumbres, M., and Pellicer, A. (1998). RAS pathways to cell cycle control and cell transformation. Front Biosci *3*, d887-912.
Mari, S., Ruetalo, N., Maspero, E., Stoffregen, M.C., Pasqualato, S., Polo, S., and Wiesner, S. (2014). Structural and functional framework for the autoinhibition of Nedd4-family ubiquitin ligases. Structure *22*, 1639-1649.
Maspero, E., Mari, S., Valentini, E., Musacchio, A., Fish, A., Pasqualato, S., and Polo, S. Structure of the HECT:ubiquitin complex and its role in ubiquitin chain elongation. EMBO reports *12*, 342-349.
Maspero, E., Valentini, E., Mari, S., Cecatiello, V., Soffientini, P., Pasqualato, S., and Polo, S. (2013). Structure of a ubiquitin-loaded HECT ligase reveals the molecular basis for catalytic priming. Nature structural & molecular biology.
Matsumoto, M.L., Wickliffe, K.E., Dong, K.C., Yu, C., Bosanac, I., Bustos, D., Phu, L., Kirkpatrick, D.S., Hymowitz, S.G., Rape, M.*, et al.* (2010). K11-linked polyubiquitination in cell cycle control revealed by a K11 linkage-specific antibody. Molecular cell *39*, 477-484.
Mattera, R., and Bonifacino, J.S. (2008). Ubiquitin binding and conjugation regulate the recruitment of Rabex-5 to early endosomes. The EMBO journal *27*, 2484-2494.
Mattera, R., Tsai, Y.C., Weissman, A.M., and Bonifacino, J.S. (2006). The Rab5 guanine nucleotide exchange factor Rabex-5 binds ubiquitin (Ub) and functions as a Ub ligase through an atypical Ub-interacting motif and a zinc finger domain. The Journal of biological chemistry *281*, 6874-6883.
Merkley, N., Barber, K.R., and Shaw, G.S. (2005). Ubiquitin manipulation by an E2 conjugating enzyme using a novel covalent intermediate. The Journal of biological chemistry *280*, 31732-31738.
Metzger, M.B., Hristova, V.A., and Weissman, A.M. (2012). HECT and RING finger families of E3 ubiquitin ligases at a glance. Journal of cell science *125*, 531-537.
Mevissen, T.E., Hospenthal, M.K., Geurink, P.P., Elliott, P.R., Akutsu, M., Arnaudo, N., Ekkebus, R., Kulathu, Y., Wauer, T., El Oualid, F.*, et al.* (2013). OTU deubiquitinases reveal mechanisms of linkage specificity and enable ubiquitin chain restriction analysis. Cell *154*, 169-184.
Meyer, H.J., and Rape, M. (2014). Enhanced protein degradation by branched ubiquitin chains. Cell *157*, 910-921.

Michel, M.A., Elliott, P.R., Swatek, K.N., Simicek, M., Pruneda, J.N., Wagstaff, J.L., Freund, S.M., and Komander, D. (2015). Assembly and specific recognition of k29- and k33-linked polyubiquitin. Molecular cell *58*, 95-109.
Nakada, S., Yonamine, R.M., and Matsuo, K. (2012). RNF8 regulates assembly of RAD51 at DNA double-strand breaks in the absence of BRCA1 and 53BP1. Cancer Res *72*, 4974-4983.
Newton, K., Matsumoto, M.L., Wertz, I.E., Kirkpatrick, D.S., Lill, J.R., Tan, J., Dugger, D., Gordon, N., Sidhu, S.S., Fellouse, F.A*., et al.* (2008). Ubiquitin chain editing revealed by polyubiquitin linkage-specific antibodies. Cell *134*, 668-678.
Nijman, S.M., Luna-Vargas, M.P., Velds, A., Brummelkamp, T.R., Dirac, A.M., Sixma, T.K., and Bernards, R. (2005). A genomic and functional inventory of deubiquitinating enzymes. Cell *123*, 773-786.
Nimmrich, I., Erdmann, S., Melchers, U., Finke, U., Hentsch, S., Moyer, M.P., Hoffmann, I., and Muller, O. (2000). Seven genes that are differentially transcribed in colorectal tumor cell lines. Cancer Lett *160*, 37-43.
Ogunjimi, A.A., Briant, D.J., Pece-Barbara, N., Le Roy, C., Di Guglielmo, G.M., Kavsak, P., Rasmussen, R.K., Seet, B.T., Sicheri, F., and Wrana, J.L. (2005). Regulation of Smurf2 ubiquitin ligase activity by anchoring the E2 to the HECT domain. Molecular cell *19*, 297-308.
Ogunjimi, A.A., Wiesner, S., Briant, D.J., Varelas, X., Sicheri, F., Forman-Kay, J., and Wrana, J.L. (2010). The ubiquitin binding region of the Smurf HECT domain facilitates polyubiquitylation and binding of ubiquitylated substrates. The Journal of biological chemistry *285*, 6308-6315.
Ohi, M.D., Vander Kooi, C.W., Rosenberg, J.A., Chazin, W.J., and Gould, K.L. (2003). Structural insights into the U-box, a domain associated with multi-ubiquitination. Nature structural biology *10*, 250-255.
Ohsumi, Y., and Mizushima, N. (2004). Two ubiquitin-like conjugation systems essential for autophagy. Seminars in cell & developmental biology *15*, 231-236.
Olsen, S.K., and Lima, C.D. (2013). Structure of a ubiquitin E1-E2 complex: insights to E1-E2 thioester transfer. Molecular cell *49*, 884-896.
Ordureau, A., Heo, J.M., Duda, D.M., Paulo, J.A., Olszewski, J.L., Yanishevski, D., Rinehart, J., Schulman, B.A., and Harper, J.W. (2015). Defining roles of PARKIN and ubiquitin phosphorylation by PINK1 in mitochondrial quality control using a ubiquitin replacement strategy. Proceedings of the National Academy of Sciences of the United States of America *112*, 6637-6642.
Osherov, N., and Levitzki, A. (1994). Epidermal-growth-factor-dependent activation of the src-family kinases. European journal of biochemistry / FEBS *225*, 1047-1053.
Page, R.C., Pruneda, J.N., Amick, J., Klevit, R.E., and Misra, S. (2012). Structural insights into the conformation and oligomerization of E2~ubiquitin conjugates. Biochemistry *51*, 4175-4187.
Pelzer, C., Kassner, I., Matentzoglu, K., Singh, R.K., Wollscheid, H.P., Scheffner, M., Schmidtke, G., and Groettrup, M. (2007). UBE1L2, a novel E1 enzyme specific for ubiquitin. The Journal of biological chemistry *282*, 23010-23014.
Penengo, L., Mapelli, M., Murachelli, A.G., Confalonieri, S., Magri, L., Musacchio, A., Di Fiore, P.P., Polo, S., and Schneider, T.R. (2006). Crystal structure of the ubiquitin binding domains of rabex-5 reveals two modes of interaction with ubiquitin. Cell *124*, 1183-1195.
Persaud, A., Alberts, P., Amsen, E.M., Xiong, X., Wasmuth, J., Saadon, Z., Fladd, C., Parkinson, J., and Rotin, D. (2009). Comparison of substrate specificity of the ubiquitin ligases Nedd4 and Nedd4-2 using proteome arrays. Molecular systems biology *5*, 333.

Persaud, A., Alberts, P., Mari, S., Tong, J., Murchie, R., Maspero, E., Safi, F., Moran, M.F., Polo, S., and Rotin, D. (2014). Tyrosine phosphorylation of NEDD4 activates its ubiquitin ligase activity. Science signaling *7*, ra95.
Petroski, M.D., and Deshaies, R.J. (2005). Mechanism of lysine 48-linked ubiquitin-chain synthesis by the cullin-RING ubiquitin-ligase complex SCF-Cdc34. Cell *123*, 1107-1120.
Peuscher, M.H., and Jacobs, J.J. (2011). DNA-damage response and repair activities at uncapped telomeres depend on RNF8. Nat Cell Biol *13*, 1139-1145.
Pickart, C.M. (2001). Mechanisms underlying ubiquitination. Annual review of biochemistry *70*, 503-533.
Plechanovova, A., Jaffray, E.G., Tatham, M.H., Naismith, J.H., and Hay, R.T. (2012). Structure of a RING E3 ligase and ubiquitin-loaded E2 primed for catalysis. Nature *489*, 115-120.
Polo, S., Sigismund, S., Faretta, M., Guidi, M., Capua, M.R., Bossi, G., Chen, H., De Camilli, P., and Di Fiore, P.P. (2002). A single motif responsible for ubiquitin recognition and monoubiquitination in endocytic proteins. Nature *416*, 451-455.
Pruneda, J.N., Stoll, K.E., Bolton, L.J., Brzovic, P.S., and Klevit, R.E. (2011). Ubiquitin in motion: structural studies of the ubiquitin-conjugating enzyme approximately ubiquitin conjugate. Biochemistry *50*, 1624-1633.
Ramanathan, H.N., and Ye, Y. (2012). Cellular strategies for making monoubiquitin signals. Critical reviews in biochemistry and molecular biology *47*, 17-28.
Redman, K.L., and Rechsteiner, M. (1989). Identification of the long ubiquitin extension as ribosomal protein S27a. Nature *338*, 438-440.
Reverter, D., and Lima, C.D. (2005). Insights into E3 ligase activity revealed by a SUMO-RanGAP1-Ubc9-Nup358 complex. Nature *435*, 687-692.
Reyes-Turcu, F.E., Horton, J.R., Mullally, J.E., Heroux, A., Cheng, X., and Wilkinson, K.D. (2006). The ubiquitin binding domain ZnF UBP recognizes the C-terminal diglycine motif of unanchored ubiquitin. Cell *124*, 1197-1208.
Rotin, D., Kanelis, V., and Schild, L. (2001). Trafficking and cell surface stability of ENaC. American journal of physiology Renal physiology *281*, F391-399.
Rotin, D., and Kumar, S. (2009). Physiological functions of the HECT family of ubiquitin ligases. Nature reviews Molecular cell biology *10*, 398-409.
Sakata, E., Satoh, T., Yamamoto, S., Yamaguchi, Y., Yagi-Utsumi, M., Kurimoto, E., Tanaka, K., Wakatsuki, S., and Kato, K. (2010). Crystal structure of UbcH5b approximately ubiquitin intermediate: insight into the formation of the self-assembled E2 approximately Ub conjugates. Structure *18*, 138-147.
Sato, Y., Yoshikawa, A., Yamagata, A., Mimura, H., Yamashita, M., Ookata, K., Nureki, O., Iwai, K., Komada, M., and Fukai, S. (2008). Structural basis for specific cleavage of Lys 63-linked polyubiquitin chains. Nature *455*, 358-362.
Scheffner, M., and Kumar, S. (2014). Mammalian HECT ubiquitin-protein ligases: biological and pathophysiological aspects. Biochimica et biophysica acta *1843*, 61-74.
Scheffner, M., Nuber, U., and Huibregtse, J.M. (1995). Protein ubiquitination involving an E1-E2-E3 enzyme ubiquitin thioester cascade. Nature *373*, 81-83.
Schlessinger, J. (2002). Ligand-induced, receptor-mediated dimerization and activation of EGF receptor. Cell *110*, 669-672.
Serniwka, S.A., and Shaw, G.S. (2009). The structure of the UbcH8-ubiquitin complex shows a unique ubiquitin interaction site. Biochemistry *48*, 12169-12179.
Shearwin-Whyatt, L., Dalton, H.E., Foot, N., and Kumar, S. (2006). Regulation of functional diversity within the Nedd4 family by accessory and adaptor proteins. BioEssays : news and reviews in molecular, cellular and developmental biology *28*, 617-628.

Shimura, H., Mizuno, Y., and Hattori, N. (2012). Parkin and Parkinson disease. Clinical chemistry *58*, 1260-1261.
Sims, J.J., and Cohen, R.E. (2009). Linkage-specific avidity defines the lysine 63-linked polyubiquitin-binding preference of rap80. Molecular cell *33*, 775-783.
Spratt, D.E., Walden, H., and Shaw, G.S. (2014). RBR E3 ubiquitin ligases: new structures, new insights, new questions. The Biochemical journal *458*, 421-437.
Staub, O., Dho, S., Henry, P., Correa, J., Ishikawa, T., McGlade, J., and Rotin, D. (1996). WW domains of Nedd4 bind to the proline-rich PY motifs in the epithelial Na+ channel deleted in Liddle's syndrome. The EMBO journal *15*, 2371-2380.
Sudol, M. (1996). Structure and function of the WW domain. Progress in biophysics and molecular biology *65*, 113-132.
Sundquist, W.I., Schubert, H.L., Kelly, B.N., Hill, G.C., Holton, J.M., and Hill, C.P. (2004). Ubiquitin recognition by the human TSG101 protein. Molecular cell *13*, 783-789.
Swaney, D.L., Rodriguez-Mias, R.A., and Villen, J. (2015). Phosphorylation of ubiquitin at Ser65 affects its polymerization, targets, and proteome-wide turnover. EMBO reports *16*, 1131-1144.
Tyrrell, A., Flick, K., Kleiger, G., Zhang, H., Deshaies, R.J., and Kaiser, P. (2010). Physiologically relevant and portable tandem ubiquitin-binding domain stabilizes polyubiquitylated proteins. Proceedings of the National Academy of Sciences of the United States of America *107*, 19796-19801.
van der Veen, A.G., and Ploegh, H.L. (2012). Ubiquitin-like proteins. Annual review of biochemistry *81*, 323-357.
Varadan, R., Walker, O., Pickart, C., and Fushman, D. (2002). Structural properties of polyubiquitin chains in solution. Journal of molecular biology *324*, 637-647.
Verdecia, M.A., Joazeiro, C.A., Wells, N.J., Ferrer, J.L., Bowman, M.E., Hunter, T., and Noel, J.P. (2003). Conformational flexibility underlies ubiquitin ligation mediated by the WWP1 HECT domain E3 ligase. Molecular cell *11*, 249-259.
Vijay-Kumar, S., Bugg, C.E., and Cook, W.J. (1987). Structure of ubiquitin refined at 1.8 A resolution. Journal of molecular biology *194*, 531-544.
Wang, J., Peng, Q., Lin, Q., Childress, C., Carey, D., and Yang, W. (2010). Calcium activates Nedd4 E3 ubiquitin ligases by releasing the C2 domain-mediated auto-inhibition. The Journal of biological chemistry *285*, 12279-12288.
Wang, M., and Pickart, C.M. (2005). Different HECT domain ubiquitin ligases employ distinct mechanisms of polyubiquitin chain synthesis. The EMBO journal *24*, 4324-4333.
Wang, S., Lu, A., Chen, X., Wei, L., and Ding, J. (2014). RABEX-5 is upregulated and plays an oncogenic role in gastric cancer development by activating the VEGF signaling pathway. PLoS One *9*, e113891.
Wang, X., Trotman, L.C., Koppie, T., Alimonti, A., Chen, Z., Gao, Z., Wang, J., Erdjument-Bromage, H., Tempst, P., Cordon-Cardo, C*., et al.* (2007). NEDD4-1 is a proto-oncogenic ubiquitin ligase for PTEN. Cell *128*, 129-139.
Wauer, T., Swatek, K.N., Wagstaff, J.L., Gladkova, C., Pruneda, J.N., Michel, M.A., Gersch, M., Johnson, C.M., Freund, S.M., and Komander, D. (2015). Ubiquitin Ser65 phosphorylation affects ubiquitin structure, chain assembly and hydrolysis. The EMBO journal *34*, 307-325.
Wenzel, D.M., and Klevit, R.E. (2012). Following Ariadne's thread: a new perspective on RBR ubiquitin ligases. BMC biology *10*, 24.
Wenzel, D.M., Lissounov, A., Brzovic, P.S., and Klevit, R.E. (2011). UBCH7 reactivity profile reveals parkin and HHARI to be RING/HECT hybrids. Nature *474*, 105-108.

Wertz, I.E., O'Rourke, K.M., Zhou, H., Eby, M., Aravind, L., Seshagiri, S., Wu, P., Wiesmann, C., Baker, R., Boone, D.L.*, et al.* (2004). De-ubiquitination and ubiquitin ligase domains of A20 downregulate NF-kappaB signalling. Nature *430*, 694-699.
Wickliffe, K.E., Lorenz, S., Wemmer, D.E., Kuriyan, J., and Rape, M. (2011). The mechanism of linkage-specific ubiquitin chain elongation by a single-subunit E2. Cell *144*, 769-781.
Wickliffe, K.E., Williamson, A., Meyer, H.J., Kelly, A., and Rape, M. K11-linked ubiquitin chains as novel regulators of cell division. Trends Cell Biol *21*, 656-663.
Wiesner, S., Ogunjimi, A.A., Wang, H.R., Rotin, D., Sicheri, F., Wrana, J.L., and Forman-Kay, J.D. (2007). Autoinhibition of the HECT-type ubiquitin ligase Smurf2 through its C2 domain. Cell *130*, 651-662.
Williamson, A., Wickliffe, K.E., Mellone, B.G., Song, L., Karpen, G.H., and Rape, M. (2009). Identification of a physiological E2 module for the human anaphase-promoting complex. Proceedings of the National Academy of Sciences of the United States of America *106*, 18213-18218.
Woelk, T., Oldrini, B., Maspero, E., Confalonieri, S., Cavallaro, E., Di Fiore, P.P., and Polo, S. (2006). Molecular mechanisms of coupled monoubiquitination. Nat Cell Biol *8*, 1246-1254.
Wu, P.Y., Hanlon, M., Eddins, M., Tsui, C., Rogers, R.S., Jensen, J.P., Matunis, M.J., Weissman, A.M., Wolberger, C., and Pickart, C.M. (2003). A conserved catalytic residue in the ubiquitin-conjugating enzyme family. The EMBO journal *22*, 5241-5250.
Xu, L., Lubkov, V., Taylor, L.J., and Bar-Sagi, D. (2010). Feedback regulation of Ras signaling by Rabex-5-mediated ubiquitination. Curr Biol *20*, 1372-1377.
Yang, B., and Kumar, S. (2010). Nedd4 and Nedd4-2: closely related ubiquitin-protein ligases with distinct physiological functions. Cell death and differentiation *17*, 68-77.
Zhang, H., Cheng, S., Wang, A., Ma, H., Yao, B., Qi, C., Liu, R., Qi, S., and Xu, Y. (2014). Expression of RABEX-5 and its clinical significance in prostate cancer. J Exp Clin Cancer Res *33*, 31.
Zhang, X., Min, J., Wang, Y., Li, Y., Li, H., Liu, Q., Liang, X., and Mu, P. (2013). RABEX-5 plays an oncogenic role in breast cancer by activating MMP-9 pathway. J Exp Clin Cancer Res *32*, 52.
Zhao, C., Denison, C., Huibregtse, J.M., Gygi, S., and Krug, R.M. (2005). Human ISG15 conjugation targets both IFN-induced and constitutively expressed proteins functioning in diverse cellular pathways. Proceedings of the National Academy of Sciences of the United States of America *102*, 10200-10205.

# ACKNOWLEDGMENT

I thank my Ph.D. supervisor Simona Polo for the opportunity to join her group and follow this project. She is always willing to help and to discuss with us.

A special thank to Elena Maspero for everyday help, not only for lab life, and support in these years that I spent with her.

I also thank my internal supervisor, Marina Mapelli, and my external supervisor, David Komander, for the useful suggestions.

This Ph.D. thesis was supported by IFOM fellowship and a personal grant from the Fondazione Italiana per la Ricerca Cancro (IG 14856).

nature structural & molecular biology

# Structure of a ubiquitin-loaded HECT ligase reveals the molecular basis for catalytic priming

Elena Maspero[1], Eleonora Valentini[1], Sara Mari[1], Valentina Cecatiello[2], Paolo Soffientini[1], Sebastiano Pasqualato[2] & Simona Polo[1,3]

**Homologous to E6-AP C terminus (HECT) E3 ligases recognize and directly catalyze ligation of ubiquitin (Ub) to their substrates. Molecular details of this process remain unknown. We report the first structure, to our knowledge, of a Ub-loaded E3, the human neural precursor cell–expressed developmentally downregulated protein 4 (Nedd4). The HECT$^{Nedd4}$~Ub transitory intermediate provides a structural basis for the proposed sequential addition mechanism. The donor Ub, transferred from the E2, is bound to the Nedd4 C lobe with its C-terminal tail locked in an extended conformation, primed for catalysis. We provide evidence that the Nedd4-family members are Lys63-specific enzymes whose catalysis is mediated by an essential C-terminal acidic residue.**



Substrate ubiquitination occurs through an E1-E2-E3 Ub conjugation cascade. The E3 ligases play a crucial part in the whole pathway, as they determine the specificity of the reaction. Members of the HECT-type ligases receive Ub from the E2 through a thioester conjugate before catalyzing Ub transfer to their substrates[1]. The human genome encodes 28 HECT E3s, and a large number of them are involved in the genesis of several human diseases[2]. They are divided into subgroups according to the presence of interaction domains, although this classification probably does not reflect the natural evolution of these enzymes[3]. The Nedd4 family is a monophyletic group represented by nine members in humans and characterized by a C2 domain and three to four WW domains responsible for substrate recognition[4].

Structural studies on HECT domains revealed their architecture. The HECT is a bilobed domain consisting of an N-terminal N lobe that interacts with the E2 and a C-terminal C lobe that contains the catalytic cysteine and is free to rotate around the flexible hinge that tethers it to the N lobe[5]. Recent studies have demonstrated the existence and relevance of two Ub-interaction surfaces within the HECT domain. The first, present in the C lobe, is essential for E2-to-E3 Ub transfer[6]; the second, in the N lobe, is critical for enzyme processivity[7,8]. Notably, the ability to build up different Ub chains appears to be an intrinsic feature of the HECT domain[8–10]. The Nedd4 family of HECTs seems to use a sequential addition mechanism by which Ub molecules are added one at a time from the catalytic cysteine to the distal lysine of the growing chain[8,9]. However, most of the mechanistic details of HECT catalysis remain elusive, owing to the lack of structures of key catalytic intermediates.

To gain insight into the ubiquitination reaction catalyzed by HECT E3 ligases, we set out to determine the crystal structure of the Ub-loaded HECT domain of Nedd4 in complex with Ub noncovalently bound in the Ub-binding domain (UBD) present in the N lobe of HECT$^{Nedd4}$ (ref. 8).

## RESULTS

### Structure of the HECT$^{Nedd4}$~Ub$^{D}$–Ub complex

Because a thioester-linked HECT~Ub is highly unstable, we generated a stable complex by bridging the HECT$^{Nedd4}$ with a modified form of Ub donor (Ub$^{D}$), G76C, by a disulfide bond (**Supplementary Fig. 1a–d**). We solved the crystal structure of the complex (HECT$^{Nedd4}$~Ub$^{D}$–Ub) at 2.51-Å resolution by molecular replacement (**Table 1** and **Fig. 1a**). As predicted[8], loading of the Ub$^{D}$ onto the HECT$^{Nedd4}$ catalytic cysteine is compatible with noncovalent Ub binding in the N lobe. Furthermore, the N lobe adopts the same conformation in the presence and absence of Ub$^{D}$ (r.m.s. deviation of 0.8 Å over 258 Cα), with free Ub kept in the binding site crafted by the N-lobe subdomains (**Supplementary Fig. 1e–g**). The N- and C-lobe organization markedly resembles that of the Nedd4-like HECT domain (HECT$^{Nedd4L}$) crystallized in complex with UbcH5B~Ub[6] (**Fig. 1b**, superposition with an r.m.s. deviation of 1.1 Å over 369 Cα), with the highly conserved N-lobe Tyr616 completely buried at the interface between the two lobes (**Fig. 1c** and **Supplementary Fig. 2**).

Notably, the Ub$^{D}$ in the HECT$^{Nedd4}$~Ub$^{D}$–Ub structure sits in the same position as does the Ub loaded on the E2 in the HECT$^{Nedd4L}$–UbcH5B~Ub structure[6] (**Fig. 1b**). The main interaction surface is contributed by hydrophobic residues Leu71, Leu73, Ile36 and Pro37 of Ub$^{D}$ and Leu861, Met888 and Ala889 of the C lobe, and it is surrounded by hydrogen bonds between Gln40 and the Leu861 main chain and between Asn892 and Leu8 and the Thr9 main chain, as well as by salt bridges between Asp39 and Lys860 (**Fig. 1d** and **Supplementary Fig. 3**). As the relative orientation between the two HECT lobes and between the C lobe and Ub$^{D}$ in our structure is unchanged with respect to that described in another study[6], we conclude that our structure represents the step that immediately follows the transfer of the thioester bond from the E2 to the E3,

[1]Fondazione Istituto FIRC di Oncologia Molecolare, Milan, Italy. [2]Crystallography Unit, Department of Experimental Oncology, European Institute of Oncology, Milan, Italy. [3]Dipartimento di Scienze della Salute, Università degli Studi di Milano, Milan, Italy. Correspondence should be addressed to S. Polo (simona.polo@ifom.eu) or S. Pasqualato (sebastiano.pasqualato@ieo.eu).

Received 3 October 2012; accepted 21 March 2013; published online 5 May 2013; doi:10.1038/nsmb.2566

**Table 1 Data collection and refinement statistics**

| | $HECT^{Nedd4}$~$Ub^{D}$–Ub | $HECT^{Nedd4}$ A889F |
|---|---|---|
| **Data collection** | | |
| Space group | *R*32:h | *P*3121 |
| Cell dimensions | | |
| *a*, *b*, *c* (Å) | 196.54, 196.54, 98.77 | 100.55, 100.55, 96.45 |
| α, β, γ (°) | 90, 90, 120 | 90, 90, 120 |
| Resolution (Å) | 56.74–2.51 (2.57–2.51)[a] | 44.58–3.00 (3.10–3.00)[a] |
| $R_{merge}$ | 8.8 (88.5) | 6.8 (69.7) |
| $I / \sigma I$ | 16.6 (2.9) | 28.4 (3.9) |
| Completeness (%) | 100.0 (100.0) | 99.3 (99.1) |
| Redundancy | 7.4 (7.5) | 13.0 (12.4) |
| **Refinement** | | |
| Resolution (Å) | 56.74–2.51 | 44.58–3.00 |
| No. reflections | 22,567 | 11,550 |
| $R_{work}$ / $R_{free}$ | 18.4 / 22.9 | 24.6 / 29.5 |
| No. atoms | | |
| Protein | 4,381 | 3,124 |
| Water | 112 | 3 |
| *B* factors | | |
| Nedd4 HECT domain | 52.8 | 136.4 |
| $Ub^{D}$ | 50.4 | |
| Ub | 82.3 | |
| Water | 46.1 | 93.9 |
| r.m.s. deviations | | |
| Bond lengths (Å) | 0.008 | 0.003 |
| Bond angles (°) | 1.12 | 0.78 |

[a]Values in parentheses are for highest-resolution shell.

in which the $Ub^{D}$ has been handed over to the C lobe and is ready to be transferred to the substrate.

### Implications for the $Ub^{D}$ C-terminal tail-locking

Differently from the aforementioned set of conserved contacts between $Ub^{D}$ and the C lobe, the last three residues of $Ub^{D}$ display a pronounced rearrangement with respect to the $HECT^{Nedd4L}$–UbcH5B~Ub structure, which locks the Ub tail in an extended conformation (**Fig. 2a**,**b**). The $Ub^{D}$ tail zips onto C-lobe β-strand β9, just upstream of the catalytic Cys867, and organizes a hydrogen bond pattern that results in β-sheet augmentation, a common motif in protein-protein interactions[11]. Furthermore, Arg74, which is involved in a single hydrogen bond with residue Ser91 of UbcH5B in the E2-loaded conformation[6], folds back onto the C lobe and contributes two hydrogen bonds with the main chain carboxylic groups of Gln825 and Phe826 (**Fig. 2a**). We reasoned that these additional tail interactions may disfavor the reversibility of the thioester transfer, so that the thioester bond could not be handed back from the E3 to the E2. Owing to the involvement of backbone carbonyls, mutational analysis is precluded, but we note that R74A-mutated $Ub^{D}$ was inefficiently released from the E2 in a pulse-chase assay[12].

A similar stretched conformation of $Ub^{D}$ was recently observed in the RNF4–UbcH5A~Ub and BIRC7–UbcH5B~Ub structures[13,14], wherein the Ub tail was shown to orient the thioester bond, held on the E2 in an optimal conformation for nucleophilic attack by the incoming lysine residue of the substrate (**Fig. 2c**,**d**). Notably, the Ub-tail stretching has been reported also in the SUMO~RanGAP1–Ubc9–Nup358 complex[15], although in this case the crystal structure trapped the reaction product, with the protein modifier already transferred to the substrate (**Fig. 2e**). In the context of the $HECT^{Nedd4}$, the rigid configuration assumed by the C-terminal tail of $Ub^{D}$ may ensure two important functions: it confers the directionality of the transthiolation reaction and, analogously to RNF4 and BIRC7, it facilitates acceptor recognition and optimizes the attack by the substrate lysine through the alignment of the thioester bond. Locking the flexible C-terminal tail of Ub in an extended conformation may be a common mechanism adopted by both E2s and E3s to prime the $Ub^{D}$ for catalytic transfer to the substrate, though further structural studies are required to confirm this hypothesis.

### Essential role of the Nedd4 C-terminal residue for catalysis

Close inspection of the sequence alignment of the HECT C-terminal tail revealed the presence of an invariable acidic residue as the last amino acid within the Nedd4 family (**Supplementary Fig. 4a**), suggesting that this might be a catalytic residue important in positioning and/or activation of the incoming lysine of the Ub acceptor ($Ub^{A}$). Indeed, mutations or even deletion of this single aspartic acid in Nedd4 supported this idea because it resulted in wild-type levels of transthiolation but completely undetectable ubiquitination (**Fig. 3a**,**b**). We obtained similar results assessing other Nedd4 family members: deletion of the last residue in Nedd4-like, Itch, Smurf2, WWP2 and Rsp5 abrogated substrate catalysis (**Fig. 3c**).

To test whether the C-terminal acidic residue could be in proximity to the catalytic site, we replaced it with a lysine. Consistently with previous mutational analysis, this single substitution abrogated Ub-chain formation (**Fig. 3d**). Notably, this terminal lysine was able to attack the thioesther bond, as demonstrated by the stoichiometric amount of Ub-modified HECT present in the reaction (**Fig. 3d**). MS analysis confirmed that the ubiquitinated peptide was the C-terminal one containing the diglycine-modified Lys900 (**Fig. 3e**). In contrast, no Ub modification of Lys900 was visible when we used the C867S catalytically impaired mutant, which proves that Lys900 did not attack the thioester-linked E2~Ub (**Fig. 3d**). Thus, upon correct positioning of the substrate or $Ub^{A}$ the catalytic core is formed with the terminal acidic residue of Nedd4 located at the active site of catalysis. Once there, this acid residue may perform its still-undefined function, either contributing to the active catalytic site or helping to position the $Ub^{A}$. Further structures are needed to uncover its specific role.

### Nedd4-family members are Lys63-specific E3 ligases

Our structure did not provide clues on the $Ub^{A}$ position. Clearly, the Ub bound in the UBD present in the N lobe of $HECT^{Nedd4}$ does not represent the $Ub^{A}$ carrying the attacking lysine (**Supplementary Fig. 1e**). Nedd4 is a Lys63-specific E3 ligase[8,9], and the UBD is not essential for chain specificity. Indeed, mutants in the critical residues required for Ub binding were defective in chain elongation but still retained Lys63 specificity[8]. Data from a previous study[9] have demonstrated that chain type specificity is an inherent property of the HECT domain itself and that the determinants of chain type specificity are located within the last 60 amino acids of the C lobe (**Supplementary Fig. 4b**). We extended this knowledge, performing absolute-quantification (AQUA) experiments on various HECTs of the Nedd4 family. Our data demonstrated that, with wild-type Ub as a source of Ub, all Nedd4-family members showed a clear preference for Lys63 linkage *in vitro* (**Fig. 4a**,**b**), although we failed to define a specific Lys63 sequence pattern by using a sequence conservation analysis (S. Polo and K. Hofmann, personal communication). Thus, we concluded that the Nedd4-family members are Lys63 specific and are characterized by a conserved and essential residue as the last amino acid.

Notably, other HECTs not belonging to the Nedd4 family do not have an acidic residue as the final amino acid (**Supplementary Fig. 4a**).

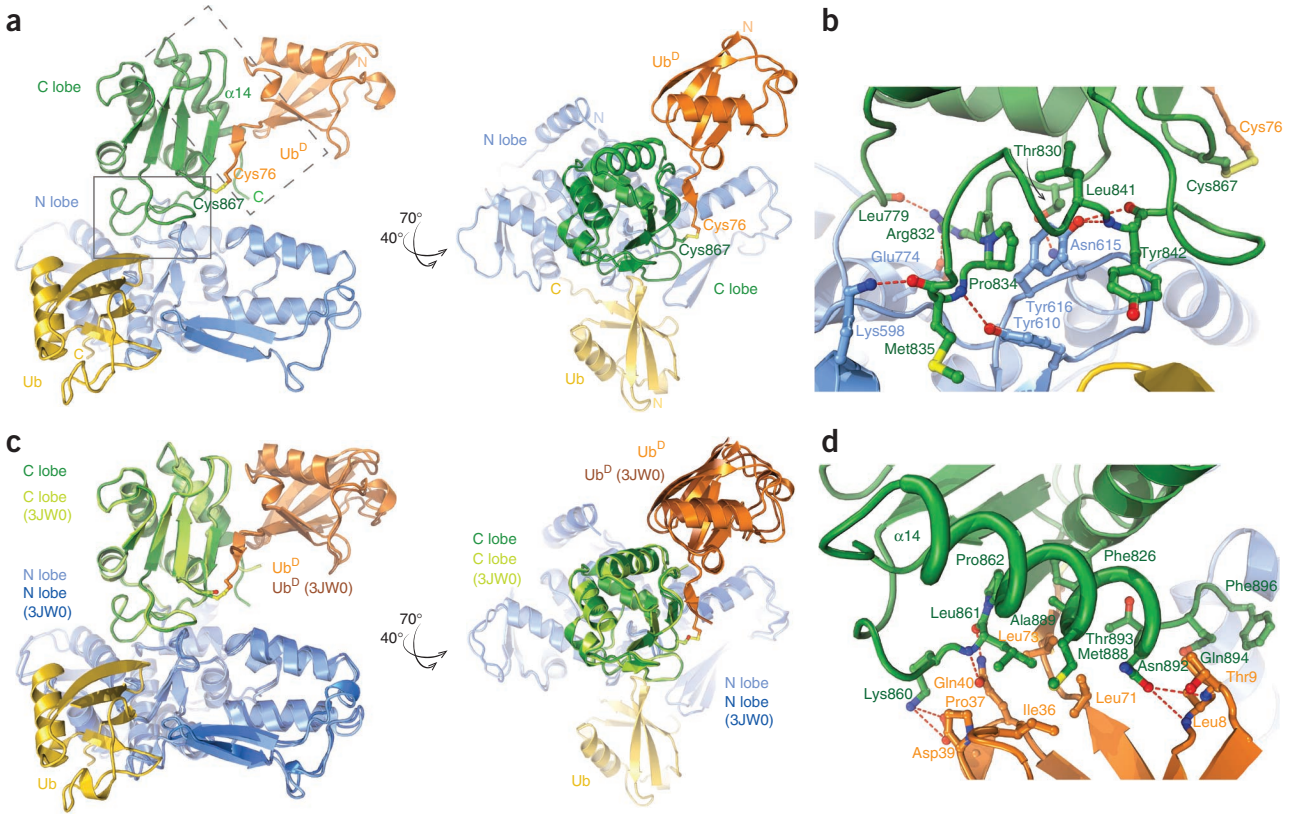


**Figure 1** Structure of the Ub-loaded Nedd4 HECT in complex with Ub. (**a**) Cartoon representation of the HECT$^{Nedd4}$~Ub$^{D}$–Ub complex. Blue and green, N and C lobes, respectively; orange, Ub$^{D}$; yellow, noncovalently bound Ub. Right, same representation, rotated as indicated. (**b**) Cartoon representation of the superposition, done through their HECTs, of HECT$^{Nedd4}$~Ub$^{D}$–Ub with HECT$^{Nedd4L}$–UbcH5B~Ub (PDB 3JW0). UbcH5B is not shown, to permit a better view of the HECT and Ub superposition. Nedd4-like N and C lobes and loaded Ub are in dark blue, light green and brown, respectively; other molecules are colored as in **a**. (**c**,**d**) Details of the interaction between the C lobe in green and the N lobe in blue (**c**, corresponding to plain rectangle in **a**) and between HECT N lobe in green and Ub$^{D}$ in orange (**d**, corresponding to dashed rectangle in **a**). Residues buried or participating at the interface are drawn in ball-and-stick representation and labeled. Hydrogen bonds are highlighted with red dashed lines.



Previous data indicated that E6AP preferentially synthesizes Lys48 chains[9,10]. Deletion of the last amino acid of E6AP did not affect its activity[16], which suggests a different catalytic mechanism. To gain insight into this difference, we substituted the last four residues after Nedd4 Phe896 with the three residues of E6AP. This short substitution showed reduced chain-formation kinetics (**Fig. 4c**), and the mutant was able to partially modify the type of the chains produced, as visualized by Lys63- and Lys48-specific antibodies (**Fig. 4d**). On the basis of these results, we concluded that the last three or four amino acids present in the C-terminal tail of the HECT ligases might participate, together with the determinants present in the C lobe[9], in determining chain specificity.

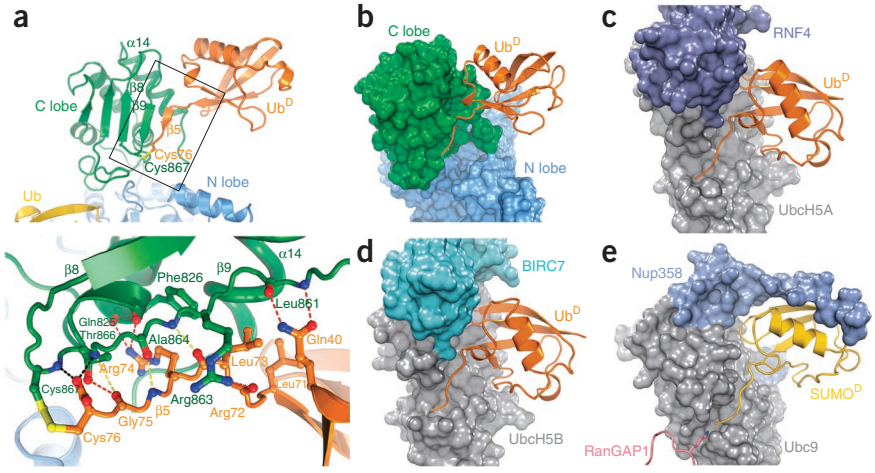


**Figure 2** Ub$^{D}$ is primed for catalysis by C-terminal tail-locking. (**a**) Details of the interactions at the interface between the HECT C lobe (green) and Ub$^{D}$ (orange), as in **Figure 1c**. Hydrogen bonds between Cys76 carboxylate and backbone amides of Thr866 and Cys867, probably artificially imposed by the glycine-to-cysteine mutation in Ub, are shown in black. Hydrogen bonds in the β-sheet are shown in yellow. (**b**–**e**) Similar extended conformation of Ub or SUMO C-terminal tails, shown for Nedd4~Ub$^{D}$ (this study) (**b**), RNF4–UbcH5A~Ub complex (PDB 4AP4) (**c**), BIRC7–UbcH5B~Ub complex (PDB 4AUQ) (**d**) and SUMO~RanGAP1–Ubc9–Nup358 complex (PDB 1Z5S) (**e**). E2 and E3 molecules are shown in surface representation, Ub, SUMO and RanGAP1 in cartoon representation.

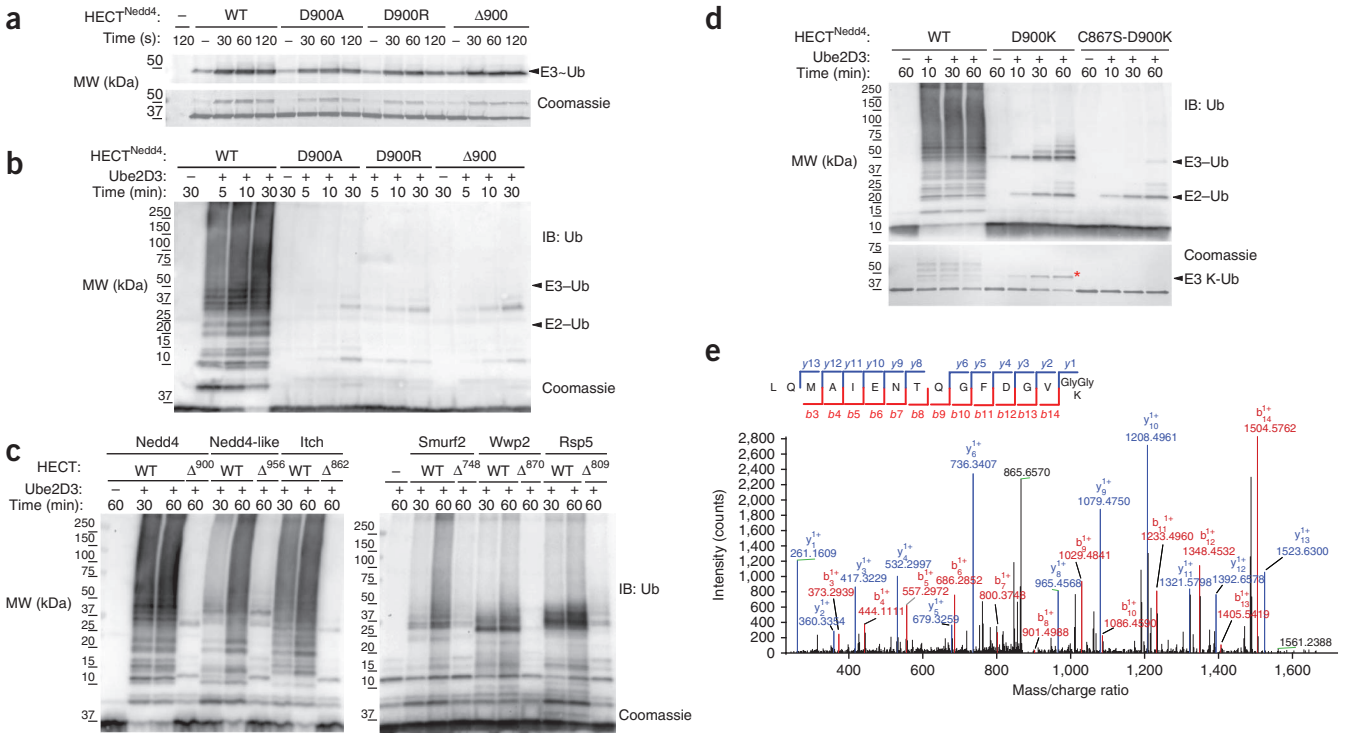


**Figure 3** The C-terminal acidic residue is critical for the catalysis of Nedd4 family members. (**a**) Pulse-chase transfer of Ub from UbcH5B to the indicated HECT$^{Nedd4}$ mutants. Top, streptavidin blot. HECT~Ub thioester is indicated. Bottom, Coomassie staining. WT, wild type. MW, molecular weight. (**b**–**d**) Ub chain formation assay with the indicated mutants and immunoblot (IB) of Ub. Arrowheads to monoubiquitinated E2 and E3 enzymes. Bottom, Coomassie staining. Red asterisk indicates the band of monoubiquitinated HECT cut for MS analysis. (**e**) MS/MS spectrum of the C-terminal peptide of Nedd4 D900K with the diglycine-modified lysine residue. Peptide sequence is shown with the annotation of the identified matched *b* ions in red and the *y* ions in blue.

### Ala889 is critical for Nedd4 C-terminal tail-positioning

To test the functional importance of the Ub$^D$ position for substrate ubiquitination, we examined various HECT mutants that elicit moderate catalytic effects in transthiolation reactions[6]. Ala889, which is conserved in all HECT ligases (**Supplementary Fig. 4a**), showed a notable behavior. Ala889 is buried largely within the C-lobe hydrophobic core, surrounded by Phe826, Leu861 and Pro862. Leu73 from Ub$^D$ conceals the residual 5-Å$^2$ surface exposed to solvent (**Fig. 1c**). Mutations of Ala889 to other hydrophobic residues are unlikely to have a marked effect on the Ub$^D$ position. Consistent with this, the transthiolation reaction occurred equally for the A889V, A889I and A889F variants. However, A889V and A889I mutants showed substantial impairment in chain elongation kinetics, whereas the A889F was a 'dead' mutant incapable of using Ub as a pseudosubstrate (**Fig. 5a**,**b**).

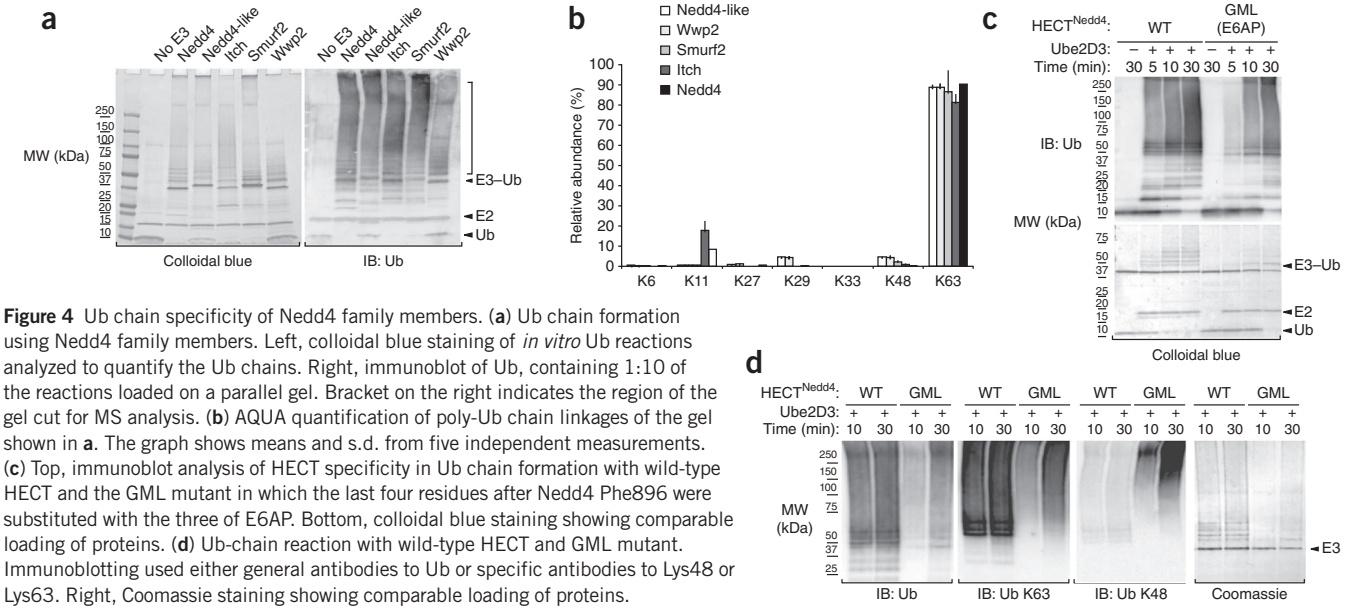


**Figure 4** Ub chain specificity of Nedd4 family members. (**a**) Ub chain formation using Nedd4 family members. Left, colloidal blue staining of *in vitro* Ub reactions analyzed to quantify the Ub chains. Right, immunoblot of Ub, containing 1:10 of the reactions loaded on a parallel gel. Bracket on the right indicates the region of the gel cut for MS analysis. (**b**) AQUA quantification of poly-Ub chain linkages of the gel shown in **a**. The graph shows means and s.d. from five independent measurements. (**c**) Top, immunoblot analysis of HECT specificity in Ub chain formation with wild-type HECT and the GML mutant in which the last four residues after Nedd4 Phe896 were substituted with the three of E6AP. Bottom, colloidal blue staining showing comparable loading of proteins. (**d**) Ub-chain reaction with wild-type HECT and GML mutant. Immunoblotting used either general antibodies to Ub or specific antibodies to Lys48 or Lys63. Right, Coomassie staining showing comparable loading of proteins.

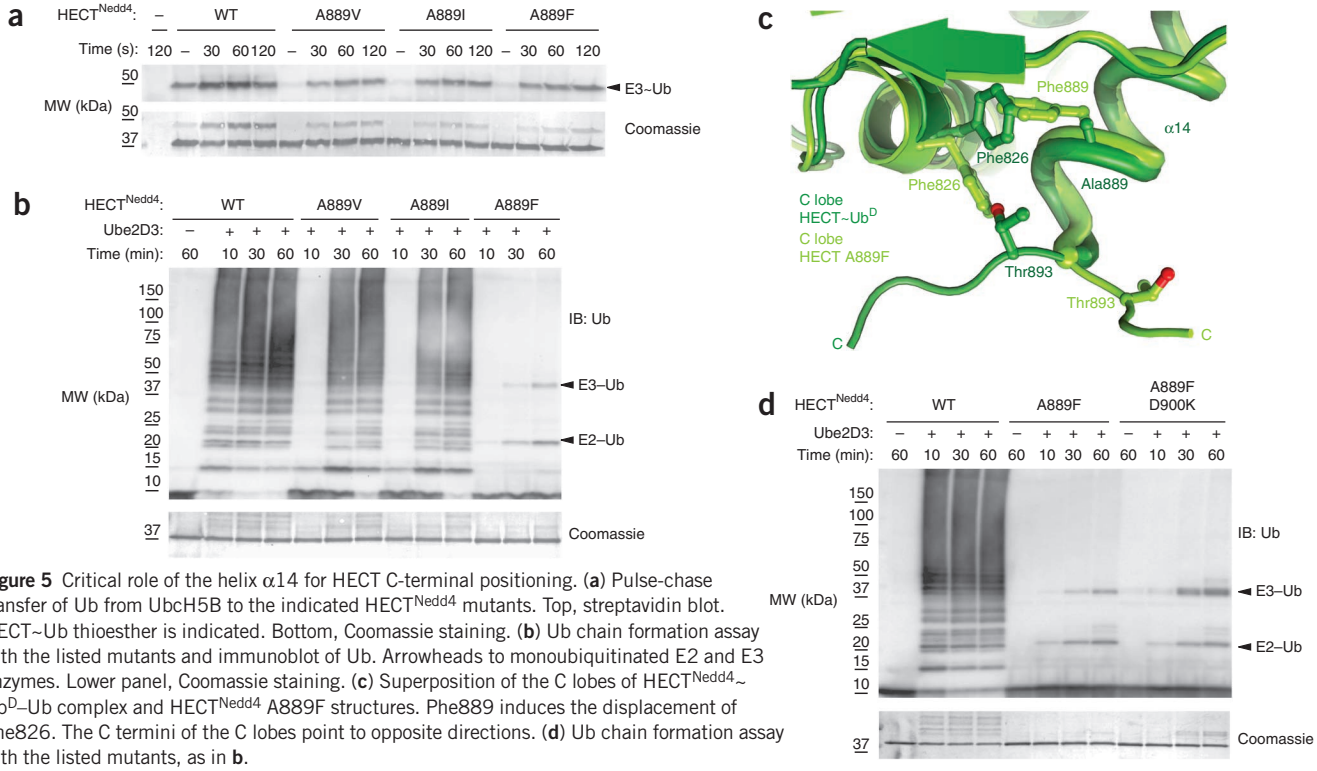


**Figure 5** Critical role of the helix α14 for HECT C-terminal positioning. (**a**) Pulse-chase transfer of Ub from UbcH5B to the indicated HECT$^{Nedd4}$ mutants. Top, streptavidin blot. HECT~Ub thioesther is indicated. Bottom, Coomassie staining. (**b**) Ub chain formation assay with the listed mutants and immunoblot of Ub. Arrowheads to monoubiquitinated E2 and E3 enzymes. Lower panel, Coomassie staining. (**c**) Superposition of the C lobes of HECT$^{Nedd4}$~Ub$^{D}$–Ub complex and HECT$^{Nedd4}$ A889F structures. Phe889 induces the displacement of Phe826. The C termini of the C lobes point to opposite directions. (**d**) Ub chain formation assay with the listed mutants, as in **b**.

Ala889 sits in helix α14, just upstream of the C-terminal tail of the HECT. One possibility is that Ala889 is not required *per se* but rather functions to position the C-terminal tail during catalysis. To investigate this possibility, we solved the structure of the Nedd4 HECT domain carrying the A889F mutation (**Table 1**). The organization of the N and C lobes is different from those previously observed for HECT$^{Nedd4}$ and closely resembles that adopted by the HECT domain of WWP1 (ref. 5 and **Supplementary Fig. 5a**). Mutation of Ala889 to phenylalanine does not induce any rearrangement in the structure of the C lobe, which superposes with that of HECT$^{Nedd4}$~Ub$^{D}$–Ub with an r.m.s. deviation of 0.6 Å over 111 Cα. The bulky side chain of Phe889 fills a hydrophobic pocket usually occupied by the Phe826 side chain, which is extruded from the C-lobe core and turned toward the C terminus (**Fig. 5c** and **Supplementary Fig. 5b**). This side chain extrusion, compatible with Ub$^{D}$ loading, pushes the C-terminal tail far from the C-lobe core, owing to steric hindrance between the newly located Phe826 and Thr893 (**Fig. 5c**). Mutational analysis of Phe826 is precluded because this residue was previously shown to be critical for E2-to-E3 transthiolation[6]. Of note, substitution of Asp900 with lysine in the context of the A889F mutant did not result in Lys900-modified peptide as in the case of the wild-type HECT (**Fig. 5d**). On the basis of these results, we concluded that the incorrect positioning of the C-terminal tail is the primary cause of the catalytic defect of the A889F mutant.

## DISCUSSION

The structure of the HECT$^{Nedd4}$~Ub$^{D}$–Ub complex offers the first glimpse, to our knowledge, of a Ub-loaded HECT primed for catalysis and, together with the biochemical data presented here, provides a framework for deciphering Lys63 specificity.

A key feature of the structure is the conserved noncovalent binding of the Ub$^{D}$ to the HECT C lobe that is preserved after the transfer of the thioester bond from the E2 to the E3 (this study and ref. 6). This finding supports the notion that formation of a Ub chain requires cycling of the E3 between E2 and the substrate and is fully consistent with the sequential addition mechanism previously hypothesized for some HECT ligases: owing to steric hindrance, a Ub-loaded E2 enzyme is unable to access the C-lobe Ub-binding site until the E3 transfers its Ub$^{D}$ to the substrate. Although molecular details may vary, Lys63 chain specificity together with sequence and structural conservation suggests that this catalytic mechanism may be general among the Nedd4 HECT–family members. This would not be necessarily true for other types of HECT ligases, such as E6AP, which is able to build a Lys48-linked chain on its HECT cysteine residue[10] and was recently suggested to carry two E2-binding sites[17]. These two features are indeed more compatible with the indexation or the seesaw models previously hypothesized[5,18].

An unresolved mystery of HECT catalysis is the role exerted by the conserved and essential phenylalanine residue[16] located most commonly at position –4 with respect to the C terminus of HECT (Phe896, position –5 in Nedd4; **Supplementary Fig. 4a**). We have been able to build this phenylalanine residue into the electron-density map (**Fig. 1d**). However, its location appears to be stabilized by interaction with a symmetry-related molecule, and it is probably not the one assumed during catalysis. We speculate that Phe896 will be positioned to exert its critical function only upon correct positioning of the substrate or the Ub acceptor. Its correct location will not necessarily be on the C lobe but possibly on an interface created by the correct orientation of the N and the C lobes. In the absence of the substrate, this binding site is not formed, as suggested by the fact that this residue has never been found ordered in HECT structures solved so far. This binding cleft should be conserved, because the phenylalanine residue is required in all the HECTs tested but has remained elusive because it is likely to be shaped only when the N and C lobes are organized with the substrate or the Ub$^{A}$ in the catalytic position.

We were able to identify a second residue within the Nedd4 family, the acidic residue present at the extreme C terminus, exclusively required for the ligation step and not for the E3 thioester formation. On the basis of our mutational analysis (**Fig. 3**) we propose a speculative model about the possible catalytic mechanism adopted by Nedd4-family members. Upon correct positioning of the substrate or of the Ub acceptor in a growing chain, the catalytic core will be formed thanks to Phe896, which works as a pivot to guide the terminal residue of Nedd4 toward the active site of catalysis. However, the role of the −4 phenylalanine remains elusive. A definitive understanding of the ubiquitination process will require additional high-resolution structures of catalytic complexes of HECT and substrates and/or Ub chains.

## METHODS

Methods and any associated references are available in the online version of the paper.

**Accession codes.** Coordinates for $HECT^{Nedd4}$~$Ub^{D}$–Ub complex and $HECT^{Nedd4}$ A889F have been deposited at the Protein Data Bank under accession codes 4BBN and 4BE8, respectively.

*Note: Supplementary information is available in the online version of the paper.*

### ACKNOWLEDGMENTS

We thank P. Romano for critically reading the manuscript and for helpful discussions and advice and the staff at the European Synchrotron Radiation Facility and Swiss Light Source for assistance in data collection. This work was supported by grants from the Associazione Italiana per la Ricerca sul Cancro (AIRC, IG11627), the European Community (Network of Excellence FP6, 100601–201012) and the European Molecular Biology Organization Young Investigator Program to S. Polo. Access to the High Throughput Crystallization Laboratory of the European Molecular Biology Laboratory Grenoble outstation was funded by the European Community's Seventh Framework Programme (FP7/2007-2013) PCUBE (grant agreement 227764).

### AUTHOR CONTRIBUTIONS

E.M. conducted the experiments with the help of E.V. and S.M.; V.C. assisted in crystallization; P.S. carried out MS analysis; S. Pasqualato performed structure determination and description; S. Pasqualato and E.M. participated in experimental design and data analysis; S. Polo conceived of the project, interpreted the results and wrote the paper.

### COMPETING FINANCIAL INTERESTS

The authors declare no competing financial interests.



1. Scheffner, M., Nuber, U. & Huibregtse, J.M. Protein ubiquitination involving an E1-E2-E3 enzyme ubiquitin thioester cascade. *Nature* **373**, 81–83 (1995).
2. Scheffner, M. & Staub, O. HECT E3s and human disease. *BMC Biochem.* **8** (suppl. 1), S6 (2007).
3. Marín, I. Animal HECT ubiquitin ligases: evolution and functional implications. *BMC Evol. Biol.* **10**, 56 (2010).
4. Rotin, D. & Kumar, S. Physiological functions of the HECT family of ubiquitin ligases. *Nat. Rev. Mol. Cell Biol.* **10**, 398–409 (2009).
5. Verdecia, M.A. *et al.* Conformational flexibility underlies ubiquitin ligation mediated by the WWP1 HECT domain E3 ligase. *Mol. Cell* **11**, 249–259 (2003).
6. Kamadurai, H.B. *et al.* Insights into ubiquitin transfer cascades from a structure of a UbcH5B~ubiquitin-HECT(NEDD4L) complex. *Mol. Cell* **36**, 1095–1102 (2009).
7. Kim, H.C., Steffen, A.M., Oldham, M.L., Chen, J. & Huibregtse, J.M. Structure and function of a HECT domain ubiquitin-binding site. *EMBO Rep.* **12**, 334–341 (2011).
8. Maspero, E. *et al.* Structure of the HECT:ubiquitin complex and its role in ubiquitin chain elongation. *EMBO Rep.* **12**, 342–349 (2011).
9. Kim, H.C. & Huibregtse, J.M. Polyubiquitination by HECT E3s and the determinants of chain type specificity. *Mol. Cell Biol.* **29**, 3307–3318 (2009).
10. Wang, M. & Pickart, C.M. Different HECT domain ubiquitin ligases employ distinct mechanisms of polyubiquitin chain synthesis. *EMBO J.* **24**, 4324–4333 (2005).
11. Remaut, H. & Waksman, G. Protein-protein interaction through β-strand addition. *Trends Biochem. Sci.* **31**, 436–444 (2006).
12. Wang, M., Cheng, D., Peng, J. & Pickart, C.M. Molecular determinants of polyubiquitin linkage selection by an HECT ubiquitin ligase. *EMBO J.* **25**, 1710–1719 (2006).
13. Dou, H., Buetow, L., Sibbet, G.J., Cameron, K. & Huang, D.T. BIRC7–E2 ubiquitin conjugate structure reveals the mechanism of ubiquitin transfer by a RING dimer. *Nat. Struct. Mol. Biol.* **19**, 876–883 (2012).
14. Plechanovová, A., Jaffray, E.G., Tatham, M.H., Naismith, J.H. & Hay, R.T. Structure of a RING E3 ligase and ubiquitin-loaded E2 primed for catalysis. *Nature* **489**, 115–120 (2012).
15. Reverter, D. & Lima, C.D. Insights into E3 ligase activity revealed by a SUMO–RanGAP1–Ubc9–Nup358 complex. *Nature* **435**, 687–692 (2005).
16. Salvat, C., Wang, G., Dastur, A., Lyon, N. & Huibregtse, J.M. The -4 phenylalanine is required for substrate ubiquitination catalyzed by HECT ubiquitin ligases. *J. Biol. Chem.* **279**, 18935–18943 (2004).
17. Ronchi, V.P., Klein, J.M. & Haas, A.L. E6AP/UBE3A ubiquitin ligase harbors two e2~ubiquitin binding sites. *J. Biol. Chem.* published online, doi:10.1074/jbc.M113.458059 (25 February 2013).
18. Hochstrasser, M. Lingering mysteries of ubiquitin-chain assembly. *Cell* **124**, 27–34 (2006).

## ONLINE METHODS

**Reagents and constructs.** Antibodies and their suppliers were: mouse monoclonal anti-Ub (ZTA10, generated in house, dilution 1:5); rabbit monoclonal anti-Lys48 and anti-Lys63 antibodies (clone Apu2 and Apu3, Millipore, dilution 1:1,000); streptavidin HRP and Imperial Protein Stain (Thermo Scientific). Biotinylated Ub was from Enzo Life Sciences. Bovine Ub was from Sigma-Aldrich. Nedd4 HECT–based constructs were engineered by site-directed mutagenesis. All other constructs were previously described[8,19]. All constructs were sequence-verified. Details are available upon request.

**Protein expression and purification.** GST fusion proteins were expressed in *E. coli* BL21 (DE3) at 18 °C for 16 h after induction with 500 μM IPTG at an $OD_{600}$ of 0.5. Cell pellets were resuspended in lysis buffer (50 mM Na-HEPES, pH 7.5, 200 mM NaCl, 1 mM EDTA, 0.1% NP40, 5% glycerol and Protease Inhibitor Cocktail set III (Calbiochem)). Sonicated lysates were cleared by centrifugation at 20,000 r.p.m. for 45 min. Supernatants were incubated with 1 ml of glutathione-Sepharose beads (GE Healthcare) per liter of bacterial culture. After 4 h at 4 °C, beads were washed with PBS and equilibrated in cleavage buffer (50 mM Tris-HCl, pH 7.4, 100 mM NaCl, 1 mM EDTA, 1 mM DTT and 5% glycerol). To cleave off GST, 10 units of PreScission protease (GE Healthcare) per mg of substrate were incubated for 16 h at 4 °C.

Untagged Ub G76C mutant was expressed in BL21 (DE3) *E. coli* at 18 °C for 16 h after induction with 1 mM IPTG at an $OD_{600}$ of 0.5. Cell pellets were resuspended in lysis buffer (25 mM ammonium acetate, 10 mM β-mercaptoethanol, 10% glycerol and protease inhibitors, pH 7.0) and lysed by sonication. Cell debris was removed by centrifugation, and the supernatant was adjusted to pH 4.5–5.0 with concentrated acetic acid. Precipitated proteins were removed by centrifugation, and the supernatant containing the Ub monomers was passed through a 0.45-mm PES filter. After dialysis, Ub was purified onto a Superdex 75 size-exclusion chromatography column equilibrated with 20 mM Tris-HCl, pH 8.0, 200 mM NaCl, 1 mM EDTA, 2 mM DTT and 5% glycerol. Bovine Ub was purified onto a Superdex 75 size-exclusion chromatography column equilibrated with 20 mM Tris-HCl, pH 8.0, 200 mM NaCl, 1 mM EDTA, 1 mM DTT and 5% glycerol.

**$HECT^{Nedd4}$~$Ub^{D}$ production.** Cleaved $HECT^{Nedd4}$ was concentrated in Vivaspin concentrators (MW cutoff 30 kDa, Sartorius Stedim Biotech) and loaded onto a Superdex 200 size-exclusion chromatography column (GE Healthcare) equilibrated with 20 mM Tris-HCl, pH 8.0, 200 mM NaCl, 1 mM EDTA, 1 mM DTT and 5% glycerol. Fractions containing $HECT^{Nedd4}$ were collected, concentrated at 0.1 mM and incubated with 0.1 mM Ub G76C in the presence of 2 mM TCEP at room temperature for 30 min to fully reduce the cysteines. Formation of disulfide bonds was conducted essentially as described in ref. 20 with a dialysis treatment in disulfide-bond buffer (100 mM $Na_2HPO_4^-$ $NaH_2PO_4$, pH 7.5, 200 mM NaCl, 5% glycerol and 25 μM $CuCl_2$) at room temperature. Disulfide-bond formation was monitored by nonreducing SDS-PAGE until Ub G76C monomer depletion (48 h). The $HECT^{Nedd4}$~Ub complex was purified through a Resource Q anion-exchange column (GE Healthcare). Fractions containing pure $HECT^{Nedd4}$~Ub complex were confirmed by nonreducing SDS-PAGE, collected and concentrated (**Supplementary Fig. 1**). $HECT^{Nedd4}$~Ub and bovine Ub were mixed at a ratio of 1:2 and concentrated at 0.5 mM for subsequent crystallization studies.

**Crystallization and structure determination.** For the $HECT^{Nedd4}$~$Ub^{D}$–Ub complex, nanovolume crystallization screening experiments were performed at the High Throughput Crystallization Laboratory (HTX Lab) of the EMBL Grenoble outstation as described[21]. Crystals were reproduced in house in sitting drops in 96-well plates set up with a Honeybee Cartesian robot, with 37 mg/ml protein complex. Diffracting crystals were obtained at 4 °C in 2.4–2.6 M sodium malonate, pH 5.7–6.2. Crystals were harvested from the 96-well plate and directly vitrified in liquid nitrogen. Data were collected at the European Synchrotron Radiation Facility (Grenoble) on beamline ID14-4 at 0.9393 Å and 100 K. For $HECT^{Nedd4}$ A889F, initial hits were obtained by screening for crystallization conditions in sitting drops in 96-well plates set up in house with a Honeybee Cartesian robot. Diffracting crystals were grown at 20 °C in hanging drops in 24-well plates with 1.15 M potassium sodium tartrate, 100 mM Tris-HCl, pH 9.0, using protein at 10 mg/ml. Crystals were cryocooled in mother liquor supplemented with 10% ethylene glycol, and data collection was performed at beamline X06DA (PXIII) of the Swiss Light Source at the Paul Scherrer Institut, at 1.0000 Å and 100 K. All data were processed with XDS/XSCALE[22] within the automated data reduction system xia2 (ref. 23) or the automated go.com procedure available in house at beamline X06DA. The structures were solved by molecular replacement with Phaser[24] within the CCP4 suite[25], using Ub, N lobe and C lobe from PDB entry 2XBB. The models were improved by iterative cycles of manual building in Coot[26] and refinement with phenix.refine[27] and Refmac[28]. For $HECT^{Nedd4}$~$Ub^{D}$–Ub, 97.9% of residues are in the favored regions of the Ramachandran plot, and no residues are in the disallowed regions. For $HECT^{Nedd4}$ A889F, 97.0% of residues are in the favored regions and no residues are in disallowed regions.

**Ubiquitination assays.** All assays were performed in ubiquitination buffer (25 mM Tris-HCl, pH 7.6, 5 mM $MgCl_2$, 100 mM NaCl, 0.2 μM DTT and 2 mM ATP) with the HECT domain cleaved and purified as previously described and Ube2D3 as the E2 enzyme. Ube2D3 was produced as a $His_6$ fusion protein and purified by using Ni-NTA agarose beads (Qiagen, manufacturer's protocol) and size-exclusion chromatography. Bovine Ub (Sigma) was purified by size-exclusion chromatography.

For the transthiolation assay, the pulse-chase was performed in two steps. First, Ube2D3 (5 μM) was loaded with biotinylated Ub (10 μM) with E1 enzyme (100 nM) in ubiquitination buffer for 15 min at 37 °C and then quenched on ice by a two-fold dilution with 0.5 M EDTA. Then the loaded E2 was mixed with E3 $HECT^{Nedd4}$ in ubiquitination buffer to the following final concentrations: E2, 1.4 μM; Ub, 2.8 μM; E3, 1 μM. Thioester formation on the $HECT^{Nedd4}$ was monitored by quenching the reaction at different time points with Laemmli buffer without reducing agent. All mutants were assayed side by side with wild-type controls.

For the Ub chain formation assay, reaction mixtures (50 μl) containing purified enzymes (20 nM E1, 250 nM purified $His_6$-tagged Ube2D3 and 500 nM $HECT^{Nedd4}$) and 1.25 μM of Ub in ubiquitination buffer were incubated at 37 °C and stopped at the different time points by addition of 4× Laemmli buffer with reducing agent (100 mM DTT).

For Ub AQUA analysis, reaction mixtures (20 μl) containing purified enzymes (50 nM E1, 1.5 μM purified $His_6$-tagged Ube2D3 and 2.2 μM HECT) and 12.5 μM of Ub in ubiquitination buffer were incubated at 37 °C for 1 h and stopped by addition of 4× Laemmli buffer with reducing agent (100 mM DTT).

**Mass spectrometry and quantitative analysis.** Proteins were resolved by SDS-PAGE on a gradient gel (4–12% TGX Precast Gel, Bio-Rad) and stained with colloidal blue (Colloidal Blue Staining Kit, Invitrogen). Gel bands corresponding to Ub-modified HECT were digested with trypsin. Briefly, samples were subjected to reduction in 10 mM DTT for 1 h at 56 °C. Digestion was carried out by saturating the gel with 12.5 ng/μl sequencing-grade modified trypsin (Promega) in 50 mM ammonium bicarbonate overnight. Peptide mixtures were acidified with trifluoroacetic acid (TFA, final concentration 3%), extracted from gel slices with 30% acetonitrile (ACN)/ 3% TFA and concentrated to 100 μl in a vacuum concentrator. Peptides were loaded onto homemade C18-stage tips, dried and dissolved in 5% formic acid (FA) before analysis on the Agilent 1100 LC system (Agilent) coupled to Ultra LTQ-FT (Thermo Fisher Scientific). MS data were analyzed for protein identification and presence of diglycine signature by using Mascot considering the following parameters: Gly-Gly (K) +114.043 Da, Leu-Arg-Gly-Gly (K) +383.228 Da, peptide tolerance 10 p.p.m., MS/MS tolerance 0.5 Da.

For AQUA analysis, samples were directly dissolved with a solution of reference peptides for Lys6, Lys11, Lys27, Lys29, Lys33, Lys48 and Lys63 polyubiquitin branched chains (Cell Signaling Technology) in 5% formic acid. Samples were analyzed by using a range of reference-peptide concentrations spanning from 1 picomole to 100 femtomoles, injecting three technical replicates per concentration. All spectra were acquired in data-dependent mode. Ion chromatograms for reference and sample peptide-pair precursor ions were manually extracted with Xcalibur v1.4 (ThermoElectron). Chromatographic coelution of reference and endogenous peptide pairs and accurate peak integration were manually confirmed.


19. Woelk, T. *et al.* Molecular mechanisms of coupled monoubiquitination. *Nat. Cell Biol.* **8**, 1246–1254 (2006).
20. Serniwka, S.A., & Shaw, G.S. The structure of the UbcH8-ubiquitin complex shows a unique ubiquitin interaction site. *Biochemistry* **48**, 12169–12179 (2009).
21. Dimasi, N., Flot, D., Dupeux, F. & Marquez, J.A. Expression, crystallization and X-ray data collection from microcrystals of the extracellular domain of the human inhibitory receptor expressed on myeloid cells IREM-1. *Acta Crystallogr. Sect. F Struct. Biol. Cryst. Commun.* **63**, 204–208 (2007).
22. Kabsch, W. Xds. *Acta Crystallogr. D Biol. Crystallogr.* **66**, 125–132 (2010).
23. Winter, G. *xia2*: an expert system for macromolecular crystallography data reduction. *J. Appl. Crystallogr.* **43**, 186–189 (2010).





doi:10.1038/nsmb.2566

24. McCoy, A.J. *et al*. Phaser crystallographic software. *J. Appl. Cryst.* **40**, 658–674 (2007).
25. CCP4. The CCP4 suite: programs for protein crystallography. *Acta Crystallogr. D Biol. Crystallogr.* **50**, 760–763 (1994).
26. Emsley, P., Lohkamp, B., Scott, W.G. & Cowtan, K. Features and development of Coot. *Acta Crystallogr. D Biol. Crystallogr.* **66**, 486–501 (2010).
27. Adams, P.D. *et al*. PHENIX: a comprehensive Python-based system for macromolecular structure solution. *Acta Crystallogr. D Biol. Crystallogr.* **66**, 213–221 (2010).
28. Murshudov, G.N., Vagin, A.A. & Dodson, E.J. Refinement of macromolecular structures by the maximum-likelihood method. *Acta Crystallogr. D Biol. Crystallogr.* **53**, 240–255 (1997).

EMBO reports

EMBO open

scientific report

# Structure of the HECT:ubiquitin complex and its role in ubiquitin chain elongation

*Elena Maspero[1], Sara Mari[1], Eleonora Valentini[1], Andrea Musacchio[2], Alexander Fish[3], Sebastiano Pasqualato[2,4+] & Simona Polo[1,5++]*

[1]IFOM, Fondazione Istituto FIRC di Oncologia Molecolare, [2]Dipartimento di Oncologia Sperimentale, Istituto Europeo di Oncologia, Milan, Italy, [3]Division of Biochemistry, The Netherlands Cancer Institute, Amsterdam, The Netherlands, [4]Crystallography Unit, IFOM-IEO Campus, Cogentech—Consortium for Genomic Technologies, and [5]Dipartimento di Medicina, Chirurgia ed Odontoiatria, Universita' degli Studi di Milano, Milan, Italy



**Several mechanisms have been proposed for the synthesis of substrate-linked ubiquitin chains. HECT ligases directly catalyse protein ubiquitination and have been found to non-covalently interact with ubiquitin. We report crystal structures of the Nedd4 HECT domain, alone and in complex with ubiquitin, which show a new binding mode involving two surfaces on ubiquitin and both subdomains of the HECT N-lobe. The structures suggest a model for HECT-to-substrate ubiquitin transfer, in which the growing chain on the substrate is kept close to the catalytic cysteine to promote processivity. Mutational analysis highlights differences between the processes of substrate polyubiquitination and self-ubiquitination.**

Keywords: catalysis; E3 ligase; polyubiquitination; structure; ubiquitin

EMBO *reports* (2011) **12**, 342–349. doi:10.1038/embor.2011.21

## INTRODUCTION

The ubiquitination process is carried out by an enzymatic cascade that includes an activating enzyme (E1), a conjugating enzyme (E2) and a ligase (E3; Dye & Schulman, 2007). The transfer of the ubiquitin moiety from the thioester-linked E3 (in HECT-type ligases) to the acceptor lysine on the substrate is the last step of this process. Subsequent chain elongation requires the modification of specific lysine residues in consecutive ubiquitin moieties. With few exceptions (Petroski & Deshaies, 2005; Jin *et al*, 2008), little is known about the mechanisms of ubiquitin-chain assembly, although various models have been proposed (Hochstrasser, 2006).

The Nedd4 family of HECT domain E3 ligases is a well-characterized class of enzymes that present a conserved modular organization with an amino-terminal C2 domain that is crucial for membrane localization, between two and four WW domains that recognize substrates and adaptor proteins and a carboxy-terminal catalytic HECT domain. In humans, there are nine members of this family that are implicated in a range of biological processes such as endocytosis, protein transport, viral budding, signalling, cellular growth and proliferation (Rotin & Kumar, 2009). This class of E3 enzymes seems to use a sequential addition mechanism, by which ubiquitin molecules are added one at a time from the catalytic cysteine to the distal lysine of the growing chain (Kim & Huibregtse, 2009). A key question is how E3 enzymes deal with the shifting position of the acceptor site during chain elongation.

Two groups have recently identified a surface implicated in non-covalent ubiquitin binding on the HECT-type E3 ligases Rsp5 and Smurf2 (French *et al*, 2009; Ogunjimi *et al*, 2010). This surface was proposed to have a role in regulating polyubiquitination, although opposite mechanisms were suggested by the groups, with the surface being required to either restrict the length of polyubiquitin chains synthesized by the HECT domain (French *et al*, 2009) or to promote polyubiquitination (Ogunjimi *et al*, 2010). In this study, we show the crystal structure of the HECT domain of Nedd4 alone and in complex with ubiquitin, and we present molecular insights into the mechanism by which Nedd4 catalyses polyubiquitination.

[1]IFOM, Fondazione Istituto FIRC di Oncologia Molecolare,
[2]Dipartimento di Oncologia Sperimentale, Istituto Europeo di Oncologia, Via Adamello 16, Milan 20139, Italy
[3]Division of Biochemistry, The Netherlands Cancer Institute, Plesmanlaan 121, Amsterdam 1066 CX, The Netherlands
[4]Crystallography Unit, IFOM-IEO Campus, Cogentech—Consortium for Genomic Technologies, Via Adamello 16, Milan 20139, Italy
[5]Dipartimento di Medicina, Chirurgia ed Odontoiatria, Universita' degli Studi di Milano, Via di Rudini' 8, Milan 20122, Italy
[+]Corresponding author. Tel: +39 02 94375172; Fax: +39 02 94375990; E-mail: sebastiano.pasqualato@ifom-ieo-campus.it
[++]Corresponding author. Tel: +39 02 574303242; Fax: +39 02 574303231; E-mail: simona.polo@ifom-ieo-campus.it

**Received 23 July 2010; revised 4 January 2011; accepted 13 January 2011; published online 11 March 2011**

## RESULTS AND DISCUSSION

### Structure of HECT$^{Nedd4}$ and HECT$^{Nedd4}$:ubiquitin

We characterized the interaction of the isolated HECT domain of Nedd4 (HECT$^{Nedd4}$) with ubiquitin in detail. The ubiquitin-binding ability resides in the N-lobe, does not show preference for Lys 63- or Lys 48-polyubiquitin chains and requires the canonical hydrophobic patch on ubiquitin, centred on Ile 44 (supplementary Fig S1 online). We extended this analysis to the other mammalian Nedd4 family members and found that only a subset of these HECT domains binds to ubiquitin, namely Nedd4, Nedd4-like and Smurf2 (Fig 1A).

To understand how ubiquitin binds to the HECT, we determined the crystal structure of the HECT$^{Nedd4}$ in isolation (at 2.5 Å) and in complex with ubiquitin (at 2.7 Å) by molecular replacement (supplementary Table S1 online and supplementary Fig S2 online). In both structures, HECT$^{Nedd4}$ displays the typical HECT fold (Huang *et al*, 1999; Verdecia *et al*, 2003; Ogunjimi *et al*, 2005) composed of two lobes connected by a flexible hinge (Fig 1B,C). The N-lobe, an elongated array of helices and β-hairpins, consists of two moieties, known as the large and small subdomains (Fig 1B). The small subdomain, which hosts the E2-binding site, comprises helices α6–α8 and β-sheets β5–β6 (Huang *et al*, 1999; Kamadurai *et al*, 2009). The large subdomain of the N-lobe is present below the C-lobe, an α/β sandwich domain that carries the catalytic cysteine. The orientation of the C-lobe differs in the two HECT$^{Nedd4}$ structures, and both orientations are distinct from those of previously reported HECT domain structures (supplementary Fig S3 online). This highlights the freedom of movement of the C-lobe, which is key for the catalytic function of HECT domains (Verdecia *et al*, 2003; Kamadurai *et al*, 2009).

Non-covalent ubiquitin binding to HECT$^{Nedd4}$ conceals a solvent-accessible interaction surface area on ubiquitin of approximately 900 Å$^2$, the largest surface identified so far for ubiquitin-binding domains (supplementary Table S2 online). Ubiquitin makes contact with Glu 554 and neighbouring residues of helix α1; Tyr 604, Tyr 605 and Tyr 610 from the region comprising helix α3′ and strand β3; Asn 628 and Glu 629 from helix α4′ and the ensuing loop; and Phe 707 and neighbouring residues of the β5–β6 beta hairpin. These residues are distributed in both the small and the large subdomains of the N-lobe (Figs 1E,2A). In the absence of ubiquitin, the relative orientation of the small and large subdomains is not fixed and varies for different structures (Huang *et al*, 1999; Verdecia *et al*, 2003; Ogunjimi *et al*, 2005). Ubiquitin binding might therefore be expected to stabilize a specific reciprocal orientation of the N-lobe subdomains. Indeed, superposition of the large subdomains of HECT$^{Nedd4}$ and HECT$^{Nedd4}$:ubiquitin (root mean square deviation of 0.6 Å over 181 $C_\alpha$) clearly indicates a relative movement of the β5–β6 hairpin of the small subdomain in the HECT$^{Nedd4}$:ubiquitin structure by approximately 5 Å towards the large subdomain of the N-lobe (Fig 1D).

As predicted by the defective behaviour of the I44A ubiquitin mutant (supplementary Fig S1C online), the interaction surface on ubiquitin involves the canonical Ile 44 hydrophobic patch, which also includes Gly 47, Leu 8 and Val 70 (Fig 2A). However, the surface of interaction is not limited to this patch, but extends to a 'second hydrophobic patch', including the residues Ile 36/Leu 71/Leu 73, the role of which has recently been discussed in the context of the E2-to-HECT ubiquitin transfer (Kamadurai *et al*, 2009; Fig 2A; supplementary Fig S4 online). The Asn 628, Tyr 634 and Glu 554 side chains on Nedd4 form hydrogen bonds with the main chain nitrogen atoms of ubiquitin-Leu 73, Arg 74 and Gly 75, whereas the ubiquitin-Leu 73 side chain is stacked between Tyr 634 and Tyr 605 of Nedd4.

We generated Nedd4 mutants that substantiate the functional importance of both interacting patches on ubiquitin. Mutation of Tyr 605 to Ala (Y605A) or Phe 707 to Ala (F707A) almost abolished HECT$^{Nedd4}$ binding to Lys 63 ubiquitin (Fig 2B). Phe 707 to Tyr (F707Y), Asn 628 to Ala (N628A) or Glu 629 to Ala (E629A) mutations had milder effects, preserving the association with higher molecular weight Lys 63 ubiquitin to varying degrees (Fig 2B). We confirmed these results by measuring the interaction between the HECT domains and monomeric and dimeric ubiquitin by fluorescence polarization and surface plasmon resonance (SPR) assay (Fig 2C; supplementary Fig S1D–F online). Both ubiquitin ligands interact with the HECT with rapid kinetics (fast $K_{on}$ and $K_{off}$ rate constants, data not shown). Wild-type HECT$^{Nedd4}$ displays a moderate affinity ($K_D$ approximately 11 μM) in the range of those reported for ubiquitin-binding domains (supplementary Table S2 online), whereas Y605A and F707A mutations show from 20- to 30-fold decreases in binding (Fig 2C; supplementary Fig S1F online).

### Role of ubiquitin binding in Nedd4 activity

Next, we analysed the catalytic activity of Nedd4 HECT mutants. In principle, the ubiquitin-binding surface might have a role at three stages of the E3 catalysis: binding to the E2, transthiolation process from E2 to E3 or substrate ubiquitination. We tested all of these possibilities using the isolated HECT, which retains the ability to ubiquitinate itself as well as substrates, albeit with reduced efficiency (not shown).

Pull-down and SPR assays showed that mutants have no significant impairment in binding with either the apo or the ubiquitin thioester-linked form of E2 enzyme Ube2D3 (Fig 3A and data not shown). Indeed, the E2 binding is built on an adjacent but non-overlapping surface on the large subdomain of the N-lobe (Huang *et al*, 1999; Fig 4C). We then tested the importance of the ubiquitin-binding surface in the E2-to-HECT transthiolation process by using a pulse-chase protocol (Fig 3B). Again, no appreciable transthiolation defects were observed for the mutants, supporting the notion that the ubiquitin-binding surface is not involved in the upstream steps of the enzymatic cascade. Of note, the thioester HECT∼ubiquitin bond is unstable and the ubiquitin moiety is immediately transferred to the lysine/s of the HECT, as demonstrated by the appearance of higher molecular-weight proteins that are resistant to dithiothreitol treatment (Fig 3B, lower panels).

These results led us to propose that the ubiquitin-binding surface on the HECT might act to bind a ubiquitin moiety that is already conjugated to a substrate, thus promoting polyubiquitination. Indeed, when we assayed F707A and Y605A in an *in vitro* ubiquitination reaction, we found that mutations in the ubiquitin-binding surface strongly impaired free-chain formation and ubiquitination of all the substrates tested (Fig 3C; supplementary Fig S5 online). The mutant enzymes were efficient in the first cycle of substrate ubiquitination and in ubiquitin dimer formation, using free ubiquitin as a pseudosubstrate (Fig 3C; supplementary Fig S5 online). This was confirmed by using a ubiquitin Lys 0 mutant and

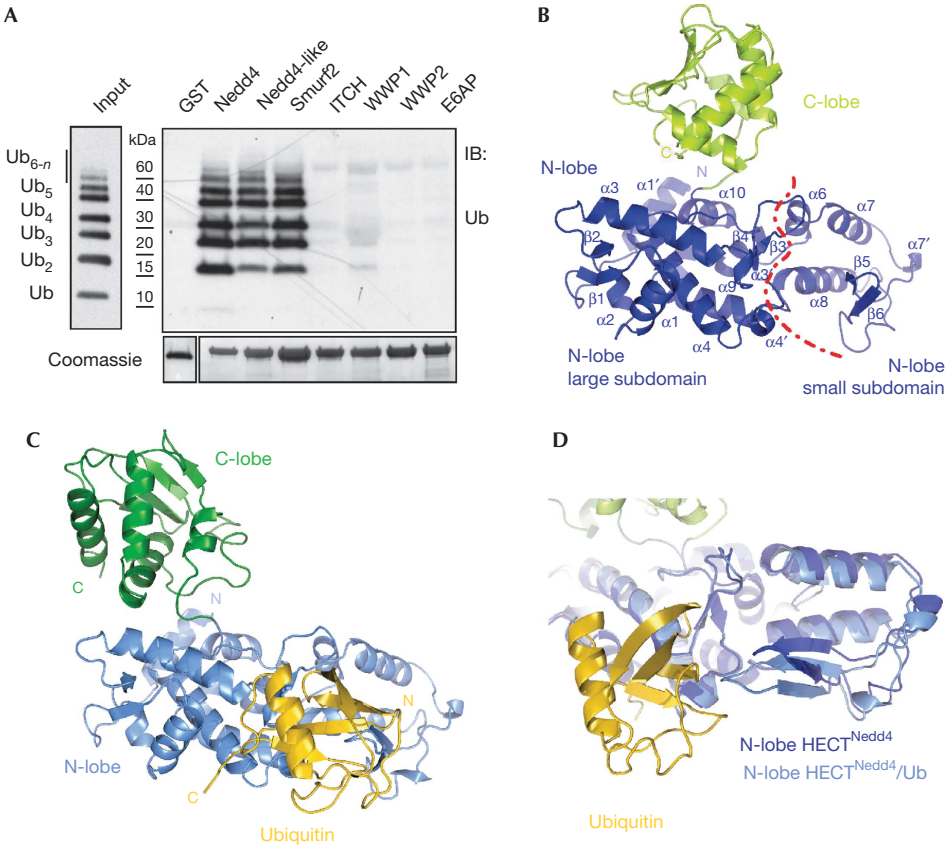


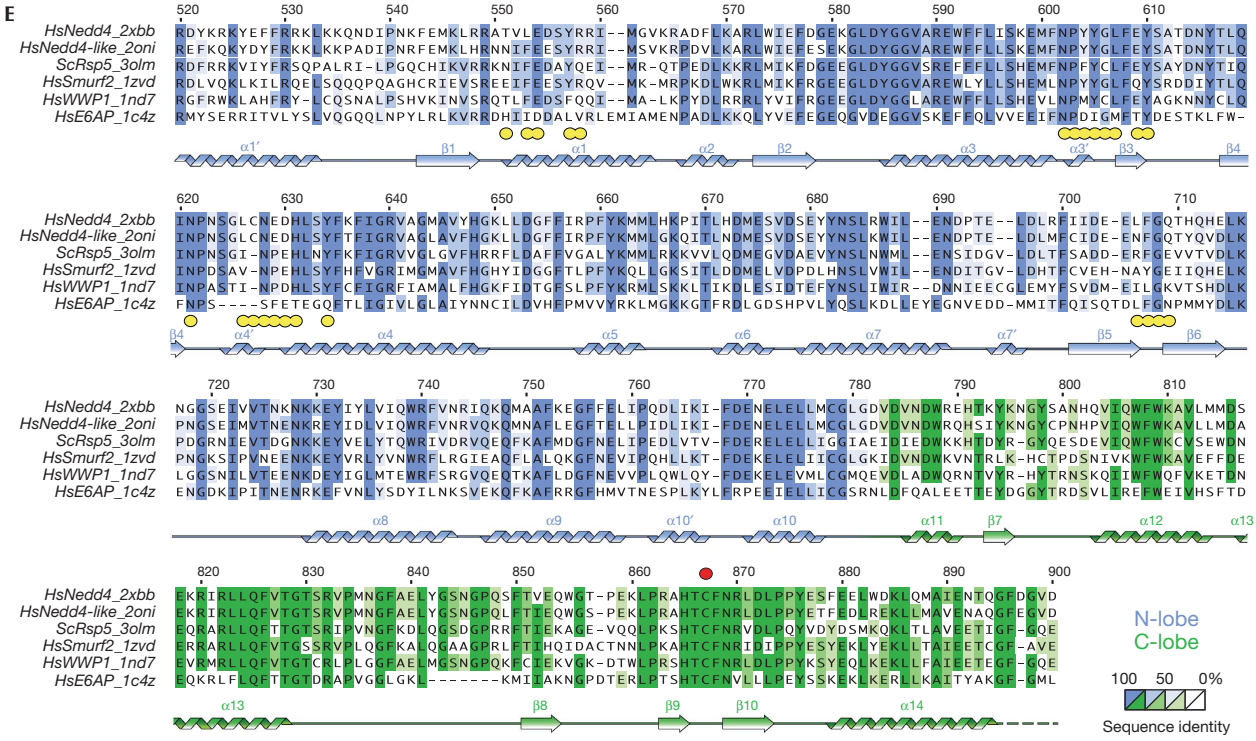

◀ **Fig 1** | Structure of the HECT$^{Nedd4}$ domain in apo form and in complex with ubiquitin. (**A**) GST pull-down assay with the HECT domains of various Nedd4 family HECT E3 ligases. GST-fusion proteins were incubated for 2 h at 4 °C in YY buffer with synthetic Lys 63-polyubiquitin chains and analysed by IB as indicated. Coomassie staining shows comparable loading of GST proteins. Similar results were obtained with linear and Lys 48-polyubiquitin chains (not shown). (**B**) Overall structure of HECT$^{Nedd4}$ (N-lobe, blue; C-lobe, green). The red dotted line indicates the boundary between the large and small subdomains of the N-lobe. (**C**) Overall structure of HECT$^{Nedd4}$ in complex with ubiquitin (yellow). The HECT structure is represented in the same orientation as in **B**; N-lobe, light blue; C-lobe, dark green. (**D**) Superposition on the large subdomain of the N-lobe of HECT$^{Nedd4}$ and HECT$^{Nedd4}$:ubiquitin. In the complex (light blue), the β5–β6 hairpin of the small subdomain of the N-lobe is closer to the large subdomain, with respect to the isolated HECT (dark blue). (**E**) Sequence alignment of the HECT$^{Nedd4}$ domain with other crystallized HECT domains. Secondary structure elements are depicted. Dotted line indicates that the residues were not visible in the electron density maps. Yellow circles indicate residues in contact with ubiquitin in the structure of HECT$^{Nedd4}$:ubiquitin (according to PISA; Krissinel & Henrick, 2007). Numbering refers to Nedd4 sequence. GST, glutathione *S*-transferase; IB, immunoblotting; Ub, ubiquitin.

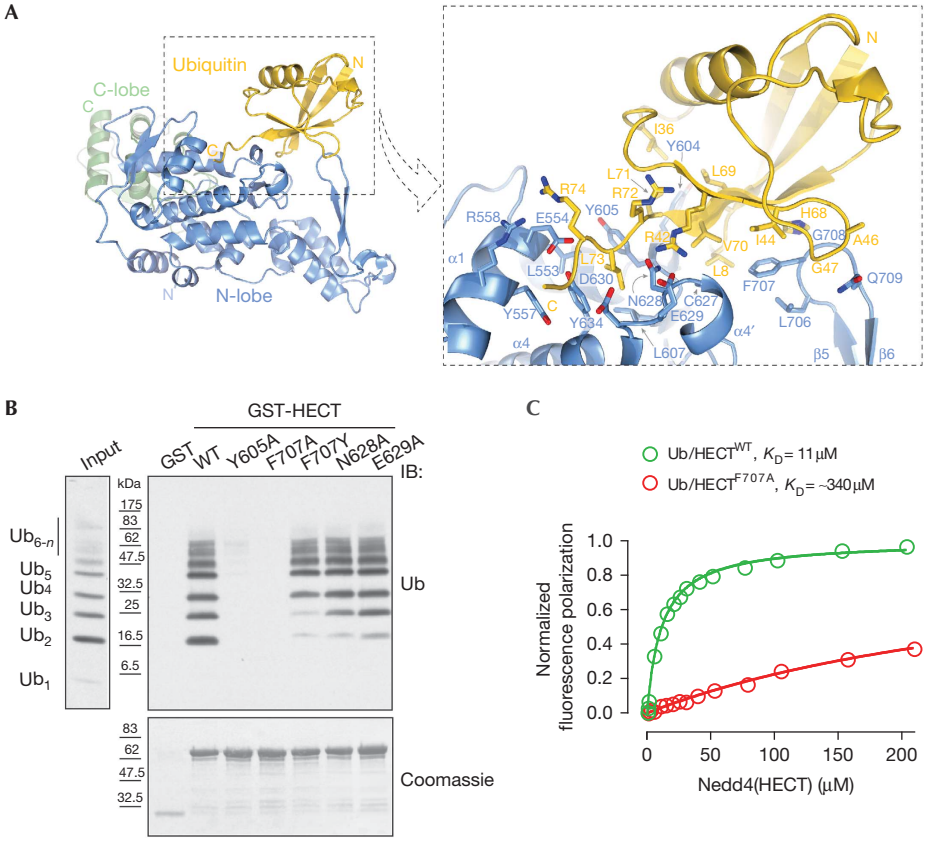


**Fig 2** | HECT$^{Nedd4}$:ubiquitin interaction and mutant validation. (**A**) Close-up view of HECT$^{Nedd4}$ N-lobe:ubiquitin interaction. (**B**) GST pull-down assay with the indicated Nedd4 constructs and Lys 63-linked polyubiquitin chains was performed as described in Fig 1A. (**C**) Fluorescence-polarization assay with the indicated Nedd4 constructs and monomeric ubiquitin was performed. The HECT$^{Nedd4}$:ubiquitin interaction displays a moderate affinity with a $K_D$ of 11 μM, F707A mutant displays a thirty times lower affinity. Details are described in the supplementary Methods online and similar results for the Y605A mutant obtained by SPR assay are in supplementary Fig S1 online. IB, immmunoblotting; GST, glutathione *S*-transferase; SPR, surface plasmon resonance; Ub, ubiquitin; WT, wild type.

quantification of the results repeated as fold differences between wild-type HECT and mutants (supplementary Fig S5A online). Interestingly, F707A and Y605A mutations did not affect self-ubiquitination of Nedd4 (Fig 3B, lower panels and Fig 3D), indicating that this *in cis* reaction is a catalytically distinct process that cannot be used as a surrogate assay for ligase activity on substrates.

Most HECT E3s synthesize polyubiquitin chains with specific linkages (Wang *et al*, 2006; Kim *et al*, 2007). To gain insight into the type of chains synthesized by Nedd4, we tested substrate ubiquitination using ubiquitin-bearing individual lysine-to-arginine mutations (KR mutants). We found that Nedd4 has a strong preference for building Lys 63-chains on substrates, a feature retained by the F707A mutant (Fig 4A). Consistent with previous data, however, F707A has defective chain elongation on substrate and shorter free chains, regardless of the type of ubiquitin used (Fig 4A). Therefore, we conclude that the ubiquitin-binding surface on the HECT acts to promote substrate polyubiquitination,

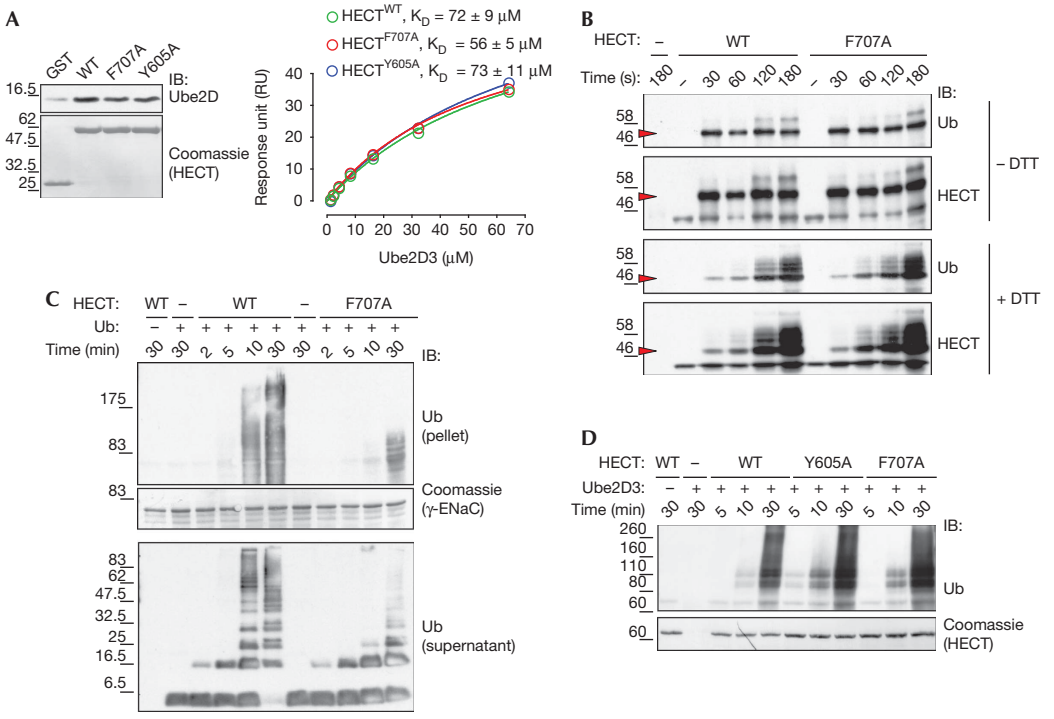


**Fig 3** | Disruption of HECT$^{Nedd4}$:ubiquitin interaction impairs substrate polyubiquitination. (**A**) Mutations do not affect E2 binding. Left panel: GST pull-down assay with the indicated HECT mutants and the E2 enzyme Ube2D3. IB was performed as indicated. Coomassie staining shows comparable loading of GST proteins. Right panel: the HECT$^{Nedd4}$:Ube2D3 interaction displays a modest affinity, that is not perturbed by the F707A and Y605A mutations. SPR assay was performed as described in the supplementary methods online. (**B**) Mutations do not affect the kinetics of the E2-to-HECT transthiolation process. The transfer of ubiquitin was monitored by quenching the reaction at different time points, with the addition of Laemmli buffer with or without the reducing agent (100 mM DTT). Arrow indicates thioesther HECT ~ ubiquitin (−DTT) or monoubiquitinated HECT (+DTT) running at the same position. DTT-resistant higher molecular bands represent self-ubiquitinated HECT. Similar results were obtained with Y605A mutant. (**C**) Mutations impair substrate polyubiquitination. Upper panel: GST-γENaC ubiquitination kinetics with WT HECT and F707A mutant (ubiquitin (pellet)). Middle panel: Coomassie staining showing comparable loading of GST proteins. Lower panel: kinetics of free ubiquitin chain formation (ubiquitin (supernatant)) during the reaction. IB was performed as indicated. (**D**) Self-ubiquitination kinetics with WT HECT and Y605A and F707A mutants. IB was performed as indicated. Coomassie staining shows comparable loading of HECT proteins. Similar results were obtained with full-length Nedd4 mutants. DTT, dithiothreitol; ENaC, epithelial $Na^+$ channel; GST, glutathione *S*-transferase; IB, immunoblotting; SPR, surface plasmon resonance; Ub, ubiquitin; WT, wild type.

but it does not dictate the preference for a specific lysine during elongation. Indeed, recent observations suggest that the C-lobe, rather than the ubiquitin-binding N-lobe, is the crucial determinant of lysine selection during elongation (Kim & Huibregtse, 2009).

## CONCLUSIONS

Collectively, our results support the hypothesis that the ubiquitin-binding surface is required for the processivity of the poly-ubiquitination reaction (Ogunjimi *et al*, 2010), rather than for limiting chain elongation, as suggested previously (French *et al*, 2009). How can this occur? It is tempting to envision a model in which the distal ubiquitin on the substrate occupies this surface, promoting retention of the ubiquitinated substrate to the E3, and also keeping the small subdomain of the N-lobe in a conformation that favours processive ubiquitin addition. This could be achieved by either reducing the gap between the catalytic cysteine of the HECT and the C-terminus of ubiquitin linked to the E2 enzyme (Kamadurai *et al*, 2009) or by facilitating the transfer of a subsequent ubiquitin to the HECT-bound substrate. In support of this model, we found that the non-covalent ubiquitin-binding surface that we mapped remains accessible in the complex of the HECT domain of Nedd4-like with the ubiquitin-loaded E2 (Kamadurai *et al*, 2009; Fig 4C).

Our data support the notion that Nedd4 adopts a simple sequential-addition model to build a chain on a substrate; after the first ubiquitin is attached, the chain is elongated through Lys 63 linkage, because of the ability of the N-lobe to maintain the growing polyubiquitin chain in close proximity. A similar conclusion about the role of the HECT ubiquitin-binding site in promoting chain elongation was reached in the accompanying study by Kim *et al* (2011) on Rsp5. Although the position of Lys 63 on bound ubiquitin does not seem to be able to orient the growing chain towards the E2 catalytic cysteine (Fig 4B), the average B factors for the ubiquitin molecules are considerably higher than those of their HECT counterparts (approximately 76 $A^2$ for ubiquitin molecules, approximately 48 $A^2$ for HECT domains; supplementary Table S1 online), suggesting freedom of movement of ubiquitin on its docking site. This could imply that the binding of

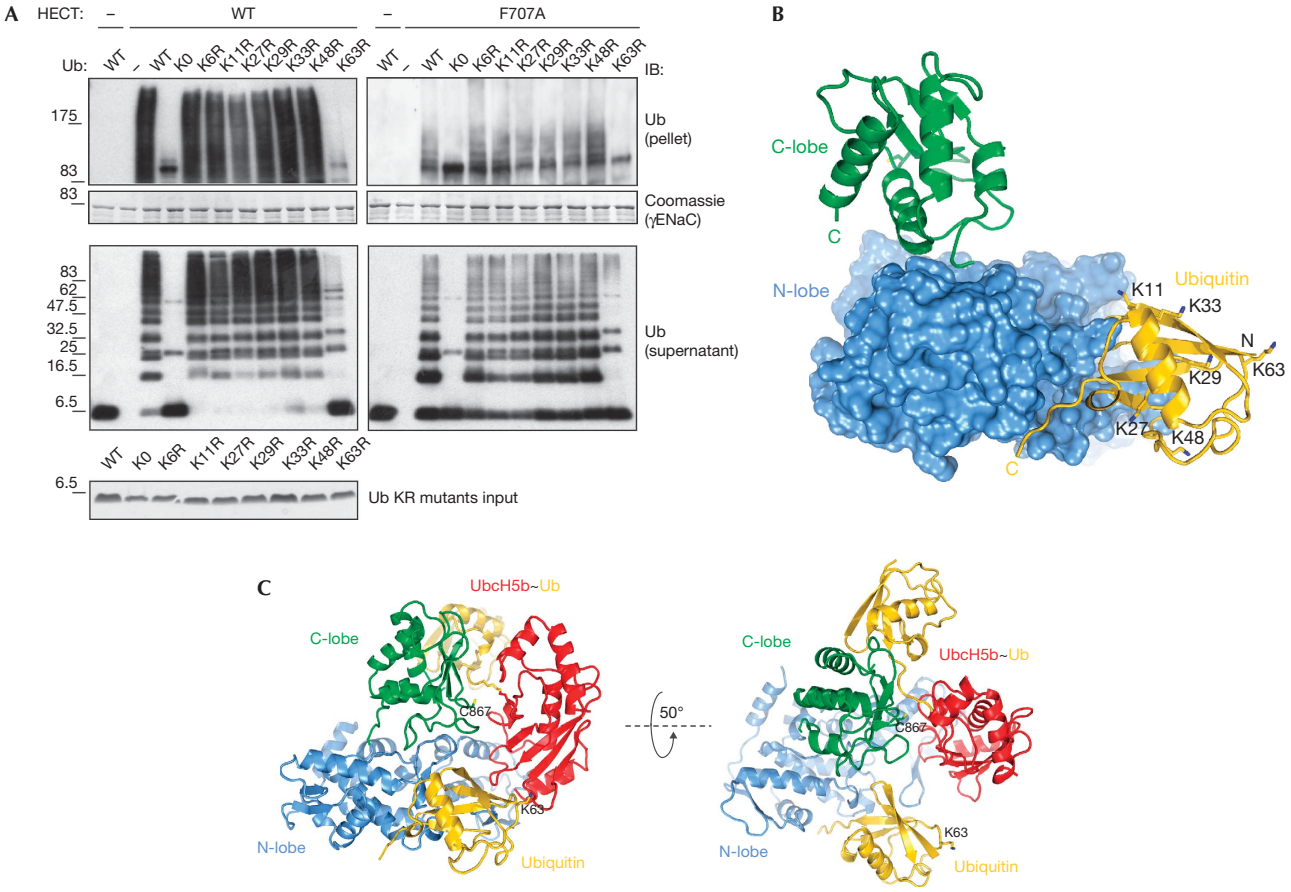


**Fig 4** | Ubiquitin binding to the HECT$^{Nedd4}$ domain is compatible with HECT$^{Nedd4\text{-}like}$:E2 ~ ubiquitin complex and does not dictate chain specificity. (**A**) Substrate ubiquitination assay with the indicated ubiquitin KR mutants was performed. The reaction was quenched after 30 min for the WT HECT and after 60 min for the F707A mutant. Upper panel: GST-γENaC ubiquitination with the indicated constructs. Middle panel: Coomassie staining showing comparable loading of GST proteins. Lower panel: free ubiquitin chain formation during the reaction. IB was performed as indicated. Lower panel: 1 μg of ubiquitin KR mutants were loaded for comparison and visualized by Coomassie staining. (**B**) Position of ubiquitin lysines in the Nedd4 HECT/ubiquitin complex. HECT N-lobe is shown as surface representation, whereas the C-lobe and ubiquitin are shown as cartoon representations. Ubiquitin lysine side chains are indicated in sticks. Six of the seven ubiquitin lysines are shown, K 6 being in the back. (**C**) Model of Ubch5B ~ Ub:C-lobe complex (Kamadurai *et al*, 2009) binding to the N-lobe:ubiquitin complex. Details are in the supplementary Methods online. C 867 on the HECT and K 63 on the Ub are shown. ENaC, epithelial $Na^+$ channel; GST, glutathione *S*-transferase; IB, immunoblotting; KR, lysine-to-arginine mutation; Ub, ubiquitin; WT, wild type.

ubiquitin to the E3 is strong enough to promote polyubiquitination, yet loose enough to allow chain growth, possibly through a slippage mechanism by which the ubiquitin-binding surface specifically binds to the distal ubiquitin at the end of the chain. The moderate affinity and fast kinetic rates of the HECT:ubiquitin interaction fit well with such a mechanism. Future structural studies with Nedd4 in complex with a ubiquitinated substrate might be required to provide a definitive picture of this dynamic process.

The detailed molecular view provided by our structure allows the identification of the crucial residues required for binding (Fig 1E), which can be used to predict the HECT E3 enzymes that are able to bind to ubiquitin. It remains to be established whether the presence of this binding surface might determine the mechanism of chain synthesis adopted by the different HECT ligases to become processive.

At our level of understanding, generalizing the mechanisms that underlie polyubiquitination would be premature, but it is interesting to note from the comparison of the small Nedd4 family of E3, that nature has used a variety of protein architectures to ensure specificity.

## METHODS

**Crystallization and structure determination.** Crystals of HECT$^{Nedd4}$ and HECT$^{Nedd4}$:ubiquitin complex were obtained by sitting-drop vapour diffusion at 20 °C, using a Honeybee Cartesian robot in 96-well plates. Diffraction-quality crystals were obtained by optimizing the initial conditions in 24-well plates, hanging drops at 20 °C. Crystals were all optimized by microseeding. For HECT$^{Nedd4}$, the optimized conditions were 100 mM Na-MES, pH 6.0, 2–4% PEG 400 or PEG 600, 30–60 mM $CaCl_2$ or $MgCl_2$, 5 mM tris(2-carboxyethyl)phosphine, with protein concentration in the 2.5–5 mg/ml range. Crystals were cryoprotected in 100 mM Na-MES, pH 6.0, 4% PEG 400, supplemented with 20% ethylene glycol. The structure was solved with a data set collected at the European

Synchrotron Radiation Facility (ESRF) at beamline ID14-2. For the HECT$^{Nedd4}$:ubiquitin complex, initial crystals were obtained in 100 mM Na-HEPES, pH 7–8, 10–20% PEG 2000 MME, 5 mM tris(2-carboxyethyl)phosphine, with proteins purified individually, then mixed in a 1:1 molar ratio and a concentration of approximately 30 mg/ml. To obtain good-quality diffraction and to overcome twinning, the complex was crystallized in the presence of excess ubiquitin (600–900 μM of complex, 1.2 × –2.3 × ubiquitin molar excess), lower concentration of PEG 2000 MME (2–10%), and the crystals were carefully frozen by equilibrating them into cryo-buffer (100 mM Na-HEPES, pH 7.5, 10% PEG 2000 MME) with increasing concentrations of glycerol, reaching a final concentration of 20%. The structure was solved with a data set collected at the ESRF at beamline ID14-1 on a crystal grown in a 1.9 × ubiquitin molar excess.

X-ray diffraction data were processed with HKL2000 (Otwinowski & Minor, 1997) or XDS (Kabsch, 2010). Both structures were solved by molecular replacement with Phaser within the CCP4 suite (CCP4, 1994), using as a search model the HECT domain of Nedd4-like (Protein Data Bank entry 2oni) in the case of HECT$^{Nedd4}$, and HECT$^{Nedd4}$ and a high-resolution structure of ubiquitin (Protein Data Bank entry 1ubi) in the case of HECT$^{Nedd4}$:ubiquitin complex. Initial models were refined with the CNS suite (Brunger, 2007), Refmac (Murshudov *et al*, 1997), the Phenix suite (Adams *et al*, 2010) and manual building in Coot (Emsley *et al*, 2010). For the HECT$^{Nedd4}$:ubiquitin complex, non-crystallographic symmetry (NCS) restraints were used in refinement. In the first cycles of refinement carried out with Refmac, HECT molecules were divided into two NCS groups (the N-lobe and the C-lobe), and ubiquitin molecules were the third NCS group. For further refinement cycles carried out with phenix.refine, five NCS groups were used: ubiquitin molecules and HECT domain residues 522:699, 724:778, 785:828 and 850:891, thus not subjecting HECT domain loops to NCS restraints. Structure representations were generated with Pymol (DeLano Scientific LLC). HECT$^{Nedd4}$ crystallized in spacegroup C2, whereas HECT$^{Nedd4}$:ubiquitin crystallized in spacegroup $P2_1$, with two complexes per asymmetrical unit. The two complexes differ slightly in the orientation of the HECT$^{Nedd4}$ C-lobe with respect to the N-lobe, and the relative orientation of HECT$^{Nedd4}$ with respect to ubiquitin, but the interactions discussed here are present in both complexes. Superpositions of pairs of domains of the asymmetrical unit indicate that they are almost identical (root mean square deviations of N-lobes: 0.36 Å over 260 $C_\alpha$; C-lobes: 0.63 Å over 115 $C_\alpha$; Ubs: 0.25 Å over 76 $C_\alpha$).

**Ubiquitination assay.** Ubiquitination assays were performed with HECT domains produced as glutathione *S*-transferase (GST) fusion proteins and cleaved with PreScission protease. The E2 enzyme Ube2D3, was produced as a $His_6$-fusion protein and eluted from Ni-NTA Agarose beads (Qiagen). Reaction mixtures contained purified enzymes (20 nM E1, 250 nM of purified $His_6$-tagged Ube2D3, 250 nM HECT$^{Nedd4}$), 300 nM of substrate (γ epithelial $Na^+$ channel and LMP2A were produced as GST fusion proteins and used attached to glutathione beads) and 1 μM of ubiquitin in ubiquitination buffer (25 mM Tris–HCl, pH 7.6, 5 mM $MgCl_2$, 100 mM NaCl, 0.2 μM dithiothreitol, 2 mM ATP). Reactions were incubated at 37 °C. At the indicated time point, samples were centrifuged to separate the pellet—containing the ubiquitinated substrates—and the supernatant—containing the enzymes and the soluble ubiquitin chains, if produced. The pellet was washed four times in YY buffer (50 mM Na-HEPES pH 7.5, 150 mM NaCl, 1 mM EDTA, 10% glycerol, 1% triton X-100) before loading on SDS–polyacrylamide gel electrophoresis gel. For self-ubiquitination reaction, the mixtures contained 20 nM E1, 250 nM of purified $His_6$-tagged Ube2D3, 250 nM of GST-HECT$^{Nedd4}$ and 0.5 μM of ubiquitin in ubiquitination buffer. Detection was performed by immunoblotting using specific antibody. Coomassie-stained membrane was used to show loading of GST-fusion protein after immunoblotting.

Reagents and constructs, protein expression and purification, transthiolation assay, pull-down experiments, fluorescence polarization assay and SPR are described in the supplementary Methods online.

**Accession codes**: Coordinates for HECT$^{Nedd4}$ and the HECT$^{Nedd4}$:ubiquitin complex have been deposited at the Protein Data Bank under accession codes 2xbf and 2xbb, respectively.

**Supplementary information** is available at EMBO *reports* online (http://www.emboreports.org).

ACKNOWLEDGEMENTS

We thank P.R. Romano for critically reading the manuscript, V. Cecatiello for assistance in crystallization, R.A. Steiner for advice, the staff at European Synchrotron Radiation Facility for assistance in data collection and M.P.A. Luna-Vargas for providing reagents. This work was supported by grants from the Associazione Italiana per la Ricerca sul Cancro (AIRC) and the European Community (FP7) to S.P. E.M. is the recipient of an AIRC fellowship.

CONFLICT OF INTEREST

The authors declare that they have no conflict of interest.

REFERENCES

Adams PD *et al* (2010) PHENIX: a comprehensive Python-based system for macromolecular structure solution. *Acta Crystallogr D Biol Crystallogr* **66:** 213–221

Brunger AT (2007) Version 1.2 of the Crystallography and NMR system. *Nat Protoc* **2:** 2728–2733

CCP4 (1994) The CCP4 suite: programs for protein crystallography. *Acta Crystallogr D Biol Crystallogr* **50:** 760–763

Dye BT, Schulman BA (2007) Structural mechanisms underlying posttranslational modification by ubiquitin-like proteins. *Annu Rev Biophys Biomol Struct* **36:** 131–150

Emsley P, Lohkamp B, Scott WG, Cowtan K (2010) Features and development of Coot. *Acta Crystallogr D Biol Crystallogr* **66:** 486–501

French ME, Kretzmann BR, Hicke L (2009) Regulation of the RSP5 ubiquitin ligase by an intrinsic ubiquitin-binding site. *J Biol Chem* **284:** 12071–12079

Hochstrasser M (2006) Lingering mysteries of ubiquitin-chain assembly. *Cell* **124:** 27–34

Huang L, Kinnucan E, Wang G, Beaudenon S, Howley PM, Huibregtse JM, Pavletich NP (1999) Structure of an E6AP–UbcH7 complex: insights into ubiquitination by the E2-E3 enzyme cascade. *Science* **286:** 1321–1326

Jin L, Williamson A, Banerjee S, Philipp I, Rape M (2008) Mechanism of ubiquitin-chain formation by the human anaphase-promoting complex. *Cell* **133:** 653–665

Kabsch W (2010) Xds. *Acta Crystallogr D Biol Crystallogr* **66:** 125–132

Kamadurai HB, Souphron J, Scott DC, Duda DM, Miller DJ, Stringer D, Piper RC, Schulman BA (2009) Insights into ubiquitin transfer cascades from a structure of a UbcH5B approximately ubiquitin–HECT(NEDD4L) complex. *Mol Cell* **36:** 1095–1102

Kim HC, Huibregtse JM (2009) Polyubiquitination by HECT E3s and the determinants of chain type specificity. *Mol Cell Biol* **29:** 3307–3318

Kim HT, Kim KP, Lledias F, Kisselev AF, Scaglione KM, Skowyra D, Gygi SP, Goldberg AL (2007) Certain pairs of ubiquitin-conjugating enzymes (E2s) and ubiquitin-protein ligases (E3s) synthesize nondegradable forked ubiquitin chains containing all possible isopeptide linkages. *J Biol Chem* **282:** 17375–17386

Kim HY, Steffen AM, Oldham ML, Chen J, Huibregtse JM (2011) Structure and function of an HECT domain ubiquitin-binding site. *EMBO Rep* **12:** 334–341

Krissinel E, Henrick K (2007) Inference of macromolecular assemblies from crystalline state. *J Mol Biol* **372:** 774–797

Murshudov GN, Vagin AA, Dodson EJ (1997) Refinement of macromolecular structures by the maximum-likelihood method. *Acta Crystallogr D Biol Crystallogr* **53:** 240–255

Ogunjimi AA, Briant DJ, Pece-Barbara N, Le Roy C, Di Guglielmo GM, Kavsak P, Rasmussen RK, Seet BT, Sicheri F, Wrana JL (2005) Regulation of Smurf2 ubiquitin ligase activity by anchoring the E2 to the HECT domain. *Mol Cell* **19:** 297–308

Ogunjimi AA, Wiesner S, Briant DJ, Varelas X, Sicheri F, Forman-Kay J, Wrana JL (2010) The ubiquitin binding region of the Smurf HECT domain facilitates polyubiquitylation and binding of ubiquitylated substrates. *J Biol Chem* **285:** 6308–6315

Otwinowski Z, Minor W (1997) Processing of X-ray diffraction data collected in oscillation mode. *Methods Enzymol* **276:** 307–326

Petroski MD, Deshaies RJ (2005) Mechanism of lysine 48-linked ubiquitin-chain synthesis by the cullin-RING ubiquitin-ligase complex SCF–Cdc34. *Cell* **123:** 1107–1120

Rotin D, Kumar S (2009) Physiological functions of the HECT family of ubiquitin ligases. *Nat Rev Mol Cell Biol* **10:** 398–409

Verdecia MA, Joazeiro CA, Wells NJ, Ferrer JL, Bowman ME, Hunter T, Noel JP (2003) Conformational flexibility underlies ubiquitin ligation mediated by the WWP1 HECT domain E3 ligase. *Mol Cell* **11:** 249–259

Wang M, Cheng D, Peng J, Pickart CM (2006) Molecular determinants of polyubiquitin linkage selection by an HECT ubiquitin ligase. *EMBO J* **25:** 1710–1719